Understanding cell lysis in fermentation and its impact on primary recovery using viscosity monitoring

A thesis submitted to University College London for the degree of

DOCTOR OF ENGINEERING

by

Joseph Matthew Newton

February 2018

Department of Biochemical Engineering

University College London

Torrington Place

WC1E 7JE

Declaration

I hereby declare that the work presented in this thesis is solely my own work and that to the best of my knowledge the work is original, except where otherwise indicated by reference to other authors.

Joseph M Newton

01 February 2018

Abstract

The high level of innovation in drug discovery in recent years has presented a significant challenge for drug manufacturing process development, which must constantly evolve to meet this increasingly diverse demand. As a result, novel process monitoring technologies to rapidly optimise these processes, reduce development costs and improve time to market are in high demand in the biopharmaceutical industry. Within the context of bioprocess development and manufacturing, the main focus of this work is on fermentation and its impact on, and interaction with, primary recovery.

Although *E. coli* is the most widely researched host organism for recombinant protein production and cell death during fermentation has been observed for decades, very little is understood about how to quantify and detect cell lysis in late stage fermentation, which leads to a number of problems in the downstream process such as product loss and poor operational performance. The complex nature of the cell broth means that it is difficult to observe lysis directly, and current analytical technologies are unable to rapidly and accurately monitor the shift between optimum intracellular product concentration and leakage to the cell broth. This thesis proposes that by monitoring the physical properties of the cell broth, i.e. by monitoring the viscosity, it may be possible to indirectly infer cell lysis, as the release of intracellular content, such as host cell protein and nucleic acids, to the cell broth at the point of lysis are known to cause an increase in the broth viscosity.

In this thesis, cell lysis was first characterised in an industrially relevant *E. coli* fermentation producing antibody fragments (Fab'), using a range of common analytical techniques. Following this, a method has been developed to rapidly detect cell lysis and product loss using at-line viscosity monitoring, and a strong correlation was shown to exist between DNA release, product leakage, cytotoxicity and viscosity. Viscosity monitoring to detect cell lysis was shown to perform better than optical density measurements and online capacitance probes, and could detect lysis faster than HPLC, flow cytometry, cytotoxicity assays and DNA quantification. Subsequently, a model has been developed to quantify cell lysis using rapid viscosity

monitoring. Viscoelasticity studies have also been performed to provide novel insight into changes in cell strength during fermentation. Finally, a case study has been carried out to demonstrate an application of viscosity monitoring in process development, and to enable insight into the impact of upstream processing conditions on the efficiency of downstream unit operations. A novel process design using crossflow filtration and flocculation achieved a 2.53-fold improvement in total product recovered, a 3-fold improvement in solids removal and a 3.6-fold improvement in product purity, in comparison to the existing Fab' primary recovery process.

This work presents the novel use of viscosity monitoring in biopharmaceutical fermentation to rapidly detect cell lysis and product loss. In doing so, a deeper understanding of changes in the physical properties of cell broths during fermentation has been obtained, as well as insight into the impact of lysis on various primary recovery unit operations. The use of viscosity monitoring to rapidly detect lysis and product loss has been shown to be a promising analytical tool to enable optimisation in process development and facilitate harvest decision making for large scale operation.

Impact statement

Cell lysis in fermentation represents a significant challenge in bioprocessing, and current technologies are unable to rapidly and accurately monitor lysis during process operation. This creates numerous problems in the downstream process such as product loss and poor operational performance. The work carried out in this thesis used rheology to characterise and provide an advanced understanding of biological processing material, and as a result developed a novel methodology to rapidly detect cell lysis and product loss in fermentation by monitoring the viscosity. This methodology can now be readily implemented into a range of industrial fermentation processes, and additionally presents a significant opportunity to carry out further research into monitoring the physical properties of process material using rheology. The dissemination of two research papers in academic journals (see Appendix) and three conference proceedings will facilitate this by encouraging the wider academic community to engage with and contribute to this research area.

Moreover, the research carried out in this thesis has demonstrated the commercial value of monitoring the viscosity of cell broths to detect cell lysis and product loss in fermentation. This has direct value for the startup sponsor company, Procellia Ltd., as it demonstrates the fundamental proof of concept for its technology. Furthermore, the academic publications and conference proceedings resulting from this thesis have provided exposure for Procellia within the bioprocessing community, and give credibility and momentum to the nascent company, for example when forming future academic or commercial partnerships.

The implementation of the methodology developed in this thesis by drug manufacturers, to detect cell lysis and product loss in fermentation, will enable informed decision making about harvesting in fermentation to maximise the product yield. By improving fundamental process understanding, it is possible to monitor critical process parameters, which can ultimately be controlled. The ability to monitor and control processes can improve the speed and efficiency of drug manufacturing process development, which enables novel therapies to be brought to market faster, and therefore patients to receive critical therapies faster. The improved

efficiency also implies that development costs can be reduced, and therefore makes treatments more affordable for patients.

The impact of cell lysis in fermentation on operational efficiency in the downstream process is also poorly understood within the bioprocessing community. Therefore, the work in this thesis also carried out a case study to clearly demonstrate the impact of upstream processing conditions on the downstream process. To solve this problem, several novel primary recovery process designs were proposed and carried out; taking an integrated approach to improve the performance of the whole bioprocess across several dimensions (i.e. total product recovered, purity, solids removal, capital costs, processing time). The novel designs achieved significant improvements in comparison to the existing process, and demonstrated the value of taking such an approach to bioprocess design.

In summary, the expertise, knowledge, methodologies and insight developed as a result of this research will facilitate beneficial impact not only in academia, but also commercially for both the sponsor company Procellia Ltd. and the wider bioprocessing community.

Acknowledgements

I would like to gratefully acknowledge the EPSRC IDTC and Procellia Ltd. for their financial support, as well as University College London for conference awards.

I would like to thank my supervisor Dr Yuhong Zhou. Apart from Yuhong's exceptional guidance and deep expertise in the field, I have, above all else, been continuously inspired by Yuhong's positive energy and enthusiasm for research, and it has been an absolute pleasure for me to work closely with her over the last 4 years.

I would also like to thank my industrial supervisor Dr Joanna Vlahopoulou, who provided a wealth of expertise in rheology and enabled me to obtain an incredibly valuable insight into the commercial side of the biotechnology industry.

Thank you to all my friends and colleagues at UCL. I am extremely grateful to Dr Desmond Schofield, Dr Alex Chatel, Dr Ioannis Voulgaris, Dr Adrian Hill and Professor Mike Hoare for mentoring me over the last 4 years. I would also like to thank Dr Desmond Schofield, Mohd Shawkat Hussain, Dr Alex Chatel, Dr Ioannis Voulgaris, Dr Andrea Rayat and Mark Turmaine for collaborating with me on various research projects.

Thank you to my parents, whose unwavering support has enabled me to keep pushing every barrier that I encounter. Thank you also for taking my phone calls every week for the last 4 years to talk through my *E. coli* problems.

Meine liebe Ariana, kaum ein Wort hier wäre ohne dich möglich gewesen. Danke für deine Geduld, deine Unterstützung, deine Ermutigung und vor allem deine Liebe. Ich verdanke dir alles und dafür ist diese Doktorarbeit dir gewidmet.

Table of contents

9

14

List of figures

List of tables

Nomenclature

$A_{membrane}$	Area of the CFF membrane, m^2
C_{cells}	Concentration of cells, g.DCW L^{-1}
C_{DNA}	Concentration of DNA, g L^{-1}
$C_{NucAc,tot;}$ $C_{NucAc,soluble;}$ $C_{NucAc,solids}$	Concentration of nucleic acids; total, soluble and in the solids fraction, mg/mL
$C_{prod,tot;}$ $C_{prod,soluble;}$ $C_{prod,solids}$	Concentration of product; total, soluble and in the solids fraction, mg/mL
$C_{prod,CFFfeed}$	Concentration of product in the CFF feed, mg/mL
$C_{prod,CFFretentate1}$	Concentration of product in the retentate after CFF in concentration mode, mg/mL
$C_{prod,CFFretentate2}$	Concentration of product in the retentate after CFF in diafiltration mode, mg/mL
$C_{prod,ext}$	Concentration of extracellular product, mg/mL
$C_{prod,int}$	Concentration of intracellular product, mg/mL
C_{prot}	Concentration of protein, g L^{-1}
C_{sol}	Concentration of solids, g L^{-1}
$C_{TotProt,tot;}$ $C_{TotProt,soluble;}$ $C_{TotProt,solids}$	Concentration of total protein; total, soluble and in the solids fraction, mg/mL
CF	Clarification factor, dimensionless
$Clarification_{cent}$	Clarification performance in centrifugation, %
d_{50}	Median particle diameter, μm
D	Number of diavolumes, dimensionless
DW	Dewatering level, %
$Flux_{CFF}$	Flux rate for CFF operation, L m^{-2} h^{-1}
$F_{v,i}$	Volume frequency distribution, where i is the channel number, dimensionless
$G*$	Complex shear modulus, Pa
G'	Loss modulus, Pa
G''	Storage modulus, Pa
g	Gravitational acceleration, m s^{-2}
K	Consistency index, Pa s^n
M_{liq}	Mass of liquid in stream, kg

$M_{NucAc,tot};$ $M_{NucAc,soluble};$ $M_{NucAc,solids}$	Mass of nucleic acids; total, soluble and in the solids fraction, kg
$M_{prod,tot};\ M_{prod,solids};$ $M_{prod,soluble}$	Mass of product; total, soluble and in the solids fraction, kg
$M_{prod,\ ext}$	Mass of extracellular product, kg
$M_{prod,\ int}$	Mass of intracellular product, kg
M_{sol}	Mass of solids in stream, kg
$M_{sol,\ aftext}$	Mass of solids after extraction, kg
$M_{sol,beforeext}$	Mass of solids before extraction, kg
$M_{sol,DFfeed}$	Mass of solids in depth filtration feed, kg
$M_{sol,\ DFpermeate}$	Mass of solids in permeate (depth filtration), kg
$M_{sol,\ feed}$	Mass of solids in feed stream, kg
$M_{sol,\ sed}$	Mass of solids in sediment stream, kg
$M_{sol,\ sup}$	Mass of solids in supernatant stream, kg
M_{tot}	Total mass in stream, kg
$M_{TotProt,tot};$ $M_{TotProt,soluble};$ $M_{TotProt,solids}$	Mass of total protein; total, soluble and in the solids fraction, kg
n	Flow behaviour index
n_p	Degree of polynomial fit
N_i	Stirrer speed, rps
N	Disc speed, rps
OD_f	Optical density of feed, 600 nm
ODs	Optical density of supernatant or permeate, 600 nm
ODw	Optical density of well-clarified sample, 600 nm
OD_x	Optical density measured at x nm
P	Mixing vessel power input, W
Pa	Pascal, Newton/m^2
r	Cone radius, m
rcf	Relative centrifugal force, g
Re	Reynolds number, dimensionless
R_i	Inner radius of centrifuge tube, m
R_o	Outer radius of centrifuge tube, m

rpm	Revolutions per minute
rps	Revolutions per second
S	Solids remaining, %
S_{CFF}	Solids remaining for crossflow filtration unit, %
S_{DF}	Solids remaining for depth filtration unit, %
t_{CFF}	Time for each CFF step, h
T	Temperature, °C
t	Time, seconds
$tan\delta$	Loss tangent, dimensionless
$V_{CFFchamber}$	Volume of the CFF chamber, mL
$V_{CFFpermeate,experimental}$	Volume of the experimentally determined CFF permeate, mL
$V_{CFFretentate}$	Volume of the CFF retentate, L
$V_{Feed,CFF}$	Volume of the CFF feed, L
V_{lab}	Volume of material in centrifuge tube, m^3
$V_{liq,DFpermeate}$	Volume of liquor in the depth filtration permeate, L
$V_{liq, sed}$	Volume of liquor in sediment stream, L
$V_{liq, sup}$	Volume of liquor in supernatant stream, L
V_{max}	Maximum volume of fluid that will pass through filter before blockage, m^3
$V_{sol, sed}$	Volume of solids in sediment stream, L
$V_{sol, sup}$	Volume of solids in supernatant stream, L
V_{tot}	Total volume, L
$V_{tot, sed}$	Total volume in sediment stream, L
$V_{tot, sup}$	Total volume in supernatant stream, L
$V_{tot, DFpermeate}$	Total volume in the depth filtration permeate, L
W_i	Particle size range of channel number i, dimensionless

Greek letters

δ	Phase angle, °
ε	Maximum energy dissipation rate, W kg^{-1}
ε_{ext}	Periplasmic extraction efficiency, %

ΔP	Pressure drop across inlet/outlet of depth filter
η	Shear viscosity, Pa s
η_L	Shear viscosity of the suspending medium, Pa s
η_{DNA}	Shear viscosity of DNA, Pa s
η_{cells}	Shear viscosity of cells, Pa s
η_{prot}	Shear viscosity of protein, Pa s
$\eta_{increase, postinduction}$	Postinduction shear viscosity increase, Pa s
η_0	Shear viscosity at induction point, Pa s
η_t	Shear viscosity at time point of interest, Pa s
ρ	Density, kg m^{-3}
ρ_{sol}	Density of solids debris, kg L^{-1}
λ	Shear strain, dimensionless
ω	Cone or angular speed, rad s^{-1}
θ	Cone angle, °
$\bar{G}$	Mean velocity gradient, s^{-1}
τ	Shear stress, Pa or dynes cm^{-2} or Newton m^{-2}
φ	Volume fraction, dimensionless
Y	Shear rate, s^{-1}
Γ	% full scale torque, dyne cm^{-1} or Newton m^{-1}
$\sum_T$	Equivalent settling area, m^2
σ	Rejection coefficient, dimensionless

Abbreviations

AU	Absorbance units
BOX	Bis-oxonol
BSA	Bovine serum albumin
CER	Carbon evolution rate
CFF	Crossflow filtration
CFU	Colony forming units
C_H, C_L	Constant regions in antibody, heavy and light
CHO	Chinese hamster ovary cells

CPP	Critical process parameter
CQA	Critical quality attribute
dAb	Domain antibody
DCW	Dry cell weight, g L^{-1}
DNA	Deoxyribonucleic acid
dsDNA	Double-stranded DNA
DoE	Design of experiments
DOT	Dissolved oxygen tension, %
DSP	Downstream processing
E. coli	*Escherichia coli*
EDTA	Ethylenediaminetetraacetic acid
Fab'	Antibody fragment or antigen-binding fragment
F_c, F_v	Constant and variable regions in antibody
FDA	Food and Drugs Administration
HPLC	High performance liquid chromatography
Hz, MHz	Hertz, megahertz
Ig	Immunoglobulin
INT	Iodonitrotetrazolium violet
IPTG	Isopropyl β-$_D$-1-thiogalactopyranoside
kDa	Kilodaltons
LDH	Lactate dehydrogenase
LMH	Litres per square metre per hour (L m^{-2} h^{-1})
LMM	Litres per square metre per minute (L m^{-2} min^{-1})
LVER	Linear viscoelastic range
mAb	Monoclonal antibody
MF	Microfiltration
NAD/NAD$^+$/NADH	Nicotinamide adenine dinucleotide
nm	Nanometre (10^{-9} m)
NWP	Normalised water permeability (to 25°C)
OD	Optical density
OUR	Oxygen uptake rate
PAT	Process analytical technology

PBS	Phosphate-buffered saline
PEI	Polyethyleneimine
PI	Propidium iodide
PID	Proportional-integral-derivative
PLS	Partial least squares
PMV	Packed mycelial volume
PSD	Particle size distribution
PPG	Polypropylene glycol
QbD	Quality by design
RNA	Ribonucleic acid
RQ	Respiratory quotient
scFV	Single chain variable fragment
SEM	Scanning electron microscopy
TMP	Transmembrane pressure, bar
UF	Ultrafiltration
USD	Ultra scale-down
USP	Upstream processing
v/v	Volume/volume
w/v	Weight/volume
w/w	Weight/weight
V_H	Heavy chain hypervariable region
V_L	Light chain hypervariable region

Chapter 1   Introduction

Advances in the pharmaceutical industry over the last hundred years, and the subsequent evolution of biotechnology, have impacted almost every aspect of our lives in the 21st century. The biopharmaceutical industry continues to grow at a rapid rate, and in fact, eight out of ten of the best-selling drugs in the world in 2016 were produced using biological methods. Throughout the industry, vast amounts of money are spent on drug discovery and development, with an estimated $1.7 billion and 12 years required to bring a drug to market (Kola, 2008). Moreover, the likelihood of a drug candidate being approved in clinical trials is estimated to be around 12% (DiMasi et al., 2016).

Despite the huge advances in our ability to treat a wide range of diseases using biopharmaceuticals, the cost of drug development and the extremely high risk of failure in clinical trials signify a strong need to improve the drug development process. By improving the efficiency of process development, and developing tools that enable process optimisation and characterisation at an early stage of development, the outcomes of the drug development process and clinical trials can be improved. The implications of such development tools are vast; not only reducing costs for the consumer but also reducing risk by bringing safer, more efficacious drugs to market, as well as improving speed to market.

This project is specifically focused on establishing and developing a novel monitoring methodology to enable process monitoring in biopharmaceutical production, with the aim of detecting cell lysis in fermentation to prevent product loss. The development of this technology has applications in process design, characterisation, optimisation, scale-up and large scale production. The following sections will provide an overview of the production of antibody fragments (Fab') using *E. coli* as a host organism, highlight some of the challenges associated with its production, specifically those associated with cell lysis and discuss recent advances in process monitoring technologies. Finally, the overall aims and objectives of this thesis will be discussed.

1.1 Biologics

Biologics can be defined as large, complex molecules (typically proteins or polypeptides) that are produced by living organisms (such as microbial or mammalian cells) (Morrow and Felcone, 2004). In contrast to chemically-synthesised drugs, biologics are more complicated to produce, harder to characterise, are more challenging to scale up and are much more sensitive to conditions such as temperature and the chemical environment. The real difference, however, between biologics and chemically-synthesised drugs lies in the genetic manipulation of a cell through the use of recombinant DNA technology, which involves isolating and often modifying human DNA before inserting it into a host cell (such as a mammalian cell or a microbial cell), and making the organism express it (i.e. express a product) (Morrow and Felcone, 2004).

The ability to manipulate the genetic information of host organisms has enabled the production of large and complex molecules that were previously not possible to produce by traditional chemical synthesis. In addition, the complexity of these molecules has opened up a vast range of possibilities to treat diseases that were previously untreatable and some examples of biologics include antibodies, vaccines, gene therapies and enzymes. As a result, their use is now widespread and the progress achieved in the last 40 - 50 years has been incredible. The hormone insulin was discovered in 1921 by Banting and Best, however it wasn't until 1982 that the first insulin product was approved by the Food and Drug Administration (FDA) for therapeutic use (Revers and Furczon, 2010), after the discovery of recombinant DNA technology by Boyer and Cohen in 1973 (Cohen et al., 1973). Since then, the huge developments in the industry have led to a wide range of treatments for various cancers (Avasti/bevacizumab, Herceptin/Trastuzumab), arthritis (Humira/Adalimumab, Remicade/Infliximab) and vaccines such as Prevnar (pneumococcal pneumonia) or Gardasil (human papillomavirus).

1.1.1 Antibodies

Antibodies, or immunoglobulins (Ig), are an extremely important class of therapeutics. Antibodies are essentially proteins that can be found in the blood, and

have a vital role in the immune system; antibodies will bind to specific targets (i.e. antigens), for example foreign bodies such as bacteria or viruses. Although knowledge of the immune system dates as far back as ancient Greece, origins of the use of antibodies as a therapy began with the discovery of von Behring and Kitasato in 1890, using small quantities of serum infected with diphtheria or tetanus as a way to pre-treat healthy animals against the respective diseases (von Behring and Kitasato, 1890). In 2016, antibodies accounted for 5 of the top 10 bestselling drugs worldwide, and sales represented around half of all biopharmaceutical revenues in 2013 (Ecker et al., 2015).

A full antibody comprises of 4 polypeptides; two identical heavy-chain and two identical light-chain regions, that form a Y-shape, as shown in Figure 1-1. Full antibodies have an average mass of ~150 kDa and the amino acid sequence at the tip of the "Y" shape is highly variable (as highlighted in Figure 1-1, both the light and heavy chains), and typically comprises of 110-130 amino acids. This variable region gives antibodies their antigen binding specificity i.e. the ability to bind to a specific antigen. Antibodies can be divided into 5 major classes, IgG, IgM, IgA, IgD and IgE; and are split as such based on their constant region structure (which confers the mechanism of antigen binding). As seen in Figure 1-1, the heavy chain region can be further subdivided into four sections; C_{H1}, C_{H2}, C_{H3} and V_H. The V_H region is hypervariable, and the C_H regions are constant. Similarly for the light chains, the V_L region is hypervariable and the C_L region is constant.

1.1.1.1 Antibody fragments

A full length antibody (i.e. ~150 kDa) is a large and intricate molecule, and producing this molecule through biological methods is therefore complex and challenging, for example, requiring the necessary host cell machinery for post-translational modifications. As seen in Figure 1-1, a full length antibody can be cleaved into smaller parts, including antibody fragments (Fab', or antigen-binding fragments), single chain variable fragments (scFv) and third generation variants of such molecules (Nelson and Reichert, 2009). Of these three fragments, Fab' is the most widely researched. In addition, genetic engineering can be employed to build various combinations of the light and heavy chains of the antibody fragment (Better

et al., 1988), in order to affect factors such as affinity, immunogenicity, half-life and effector function (Abuchowski et al., 1977).

Antibody fragments that exhibit antigen-binding properties are a relatively new class of therapeutics entering the market (Nelson and Reichert, 2009). Although the nascent research into Fab' fragments has focused on cancer treatments, none of the three FDA approved fragments (as of 2009; ReoPro (used to prevent cardiac ischemic complications for patients undergoing percutaneous coronary intervention (PCI) treatment for both coronary heart disease and unstable angina, Janssen/Eli Lily), Lucentis (used to treat patients with wet age-related macular degeneration, Roche-Genentech) and Cimzia (used to treat both Crohn's disease and rheomatoid arthritis, UCB)) were for cancer indications (Nelson and Reichert, 2009). As of 2009, a further 19 Fab' fragments were in clinical trials, and their application and interest in therapies has been rapidly growing (although they remain a relatively small percentage of full mAb's).

In comparison to full sized antibodies, Fab' fragments have several advantages and disadvantages. The smaller size of Fab' fragments means that they can be synthesised more easily, require less resources, have lower costs and have a lower burden on the host cell, for example there is no need for glycosylation (Li et al., 2013). Another advantage of Fab' fragments is that their smaller size enables faster and deeper penetration into tissue and tumours (Ward et al., 1989; Jain, 1990; Yokota et al., 1992). It has also been suggested that the smaller size of the fragment means that they can access epitopes that full antibodies cannot reach (Ward et al., 1989).

Additionally, there are a number of challenges with antibody fragments, such as a short half-life in humans (Larson et al., 1983), or undesirable aggregate formation (Bird et al., 1988). However, efforts have been made to alleviate the various challenges (Wörn and Plückthun, 2001), such as developing antibody fragments that are resistant to heat denaturation (Jespers et al., 2004). Therefore, antibody fragments are an interesting and rapidly evolving therapy, which present a unique opportunity for further study.
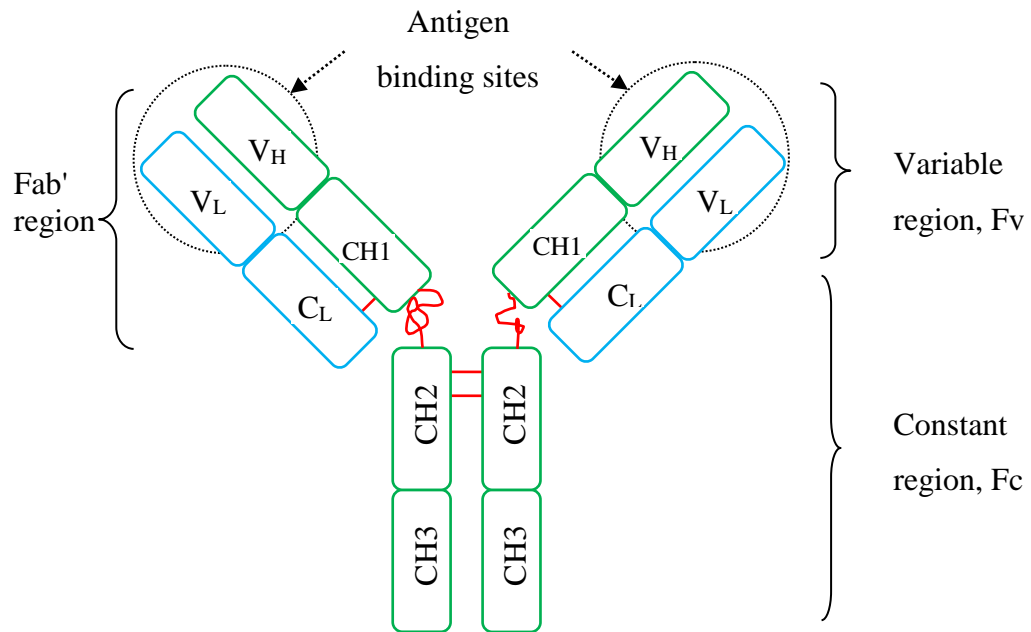
Figure 1-1: Schematic of a general immunoglobulin (Ig) molecule, highlighting the heavy chains in green (V_H, C_{H1}, C_{H2} and C_{H3}), the light chains in blue (V_L and C_L), the Fab' region, the constant region (Fc) and the variable region (Fv). Red lines show disulfide bonds.

1.2 Methods of production and challenges

There are a range of host cells available for recombinant protein expression. Although full length antibodies are typically produced in mammalian cells, such as chinese hamster ovary cells (CHO cells), the smaller size of the Fab' fragments means that they can be produced in microbial host cells, such as *E. coli*. Each host cell has advantages and disadvantages, and a selection of commonly used hosts will briefly be discussed in this section. Other host cells not covered here, but gaining increasing importance in nascent biopharmaceutical research include insect cells and plant cells.

1.2.1 Recombinant protein expression

In order to achieve recombinant protein expression, the host cell is genetically modified by inserting a plasmid into the cell. A detailed review of the transformation procedure is not in the scope of this review, however it is a well established and robust technique. To briefly summarise; a plasmid is a segment of DNA, separated from chromosomal DNA and capable of replicating autonomously within the nucleus of the host cell. The plasmid usually includes the coding for antibiotic resistance, as well as the coding for the required sequence of amino acids, which enables production of the protein of interest.

1.2.2 Host cells

1.2.2.1 Eukaryotic hosts

Eukaryotes such as yeast or mammalian cells have a more complicated genetic structure, which has the advantage that they can carry out post-translational modifications, can secrete proteins outside of the cell, can carry out advanced folding and can produce full length antibodies (Frenzel et al., 2013).

Some common microbial eukaryotic hosts include filamentous fungi, such as *Aspergillus* which has the ability to secrete Fab' fragments and antibody fusion proteins to the medium (Joosten et al., 2003), and can achieve high product titres, for example yields of up to 1.2 g/L IgG with *Aspergillus niger* (Ward et al., 2004).

Pichia pastoris is the principally used yeast host cell, and its main advantage is the extremely high cell densities achievable in fermentation (Jeong et al., 2011). In addition, its growth rate and induction can be controlled via methanol feeding and it can secrete recombinant proteins into the medium. However, yields of Fab' in *P. pastoris* achieved only up to 0.5 g/L in bioreactor fermentation (Gasser et al., 2006), and issues can arise in yeast expression in general, such as proteolysis during high cell density fermentation (Frenzel et al., 2013), or non-homologous recombination (Spadiut et al., 2014).

CHO cells are the most commonly used host cell across the biopharmaceutical industry, accounting for 60-70% of all processes and represented 95% of all approved therapeutic antibody production in 2013 (Frenzel et al., 2013). The significant advantage of CHO cells is their ability to fold, secrete and carry out post-translational modifications for complex, full length antibodies, as well as achieve high product titres, currently in the 1-10 g/L range. However, there are relatively high costs associated with CHO cell production and cell culture takes up to 3 weeks (in comparison to microbial fermentation which would typically last up to 1 week), as the growth rate of CHO cells is slow.

1.2.2.2 Prokaryotic hosts

There are several prokaryotic hosts that are used to produce recombinant proteins, including both gram-negative (*E. coli, Pseudomonas putidas*) and gram-positive (*Bacillus subtilis, Bacillus brevis and Lactobacillus paracasei)* bacteria. However, as *E. coli* is so prevalent in the biopharmaceutical industry, this section will focus solely on its use.

1.2.2.2.1 *Escherichia coli* as a host cell

E. coli is a gram-negative, rod-shaped bacteria, that is facultatively anaerobic and has typical dimensions around 2 μm in length and 0.5 - 1 μm diameter. Under optimum conditions, *E. coli* will double every 20 minutes in exponential phase (i.e. it will outgrow any other orgamism). The *E. coli* K12 strain (used in the research presented in this thesis) is one of the most widely studied strains of *E. coli*, largely because of

its debilitated state that does not usually affect the human colon, making it safer to use for industrial scale applications.

E. coli is heavily used as a microbial host to express recombinant proteins such as Fab', as glycosylation is not needed (Nelson and Reichert, 2009; Li et al., 2013), it has well-characterised genetic properties and has lower associated production costs than mammalian cells or other expression systems, for example it can be grown using inexpensive, chemically-defined media (Spadiut et al., 2014). *E. coli* was first used to successfully express antibody fragments in 1988 (Better et al., 1988), and is now classed as the most important expression system for recombinant protein production (Frenzel et al., 2013), achieving yields in the gram per litre range (Schmidt, 2004), including when using novel extracellular secretion methods (Ni and Chen, 2009). Advances in genetic engineering technology have led to high cell density fermentations, which has also significantly increased the achievable product titre (Kleman and Strohl, 1994; Riesenberg and Guthke, 1999; Shiloach and Fass, 2005). *E. coli* can also be used to produce a range of other recombinant proteins such as scFv fragments at high yields (1.2 g/L) (Sletta et al., 2004).

1.2.2.2.1.1 Periplasm

The periplasm is a concentrated gel-like matrix in the space between the inner cytoplasmic membrane and the bacterial outer membrane (Spadiut et al., 2014). *E. coli* produce Fab' fragments in the cytoplasm, that can be routinely targeted to the periplasmic space. This is important because the oxidising conditions in the periplasm enable correct folding and formation of disulfide bonds (Better et al., 1988; Skerra and Plückthun, 1988) and secretion to the periplasm also minimises formation of inclusion bodies, which can be a significant problem for *E. coli* production. The secretion to the periplasm presents a large advantage for *E. coli* as a host, in comparison to other microbial systems.

1.2.3   Bioprocessing challenges

The bioprocess as a whole comprises many steps involving either the production (upstream) or the recovery (downstream) of a therapeutic product. The upstream

process and downstream process are closely related, and the conditions set in the upstream process can significantly impact the downstream efficiency. However, many unit operations are currently considered in isolation, which is detrimental to the overall objective to optimise the total yield across the bioprocess (typically a trade-off is involved). Some of the upstream factors that impact the efficiency and costs of the downstream process include the product titre in the fermentation broth, solids concentration, the level of contaminants and the viscosity. Furthermore, characterising and understanding the behaviour of the process material when scaling up from the lab to industrial scale presents a significant challenge, and effective scale-up is essential to drive improvements in the efficiency of the development process.

The industry has seen rapid advances in the upstream process in recent years, and above all, this has been driven by the developments in synthetic biology, which have led to our ability to treat an increasing number of diseases, as well as advances such as achieving high cell density fermentation and reaching higher and higher product titres. However, these improvements also increase the complexity and challenges in the fermentation process, for example achieving sufficient mass and oxygen transfer due to the high cell density fermentation broth.

As such, the bioprocess still has many challenges to overcome, particularly relating to meeting the demands of the diverse and constantly evolving range of therapies that are required to be produced. Therefore, there remains a need for the rapid and efficient development of novel therapies, in order to bring these therapies to market as quickly as possible (the pharmaceutical industry has notoriously long development times), and according to regulatory standards. This means that there is a strong need to both improve our understanding of the bioprocess from a holistic perspective, as well as develop novel technologies that will facilitate rapid characterisation, optimisation and scale-up.

1.3   Cell lysis

Cell lysis is one of many significant challenges in the bioprocess and occurs in the late stage of the fermentation process and is difficult to both define and to detect its

47

onset. As highlighted in the previous section, process conditions in fermentation can have a significant impact on the efficiency of many downstream unit operations. This section will highlight some of the key challenges relating to cell lysis in fermentation, and provide an overview of the impact of lysis on downstream processing.

1.3.1   Defining cell lysis and cell viability

The definitions of cell lysis and cell viability differ. Cell lysis is defined as the release of DNA from a cell due to the total disruption of the cell membrane. However, cell viability relates to the intactness of the cell membrane, i.e. if the cell membrane is non-intact, intracellular content may leak from the cell through porous membrane channels. It is believed that cells with non-intact membranes, i.e. leaking product or other intracellular content, may have the potential to recover if transferred to fresh media. However if DNA is lost from the cell, the cell can be classed as dead.

1.3.2   Understanding cell lysis

Bacterial cell death is often observed in the late stage of the fermentation process. Understanding this phenomenon has significance both scientifically and commercially; deeper process understanding enables higher quality manufacturing processes to be built, for example by identifying key parameters to be monitored and controlled (Food and Drug Administration, 2004). Traditionally, cell lysis is considered to be a consequence of "unbalanced growth" at the end stage of the bacterial life cycle (i.e. one or more essential nutrients in the media are at a sub-optimal concentration). However, despite the numerous studies on autolysis, our knowledge is still limited. In addition, cell lysis can be extremely detrimental to a process. For example, for processes where the host cell produces and stores the product intracellularly, product loss can occur at the point of lysis. The release of intracellular content at the point of lysis not only affects the product yield, however can also impact downstream unit operations, as well as the robustness of the process (i.e. the sensitivity of the unit operations to variations in the process material).

Lysis phenomena in microbial fermentations may be influenced by a variety of different factors, including:

- Environmental conditions in the fermenter such as shear stress, osmotic imbalance or poor mass and oxygen transfer;
- Toxic waste product build-up in the cell broth;
- A lack of nutrients available in the media;
- Metabolic burden from excessive recombinant protein expression;
- Internal stresses from a build-up of product in the periplasm or cytoplasm.

There is a metabolic burden associated with recombinant protein expression, which typically has a high energy requirement (Sørensen and Mortensen, 2005), and the growth rate and productivity of cells are subsequently impacted when a plasmid is inserted into the cell. The metabolic burden can be defined as the amount of resources (raw material and energy) that are withdrawn from the host metabolism for maintenance and expression of the foreign DNA (Bentley and Kompala, 1990). The metabolic burden occurs for several reasons, for example the additional strain placed on the host cell by plasmid replication, rDNA transcription and plasmid-encoded mRNA translation (Bentley et al., 1990), as well as changes in metabolic fluxes, enzyme composition and drainage of precursors (Hoffman and Rinas, 2004).

E. coli produce Fab' fragments that can be routinely targeted to the periplasmic space. However, the capacity of the periplasm is limited, for example Fab' fragments will leak when exceeding 6% of the volume of the periplasm (Schofield et al., 2016). During fermentation, as the limit of the periplasm is reached, cells begin to lose viability and leak the Fab' product and other intracellular content to the fermentation broth.

As discussed in section 1.2.2.2.1, high cell density fermentation has led to increasing product titres, however this has created additional challenges such as mass and oxygen transfer in the fermenter (Kleman and Strohl, 1994; Riesenberg and Guthke, 1999; Shiloach and Fass, 2005). As cell lysis occurs in fermentation, mass transfer

will reduce further, due to the release of intracellular content which interferes with mass transfer in the cell broth. In response to this, the fermenter control system will increase the agitation and oxygen feeding in order to maintain the appropriate dissolved oxygen tension in the media.

In addition, as the cell population ages and the fermentation progresses, cells in the fermenter become weaker (Perez-Pardo et al., 2011) and the shear stresses from the high agitation and aeration rates (i.e. particularly at gas-liquid interfaces) can exacerbate cell lysis. Furthermore, as the fermentation progresses, toxic waste product builds up in the cell broth, which can worsen the conditions for the cells, and the nutrient content (e.g. salts or the nitrogen source) in the media continually diminishes over time.

These phenomena all act simultaneously to cause the rapid onset of cell lysis in late stage fermentation. For large scale bioreactors, heterogeneity poses additional challenges with the availability of dissolved oxygen in the media, availability of nutrients in the media and the presence of carbon dioxide (carbon dioxide can stimulate lactate formation, which subsequently reduces productivity in the bioreactor) (Chen et al., 1992).

1.3.3   Impact of cell lysis on the downstream process

Apart from product loss in late stage fermentation, cell lysis has adverse consequences on the efficiency of subsequent downstream processing steps including homogenisation, microfiltration and centrifugation, and therefore a trade-off exists between harvest time and total product yield (Ambler, 1961; Okamoto et al., 2001; Meireles et al., 2003; Chan et al., 2006; Balasundaram et al., 2009; Nesbeth et al., 2011; Perez-Pardo et al., 2011; Aucamp et al., 2014). For example, the remaining viable cells at harvest point will become more fragile and break four-fold more than those harvested at an earlier stage, if subjected to the equivalent shear level of that in an industrial centrifuge (Perez-Pardo et al., 2011).

As cell lysis occurs in late stage fermentation, leakage of product to the fermentation broth also acts to increase the broth viscosity, as large quantities of chromosomal

DNA and other intracellular content are released simultaneously into the broth (Balasundaram et al., 2009; Nesbeth et al., 2011). High viscosity broths cause additional complications downstream. For example, clarification efficiency in centrifugation is inversely proportional to the viscosity (Ambler, 1961) and studies have previously been carried out investigating the effects of bacterial cell culture age on microfiltration performance (Okamoto et al., 2001; Meireles et al., 2003), showing that release of intracellular material (such as DNA) due to cell death was found to increase fouling and resistance, hence reducing process performance.

In summary, cell lysis and product loss in late stage fermentation can dramatically reduce the overall product yield of the bioprocess. In addition, the release of intracellular content such as nucleic acids and host cell protein significantly affect the performance of subsequent downstream unit operations. Although many studies have been carried out on this, our knowledge is limited, particularly relating to understanding the changes in physical properties of fermentation broths during lysis, and the impact on the bioprocess. Furthermore, due to both the complexity and a lack of understanding, there is a limited ability to directly monitor the onset of cell lysis in fermentation.

1.4   Bioprocess monitoring technologies

Having highlighted some of the key issues associated with cell lysis in fermentation and our limited ability to detect and monitor lysis, this section will discuss the aims of process monitoring technologies in the biopharmaceutical industry, provide an overview of commonly used monitoring technologies in upstream production and outline the key challenges.

1.4.1   Process analytical technologies

Process analytical technologies (PAT) are highly desired in the biotechnology industry to aid bioprocess development, monitoring and control (Chew and Sharratt, 2010; Glassey et al., 2011), and are particularly important for the implementation of quality-by-design (QbD) initiatives (Read et al., 2009). This initiative has been strongly promoted by the FDA since 2002 (Beutel and Henkel, 2011), which brings

together process analysis, process knowledge and modelling to create a "built-in" quality process (Biechele et al., 2015), by identifying, monitoring and ultimately enabling process control of critical parameters.

The overall aim of the FDA's PAT initiative is to support the innovation and efficiency of bioprocess development, manufacturing and quality assurance across the industry (Food and Drug Administration, 2004). Building quality into a process (i.e. QbD), rather than testing quality in a product enables a more efficient process, however requires a deep level of process understanding (Food and Drug Administration, 2004). Therefore, before an analytical technology can be built to monitor and control a critical process parameter (CPP) or critical quality attribute (CQA) in the bioprocess, the parameter must first be identified, understood and characterised.

Critical process parameters are therefore key operating variables that influence the production process and some examples in fermentation include cell density, cell viability, pH, temperature and dissolved oxygen tension. There are also separate aims concerning CPP's in the fermentation process. Firstly, some parameters have a direct influence on the host organism, for example the dissolved oxygen tension in the media will affect the growth and viability of the cells. Secondly, some parameters are critical because they affect the biological activity of the product, such as temperature or pH (Ozturk and Hu, 2004).

Therefore, different process monitoring technologies will focus on different applications, and the majority of these technologies are focused on either monitoring biomass growth or cell viability in fermentation. Bioprocess variables can include physical variables (temperature, foam, viscosity, pressure), chemical variables (oxygen, carbon dioxide, metabolites, substrates) or biological variables (biomass, cell morphology, cell metabolism) (Biechele et al., 2015).

1.4.2   Challenges with developing monitoring technologies in fermentation

Fermentation broths are complex and diverse, and can comprise a whole host of material capable of interfering with the desired monitoring or control strategies.

52

Typical suspensions may include cells, a carbon source, a nitrogen source, gas bubbles (oxygen, carbon dioxide), micronutrients, the product, the aqueous phase and often intracellular content from autolysed cells. This complexity can make it difficult to achieve the desired sensitivities and specificities of the analytical instrument, and the problem is further exacerbated when cell autolysis takes place as the intracellular content such as host cell protein and nucleic acids can interfere with chemical-based, biological-based and physical-based measurements.

The development of in-line process monitoring technologies presents the need for sterilisation, including stability of the analytical instrument at high temperatures. For offline or at-line technologies, the key issue is contamination when sampling (Beutel and Henkel, 2011). For spectroscopic applications in general, which comprise a significant proportion of the most promising PAT applications, calibration is a significant issue. This is important as fermentations can last for several weeks, and once started, it is not possible to recalibrate the instrument. The configuration of PAT when applied to disposable technologies must also be considered (Beutel and Henkel, 2011).

Technologies to monitor cell growth are widespread and well developed. However, monitoring cell viability or lysis remains a key challenge, and is particularly important for processes with host cells that store the product in the periplasmic space (or intracellularly), as product loss due to leakage occurs at the point of lysis. However, lysis is difficult to observe directly in fermentation because of its inherent complexity, and current analytical technologies are unable to rapidly and accurately monitor the shift between optimal intracellular product concentration and leakage to the fermentation broth. Current industrial processes typically focus on solving this problem by monitoring cell density, product titres, product leakage and cell viability offline to determine harvesting time (Bowering, 2004; Perez-Pardo et al., 2011).

1.4.3   Process monitoring strategies

An in-line monitoring technology can be defined as a sensor that operates within the bioreactor system. An at-line sensor operates outside of the bioreactor and sampling is necessary (Biechele et al., 2015). Ex-situ monitoring technologies are able to

monitor online whilst avoiding contamination and sterilisation issues as they are situated on the outside of the bioreactor, however measurements at the bioreactor wall may not be representative of the cell population due to axial variations and dead-zones, particularly for large scale production. Flow-through cells are able to avoid issues such as signal interference from the highly agitated and aerated environment within the bioreactor, and can be multiplexed, however sterility becomes an issue and more importantly, samples may not be representative of the cell population in the bioreactor. Offline sampling is not ideal as it is typically carried out after a fermentation, which is inefficient, unreliable and time consuming. Most importantly, it removes the possibility to make decisions in real-time.

1.4.4 Common bioprocess monitoring technologies

This section will provide an overview of some of the most commonly used monitoring technologies in upstream processing and highlight some of the key advantages and challenges with each technique.

1.4.4.1 Routine fermenter monitoring and control

Online monitoring and control technologies routinely used in biopharmaceutical fermentation include temperature (T), dissolved oxygen tension (DOT) and pH. Frequently, foaming in the fermenter headspace is controlled via addition of antifoam (e.g. a surfactant such as polypropylene glycol, PPG). These parameters are controlled to ensure optimal growth of the cell population. A PID (proportional-integral-derivative) controller is applied to each parameter.

1.4.4.2 Offline analytical technologies

There are several technologies that are used to monitor fermentation broths offline. A method that is frequently coupled with optical density measurements to measure biomass growth is the measurement of wet cell weight and dry cell weight. Wet cell weight is typically unreliable due to the variation in water content in a sample (i.e. it is limited by the efficiency of centrifugation and subsequent manual removal of supernatant from an Eppendorf tube). However, dry cell weight is a robust

measurement although sample preparation is time consuming as the sample must be dried in an oven overnight.

Flow cytometry is regularly employed to monitor cell viability offline in fermentation; however it requires a lengthy and complicated staining procedure that also requires post-measurement data analysis. In fact, all cell-based monitoring techniques can only detect existing cells and are unable to measure the lysed cells, making it infeasible to monitor the extent of cell lysis effectively.

However, the intracellular content from lysed cells will still remain in the bioreactors. Thus, measuring the protein or DNA leakage can give an indication of cell lysis. DNA analysis, using assays such as Picogreen™ or spectrophotometric absorption devices such as the NanoDrop™ offer another option to monitor cell lysis in fermentation. However, Picogreen™ assay requires a comparatively complicated protocol and is time-consuming, and proteins can interfere in NanoDrop™ measurements as they are absorbed at the same wavelength as nucleic acids (Neves et al., 2000). In general, techniques for DNA analysis are susceptible to errors from losses due to degradation of DNA or from losses in sample preparation steps such as centrifugation (Neves et al., 2000). Lactate dehydrogenase (LDH), a stable cytosolic enzyme is also used in microbial and mammalian cultures to detect cell viability, however the assay is also offline and relatively time-consuming. In addition, HPLC is commonly used to monitor product leakage to the cell broth. HPLC is able to accurately quantify the product in the broth, however is time-consuming due to set up and sample preparation steps (e.g. centrifugation).

1.4.4.3 Electrochemical sensors

Electrochemical sensors are based on the principle that chemical reactions undergo changes in electrical properties due to charge transport, such as potential, charge or current changes. There are three broad classes of electrochemical sensors; potentiometric (measures the potential difference between two electrodes), conductometric (measures conductance), and voltametric (measures current by varying the potential and determining differences based on charge transport) (Beutel

and Henkel, 2011). Standard electrochemical sensors in fermentation include dissolved oxygen and pH sensors (as described in section 1.4.4.1).

1.4.4.3.1 Capacitance sensors

Dielectric spectroscopy (also called electrochemical impedance spectroscopy) is able to measure the number of viable cells in a cell suspension. Dielectric spectroscopy works by applying an alternating electric field to the sample (Zhao et al., 2015) and measuring the resulting capacitance.

The plasma membranes of cells are non-conductive, however can hold charge. Therefore, intact plasma membranes will hold charge when an electric field is applied, enabling the capacitance to be measured (i.e. the measured difference between the detected amplitude or frequency when the electric field is reversed) (Justice et al., 2011). The capacitance is therefore proportional to the total number of intact cells in the culture. Cells that have lysed or are leaking intracellular content, i.e. cells with non-intact plasma membranes, have a negligible contribution to capacitance, so capacitance measurements can be used to give an indication of viable biomass in the culture. The units of capacitance are farads (SI units) or picofarads. This is quoted as pF/cm for cell suspensions and can be converted to viable cells/mL, grams per litre, or packed mycelial volume (PMV) with the appropriate correlation (specific to the species). The capacitance can also be calibrated to offline data such as flow cytometry.

One of the most promising in-line monitoring technologies in fermentation is the Aber Instruments Futura biomass probe (Aber Instruments Ltd, Aberystwyth, UK), which gained initial popularity due to its success in the brewing industry. This has now been used not only in brewing, but also extensively in biopharmaceutical production including for yeast fermentation (Fehrenbach et al., 1992; Xiong et al., 2008; Chopda et al., 2016), *E. coli* fermentation (Franz et al., 2005; Kaiser et al., 2008) and mammalian cell culture (Justice et al., 2011; Lee et al., 2015). Furthermore, this has recently included integration with control systems, for example for online feedback on the specific growth rate to control glucose addition in fed-batch glutathione production with *Saccharomyces cerevisiae* (Xiong et al., 2015).

Capacitance probes have been widely researched and have been shown to be able to monitor the viable biomass and specific growth rate in a range of fermentations. However, capacitance measurements tend to perform poorly in late stage fermentation, often missing the onset of cell lysis; this is because non-viable cells will still hold a certain amount of charge and exhibit some form of capacitance (Sarra et al., 1996; Neves et al., 2000). Therefore, although the technology is incredibly useful in the early growth stages of fermentation, for the purpose of monitoring cell lysis, product loss and viability, its use is limited.

1.4.4.4   Spectroscopic monitoring technologies

Spectroscopy is the study of the interaction between electromagnetic radiation and matter, and is one of the most advanced and powerful analytical tools available to investigate chemical samples.

1.4.4.4.1   Optical density measurements

Optical density (OD) is commonly used to measure biomass growth in fermentation and some of its benefits include rapid and robust analysis. Optical density is typically measured offline; spectrophotometers are widely available in research labs and are relatively cheap. In fact, optical density measurements are considered to be a benchmark in the industry for monitoring biomass concentration (Biechele et al., 2015).

Several in-situ, online optical density probes have been developed for application in fermentation and are commercially available (Wu et al., 1994; Kiviharju et al., 2008) and can be based on transmission, absorption, reflection or light scattering (Vojinovic et al., 2006; Mandenius and Titchener-Hooker, 2013). In addition, an in-situ, steam sterilisable optical density probe has previously been developed for microbioreactors (in the microlitre range) (Zanzotto et al., 2004). However, in-line optical density measurements are often highly susceptible to interference from agitation and aeration in the bioreactor.

Moreover, although optical density measurements provide a good representation of cell growth in bioreactors, OD gives an indication of the total biomass obscuring the light path, which offers no insight into the viable biomass (a highly desirable parameter to monitor in fermentation) (Hewitt and Nebe-Von-Caron, 2004). This means that OD measurements systematically underestimate cell lysis in late stage fermentation and miss the critical point of product leakage in fermentation; causing issues with determining the optimal harvest time.

1.4.4.4.2 Near-infrared spectroscopy

In-situ infrared spectroscopic monitoring probes are available on the market and have been extensively studied (Doak and Phillips, 1999; Arnold et al., 2002; Navratil et al., 2005; Vojinovic et al., 2006; Kiviharju et al., 2008). Due to its high specificity, infrared spectroscopic applications are capable of monitoring the chemical properties of fermentation broths, including biomass, glucose and protein concentration. Most infrared spectroscopy-based research for the purpose of bioprocess monitoring has focused on near-infrared spectroscopy, as near-infrared requires no sample preparation and its spectra are not affected by the absorption of water (whereas these are the greatest challenges for mid-infrared spectroscopy). In fact, it can be argued that near-infrared spectroscopy has shown the most promising results of the available fermentation monitoring technologies; delivering highly specific insight into the chemical properties of complex cell broths, particularly when used in combination with advanced multivariate statistical analysis (such as principal component analysis or partial least squares regression) (Tosi et al., 2003; Crowley et al., 2005; Finn et al., 2006).

Near-infrared spectroscopy is a rapid, non-destructive and non-invasive spectroscopic technique that uses infrared light in the 800 - 2500 nm wavelength region of the electromagnetic spectrum. One of the main benefits is its high chemical specificity that enables differentiation of molecules based on chemical content, due to the uniqueness of the absorption of infrared light by molecular vibrations at different wavelengths for different chemical bonds. Fundamental absorptions of infrared light occur in the mid-infrared region, however, overtones and combinations

of bands are perceptible within the near-infrared region, which can present specific information about the analyte.

The use of at-line, near-infrared spectroscopy has been demonstrated in high cell density *Saccharomyces cerevisiae* fermentation (Finn et al., 2006) to quantify biomass, ethanol and glucose concentration; in high cell density *Pichia pastoris* fermentation to measure biomass, product, glycerol and methanol (Crowley et al., 2005); in a CHO cell culture producing a monoclonal antibody (mAb) to define batch trajectories and implement control strategies such as adjusting the feeding rate (Hakemeyer et al., 2012); in high cell density *E. coli* fermentation to monitor biomass, acetate, ammonia and glycerol concentration (Hall et al., 1996); and Sartorius have developed an ex-situ, flow-through cell (*BioPAT® Spectro,* Sartorius AG, Göttingen, Germany) to monitor cell growth, viability and various analytes in mammalian cell culture, which has a "golden batch modelling" feature, to inform the operator about deviations from the optimal growth trajectory (Sandor et al., 2013). For the latter study, cell viability was able to be predicted between 28-100% with a standard error of 4.2%, using principal component analysis with no pre-processing of data.

However, it was also shown that near-infrared was not capable of discriminating between three different types of bacterial strains, demonstrating its poor applicability for low biomass concentrations in biological systems, or to detect contamination in the batch (Tosi et al., 2003). In addition, infrared spectroscopic techniques have a high cost and have issues with calibration, which is challenging when fermentations can run for 7-14 days (Harms et al., 2002). Although the available technologies are able to measure the carbon source, product and biomass concentrations, fermentation broths are extremely complex and infrared spectroscopy can have problems with sensitivity when analysing molecules at low concentration, such as protein products or substrates such as glycerol or glucose.

1.4.4.4.3 Fluorometry

Fluorescence-based spectroscopic sensors are widely used for both research and industrial applications, and offer several benefits such as the ability to monitor in-situ

and online (Beutel and Henkel, 2011). Fluorometry enables the determination of protein content for various applications (Shibasaki et al., 2001), and can also be used for biomass estimation in fermentation as fluorophores are present inside cells (Zabriskie and Humphrey, 1978). The use of a commercially available technology, the *BioView™* fluorescence spectrometer (DELTA Lights & Optics, Hørsholm, Denmark) using 2-dimensional fluorescence spectrocopy has been demonstrated with *Saccharomyces cerevisiae* to monitor changes in fluorophores such as tryptophan and NADH in real-time, and the different growth phases of fermentation could be recognised by combining the online data with principal component analysis (Assawajaruwan et al., 2017), as NADH is a marker for cell viability. The successful application of fluorometry has also been demonstrated in CHO cell culture and fungi cultivation (*Claviceps purpurea*) (Boehl et al., 2001).

In addition, combining fluorometry with chemometrics has been shown to enable indirect estimation of non-fluorescent material such as nitrates and succinates (Ulber et al., 2003). However, a significant challenge with fluorometry is that complex spectra are obtained, with overlapping peaks (i.e. fluorophore interactions are present) that make it difficult to interpret results accurately. This requires complex, computationally intensive multivariate statistical analysis that is difficult to implement (Beutel and Henkel, 2011).

1.4.4.4.4 UV/Vis spectroscopy

UV/Vis spectroscopy is based on the excitation of electrons using ultraviolet light and visible light, in the range of 10-740 nm. UV/Vis spectroscopy is based on the excitation of unsaturated bonds (Pons et al., 2004). The application of UV/Vis spectrophotometers has the same benefits as for optical density measurements (for *E. coli*, OD is typically measured at 600 nm), i.e. they are robust, cheap and widely available (Beutel and Henkel, 2011). However, measurement of optical density is carried out for the purpose of biomass monitoring, whereas UV/Vis spectroscopy here refers to the analysis of proteins, analytes and substrates, such as product quantification. For example, antibody fragments (Fab'), the product investigated in this thesis, is analysed at 220 nm (protein is often analysed between 220 - 280 nm).

A charged coupling device (CCD) (using an at-line UV/Vis spectrophotometer) has previously been developed for bioprocess monitoring, to detect and measure both RNA and protein (BSA) continuously (Noui et al., 2002) in combination with partial least squares (PLS). This was demonstrated using *Saccharomyces cerevisiae* homogenate. However, as for all spectroscopic applications, the challenge lies in appropriate calibration procedures (using chemometrics) and data treatment (Biechele et al., 2015). Although this technology appears promising, there are few published examples available related to fermentation monitoring, and it is not widely in use in the industry (Biechele et al., 2015).

1.4.4.4.5 Raman spectroscopy

Raman spectroscopy is similar to infrared spectroscopy, in that it is a form of vibrational spectroscopy. However, Raman spectroscopy is concerned with the scattering of light and infrared spectroscopy is concerned with the absorption of light. Several analytes can be measured simultaneously in bioprocesses, including glucose, acetate and lactate in *E. coli* fermentation (Lee et al., 2004; Beutel and Henkel, 2011; Biechele et al., 2015). Raman spectroscopy is susceptible to light scattering, however it has been shown that this can be corrected (Lee et al., 2004).

The greatest challenge with Raman applications in bioprocessing is the strong fluorescence activity of many biological samples, which can overlay and significantly interfere with the Raman scattering bonds (Becker et al., 2007; Biechele et al., 2015). The future of Raman spectroscopy lies in the ability to resolve this issue, in order to enable its application in a wider range of bioprocesses (Becker et al., 2007).

1.4.4.4.6 In-situ microscopy

In-situ microscopy is a technique based on the light microscope, developed since 1995 (Suhr et al., 1995), and allows online, non-invasive imaging of cell cultures in bioreactors to determine cell density, cell size distribution and morphology (Biechele et al., 2015). The analysis can also be automated using image-processing algorithms. Visualisation of cell cultures in real-time is an extremely useful tool, however may

61

have limitations in the accuracy of its haemocytometer-style cell counting. Online, automated monitoring of cell viability is not possible with this method, as non-viable cells cannot be visually distinguished from viable cells in the bioreactor.

1.4.4.5   Off-gas analysis

Online mass spectrometry is frequently employed for off-gas analysis in fermentation, using a quadrupole mass spectrometer (Coppella and Dhurjati, 1987). This can be used to monitor both carbon dioxide evolution rate (CER), oxygen uptake rate (OUR) and hence determine the respiratory quotient (RQ), which give a strong indication of a cell's metabolic activity. From these measurements, it is possible to determine the specific growth rate of the cells. In some cases, infrared spectroscopy is used to monitor off-gas, for example carbon dioxide in the AMBR bioreactor system (Sartorius AG, Göttingen, Germany). Mass spectrometry has also been used in *E. coli* fermentation to control the rate of nutrient feeding, as the CER is roughly proportional to the rate of consumption of the carbon source (Lee, 1996). Although a mass spectrometer is expensive, it can be multiplexed to reduce the cost per fermentation, and has gained widespread acceptance in the biofuels area, due to its ability to also detect simple alcohols such as ethanol (McNeil et al., 2013). However, there are some challenges with its use, for example in *P. pastoris* fermentation, methanol (carbon source) has the same molecular mass as oxygen, which can affect the accuracy of OUR determination (even when a filter is applied to remove the methanol from the mass spectrometer feed).

1.4.5   Summary of process monitoring technologies

In summary, process analytical technologies are highly desired in the biopharmaceutical industry. There are some very interesting monitoring technologies in development or that are already commercially available, and significant advances have been made in the field in recent years. The available technologies can monitor a range of chemical, physical and biological properties, such as biomass concentration, viable biomass concentration, carbon source concentration, product concentration or markers of cell lysis such as lactate formation or product leakage. However, many of the technologies are limited in their accuracy, cost, incompatibility with sterilisation

procedures, complexity or even the expertise required for analysis and data interpretation. In addition, there are few technologies available that are able to monitor the physical properties of a cell broth, in particular to provide useful information regarding cell health. The future of PAT lies in the further development of some of the most promising technologies, and their subsequent integration into a single bioreactor platform, in order to obtain a comprehensive picture of the bioprocess, for example by monitoring the physical, biological and chemical properties of a cell broth. This will facilitate a deeper, holistic understanding of the process, enable process control and therefore further automation in the industry.

1.5 Rheology

Rheology can be defined as the study of the deformation and flow of matter, which can be divided into two types of physical properties; viscosity and viscoelasticity.

Viscosity relates to the internal friction of a fluid and is a measure of its resistance to flow, and therefore provides a way to quantify a materials' resistance to flow. However, not all materials behave as pure solids or pure liquids. In fact, most materials exhibit some form of both types of property, and these materials can be classed as viscoelastic. Therefore, viscoelasticity describes both the solid-like (elastic) and liquid-like (viscous) characteristics of a material undergoing deformation (which can be temporary or permanent). Essentially, viscoelasticity can help to classify and quantify the properties of the internal structure and strength of a material.

Rheology is frequently used to characterise materials in the processing industry, from oil and gas (e.g. in exploration and drilling) to cosmetics such as toothpaste and hand cream. In the biopharmaceutical industry, rheology is typically used in formulation for therapeutics.

This section will discuss the theory, development and use of rheology within the context of bioprocessing, with a particular focus on monitoring in fermentation.

1.5.1 Rheology definitions

For all rheological testing, a "shear" is applied to a sample. This can be seen in Figure 1-2, where a sample is placed between the upper and lower plates of a rheometer, and the upper plate applies shear (lower plate is fixed). For viscosity testing, this shear force, *f*, is a constant shear rate, and for viscoelastic testing an oscillation is applied, or strain rate (which oscillates at a defined frequency and strain amplitude). Figure 1-3 illustrates the terms required to define shear. Rheology involves some standard variables, such as shear stress, shear strain and shear rate, which can be described mathematically, in order to develop a picture of rheology (in combination with Figure 1-3). Therefore, shear stress can be defined as:

$$Shear\ stress\ =\ \frac{Shear\ force}{Surface\ area} \qquad \textbf{Equation 1-1}$$

where shear stress is in units of pascal (Pa), shear force is in units of Newtons (N) and surface area is in units of m^2.

Shear strain can be defined as:

$$Shear\ strain\ =\ \frac{Displacement}{Height} \qquad \textbf{Equation 1-2}$$

where shear strain is dimensionless (often plotted as a percentage, %), and displacement and height are in units of length (m).

The shear rate can also be defined as:

$$Shear\ rate\ =\ \frac{Change\ in\ strain}{Change\ in\ time}$$ **Equation 1-3**

where the change in time is in seconds (s) and shear rate is in units of s^{-1}.

Therefore, having defined these terms, the shear viscosity can subsequently be described by:

$$\eta = \frac{\tau}{\gamma}$$ **Equation 1-4**

where η is the shear viscosity (Pa s), τ is the shear stress (Pa) and γ is the shear rate (s^{-1}).

The complex shear modulus, or G^*, a measurement of viscoelasticity can also be defined as:

$$G^* = \frac{\tau}{\lambda}$$ **Equation 1-5**

where G^* is the complex shear modulus, in units of pascal (Pa), τ is the shear stress (Pa) and λ is the shear strain.
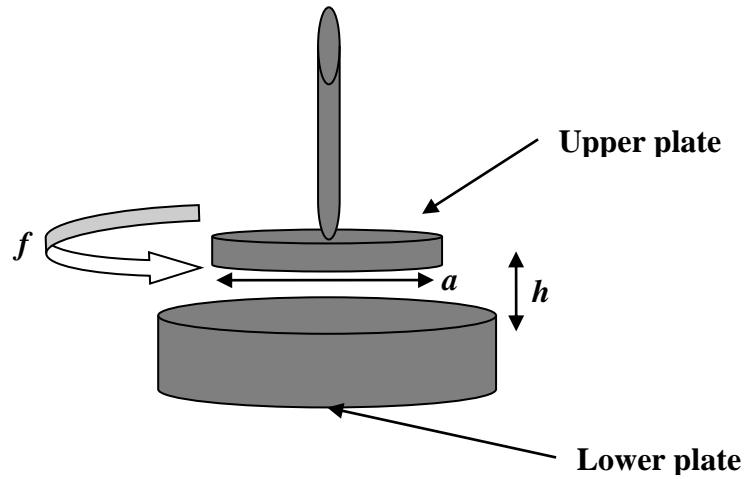
Figure 1-2: Illustration of rheometer operation. Diagram shows fixed lower plate, and upper plate of surface area, a, that rotates with shear force, f. Sample inserted between the upper and lower plates, and sample height (or gap size), h, is kept constant during measurement.
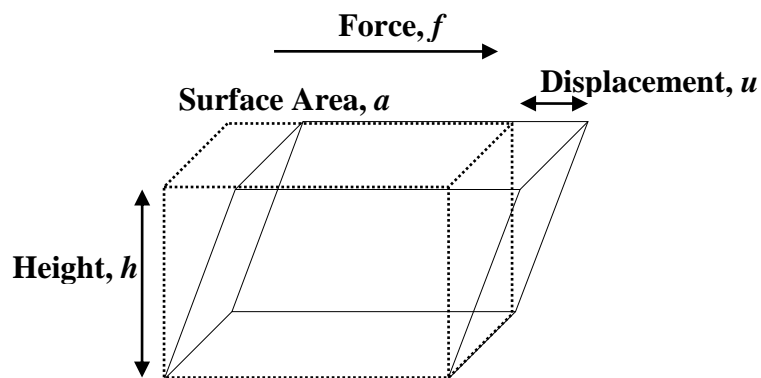
Figure 1-3: Definition of shear terms. A rheometer applies a constant shear force, f, to a sample of height, h, over a surface area, a, which is displaced by amount, u.

66

1.5.2   Viscosity

1.5.2.1   Viscosity theory

The shear viscosity of a material must always be defined within a particular context, i.e. under a set of stated conditions. This is because the viscosity is a function of these conditions and will therefore be different for each condition. For example, the shear viscosity of water can be said to be η Pa s, at a temperature of $T°$C.

A material will have three general flow behaviours; Newtonian, shear thinning (pseudoplastic) or shear thickening (dilatant). A Newtonian fluid is where the viscosity is independent of shear rate, and examples include water, oil or alcohol. The viscosity of non-Newtonian fluids, i.e. shear thinning or shear thickening fluids, changes with the shear rate. The viscosity of a shear thinning or pseudoplastic fluid will decrease as the shear rate increases, and the viscosity of a shear thickening or dilatant fluid will increase as the shear rate increases. This is highlighted in Figure 1-4 below. Some examples of shear thinning fluids include blood, ketchup and polymers. An example of a shear thickening fluid is corn flour.

In fact, non-Newtonian fluids are very common; most real samples are shear thinning with Newtonian regions (i.e. they exhibit Newtonian behaviour at low shear rates). Additionally, more materials are shear thinning than shear thickening.

Non-Newtonian behaviour can be described by the flow behaviour index, n, where a Newtonian fluid has a flow behaviour index of 1, a shear thickening fluid has a flow behaviour index greater than 1 and a shear thinning fluid has a flow behaviour index less than 1. The more pronounced the non-Newtonian behaviour is, the further the flow behaviour index is from 1. This will be discussed in more detail in Materials & methods section 2.5.

There are several other types of viscometry tests that can be carried out to determine rheological properties such as thixotropy or yield stress, however they are not the focus of this work.
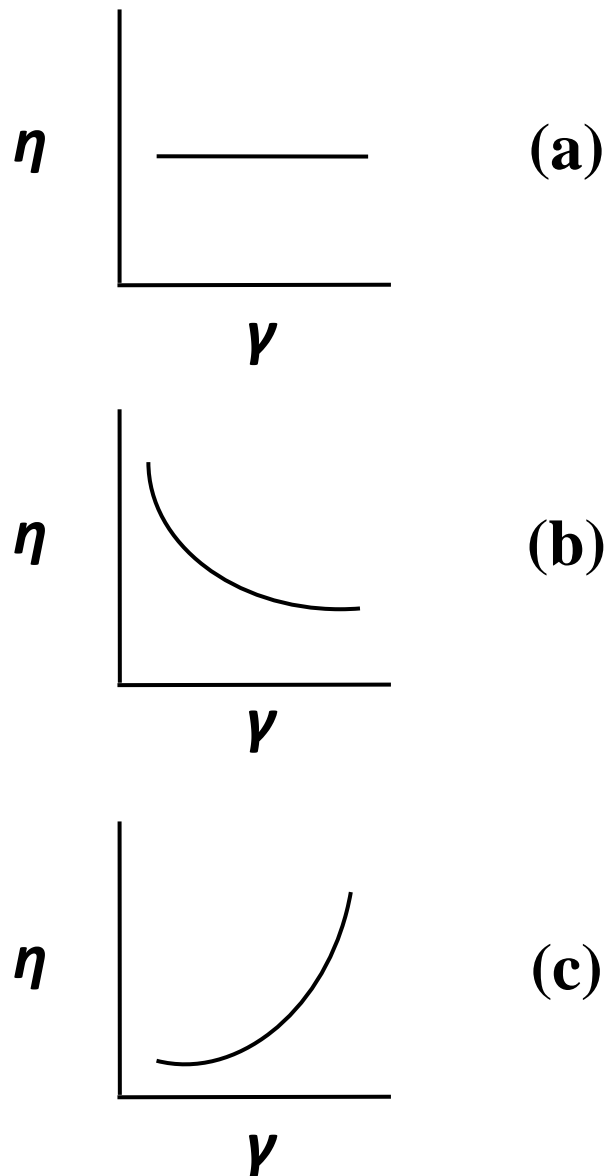
Figure 1-4: Illustration of three general flow behaviours. Shear viscosity, η, vs. shear rate, γ, for (a) a Newtonian fluid, (b) a non-Newtonian, shear thinning fluid and (c) a non-Newtonian, shear thickening fluid.

1.5.2.2   Viscosity applications in bioprocessing

Viscosity has previously been used in bioprocessing to monitor various physical properties, and has most commonly been applied in fermentation to monitor the cell broth. Viscosity monitoring in fermentation gained interest in the 1970's and 80's, however lost momentum in the 90's, due to a lack of adequate technology to accurately monitor viscosity in complex biological systems. Nevertheless, with much more advanced technologies (e.g. more powerful rheometers) entering the marketplace recently, its use is starting to gather interest again.

Studies in the 70s, 80s and early 90s attempted to monitor viscosity in fermentation to determine biomass concentration, as cell concentration is directly related to viscosity (Leduy et al., 1974; Shimmons et al., 1976; Perley et al., 1979; Picque and Corrieu, 1988; Bryan and Silman, 1990; Dhillon et al., 2013). For example, viscosity measurements have been used previously to monitor cell concentration in filamentous fermentation broths; a capillary-type viscometer has been used to monitor the broth viscosity of *Hansenula polymorpha* (a methylotrophic yeast), using cells harvested in both exponential phase and in stationary phase (Perley et al., 1979). The viscosity was shown to increase non-linearly (second order polynomial fit) with cell concentration (Perley et al., 1979), and the small coefficients in the polynomial regression indicated that viscosity is a weak function of cell concentration. For analysis, the viscosity was normalised by dividing the viscosity of the cell suspension by the viscosity of the supernatant, and it was observed that the normalised viscosity increased by only a factor of 1.06 as the cell concentration doubled from 7.5 g/L to 15 g/L. This result showed that for filamentous organisms, other factors significantly influence the viscosity at low cell concentrations, such as changing morphology and extracellular product secretion (Perley et al., 1979), which could be minimised at high cell concentrations.

Using a rotational viscometer for *Saccharomyces cerevisiae* showed better results, although mixing experiments were carried out with yeast cells re-suspended in buffer solution (Shimmons et al., 1976). The results showed that below volume fractions of 0.15, a linear relationship between the apparent viscosity and cell concentration was evident, however at high cell concentrations the behaviour was non-linear.

Interestingly, the apparent viscosity was used to control the cell concentration during the mixing of the yeast with distilled water, by controlling the rate of distilled water addition using a PI controller. Such an application has crossover to perfusion bioreactor systems in biopharmaceutical production, which have also gained significant interest in recent years, and which require novel PAT approaches for monitoring and control. This result also confirmed that viscosity-cell concentration relationships are useful for systems where the effect of other factors, such as extracellular solute concentration and cell morphology, are small (Shimmons et al., 1976).

A vibrating rod sensor has also been used to characterise the viscosity in xanthan production (*Xanthomonas campestris*) and yoghurt fermentation (*Streptococcus thermophilus* and *Lactobacillus bulgaricus*). As the viscosity increased, the vibration of the rod was dampened and the output signal could be transformed from voltage into arbitrary viscosity units (Picque and Corrieu, 1988). In addition, the vibrating rod was implemented in-line in the fermenter. However, this empirically-based method must be calibrated (with sucrose solution) before each fermentation and a non-linear correlation was shown, which resulted in a lack of sensitivity at higher viscosities. For example, the sensitivity was 4.4 mV/mPa s for sucrose viscosities in the range 1 - 50 mPa s, and 0.9 mV/mPa s in the 200 - 300 mPa s range (Picque and Corrieu, 1988). In addition, for the xanthan fermentation studied, a highly viscous polysaccharide product, the vibrating rod signal could be correlated to the product concentration (in the range 0 - 8.5 g/L) via a second order relationship with a high R^2 value of 0.992.

Of particular note, Badino et al. (Badino et al., 1999; Badino et al., 2001) have previously carried out studies using a custom online rheometer to develop empirical correlations between the rheological properties of the cell broth (such as the flow consistency index, K, which can be used to give an indication of the non-Newtonian behaviour of a material) and biomass concentration, agitation rate and mycelial morphology in *Aspergillus awamori* fermentation. However, agitation rate is not a reliable indicator of viscosity when a cascade control system is used because both stirrer rate and oxygen gas blending are used to control the dissolved oxygen tension.

In addition, the agitation rate is constantly fluctuating significantly during fermentation, for example in the fermentation system presented in this thesis (see results in Chapter 3, Chapter 4 and Chapter 5), the stirrer rate varied between 300 - 1200 rpm, which makes it difficult to establish a distinct correlation.

More recently, a method was developed to determine the viscosity of a *Xanthomonas campestris* fermentation (producing xanthan) by measuring the heat transfer capacity (Wunderlich et al., 2016; Schelden et al., 2017) online and in-situ. The heat transfer capacity is influenced by the thickness of the boundary layer between the bulk liquid in the bioreactor and the wall, which is a function of flow conditions and therefore of the viscosity. The results achieved a good correlation with offline data (R^2 value of 0.93), however the method is only applicable for processes with formation of biopolymers and filamentous growth (Schelden et al., 2017).

Monitoring viscosity in fermentation broths where the cells undergo significant morphological changes during the various growth phases (i.e. filamentous fermentation) has typically shown an increase in viscosity in relation to cell density in the exponential phase, followed by a subsequent immediate decrease in viscosity in stationary phase (Leduy et al., 1974; Bryan and Silman, 1990; Dhillon et al., 2013). This is related to changes in cell morphology (for example, during spore formation) which significantly affect broth viscosity (Neves et al., 2000). Filamentous organisms are considered to be the most challenging expression systems due to such high viscosities which lead to problems with mass transfer during fermentation (Formenti et al., 2014), and this is the primary reason why so much work relating to biomass monitoring using viscosity has been carried out in this area.

For the case of *E. coli* cell broths, fewer rheological studies have been carried out. The change in viscosity of *E. coli* suspensions has previously been observed whilst undergoing chemical (alkaline) lysis, however this study monitored the change in viscosity over the course of the chemical reaction to understand genomic DNA denaturation. Additionally, samples were taken at the beginning of stationary phase where the cells reached a low optical density, no product was being produced, and the analysis method took 30 - 60 minutes (Kong et al., 2009). Nonetheless, this

71

verifies an important consideration; a significant change in viscosity takes place during *E. coli* cell lysis. Additionally, chromosomal DNA was attributed to the largest change in rheological properties during lysis. Further to this, the co-expression of nuclease in *E. coli* fermentation has been shown to produce a step change in the efficiency of centrifugation due to the reduction of the viscosity of the cell broth (up to 75%), by removing chromosomal DNA (Balasundaram et al., 2009).

A recent study focusing on the evaluation of primary recovery options (centrifugation and depth filtration) reported an increase in the flow consistency index, *K*, during fermentation, from 0.01 Ns^n/m^2 at 15 h postinduction to over 0.12 Ns^n/m^2 at ~40 h postinduction. This demonstrated that the broth viscosity and the non-Newtonian behaviour increased during *E. coli* fermentation producing a domain antibody (dAb) (Voulgaris et al., 2016), and indicated that monitoring the change in various rheological parameters such as flow consistency index may be feasible for industrial fermentations to determine harvest time.

In summary, for filamentous cell broths, which undergo morphological changes during fermentation, the broth viscosity is significantly affected by changes in morphology (Picque and Corrieu, 1988). However, in general (i.e. for fermentations that do not undergo significant morphological changes), the viscosity in fermentation is determined by both the cell concentration and solute concentration in the broth (Reardon and Scheper, 1991).

Solute concentration often refers to the production of exopolysaccharides (for example, in *A. pullulans* fermentation where the product is a polysaccharide that is secreted to the broth (Leduy et al., 1974)), which can significantly affect broth viscosity due to its high molecular weight. In addition, for bioprocesses that produce plasmid DNA as products, or that have high polysaccharide or protein concentrations, the viscosity and non-Newtonian behaviour of the broth can be significant (Picque and Corrieu, 1988). This can have a major impact on mass transfer, bioreactor design, pumping and power consumption.

However, for *E. coli* cell broths, it is well known that other factors affect the viscosity, such as the release of chromosomal DNA from inside the cell during homogenisation (Balasundaram et al., 2009). When cell lysis occurs (for example, in fermentation, homogenisation or chemical lysis), the intracellular content will leak to the broth and the viscosity will increase. Therefore, although viscosity monitoring in fermentation has typically been used to determine the biomass concentration, there are other factors that affect the viscosity such as the solute concentration in the broth (Reardon and Scheper, 1991) that have not previously been considered for *E. coli* fermentation. In addition, detailed characterisation of viscosity changes during cell lysis in fermentation have not been carried out for the purpose of fermentation monitoring.

1.5.2.2.1 Einstein equations

In 1906, Einstein proposed a relationship for the viscosity of a dilute suspension of spherical particles, based on hydrodynamics (Einstein, 1906):

$$\eta = \eta_L (1 + 2.5\phi)$$
Equation 1-6

where η is the viscosity of the suspension, η_L is the viscosity of the suspending medium and ϕ is the volume fraction (i.e. for fermentation broths, the volumetric biomass concentration).

This theory assumes that all particles are spheres (*E. coli* are non-spherical) and assumes no interactions between particles due to being in a dilute suspension. It also assumes that Stokes flow applies, and inertia is neglected (Mewis and Wagner, 2012). This linear relationship is valid up to a volume fraction of 0.05 or 5%.

There are various extensions to the Einstein equations for suspensions at higher volume fractions, where more complex interactions are present (such as hydrodynamic interactions and particle-particle interactions). For semi-dilute

73

suspensions, i.e. up to a 14% volume fraction, the following correlation has been developed (Blanch and Bhavaraju, 1976):

$$\eta = \eta_L(1 + 2.5\phi + 7.25\phi^2)$$
Equation 1-7

This correlation was validated for yeast suspensions (Deindoerfer and West, 1960), and is termed the "Vand equation" (Blanch and Bhavaraju, 1976). At higher volume fractions, complex hydrodynamic interactions, cell-cell interactions and random Brownian motion become significant, making it extremely challenging to characterise the properties of the broth (Mewis and Wagner, 2012).

Such equations are useful for determining the viscosity of fermentation broths based on the volume fraction. However, as discussed above in section 1.5.2.2, factors contributing to the viscosity of cell broths include biomass concentration, the solute concentration in the broth and for filamentous fermentations, the cell morphology. Therefore, the Einstein equations (and extensions to the Einstein equations) assist with the determination of one part of the picture of cell broth rheology. This will be discussed in more detail in Chapter 4.

1.5.3   Viscoelasticity

1.5.3.1   Viscoelasticity theory

While viscosity measures a materials' resistance to flow, viscoelasticity provides a way to understand how a sample behaves before it flows, i.e. at near-rest conditions. This is useful as it enables the classification of a material in terms of its internal structure and strength. Viscoelasticity describes both the solid-like (elastic) and liquid-like (viscous) properties of a material (most materials are a mixture of both). A viscoelastic material exhibits non-Newtonian behaviour, however non-Newtonian fluids are not necessarily viscoelastic. An example of a viscoelastic material is paint; during storage, the paint behaves as a solid (preventing sedimentation), however

when painting, it behaves as a fluid, i.e. it will flow in the bristles of a brush and can be evenly distributed on a surface.

The complex shear modulus, G* (defined in section 1.5.1), is a commonly used parameter to describe viscoelasticity. G* is comprised of the shear stress over the shear strain, and the higher the modulus, the tougher the material. G* can alternatively be described by:

$$G^* = G' + iG''$$ **Equation 1-8**

where i is the imaginary number ($\sqrt{-1}$), G' is the storage (elastic) modulus and G'' is the loss (viscous) modulus.

The storage modulus, G' (Pa) can also be expressed as:

$$G' = \frac{\tau}{\lambda} \times \cos(\delta)$$

Equation 1-9

where δ is the phase angle (°), τ is the shear stress (Pa) and λ is the shear strain.

The loss modulus, G'' (Pa) can therefore be defined as:

$$G'' = \frac{\tau}{\lambda} \times \sin(\delta)$$

Equation 1-10

The phase angle, δ, is an important rheological parameter. When applying a sinusoidal (oscillatory) signal to a sample, different materials will have different response times, i.e. a different lag or phase angle between the applied and measured sinusoidal signal. This is demonstrated in Figure 1-5. For a purely elastic (solid-like) material, the stress and strain are exactly in phase, i.e. the phase angle is 0°. For a purely viscous (liquid-like) material, the stress and strain are 1/4 of a cycle out of phase, i.e. the phase angle is 90°. Therefore, if G' is greater than G'', the phase angle is less than 45° and the material can be said to be "solid-like". In contrast, if G'' is greater than G', the phase angle is greater than 45° and the material can be classified as "liquid-like", i.e. the material behaves more as a liquid than a solid.

In addition, the loss tangent can be used to quantify the elasticity of a material, and is a ratio of the loss modulus to the storage modulus:

$$\tan\delta = \frac{G''}{G'}$$

Equation 1-11

There are two main types of measurements used to determine viscoelastic properties; the amplitude sweep and the frequency sweep. When a sinusoidal, oscillatory signal is applied to a sample, the oscillation is a function of both the amplitude and the frequency. Therefore, the two tests are called amplitude sweeps and frequency sweeps and are carried out by holding one variable constant whilst varying the other.

The amplitude sweep experiment is ran to determine the linear viscoelastic range (LVER), which is the critical strain limit at which a material starts to break down. The frequency sweep experiment is then carried out to record a fingerprint spectrum of the material, whilst the amplitude is held constant within the LVER. A frequency sweep can classify a material into three general behaviours; a gel, a viscoelastic solid, or a viscoelastic liquid.

There are several other types of viscoelastic tests, such as creep or relaxation tests, however they are not the focus of this work.

Measured strain

Input stress

Time

δ
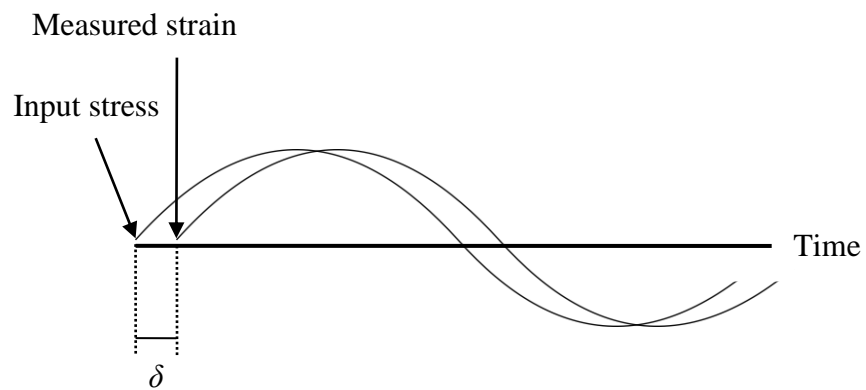
Figure 1-5: Phase angle (δ) illustration. showing the input applied sinusoidal stress and the measured strain response, with a phase angle of δ.

1.5.3.2 Viscoelasticity applications in bioprocessing

Viscoelastic measurements have also been used in bioprocess research and development. Oscillatory testing was previously used to investigate the effect of cell biomass and exopolysaccharides produced by *Streptococcus theromphilus* and *Lactobacillus bulgaricus* strains during yoghurt fermentation (Vlahopoulou and Bell, 1993; Vlahopoulou et al., 1994; Vlahopoulou et al., 2001). This work used oscillatory testing to gain insight into the metabolic activity of lactic acid bacteria, and to understand the contribution of exopolysaccharides to the physical structure of fermented milks (Bensmira et al., 2010), assuming that the bacterial cells interacted with milk proteins through the production of exopolysaccharides.

Oscillatory testing has been carried out on flocculated gels of *E. coli* lysate after undergoing chemical lysis (Ciccolini et al., 1999; Levy et al., 1999), demonstrating the sensitivity of the elastic modulus of the gel-matrix to shear strain, and results from the rheological studies were used to inform research strategies for process synthesis. Viscoelasticity has also been used to study mixing and fluid flow in simulated xanthan fermentation broths (Galindo and Nienow, 1992) and to analyse the viscoelastic nature of filamentous fermentation broths (Mohseni et al., 1997). Essentially, viscoelasticity has been shown to be a very useful method to analyse the material properties of fermentation broths.

In terms of understanding the rheological properties of an *E. coli* cell broth, these studies are interesting because they suggest the possibility to derive useful insight from viscoelastic testing regarding cell lysis (whether in fermentation or chemical lysis). Moreover, rheological testing has also been carried out on calf thymus DNA, to understand the formation of a network at high DNA concentrations (Mason et al., 1996). This shows the sensitivity of oscillatory testing to differences in high molecular weight molecules such as DNA; which is known to be an important marker for cell lysis (Balasundaram et al., 2009). In addition to viscoelastic testing relating to cell lysis, monitoring viscoelastic properties may also be able to provide novel insight into the physical properties of cells, such as changes in the strength, stability and robustness of the cell population during fermentation, as well as

providing insight into any interactions present in the system, for example between protein, nucleic acids and cell debris during cell lysis.

In summary, although few rheological studies on *E. coli* cell broths have been carried out, there is sufficient literature to be able to draw several conclusions regarding rheology applications in fermentation. Firstly, viscosity can be used to monitor the cell concentration in the fermentation, as cell concentration (volume fraction) is directly related to viscosity. Secondly, rheological testing on *E. coli* cell broth during chemical lysis provided useful information regarding changes in the material properties of the cell broth (Levy et al., 1999).

The ability to detect and monitor cell lysis in fermentation remains a significant challenge and detailed characterisation of rheological changes during cell lysis in fermentation has not been carried out for the purpose of fermentation monitoring. There remains a substantial need for novel process monitoring technologies in the biopharmaceutical industry to drive improvements in process development and large scale production, in order to bring safer and more efficacious drugs to market in a shorter time. The development of a novel rheology-based monitoring technology may therefore be able to deliver insight into the changes in physical properties of cell broths during fermentation, which will aid both our understanding of cell lysis, as well as our ability to monitor and subsequently control lysis. Improving understanding of cell lysis from a bioprocessing perspective may have useful applications in process design, monitoring and optimisation.

1.6   Aims and objectives

Cell lysis is often observed in microbial fermentation and remains a key challenge that is poorly understood. For host cells with intracellularly-stored products, product loss occurs at the point of cell lysis, which can have a huge impact on the final product yield. Moreover, when cell lysis occurs, intracellular content such as host cell protein and nucleic acids leak to the broth, which acts to increase the viscosity of the broth and can have major consequences on the performance of subsequent downstream unit operations.

The fermentation process itself is characterised by many different and complex variables, which make it challenging to monitor and control cell lysis directly. Process analytical technologies (PAT) and quality-by-design (QbD) initiatives are beginning to demonstrate tangible improvements in the biopharmaceutical industry's approach to process development, however due to the inherent complexity of the fermentation broth, there remains a significant need for new monitoring technologies in fermentation.

The inability to monitor and control cell lysis in fermentation leads to problems with process robustness, such as variations in the material properties of the cell broth which in turn affects many of the downstream processing unit operations such as unit sizing or the operational performance, for example cake formation in microfiltration.

Current analytical technologies are unable to rapidly and accurately monitor the shift between optimal intracellular product concentration and product leakage to the fermentation broth. Using viscosity monitoring in fermentation may facilitate a deeper understanding of the physical properties of cell broths, and may provide an efficient way to indirectly infer cell lysis, which would enable decision-making about harvest time in fermentation and improve our understanding of the impact of lysis on the performance of downstream unit operations.

The overall aim of this thesis is to use viscosity monitoring to detect cell lysis in fermentation, in order to gain a deeper understanding of the effects of lysis on the physical properties of cell broths and demonstrate its application in process design and optimisation by considering the impact on primary recovery unit operations.

The specific objectives for each chapter are outlined below:

- Develop a method to rapidly detect cell lysis and product loss in fermentation using viscosity monitoring. This will involve characterising cell lysis using a range of analytical techniques and then evaluating them in comparison to viscosity monitoring

- Investigate the effects of cell lysis on the rheological properties of cell broths in fermentation. This will involve using advanced rheological testing to gain a deeper understanding of the physical properties of cell broths and then using this insight to develop a model to quantify cell lysis in postinduction fermentation using viscosity monitoring

- Carry out a case study demonstrating an application of viscosity monitoring in fermentation. This will involve using viscosity monitoring to make decisions about harvest time and to influence an approach to create a novel process design in primary recovery

Chapter 2   Materials & methods

All chemicals were provided by Sigma-Aldrich (Dorset, UK) unless otherwise stated and used as supplied.

2.1   Host strain

An *E. coli* K12 w3110 strain (ATCC 27325) containing the plasmid pTTOD A33 IGS2 (with specificity for human IL-17) was kindly donated by UCB Pharma Ltd. (Slough, UK), coding for a 46 kDa antibody fragment (Fab') utilising a *tac* promoter. The plasmid also codes for tetracycline resistance and is shown in Figure 2-1.
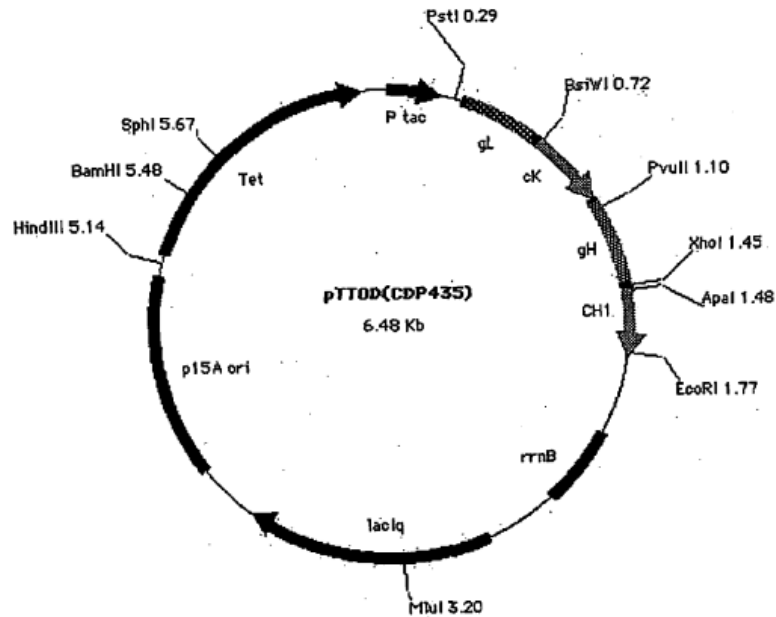
Figure 2-1: pTTOD A33 IGS2 plasmid used in *E. coli* w3110, coding for Fab' expression and tetracycline resistance, utilising a *tac* promoter (Adams et al., 2009).

2.2   Fermentation

High cell density fed-batch fermentations were carried out using an autoclavable 7 L Applikon vessel (vessel diameter 160 mm, aspect ratio 2.3:1; Applikon Biotechnology B.V., Schiedam, Holland), with a 5 L working volume using an overhead driven double Rushton 6-blade impeller (60 mm diameter).

2.2.1 Working cell bank preparation

A master cell bank vial was kindly provided by UCB Pharma Ltd. (Slough, UK), and used to inoculate 200 mL complex LB broth (10 g L^{-1} tryptone, 5 g L^{-1} yeast extract and 5 g L^{-1} NaCl) in 1 L baffled shake flasks. Tetracycline was supplemented in each shake flask to a working concentration of 10 μg mL^{-1}. The shake flasks were subsequently incubated at 37°C and 250 rpm until an optical density (OD_{600}) of 1-1.5 was reached (4.5-5 h) where the cells were in exponential phase. To make the working cell bank, 1 mL of cell broth was added to 1 mL of 50% (v/v) glycerol solution and stored in 2 mL cryovials at -80°C.

2.2.2 SM6Gc defined media

The formula for SM6Gc defined media is defined in Table 2-1 and Table 2-2, and was previously described by Garcia-Arrazola et al. (2005).

Table 2-1: SM6e trace elements formula for SM6Gc defined media (Garcia-Arrazola et al., 2005).

Compound	Concentration (g/L)
Citric acid	100
$CaCl_2.6H_2O$	5
$ZnSO_4.7H_2O$	2.46
$MnSO_4.4H_2O$	2
$CuSO_4.5H_2O$	0.5
$CoSO_4.7H_2O$	0.427
$FeCl_3.6H_2O$	9.67
H_3BO_3	0.03
$NaMoO_4.2H_2O$	0.024

Table 2-2: Media components for SM6Gc defined media (Garcia-Arrazola et al., 2005).

Compound	Concentration (g/L)
$(NH_4)_2SO_4$	5.2
$NaH_2PO_4.H_2O$	4.4
KCl	4
$MgSO_4.7H_2O$	1.04
SM6e trace elements	10 mL
Citric acid. H_2O	4.2
Glycerol	141.12
PPG	0.2 mL
$CaCl_2.H_2O$	0.25

2.2.3 Fermentation protocol

Using the working cell bank, the seed train was initiated in the same way as described above (in section 2.2.1), and incubated for 4.5-5 h in complex LB media with tetracycline (working concentration of 10 µg mL^{-1}) until reaching an OD$_{600}$ of 1-1.5. 40 mL of culture was then transferred to a total working volume of 400 mL in 2 L baffled shake flasks containing tetracycline (working concentration of 10 µg mL^{-1}) and SM6Gc media (method previously described by Garcia-Arrazola et al. (2005)). The cells were grown in a shaker-incubator in defined SM6Gc media for 20 h at 30°C and 200 rpm, until reaching an OD$_{600}$ of 5 (cells in exponential phase).

600 mL of seed culture was then used to inoculate (at 15 % v/v) the 7 L Applikon fermenter. pH was maintained at 6.95 ± 0.05 using an automated PID controller with ammonia solution (12% v/v) and phosphoric acid (12% v/v). Dissolved oxygen tension (DOT) was controlled (PID controller) at $30\% \pm 5$, using a cascade control system with agitation (300-1200 rpm) and oxygen gas blending. Temperature was initially controlled (PID controller) at $30°C \pm 1$ and dropped to $25°C \pm 1$ thereafter upon reaching an optical density (OD$_{600}$) of 38. At an OD$_{600}$ of 38, a 32 mL shot of $MgSO_4.7H_2O$ (246.7 g L^{-1}) was added to the fermenter. At an OD$_{600}$ of 54, 24 mL of $NaH_2PO_4.H_2O$ (232.8 g L^{-1}) was added, and at an OD$_{600}$ of 80, a further 32 mL was

added. These shots are added to help stabilise the structure of the outer cell membrane of the cells during rapid (exponential) growth by binding with lipopolysaccharide (Chen et al., 2004).

At an OD_{600} of around 200 (~36-38 h postinoculation), a DOT spike indicated that the culture had utilised all of the glycerol carbon source in the media. At this point, isopropyl β-$_D$-1-thiogalactopyranoside (IPTG) (Generon Ltd., Maidenhead, UK) was added to a target bioreactor concentration of 0.03 g L^{-1} in order to induce Fab' expression, and 80% (w/w) glycerol solution was fed at a rate of 6.4 mL h^{-1}. To control foaming, 1 mL of 100% polypropylene glycol (PPG) was added to the fermenter prior to inoculation, and as necessary thereafter up to a maximum of 2 mL total PPG. Samples were taken from the bioreactor throughout the fermentation and the fermentation was typically continued up to 60 h postinduction.

2.2.4   Fermentation process control

As discussed in section 2.2.3, several parameters were controlled during the fermentation process including temperature, pH, and dissolved oxygen tension. After initially setting up the bioreactor, the controller performance for these parameters was poor. Therefore, the proportional-integral-derivative (PID) controller for each of the parameters was improved. This was done sequentially by trial and error, first establishing the P-term, followed by an I-term and finally a D-term where necessary. The improved PID terms are displayed in Table 2-3 below.

Table 2-3: Improved PID controller settings for pH, temperature and dissolved oxygen tension (DOT) for the Applikon 7 L fermenter

	pH	Temperature	DOT
P-term	50	20	1.25
I-term	250 s	2700 s	250 s
D-term	0 s	0 s	25 s

2.3   Analytical methods

2.3.1   Measurement of cell density

Optical density was measured at 600 nm using an Ultrospec 500 Pro spectrophotometer (Amersham Biosciences Ltd., Amersham, UK). Samples were diluted in distilled water, where appropriate.

Dry cell weight was measured by aliquoting 1 mL of cell broth into pre-dried and pre-weighed 2 mL Eppendorf tubes, centrifuging at max rcf (16,100 rcf or 13,200 rpm, Eppendorf Centrifuge 5415R, Eppendorf, Germany) for 10 min, removing the supernatant and drying in an oven overnight at 100°C.

2.3.2   Capacitance measurements

The Aber Instruments (Aber Instruments Ltd., Aberystwyth, UK) Futura biomass probe (320 mm x 12 mm) was used in fermentations to obtain online, in-situ measurements of viable cells/mL. The online biomass probe fits into a standard 325 mm port on the fermenter headplate and measures the electrical capacitance of cell suspensions at various radio frequencies. The probe was set up to measure in dual frequency mode, at 1.12 MHz and 15 MHz, which has been optimised by Aber Instruments for bacteria. A detailed explanation of dielectric spectroscopy theory was discussed in the Introduction (section 1.4.4.3.1).

2.3.3   Sonication

Where appropriate, samples were sonicated in order to release intracellular content for subsequent analytical measurement. Sonication was carried out using a Soniprep 150 (MSE Ltd., London, UK), with 4 cycles each consisting of 10 seconds on, 10 seconds off, at an amplitude of 10 μm. The samples were held in an ice bath during sonication.

2.3.4   Cytotoxicity assay

The cytotoxicity assay, Cytotox-96 (Promega Inc., Madison, USA), was used to determine cell viability, based on lactate dehydrogenase (LDH) release from the cell

to extracellular space. The method is non-radioactive and colorimetric based, using absorbance spectrophotometry to quantify the amount of LDH present. Cells that have lost membrane integrity release LDH to extracellular space. LDH is a stable cytosolic enzyme that is released upon cell lysis (similar to $[^{51}Cr]$ release in radioactive assays). LDH is deemed to be an effective marker because it does not lose its activity or degrade during cell lysis assays.

In the assay, a tetrazolium salt (iodonitrotetrazolium violet; INT) is converted into a red formazan product (by supplying LDH, lactate and NAD^+ (nicotinamide adenine dinucleotide) as substrates), which can be determined quantitatively using a spectrophotometer. The amount of colour is proportional to the amount of lysed cells (i.e. concentration of LDH). This reaction sequence is detailed in the equations below:

LDH

$$NAD^+ + Lactate \xrightarrow{\quad LDH \quad} Pyruvate + NADH \qquad \textbf{Equation 2-1}$$

Diaphorase

$$NADH + INT \xrightarrow{\quad Diaphorase \quad} NAD^+ + Formazan \qquad \textbf{Equation 2-2}$$
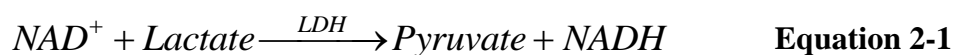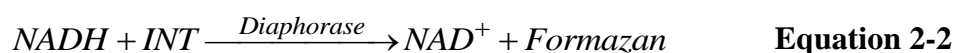
The assay was carried out and measured using a Tecan Safire^2 spectrophotometer (Tecan Group Ltd., Reading, UK) in 96-well plate format at an optical density of 490 nm, according to the manufacturer's instructions.

The assay does not give the concentration of its "positive control" standard, which means that a standard curve cannot be produced. Therefore, it is necessary to plot % cytotoxicity at each time point by determining the absorbance for both the supernatant of undisrupted cells and total LDH release from the supernatant of sonicated cells. This is shown in the equation below:

88

$$\% \text{ cytotoxicity} = \frac{\text{Experimental LDH release (OD}_{490})}{\text{Maximum LDH release (OD}_{490})} \times 100\% \qquad \textbf{Equation 2-3}$$

2.3.5 Flow cytometry: BP staining

Flow cytometry was performed using an Accuri C6 flow cytometer (BD Biosciences, California, USA), using bis-oxonol (BOX) and propidium iodide (PI) stains. Analysis using this method for *E. coli* analysis has been described elsewhere (Lewis et al., 2004). Fermentation samples were diluted to an OD_{600} of 1.0 AU and 10 µL combined with 990 µL of staining solution (50 µg/mL bis-oxonol, 40mM EDTA, 20 µg/mL propidium iodide, in PBS). Samples were stained for 8 minutes before analysis. Cells which remained unstained or stained with bis-oxonol were counted to provide an overall measurement of viable cells/mL. Flow cytometry measurements were verified by carrying out cell counts using the colony forming units (CFU) method. This work was carried out by Dr Desmond Schofield (Department of Biochemical Engineering, University College London).

2.3.6 Nucleic acid and protein quantification

2.3.6.1 Picogreen assay

Quant-iT Picogreen assay (Life Technologies Ltd., Warrington, UK) was used to determine double-stranded DNA (dsDNA) concentration. Picogreen is a highly sensitive method of nucleic acid staining, based on fluorescence spectroscopy, to quantify double-stranded DNA in solution.

Picogreen can quantify dsDNA over three orders of magnitude (linear relationship), without interference from other artefacts such as RNA and single-stranded DNA, using a standard bacteriophage lambda DNA as a reference to quantify dsDNA in unknown samples. The standard DNA curve can be plotted as fluorescence vs. DNA concentration.

The assay was carried out according to the manufacturer's instructions. Samples were diluted as appropriate in the assay buffer provided (to 100 μL total volume). Samples were incubated in the dark for 5 min, after addition of 100 μL of reagent to each sample, and then measured using a Tecan Safire[2] spectrophotometer (Tecan Group Ltd., Reading, UK) in 96-well plate format, excited at 480 nm and fluorescence emission intensity was measured at 520 nm.

2.3.6.2 Bradford assay

Bradford assay (Bio-Rad Laboratories, Inc., Hercules, California, USA) was used to determine total protein concentration in samples of cell broth. The assay uses Coomassie Brilliant Blue which shifts its absorbance in visible light from 465 nm to 595nm in the presence of protein, causing a visible colour change.

Bovine serum albumin (BSA) was used to prepare the standard curve. Samples were diluted as appropriate (total volume of 10 μL), and 200 μL of Bradford reagent was added to each sample, according to the manufacturer's instructions. Following this, samples were immediately measured using a Tecan Safire[2] spectrophotometer (Tecan Group Ltd., Reading, UK) in 96-well plate format, at 595 nm.

2.3.6.3 Nanodrop measurements

A Nanodrop 1000 spectrophotometer (Thermo Scientific, Wilmington, DE, USA) was used to quantify total soluble protein (at 280 nm) and total nucleic acids (at 230 nm) of clarified cell broth, according to the manufacturer's instructions. Samples (total volume of 3 μL per sample) were diluted where appropriate.

2.3.7 Product quantification

Product concentration (Fab') in the supernatant and total product concentration were analysed by HPLC (Agilent 1200, Agilent Technologies Inc., California, USA) using a 1 mL protein G column (HiTrap, GE Healthcare, Uppsala, Sweden). To measure total Fab' concentration, sonication was carried out, followed by centrifugation at max rcf (16,100 rcf or 13,200 rpm, Eppendorf Centrifuge 5415R, Eppendorf, Germany) for 10 min at 10°C, removing the supernatant and centrifuging for a

further 10 min. Bind and elute 20 mM phosphate buffers were used to process the samples, at pH 7.4 and pH 2.5 respectively. The concentration of eluted Fab' was measured by absorbance at 220 nm. Purified Fab' was kindly provided by UCB Pharma Ltd. (Slough, UK), and diluted as appropriate to generate the standard curve for calibration. Product peak area was automatically integrated using Agilent's software (Agilent Chemstation, Agilent Technologies Inc., California, USA).

2.3.8   Particle size distribution

The particle size distribution of the cell broth was analysed by blue and red laser light diffraction across the size range 0.01-2,000 μm, using a Malvern Instruments Mastersizer 3000 (Malvern Instruments, Malvern, UK).

The scattering of light as it passes through a dispersed particulate sample can be used to determine the Brownian motion velocity, and can therefore establish the hydrodynamic diameter of the particle from the Stokes-Einstein equation. The Mastersizer 3000 employs multiple detectors to measure the intensity of light scattered over a wide range of angles, and each detector analyses particles within a certain size range.

Refractive and absorbance indices used were 1.59 and 0.00 respectively, based on latex particles, as the refractive indices of most biological materials are unknown. The cell broth sample volume required was dependent on the cell concentration, therefore the laser obscuration was held at 12-15% for all samples, and samples were added drop-wise until the desired obscuration was achieved (the obscuration value was displayed live on the computer). Measurements were taken in triplicate, averaged, and recorded as volume percentage vs. particle size interval. The raw data were treated, as previously described (Chatel et al., 2014), by converting into volume frequency vs. average particle size.

2.3.8.1   Treatment of raw data

The measurement of particle size distribution with the Mastersizer produces a histogram of volume percentage vs. particle size interval. This covers six orders of

magnitude on a logarithmic scale, allowing the entire sample range to be visually represented. However, the plot of percentage volume can actually misrepresent data, particularly if the distribution has more than one peak. This is because volume is a cubic factor of radius, thus the percentage volume of larger particles dominates the histogram compared to smaller particles, and also misrepresents the data as the particle size ranges are not equal throughout the histogram.

Therefore, the percentage volume can be converted into volume frequency by dividing the percentage volume by the size range for that band, i.e. for the size range of channel *i*:

$$F_{v,i} = V_i \big/ W_i$$

Equation 2-4

where $F_{v,i}$ is the volume frequency distribution, V is the % volume and W is the particle size range of the channel. In addition, the particle size range can be converted to the average particle size between the size range (Chatel et al., 2014).

2.4 Scanning electron microscopy

Cell broth was centrifuged, the supernatant was removed and the pellet was stored at -20°C before carrying out analysis with scanning electron microscopy. Cells were re-suspended for analysis in a primary fixative (2% glutaraldehyde in 0.1 M sodium cacodylate buffer (pH 7.3)) and left for 24 h at 3°C. The cells were then washed in 0.1 M cacodylate buffer and fixed in 1% osmium tetraoxide in 0.1 M cacodylate buffer at 3°C for 1.5 h. The cells were washed again in 0.1 M cacodylate buffer and washed with dH_2O before dehydrating in a graded ethanol-water series to 100% ethanol. The samples were then critical-point dried using CO_2, and mounted on aluminium stubs using sticky carbon taps. The samples were then coated with a thin layer of Au/Pd (~2 nm thick) using a Gatan ion beam coater. The samples were viewed and imaged with a 7401 FEGSEM (Jeol, Massachusetts, USA). This work

was carried out by Mr Mark Turmaine (Department of Biosciences, University College London).

2.5   Rheological characterisation

Rheological experiments were carried out using two different instruments in order to compare results between the two instruments. The first instrument, a Brookfield DV-2+ viscometer (Brookfield Engineering Laboratories, Inc., Middleboro, MA, USA) was used to determine the viscosity of the cell broth during fermentation. The second instrument, a Malvern Instruments Kinexus Lab + rheometer (Malvern Instruments, Malvern, UK) was used to carry out a range of rheological measurements, including measuring the viscosity and viscoelasticity of the cell broth during fermentation.

2.5.1   Brookfield viscometer

The Brookfield DV-2+ viscometer (Brookfield Engineering Laboratories, Inc., Middleboro, MA, USA) was used to carry out viscometry experiments with a cup and bob setup (CP-40 cup, coaxial cylinder rotary viscometer). A water bath was used to control the temperature at 25°C in order to mimic conditions found inside the fermenter, and 0.9 mL sample was required to fill the cup. The viscometer applied a fixed rotational speed (revolutions per minute, rpm, which can be converted to shear rate, s^{-1}) to the sample and the resultant shear stress (measured as % torque or Newton/m, which can be converted to shear stress, Pa, or Newtons/m^2) can be recorded manually from the viscometer readout. The gap size between the cup and the bob was manually adjusted between each measurement.

The shear rate can be calculated, according to the Brookfield DV-2+ viscometer manufacturer's instructions (Brookfield Engineering Laboratories, Inc., Middleboro, MA, USA), by:

$$\gamma = \frac{\omega}{\sin\theta} \qquad\qquad \textbf{Equation 2-5}$$

where γ is shear rate in s^{-1}, ω is the cone speed in rad/sec and θ is the cone angle in $°$, which for the CP-40 spindle is 0.8°.

The shear stress can be calculated from the torque by:

$$\tau = \frac{\Gamma}{\frac{2}{3}\pi.r^3}$$

Equation 2-6

where τ is shear stress in dynes/cm^2 (1 dyne/cm^2 is equivalent to 0.1 Pa), Γ is the % full scale torque (dyne-cm) and r is the cone radius, which for the CP-40 spindle is 2.4 cm.

A flow curve can be generated to produce a graph of shear stress vs. shear rate and the viscosity can then be determined as the gradient of the line (for Newtonian suspensions). Experiments were carried out using a shear rate of 50 s^{-1} to 1500 s^{-1}, selected due to the limitation imposed by the Brookfield instrument.

2.5.2   Malvern Instruments Kinexus rheometer

Rheological experiments were carried out with a Malvern Instruments Kinexus Lab + rotational rheometer (Malvern Instruments, Malvern, UK), using 1 mL sample volume with 50 mm parallel plates at 25°C and a 300 μm gap size. The rotational rheometer applies controlled shear deformation to the sample under examination, to measure various rheological properties. Temperature was controlled using a peltier plate heating system at 25°C in order to mimic conditions found inside the fermenter. All parameters, such as gap size, could be adjusted and controlled using the rSpace software (rSpace, Malvern Instruments, Malvern, UK).

All rheology-based results presented in this thesis were carried out using the Malvern Instruments Kinexus Lab + rheometer, except where stated.

2.5.2.1 Viscosity measurements

Viscosity measurements were taken by applying a controlled shear rate over a range of 100-1000 s^{-1} and measuring the shear stress response (automated on the rSpace software (rSpace, Malvern Instruments, Malvern, UK)). Measurements were recorded at each shear rate after reaching a stable response value i.e. after being maintained at steady state for 10 s. Results were automatically plotted in the rSpace software and data could be exported to an Excel file. The flow curve can be plotted as shear stress vs. shear rate or shear viscosity vs. shear rate. However, current "best practice" in scientific publications is to present the data as shear viscosity vs. shear rate, on a logarithmic scale.

2.5.2.2 Viscoelasticity measurements

Oscillatory testing was carried out via amplitude and frequency sweeps. Amplitude sweeps were taken over a shear strain range 0.05-10%, holding frequency constant at 1 Hz to determine the linear viscoelastic range (LVER); the critical strain limit at which a material starts to break down. Frequency sweeps were taken over the range 1-10 Hz, with shear strain held constant at 0.1 %, within the critical strain region (LVER).

The loss tangent, *tanδ*, is a ratio of the loss modulus (*G''*) to storage modulus (*G'*), and can be described:

$$\tan \delta = \frac{G''}{G'}$$

Equation 2-7

where units of both the storage and loss moduli are in pascal (Pa). The loss tangent can be used to quantify the elasticity of a material. A loss tangent value of less than one indicates predominantly elastic or solid-like behaviour and a loss tangent greater than one indicates predominantly viscous or liquid-like behaviour.

2.5.3 Treatment of raw viscosity data

For Newtonian fluids, the viscosity is the gradient of the straight line plot of shear stress vs. shear rate:

$$\tau = \eta.\gamma \qquad \qquad \textbf{Equation 2-8}$$

where τ (Pa) is shear stress, γ (s^{-1}) is shear rate and η is shear viscosity (Pa s).

For a non-Newtonian fluid, i.e. where the viscosity changes as the shear rate changes, and therefore exhibits shear thinning or shear thickening behaviour, may be described by the Power Law:

$$\tau = A + B.\gamma^{n} \qquad \qquad \textbf{Equation 2-9}$$

where A is zero, B is equal to K, the consistency index (Pa s^{n}) and n, the flow behaviour index, is a measure of non-Newtonian behaviour (i.e. a measure of the non-linearity of the flow curve, shear stress vs. shear rate). For a shear thinning or pseudoplastic fluid, n is less than one and for a shear thickening or dilatant fluid, n is greater than one.

The Power Law can then be rewritten:

$$\tau = K.\gamma^{n} \qquad \qquad \textbf{Equation 2-10}$$

Taking logarithms and separating out the variables, it is possible to obtain a straight line plot of log-shear stress vs. log-shear rate, where n is the gradient of the line and K is the y-intercept:

$$n = \frac{\log(\tau_2 / \tau_1)}{\log(\gamma_2 / \gamma_1)}$$ **Equation 2-11**

and

$$K = \frac{\tau_2}{\gamma_2^n}$$ **Equation 2-12**

Therefore, the apparent viscosity can be determined as:

$$\eta_{app} = K.\gamma^{n-1}$$ **Equation 2-13**

For fluids that exhibit strong non-Newtonian behaviour, the Power Law is often employed to determine the viscosity and to quantify the flow behaviour index, n.

2.5.3.1 Calculating the average shear rate in the bioreactor

Flow curves can be generated for each sample measured, however in order to plot shear viscosity vs. fermentation time, a single viscosity value was desired. This is challenging when the flow curve is non-linear (i.e. non-Newtonian behaviour is exhibited), as the viscosity changes depending on the rate of shear. The viscosity can either be derived from the Power Law or can instead be determined by using a single value of viscosity from a fixed shear rate.

By using a single value of viscosity from a fixed shear rate, the measurement and analysis time can be significantly decreased (i.e. from 10-15 min to 1-2 min). However, it was desired to obtain viscosity values at a shear rate that relates to the shear rate experienced inside the fermenter. Therefore, it was important to determine the average shear rate in the fermenter. Metzner and Otto describe the average shear

rate inside a stirred vessel as a linear function of stirrer speed (Metzner and Otto, 1957; Doran, 1995):

$$\gamma_{average} = k.N_i$$

Equation 2-14

where $\gamma_{average}$ is the average shear rate in the stirred vessel (s^{-1}), N_i is the stirrer speed in revolutions per second and k is a constant which for Rushton impellers is 10-13.

The 7 L Applikon fermenter operates between 300-1200 rpm, as a cascade control system is used to control dissolved oxygen tension at 30%. This makes the minimum and maximum average shear rate in the fermenter 50 s^{-1} and 200 s^{-1} (using $k = 10$). These values are average shear rates, as the shear rate inside the bioreactor is strongly dependent on the distance from the impeller.

Therefore, a fixed shear rate of 100 s^{-1} was chosen to obtain apparent shear viscosity data for cell broth during fermentation, as this provides a more accurate representation of the average shear rate found inside the fermenter whilst allowing rapid measurement and analysis.

2.5.4 Preparation of material for rheological characterisation

2.5.4.1 Cell paste and supernatant

Cell paste was obtained for rheological measurements by taking 50 mL samples from the fermenter, and clarifying twice for 30 minutes each, at 10°C and 1,431 rcf (4,000 rpm), using an Eppendorf Centrifuge 5810R (Eppendorf AG, Germany), and removing the supernatant after each run.

2.5.4.2 DNA and protein

Herring Sperm DNA (Promega, Madison, Wisconsin, USA) was used as representative DNA to fabricate lysed cell suspensions. Bovine serum albumin (BSA) was used as a representative protein to fabricate lysed cell suspensions.

2.6 Cell broth processing: primary recovery studies

2.6.1 Flocculation studies

A 25% w/v polyethyleneimine (PEI, $(C_2H_5N)n$, M_w = 50,000-100,000; MP Biomedicals SARL, Illkirch Cedex, France) water-based solution was prepared and mixed for 1 h at 21°C (dilution was necessary because 100% PEI is extremely viscous). The PEI solution was then added dropwise to the cell broth to a total of 100 mL (final concentration of 0.5-1.5% w/v), at the tip of the impeller in a 200 mL baffled mixing vessel fitted with a Rushton impeller (six-bladed, 2.5 cm diameter, stirred at 1,080 rpm, Re = 2,250, $\bar{G} = (P/V\eta)^{0.5}$ = 700 s^{-1}, where $\bar{G}$ is the mean velocity gradient, P/V is the power dissipated per unit volume, η is the suspension viscosity (Pa s) and Re is the Reynolds number), and controlled by a Caframo Stirrer (BDC1850-220, Caframo Limited, Ontario, Canada). To reach maximum floc strength (Bell and Dunnill, 1982), the solution was left to mix for 0.5 h at 21°C, where $\bar{G}t \sim 1.25 \times 10^6$ ($\bar{G}t > 1 \times 10^5$ is required to reach maximum floc strength).

2.6.2 Periplasmic extraction

Periplasmic extraction was carried out according to UCB Pharma (Slough, UK) protocol using extraction buffer containing 10 mM EDTA and 100 mM Tris, at pH 7.4. After centrifugation, cells were re-suspended in a 1:7 w/v ratio (cells: buffer) and incubated in a shaker-incubator at 60°C and 250 rpm for 12 h.

2.6.3 Ultra scale-down studies

2.6.4 Ultra scale-down centrifugation

In order to mimic large scale centrifugation, the shear (e.g. shear experienced in the feed zone of a large scale centrifuge or due to solids discharge in centrifugation) and centrifugation steps were decoupled, as carried out and described in detail elsewhere (Chatel et al., 2014; Rayat et al., 2016; Voulgaris et al., 2016).

2.6.4.1 Ultra scale-down shear studies

Samples were exposed to shear stress in an ultra scale-down (USD) rotary disc shear device (kompAs^{TM} shear device, 20 mL stainless steel chamber of 50 mm internal diameter and 10 mm height, fitted with a stainless steel rotating disc of 40 mm diameter and 1 mm thickness, with disc speed 0-20,000 rpm) for 20 s, controlled by a custom designed power pack (UCL Mechanical Workshop) at either 14,000 rpm or 8,000 rpm (equivalent to 1.04 x 10^6 W kg^{-1} and 1.30 x 10^5 W kg^{-1} maximum energy dissipation rates (ε) respectively, determined by a computational fluid dynamics empirical correlation (Figure 2-2), as described by Chatel et al. (2014)) and adapted from Levy et al. (1999).
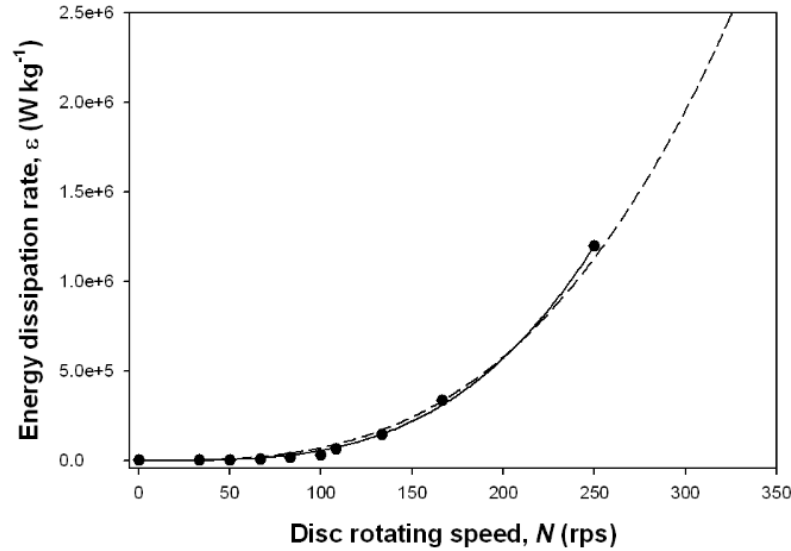
Figure 2-2: Correlation for the predicted maximum energy dissipation rate, ε, (W kg^{-1}) as a function of disc speed, N, (revolutions per second, rps), at the tip of the rotating disc in the USD shear device. Correlation developed by computational fluid dynamics (adapted from Levy et al. (1999)), ● (where — is the line of best fit), and relationship determined based on fluid dynamic analysis ($\varepsilon = 1.7 \times 10^{-3} N^{3.71}$), − − −, (Chatel et al., 2014).

2.6.4.2 Ultra scale-down centrifugation studies

Following USD shear studies, centrifugation was carried out at small scale (Eppendorf Centrifuge 5810R, Eppendorf, Germany) for 5 min at 6,800 rpm (5,945 rcf) based on a $V_{lab}/t\sum_T$ of 1.96×10^{-8} m/s (corresponding to a mid-range flow rate of an industrial CSA disc stack centrifuge of 48 L h^{-1}, by correlating the corresponding flow rate and equivalent settling areas, as previously described (Chatel et al., 2014; Voulgaris et al., 2016)), following the equation:

$$\Sigma_T = \frac{(V_{lab}.\omega^2)}{(2.g.\ln(2.R_o / (R_o + R_i)))} \qquad \textbf{Equation 2-15}$$

where $\sum_T$ is the equivalent settling area (m^2), V_{lab} is the volume of process material in the centrifuge tube (m^3), ω is the radial speed (rad s^{-1}), g is acceleration due to gravity (m s^{-2}), and R_i and R_o are the inner and outer radii of the centrifuge tube (m).

All centrifugation was carried out at 10°C. Well-clarified supernatant was prepared by centrifugation for 30 min at maximum rcf (16,100 rcf or 13,200 rpm, Eppendorf Centrifuge 5415R, Eppendorf, Germany).

The solids remaining (S) was characterized by:

$$S = \frac{(OD_s - OD_w)}{(OD_f - OD_w)} \times 100\%$$

Equation 2-16

where OD_s is the optical density (at 600 nm) of the supernatant, OD_w is the optical density of the well-clarified sample and OD_f is the optical density of the feed sample.

2.6.5 Ultra scale-down depth filtration

Ultra scale-down depth filtration was performed on a liquid handling robotic platform (Tecan Freedom EVO₁, fitted with a TeVacS two-position vacuum filtration manifold, Tecan Group Ltd., Reading, UK). Custom made filter housings (UCL Mechanical Workshop) were fitted with $2.8 \times 10^{-5}\,m^2$ coupons of depth filter media, using a 90SP filter (0.1 μm nominal pore size, Zeta Plus SP Series, 3M, Diegem, Belgium). Each pre-cut filter was wetted with 4 mL milliQ water (milliQ water purification system, Merck Millipore, Abindgon, UK), followed by 5 mL of process material. Vacuum filtration was carried out at constant pressure ($\Delta P = 300$ mbar), with the feed volume monitored at 5 s intervals by the liquid handling arm of the Tecan robot. A script automatically plotted the permeate vs. time on an Excel spreadsheet.

2.6.6 Ultra scale-down crossflow filtration

Experiments were carried out using an automated crossflow filtration (CFF) system, ÄKTA Crossflow (GE Healthcare Life Sciences, UK), with a custom-made rotating disc filter (RDF) system (UCL Mechanical Workshop), geometrically similar to the rotating disc filter system used by Ma et al. (2010), however houses a 35 mm

diameter stainless steel disc and has a working volume of 5.3 mL. The USD membrane filtration device is designed to allow filtration of the material across the membrane at variable flux and pressure, and mimics crossflow filtration (representative of CFF at large scale) whilst operating in dead-end mode (using a similar approach to Ma et al. (2010)). The USD membrane filtration device is equipped with a motor, controlled by a speed control unit (UCL Mechanical Workshop), which ensures a constant rotational speed of the disc at a given rpm (4,000 - 6,000 rpm, corresponding to a feed flux of 1350 - 1950 L/m^2/h for large scale operation using a V-screen cassette). The device was equipped with a cooling jacket to maintain constant temperature, measured via a K-type thermocouple and logged using an USB Data Logger (Lascar Electronics Ltd, UK). 47 mm diameter membrane discs (effective membrane area of 13.2 cm^2, Merck Life Sciences KGaA, Germany) with a pore size of 500 kDa were used in the USD membrane filtration device. An illustration of the device can be seen in Figure 2-3.
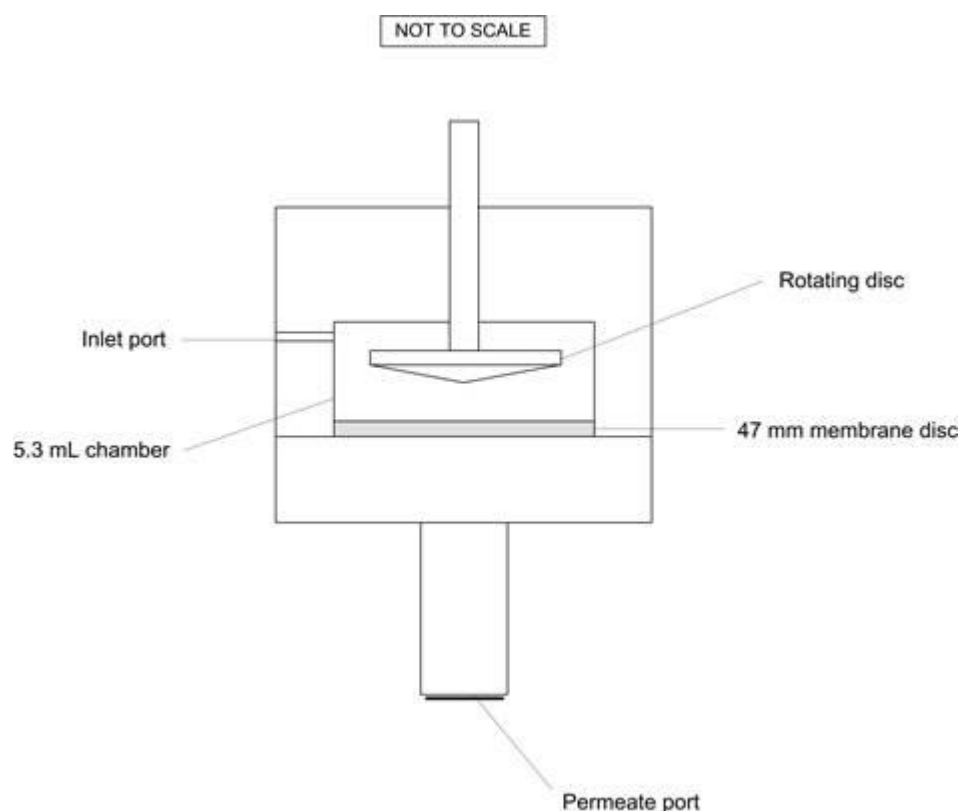
Figure 2-3: Cross-sectional illustration of the USD crossflow filtration device.

A new membrane was used for each run, pre-soaked and flushed with milliQ water, and water flux tests were carried out before and after to compare the normalised water permeability (NWP, normalised to 25°C). The feed flow rate was set using UNICORN v5.11, the control software, which also records the feed pressure (which, in the case of dead-end flow, is equal to the transmembrane pressure). Data was logged every 1.5 - 3 seconds. This work was carried out with Mr Mohd Shawkat Hussain (Department of Biochemical Engineering, University College London).

2.7 Computational methods

2.7.1 Modelling cell lysis

An empirical model was created to determine the extent of cell lysis from viscosity measurements using the "polyfit" function and the fit was evaluated using the "polyval" function in Matlab (The Mathworks, Inc., Natick, Massachusetts, USA). The model was created using a linear polyfit function (n_p=1, where n_p is the degree of polynomial fit). Data was normalised to perform the modelling, and de-normalised to obtain final results.

Chapter 3   Detecting cell lysis in *E. coli* fermentation using viscosity monitoring

The results presented in this chapter have been published in the journal Biotechnology Progress, "Detecting cell lysis using viscosity monitoring in *E. coli* fermentation to prevent product loss" (see Appendix).

3.1   Introduction

Cell lysis is often observed in the late stage of the fermentation process. Understanding this phenomenon has significance both scientifically and commercially. Traditionally, cell lysis is considered to be a consequence of "unbalanced" growth at the end stage of the bacterial life cycle. However, despite the numerous studies on autolysis, our knowledge is still limited. Lysis phenomena in microbial fermentations may be influenced by a variety of factors, including environmental conditions in the fermenter such as shear stress or poor mass and oxygen transfer, toxic waste product build-up in the media, metabolic burden from excessive recombinant protein expression, as well as internal stresses from a build-up of product within the intracellular environment. Advances in fermentation technology in recent years have led to the development of high cell density fermentation, which not only increases the product titre but also increases complications with respect to mass transfer in the dense population (Kleman and Strohl, 1994; Riesenberg and Guthke, 1999; Shiloach and Fass, 2005).

E. coli produce antibody fragments (Fab') that can be routinely targeted to the periplasmic space, a concentrated gel-like matrix in the space between the inner cytoplasmic membrane and the bacterial outer membrane (Spadiut et al., 2014). However, the capacity of the periplasm is limited; Fab' fragments will leak when exceeding 6% of the volume of the periplasm (Schofield et al., 2016). During fermentation, as the limit of the periplasm is reached, cells begin to lose viability and leak the Fab' product and other intracellular content to the fermentation broth.

Apart from product loss in late stage fermentation, the remaining viable cells become more fragile which can significantly impact the performance of many downstream

unit operations. For example, cells will break four-fold more than those harvested at an earlier stage, if subjected to the equivalent shear level of that in an industrial centrifuge (Chan et al., 2006; Balasundaram et al., 2009; Perez-Pardo et al., 2011; Aucamp et al., 2014). Lysis can also reduce microfiltration performance, for example increasing fouling and resistance (Okamoto et al., 2001; Meireles et al. 2003).

Therefore, monitoring cell lysis is particularly important for processes with host cells that store the product in the intracellular space. However, lysis is difficult to observe directly in fermentation, because it is inherently complex and current analytical technologies are unable to rapidly and accurately monitor the shift between optimal intracellular product concentration and leakage to the fermentation broth. Current industrial processes focus on solving this problem by monitoring cell density, product titre, product leakage and cell viability to determine harvesting time (Bowering, 2004; Perez-Pardo et al., 2011).

As cell lysis occurs in late stage fermentation, leakage of product to the fermentation broth also acts to increase the broth viscosity, as large quantities of chromosomal DNA and other intracellular content are released simultaneously into solution (Balasundaram et al., 2009; Nesbeth et al., 2011). Therefore, it is proposed that monitoring the viscosity of the cell broth during fermentation may be an efficient way to indirectly infer cell lysis, which would enable decision making about cell harvesting to prevent product loss in late stage fermentation.

The aim of this chapter is to develop a method to rapidly detect cell lysis in fermentation using viscosity monitoring. The specific objectives of this chapter are to:

- Characterise cell lysis in an industrially relevant *E. coli* fermentation using a range of analytical techniques

- Develop a method to rapidly detect cell lysis and product loss in fermentation using viscosity monitoring

- Evaluate viscosity monitoring against other common fermentation monitoring techniques

3.2   *E. coli* **fermentation**

The high cell density fermentation of *E. coli* w3110 was carried out in fed-batch mode in a 5 L working volume Applikon fermenter. As described in the Materials & methods (section 2.2), the cells were initially seeded in shake flasks using LB media before being transferred to a second shake flask with SM6Gc media, and grown to an optical density (OD_{600}) of 5 (cells in exponential phase) before inoculating the fermenter at 15% v/v.

The growth profile of two typical fermentation runs is shown in Figure 3-1. After inoculation, the lag phase in fermentation lasted until ~24 h, when the exponential phase subsequently began. Cells grew to a maximum dry cell weight (DCW) of 48 g/L for Figure 3-1 (a) and to 61 g/L for Figure 3-1 (b), which corresponded to an optical density of ~200 - 220. A dissolved oxygen tension (DOT) spike and a pH spike were observed at 36 - 38 h (see also Figure 3-2), which indicated complete utilisation of the carbon source (glycerol). At this point, isopropyl β-$_D$-1-thiogalactopyranoside (IPTG) was added to the fermenter, which triggered the over-expression of the TTOD A33 plasmid coding for antibody fragment (antigen-binding, Fab') production. At induction point, glycerol feeding began and was fed at a constant rate throughout the postinduction phase (6.4 mL h^{-1}). Fermentation runs were typically continued up to 60 h postinduction.

Cells growing in exponential phase allocate the vast majority of their energy to reproduction and growth, therefore only a very small concentration of Fab' product can be seen at induction point (36 - 38 h, Figure 3-1) and the rapid production of Fab' can be seen in stationary phase (after induction with IPTG), reaching 1.6 - 1.85 mg/mL total product by the end of the fermentation.

Taking Figure 3-1 (a) as an example; immediately after 38 h, a slight drop in cell density was observed, which can be attributed to a time lapse of ~30 min between the DOT spike and induction point (IPTG addition, plus starting the glycerol feed).

Following this, cell density (OD_{600} and DCW) was relatively constant in the stationary phase, although increased slightly between induction point at 38 h and 82 h, which is likely to be a result of mild overfeeding of glycerol in stationary phase. Nonetheless, Figure 3-1 (a) and (b) represents typical fermentation runs in terms of the growth profile and the Fab' production profile.

It can be seen in Figure 3-1 (a) that the stationary phase appears to continue until a drop in cell density was observed from 82 h onwards (44 h postinduction, seen from both OD_{600} data and DCW data). This coincided with a change in the rate of Fab' production, which also dropped significantly after 82 h. During fermentation runs it was observed that foaming occurred in exponential phase, and PPG (antifoam) addition was required (manually added drop-wise), however very little or no foaming occurred in stationary phase.

Figure 3-2 shows the corresponding online control data during two typical fermentation runs. As described in Materials & methods (section 2.2.4), the proportional integral derivative (PID) control systems for temperature, pH and DOT were improved in early fermentation runs, and displays an enhanced control system Figure 3-2for the Applikon fermenter. Data points were recorded every 2 min from the Applikon control system and smoothed using the "prune" function in Prism software (GraphPad Prism 7, Inc., La Jolla, California, USA) in order to plot Figure 3-2 (every two data points were averaged).

Taking Figure 3-2 (a) as an example, pH was controlled at 6.95 ± 0.05, however two spikes are noticeable between 20-30 h, due to the addition of sodium phosphate shots (sodium phosphate is acidic). These shots are added to help stabilise the structure of the outer cell membrane of the cells during rapid (exponential) growth by binding with lipopolysaccharide (Chen et al., 2004). A pH spike was also observed at induction point. This is because the *E. coli* cells produce (and release) lactic acid during cell growth, therefore base (12% v/v ammonia solution) is added throughout the exponential phase. At the point that cells run out of glycerol, lactic acid suddenly stops being produced, and the continued addition of base causes the pH to shoot up

(i.e. before the PID control system kicks in). After induction with IPTG, pH control was very good.

Temperature was controlled at 30°C ± 1 until an OD_{600} of 38 was reached, and reduced to 25°C ± 1 thereafter. Temperature was accurately controlled using a mixture of a cooling coil (water cooled to 6°C) that runs inside the fermenter and a heating jacket that surrounds the vessel.

Dissolved oxygen tension (DOT) was controlled at 30% ± 5 for the duration of the fermentation, except in Figure 3-2 (a) between 30-52 h, where DOT fluctuated significantly (in exponential phase and immediately after), i.e. ± 10%. Therefore, in order to protect the cells and ensure that excess oxygen was present in the media, the DOT set point was increased to 32% for this duration. This strategy was not adopted for all fermentation runs. Figure 3-2 (b) also shows some fluctuation in the DOT and stirrer rate data in exponential phase, with occasional spikes above ± 10%. However, in postinduction culture, DOT control for all fermentation runs was very good.

DOT was maintained at 30% using a cascade control system, with agitation (stirrer rate controlled between 300-1200 rpm) and oxygen gas blending, so that the oxygen gas addition was implemented as the stirrer rate increased to the maximum of 1200 rpm. In the early stage of the fermentation, the stirrer rate increased to cope with the increased oxygen demand of the growing cell population, until early exponential phase (~24 h) where the stirrer rate continued increasing, however started to fluctuate significantly. This was also reflected in the fluctuation of the DOT. This fluctuation was caused by oxygen gas blending, which began in exponential phase and continued until induction point. After the dissolved oxygen spike at 36 - 38 h, the stirrer rate dropped to ~700 - 800 rpm and steadily increased during stationary phase until ~65 - 80 h, where the stirrer rate began to rapidly increase. The increase in stirrer speed from 65 h reflects the challenges of mass and oxygen transfer in late stage fermentation as the broth viscosity increases during cell lysis.

Although the DOT was generally well controlled, the PID controller for DOT could be further optimised in the future as there was some fluctuation in the stirrer rate and

DOT in exponential phase, particularly when oxygen gas blending was implemented. This is because the addition of oxygen presents a burden on the PID controller, i.e. the cascade control system must handle two control loops; stirrer rate and oxygen gas addition. The fermenter setup may therefore require more controlled oxygen addition or a different PID control for different growth phases i.e. different controller settings for exponential phase, stationary phase etc. However, this was not the focus of the present study.

However, Figure 3-1 and Figure 3-2 demonstrate that although there was some variation between dry cell weight, OD and total Fab' concentration between runs (which is to be expected in fermentation), the reproducibility of the fermentation system was good.
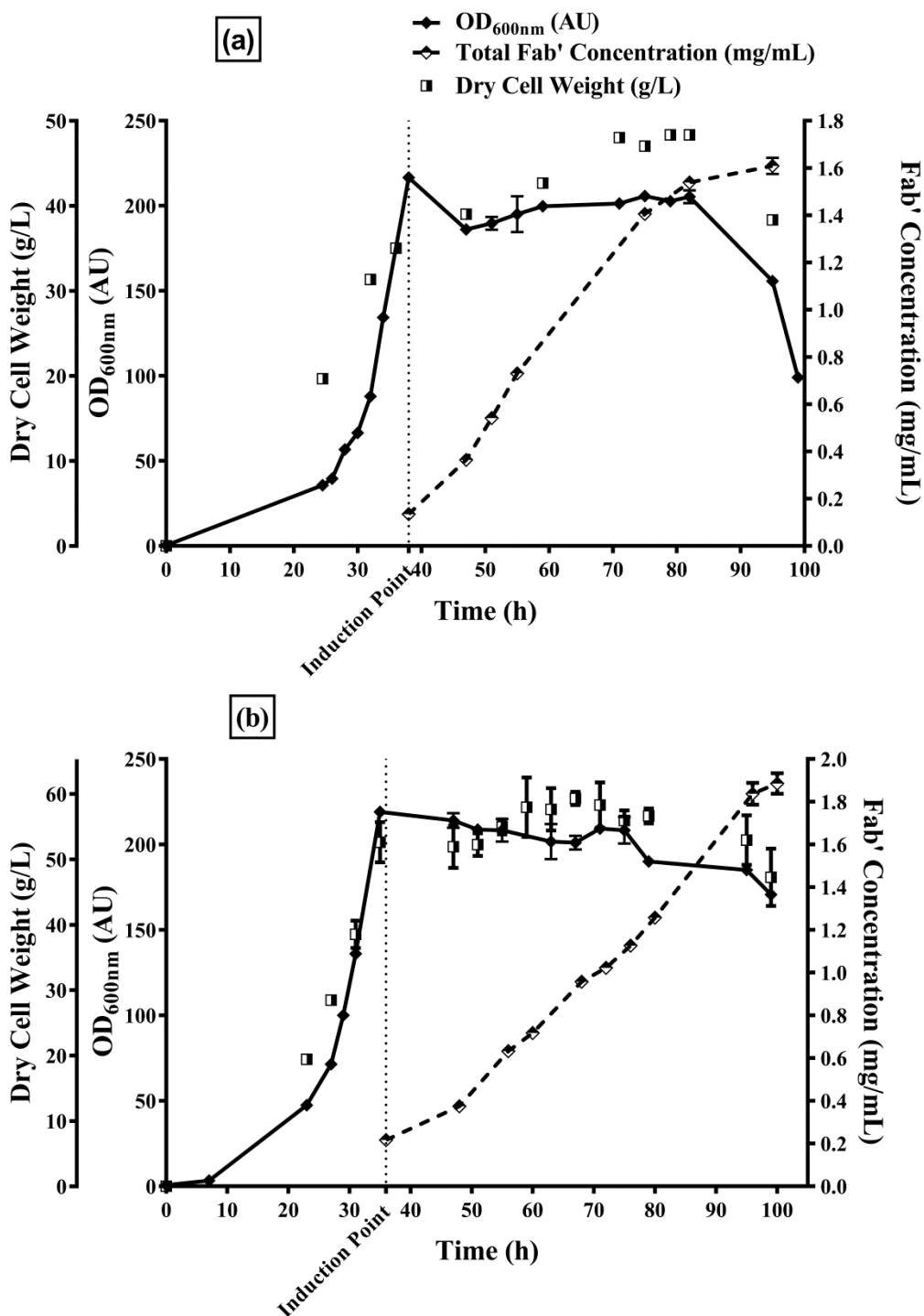
Figure 3-1: Characterisation of two typical *E. coli* fermentation runs. Optical density at 600 nm (absorbance units (AU), in triplicate), dry cell weight (g/L, in triplicate) and total Fab' concentration (mg/mL, in duplicate). Cells induced with IPTG at 36 - 38 h, after a dissolved oxygen tension spike was observed. Dry cell weight reached a maximum of 48 g/L and 61 g/L, respectively; total Fab' concentration reached 1.6 mg/mL and 1.85 g/L respectively at the end of the fermentation. Error bars show standard deviation.

111
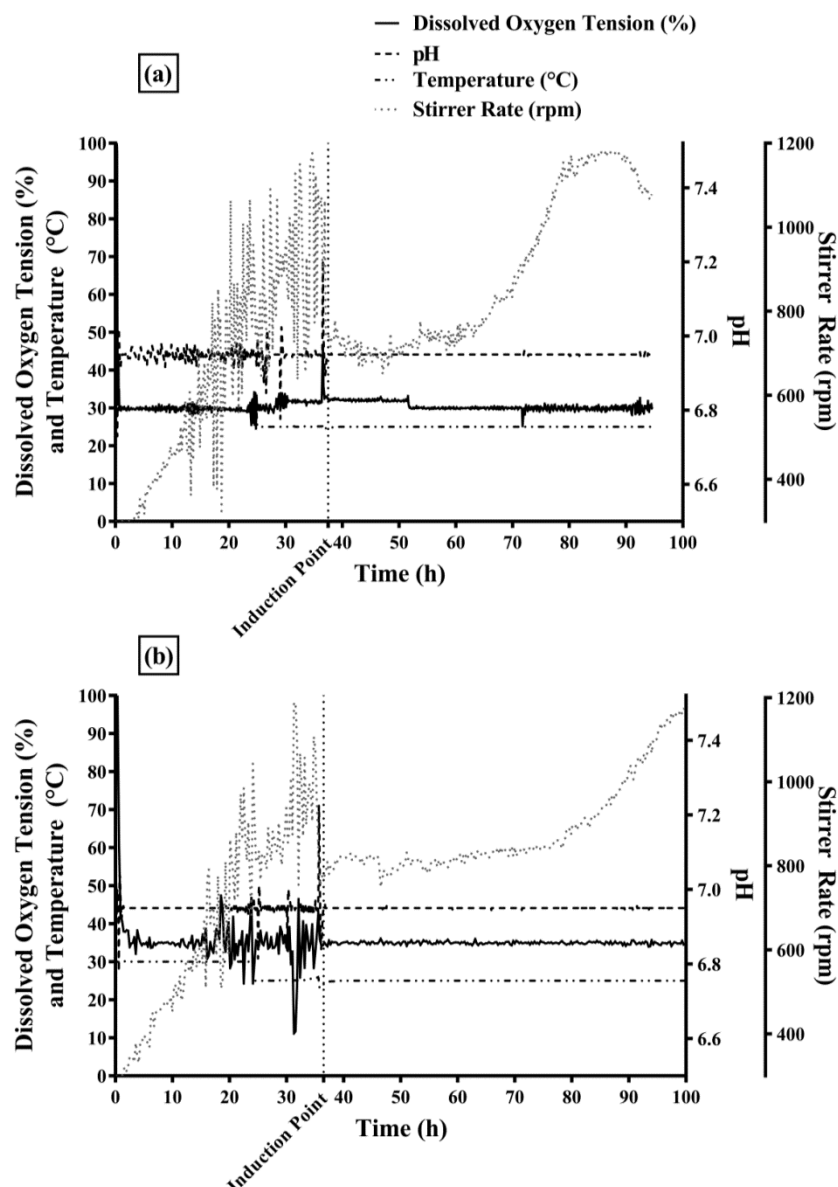
Figure 3-2: Online fermenter controls for two typical *E. coli* fermentation runs. Cells were induced with IPTG at 36 - 38 h, after a dissolved oxygen tension spike was observed. Temperature was controlled at 30°C ± 1 until an OD_{600} of 38 was reached, and maintained at 25°C ± 1 thereafter. pH was controlled at 6.95 ± 0.05; two spikes between 20-30 h correspond to sodium phosphate shot additions (see Materials & methods), and a spike at 36 - 38 h corresponds to the induction point. Stirrer rate was controlled between 300-1200 rpm. Dissolved oxygen tension (DOT) was controlled at 30% ± 5 for the fermentation duration, except for (a) between 30-52 h, where DOT fluctuated significantly (± 10%) and was subsequently controlled at 32%. (b) also shows fluctuation in the DOT and stirrer rate data in exponential phase, with occasional spikes above ± 10%. Data was recorded every 2 min, and smoothed using the "prune" function in Prism software (GraphPad Prism 7, Inc., La Jolla, California, USA) to reduce the number of data points (every two data points averaged).

112

3.3 Characterising cell lysis in fermentation

Before assessing the ability of viscosity to detect and monitor cell lysis in fermentation, it was first necessary to characterise cell lysis using a range of analytical techniques, in order to better understand the mechanisms of lysis.

3.3.1 Defining cell lysis and cell viability

The definitions of cell lysis and cell viability differ. Cell lysis is defined as the release of DNA from the cell due to total disruption of the cell membrane. Cell viability relates to the intactness of the cell membrane, i.e. if the cell membrane is non-intact, intracellular content will leak from the cell through porous membrane channels. It is believed that cells with non-intact membranes, i.e. leaking product or other intracellular content, may have the potential to recover. However if DNA is lost from the cell, the cell can be classed as dead.

3.3.2 Determining the optimal harvest time

In the fermentation system under study, the Fab' product is produced and then targeted to the periplasm of the *E. coli* cell, until the cells lose viability, product leaks to the broth and cell lysis occurs. Traditionally, it is desired to maximise the intracellular product concentration in fermentation, and therefore harvest the cells before significant product loss occurs. For this reason, it is important to characterise the product profiles in fermentation, in order to determine the point of loss of viability and hence product loss, and subsequently define the optimal harvest point.

Having observed the rate of total production of the Fab' product in Figure 3-1, the intracellular Fab' concentration and Fab' leakage profiles are shown (postinduction) in Figure 3-3 (a) from the fermentation run presented in Figure 3-1 (a). It can be seen that the intracellular product concentration increased rapidly after induction and reached a maximum of 1.2 mg/mL at 36 h postinduction (74 h total fermentation time), decreasing quickly thereafter.
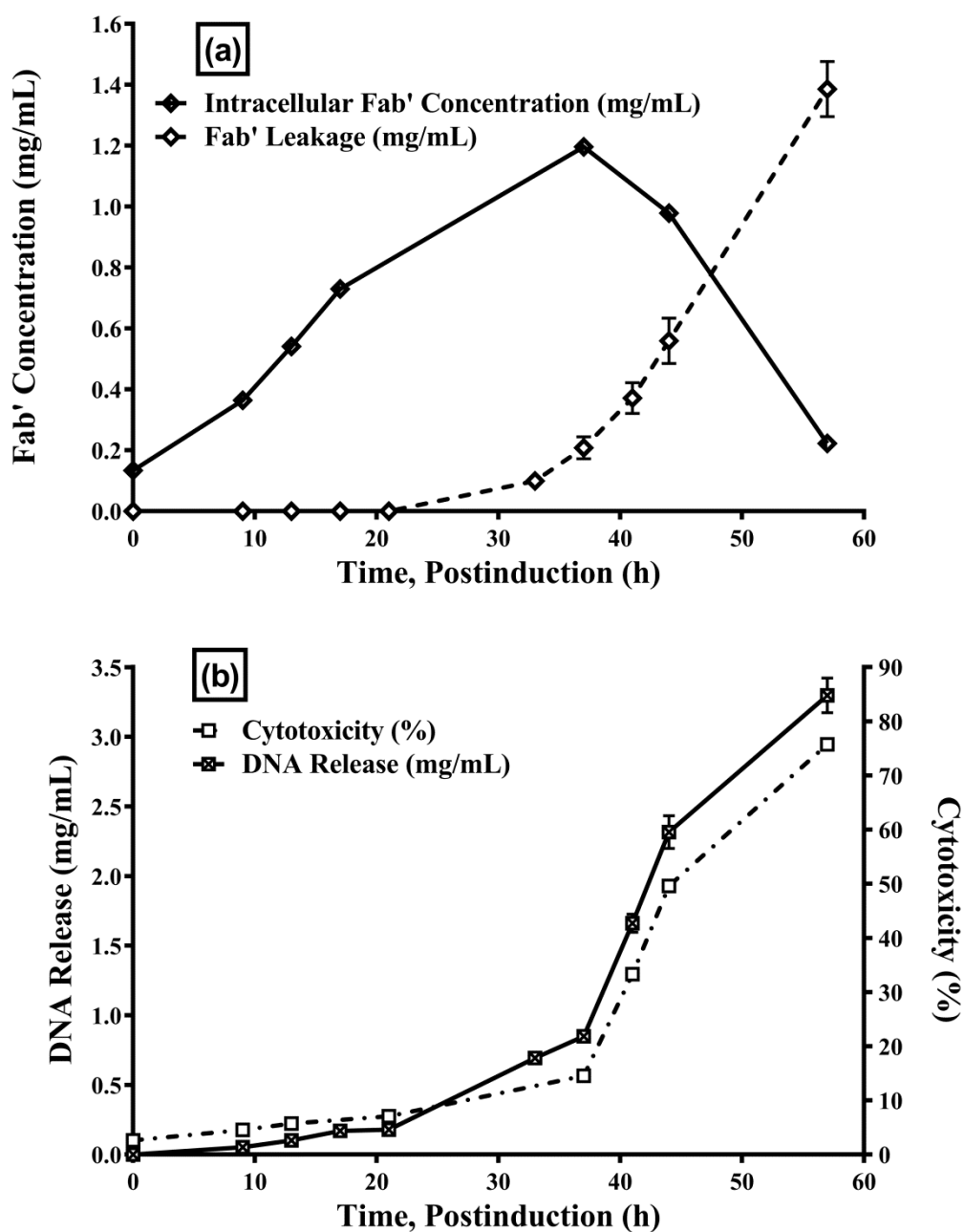
Figure 3-3: Analytical characterisation of cell lysis in an *E. coli* Fab' fermentation. (a) Intracellular Fab' concentration and Fab' leakage to the cell broth (data shown postinduction, mg/mL, in duplicate). (b) Cytotoxicity data (based on lactate dehydrogenase (LDH) release to the cell broth, data shown postinduction, %, in triplicate) and double stranded DNA (dsDNA) release (data shown postinduction, mg/mL, in triplicate). Error bars show standard deviation.

In contrast, the product leakage profile (i.e. product leaked to the broth) shown in Figure 3-3 (a) is at zero initially after induction, until 10% product leakage (calculated as a percentage of the total product at each time point) was observed at 33 h postinduction (71 h total fermentation time), and product loss increased rapidly from this point. At 36 h postinduction, 25% of the product had already leaked to the broth, although the maximum intracellular product concentration corresponded to this time point. If cells were harvested at 36 h postinduction at manufacturing scale, the risk of additional cell lysis and product loss in subsequent unit operations (i.e. holding time after harvesting, microfiltration and centrifugation) is extremely high due to the shear environment and processing time in the respective unit operations.

HPLC is a robust method to characterise and quantify product profiles such as leakage, and shows the rapid deterioration of cells from 33 h postinduction onwards. Therefore, for this fermentation system, 33 h postinduction was chosen as the optimal harvest time in order to minimise product loss in subsequent downstream unit operations.

3.3.3 Understanding the relationship between cell lysis and viability

As cells lose viability and cell lysis occurs in fermentation, intracellular content such as the product, host cell protein and nucleic acids are released to the cell broth. In Figure 3-3 (b), the postinduction profiles for double stranded DNA (dsDNA) and cell cytotoxicity are shown. The cytotoxicity assay is based on lactate dehydrogenase (LDH); a stable marker (cytosolic enzyme) that is released due to the loss of cell membrane integrity. Loss of membrane integrity implies loss of cell viability and hence product leakage. Cytotoxicity is presented as a ratio of LDH in the supernatant to total LDH, at each time point.

As shown in Figure 3-3 (b), dsDNA release and cytotoxicity were both low immediately after induction. dsDNA content remained below 0.5 mg/mL and cytotoxicity was below 10% until 33h postinduction, where a rapid increase in both dsDNA release and cytotoxicity were observed thereafter. The dsDNA release and cytotoxicity profiles both correlated well with each other and with the Fab' leakage profile shown in Figure 3-3 (a).

The flow cytometry plots in Figure 3-4 demonstrate this phenomenon further. For each plot, the upper left (UL) quadrant denotes dead cells and cell fragments, the upper right (UR) quadrant denotes PI stained cells (nonviable), the lower left (LL) quadrant denotes viable, polarised cells, and the lower right (LR) quadrant denotes viable cells that have been stained by BOX (depolarised cell membranes).

Plot (a) in Figure 3-4 shows highly viable cells in mid-exponential phase; 99.6% were viable (LL and LR quadrants), and in mid-stationary phase (36 h postinduction; as seen in plot (b)), 98.1% of cells were viable. However at this point, 25.5% of these cells have been stained by bis-oxonol (BOX) and therefore had depolarised membranes. Technically, cells with depolarised membranes are classed as viable cells as they have the potential to recover if transferred to fresh media, however, their membranes are non-intact and will leak considerable quantities of product and other intracellular content if left exposed to the harsh shear environment inside the fermenter.

At 57 h postinduction, shown in Figure 3-4 (c), 93% of the cells were viable; 33.2% had polarised membranes and 59.8% had depolarised membranes, and 6.8% of cells were nonviable (i.e. stained with propidium iodide (PI)). However, at 57 h postinduction, almost 90% of the Fab' product had been lost to the fermentation broth. Therefore, although cells with depolarised membrane channels are still technically "viable," in terms of fermentation; it can be said that they have lost the ability to produce and retain product in the periplasm.

According to the traditional definitions of cell lysis and viability stated at the beginning of this section (3.3), if cells are leaking DNA then lysis is occurring. With regards to the fermentation of cells producing a product that is stored in the intracellular space (i.e. inside the periplasm); if the cells are leaking product, that is, have depolarised, non-intact cell membranes, they can be classed as nonviable. Figure 3-3 and Figure 3-4 therefore demonstrate that lysis, loss of cell viability and product loss occur simultaneously in fermentation.

(a)

(b)

(c)
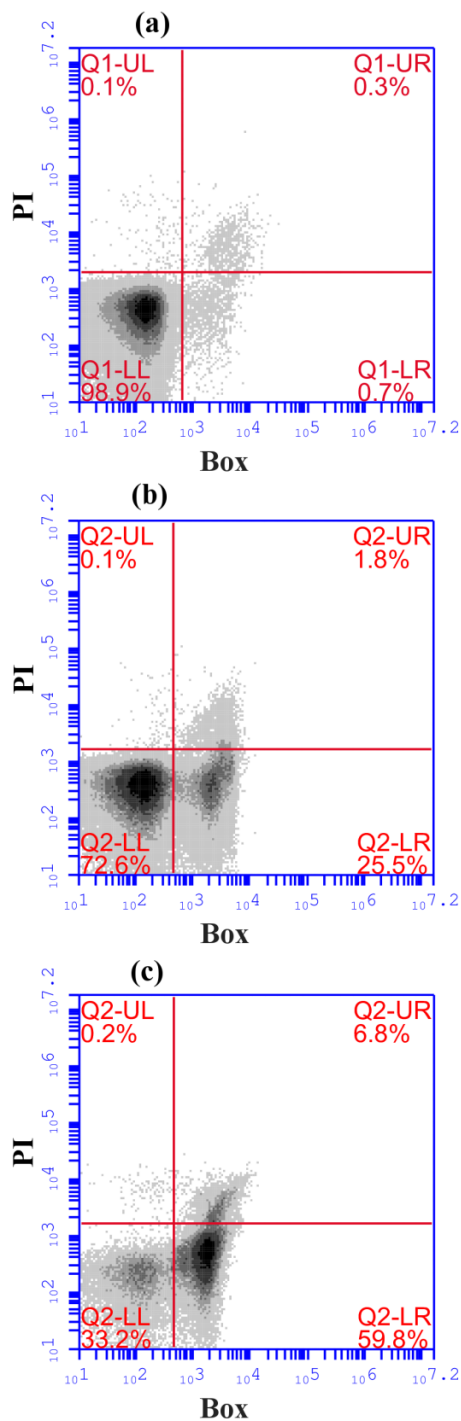
Figure 3-4: Flow cytometry plots for BOX (bis-oxonol) and PI (propidium iodide) stains. For each plot, UL quadrant denotes dead cells and cell fragments, UR quadrant denotes PI stained cells (nonviable), LL quadrant denotes viable, polarised cells, and LR quadrant denotes viable cells that have been stained by BOX (depolarised cell membrane). (a) Sample was taken in mid-exponential phase, (b) sample was taken in mid-stationary phase at the onset of cell lysis (36 h postinduction), and (c) sample was taken in late stationary/decay phase (57 h postinduction). Samples were measured in triplicate.

117

Scanning Electron Microscopy (SEM) images were taken of *E. coli* cells throughout a fermentation to provide qualitative observation of cell lysis and are shown in Figure 3-5. Figure 3-5 (a) shows highly viable cells, with largely intact cell membranes in early stage postinduction culture (i.e. early stationary phase). Figure 3-5 (b) shows three things in late stage postinduction culture (i.e. late stationary/decay phase); (1) some healthy, viable cells, (2) swollen cells and (3) empty shells of lysed cells. This suggests that the over-expression and subsequent build-up of product within the periplasm (the capacity of the periplasm is limited to 6% (Schofield et al., 2016)) has a significant stress on the metabolism of the cells, leading to a loss of the cell's ability to maintain their osmotic balance in late-stage fermentation, seen by the swelling and bursting of the cells in Figure 3-5 (b).
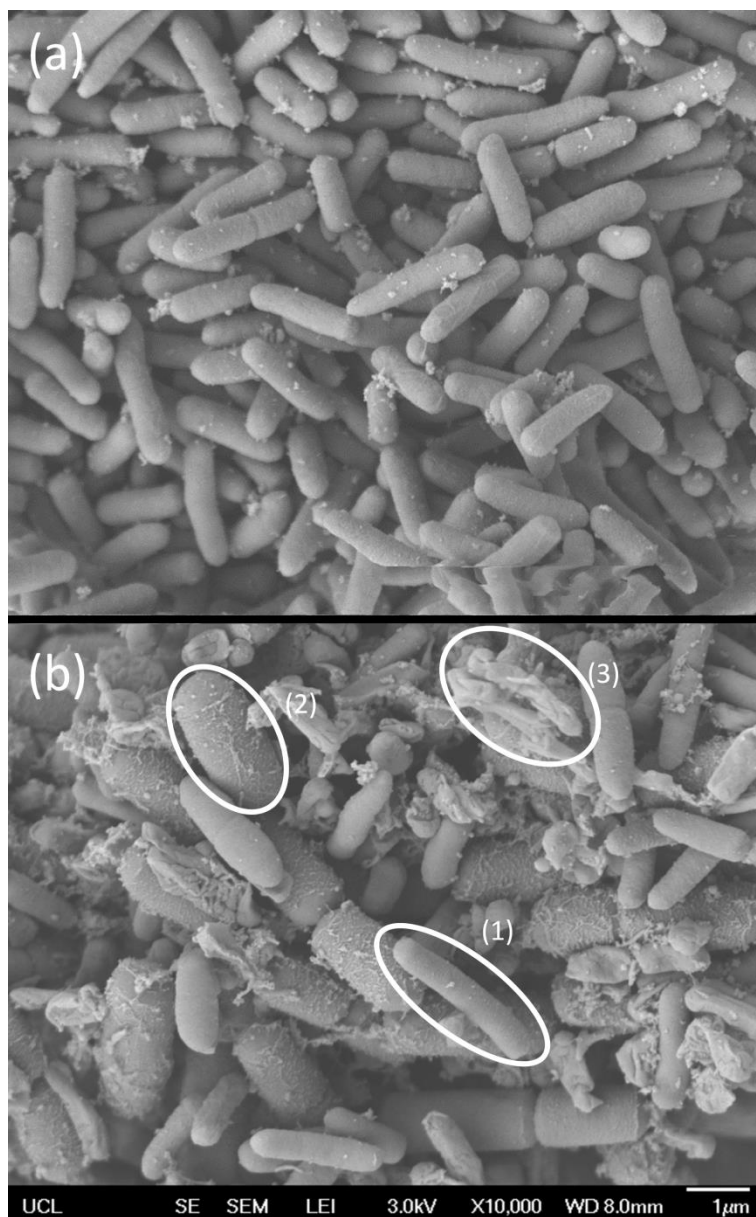
Figure 3-5: Scanning Electron Microscopy (SEM) images at x10,000 magnification. (a) SEM image of an *E. coli* fermentation sample in early stationary phase. (b) SEM image of an *E. coli* fermentation sample in late stationary phase/decay phase, showing; (1) healthy cells, (2) swollen cells, and (3) shells of lysed cells.

3.4 Developing a method to detect cell lysis using viscosity

3.4.1 Determining the viscosity profile of an *E. coli* fermentation

After characterising cell lysis in an *E. coli* fermentation, it was important to establish the viscosity profile of the cell broth under study, in order to assess the feasibility of using viscosity as a monitoring tool to detect cell lysis and product loss.

3.4.1.1 Flow curves

The classic method to determine a fluid's resistance to flow i.e. its viscosity, is to carry out viscometry testing to obtain the flow curve (shear viscosity vs. shear rate). Therefore, viscometry measurements were carried out over the course of a fermentation to obtain flow curves, observe any changes in the rheological behaviour of the cell broth and determine the shear viscosity profile.

No sample preparation was required to obtain the flow curves, and the cell broth (1 mL sample volume) was added directly to the Malvern Instruments Kinexus Lab + rheometer. Viscometry measurements were taken over a shear rate range of 100-1000 s^{-1}, and the resultant shear stress was measured and recorded automatically after a steady state value was maintained for 10 seconds. Measurements were carried out using 50 mm parallel plates at 25°C and a 300 μm gap size. As a general heuristic, the gap size used should be at least 3-fold larger than the largest particle in the sample (*E. coli* cells are ~1-2 μm). Single measurements were carried out for the Kinexus rheometer as the steady state measurement allowed multiple readings to be taken and averaged over 10 seconds.

The flow curves for a typical fermentation run, taken at various points throughout the fermentation, are presented in Figure 3-6. The flow curve of the SM6Gc media is presented for reference (~0.00114 Pa s), and has a higher viscosity than that of water at 25°C (0.001 Pa s), due to the presence of glycerol and other components such as salts in the media (see Table 2-1 and Table 2-2 in Materials & methods). Figure 3-6 shows that the viscosity increased during exponential phase and then continued to increase significantly as the fermentation progressed from stationary phase to cell lysis (induction with IPTG was at 38 h). Importantly, the flow curves presented in

Figure 3-6 show a clear difference in the viscosity over the course of the fermentation.

Shear thinning behaviour is often observed in high cell density fermentation broths that have been partially or wholly disrupted to release their intracellular content, for example, after homogenisation using low pressures and a minimum number of passes (Li et al., 2012), or during fermentation (Furuse et al., 2002), particularly for yeast and filamentous fungi. The extent of non-Newtonian behaviour has implications on various processing conditions such as pumping requirements, and is often used in quality control to characterise materials. The non-Newtonian behaviour of a fluid can be determined by the flow behaviour index, n, which is a measure of the linearity of the flow curve. A Newtonian fluid has a flow behaviour index of 1 (where the viscosity is independent of the shear rate, i.e. the flow curve is linear); a shear thinning fluid has a flow behaviour index of less than 1; and a shear thickening fluid has a flow behaviour index of greater than 1. As the flow behaviour index moves further away from 1, the non-Newtonian behaviour becomes increasingly apparent.

In Figure 3-6, it can be seen that the shear thinning behaviour increases as the fermentation progresses; the flow curves for early stage stationary phase, late stage stationary phase and cell lysis show that the viscosity decreases as the shear rate increases, and becomes increasingly apparent as the fermentation progresses. Table 2-1 presents the values of flow behaviour index for each sample in Figure 3-6, demonstrating that the shear thinning behaviour increased to 0.860 as significant cell lysis took place. This shear thinning behaviour is thought to be caused by structural interactions between cells, cell debris and high molecular weight species, such as nucleic acids, that are released to the fermentation broth during cell lysis. As seen in Figure 3-3 (b), significant quantities of high molecular weight dsDNA and other intracellular content were released to the broth as the fermentation progressed, which contributed to the increase in shear thinning behaviour seen in Figure 3-6.

However, the flow behaviour index, n, remained above 0.85 for all samples, demonstrating that the shear thinning behaviour was relatively mild in this *E. coli* fermentation system. This implies that there is only a slight structure in the cell broth

during fermentation, as low cell concentrations are present in fermentation broths in comparison to homogenisation feeds (which typically have significant structure).
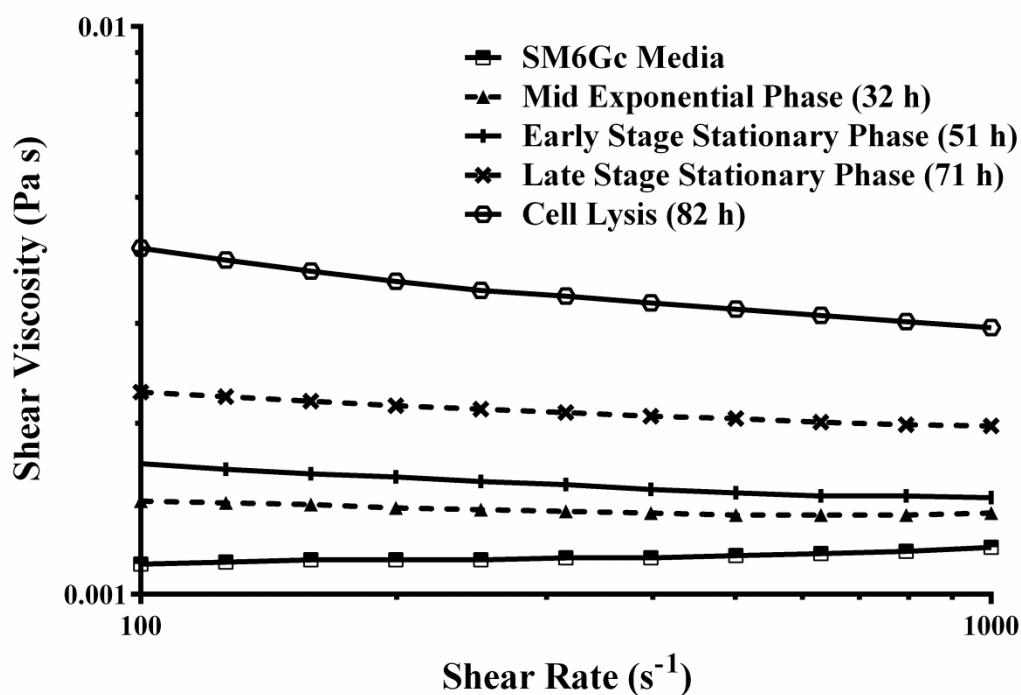
Figure 3-6: Viscometry flow curves of *E. coli* cell broth at various times throughout fermentation, over a shear rate of 100-1000 s^{-1}, using a Malvern Instruments Kinexus Lab + rotational rheometer. Induction time was at 38 h using IPTG. Measurements were carried out at 25°C using 50 mm parallel plates and a 300 μm gap size. An increase in shear thinning behaviour is evident as the fermentation proceeded (flow behaviour index, n, was greater than 0.85 for all samples). Single viscometry measurements were recorded at each shear rate, and held at steady state for 10 seconds.

Table 3-1: Flow behaviour index (n) values for the flow curves presented in Figure 3-6 of *E. coli* cell broth at various times throughout fermentation, over a shear rate of 100-1000 s^{-1}, using a Malvern Instruments Kinexus Lab + rotational rheometer. Induction time was at 38 h using IPTG. Measurements were carried out at 25°C using 50 mm parallel plates and a 300 μm gap size. An increase in shear thinning behaviour is evident as the fermentation proceeded (flow behaviour index, n, was greater than 0.85 for all samples). Single viscometry measurements were recorded at each shear rate, and held at steady state for 10 seconds.

Sample	Flow behaviour index, n
SM6Gc media	1.028
Mid exponential phase (32 h)	0.977
Early stage stationary phase (51 h)	0.939
Late stage stationary phase (71 h)	0.939
Cell lysis (82 h)	0.860

3.4.1.2   Viscosity profile in fermentation

After obtaining the flow curves for the cell broth throughout a fermentation, it was essential to assess the shear viscosity of the cell broth vs. fermentation time. For this, a single value of viscosity was required to plot vs. time.

For Newtonian fluids, the viscosity is independent of the shear rate, therefore the viscosity can be determined from the gradient of the straight line curve of shear stress vs. shear rate. However, for fluids that exhibit non-Newtonian behaviour, the viscosity changes as the shear rate changes. Therefore, for non-Newtonian fluids, either the apparent viscosity can be determined or a single value of viscosity can be used from a single shear rate. The methodology for viscosity determination was discussed in detail in Materials & methods (section 2.5). Therefore, measurement of viscosity at a single shear rate was used to determine the viscosity of the broth. This has two main advantages.

First, in order to mimic the shear environment experienced inside the fermenter, the average shear rate in the fermenter could be calculated (see section 2.5 in Materials & methods) and the viscosity of the cell broth could then be determined at this shear rate using the rheometer. The average shear rate was determined to be 50-200 s^{-1}. This is because the fermenter uses a cascade control system, where agitation varies between 300-1200 rpm in order to control DOT at 30%.

Secondly, in order to rapidly determine the viscosity of the cell broth at-line, and enable decision-making about cell harvesting; viscosity determination at a single shear rate removes the need to obtain the entire flow curve (in order to then calculate the apparent viscosity), and reduces the measurement time from 10 min to under 2 min.

Therefore a shear rate of 100 s^{-1} was chosen as the characteristic parameter to obtain shear viscosity values. This enabled rapid data acquisition and was representative of the shear environment within the bioreactor (between 50-200 s^{-1}). Although the impeller speed fluctuated significantly during exponential phase, this did not happen in postinduction fermentation, where the impeller speed can be seen to be stable (see

Figure 3-2). Therefore, for the purpose of detecting cell lysis in postinduction fermentation, the average shear rate calculated in section 2.5 (Materials & methods) is appropriate for this growth phase.

Another important consideration is that at lower shear rates, the measurement will pick up more of the polymer interactions (e.g. nucleic acids) that are thought to cause an increase in viscosity during cell lysis, and hence enables more precise observation of cell lysis.

The viscosity of fermentation broths is determined by two factors; cell concentration and solute concentration in the broth (assuming other factors such as media composition, temperature, aeration and agitation are constant) (Reardon and Scheper, 1991).

Figure 3-7 (a) shows the viscosity profile obtained using the Kinexus rheometer during a typical fermentation run. The growth profile (OD_{600}) is presented as a reference. The shear viscosity of the cell broth increased correspondingly to the increase in cell density during exponential phase, up to 38 h when a dissolved oxygen spike was observed and the cells were subsequently induced with IPTG. At this point, the cell density in stationary phase remained constant, and a relatively flat viscosity profile was observed, until 71 h (33 h postinduction), where a rapid increase in the viscosity was seen. Although the cell density increase in exponential phase was large, the resulting increase in viscosity was relatively small. As cell lysis progressed, a much larger increase in viscosity was observed (~2.5-fold increase in viscosity observed at the end of the fermentation, in relation to the viscosity in early stationary phase).

The viscosity profile shown in Figure 3-7 (a) correlates well with the increase in cell density in the growth phase. Additionally, the postinduction viscosity profile closely follows the cell lysis trends observed through HPLC (product leakage), flow cytometry, DNA release and cytotoxicity.
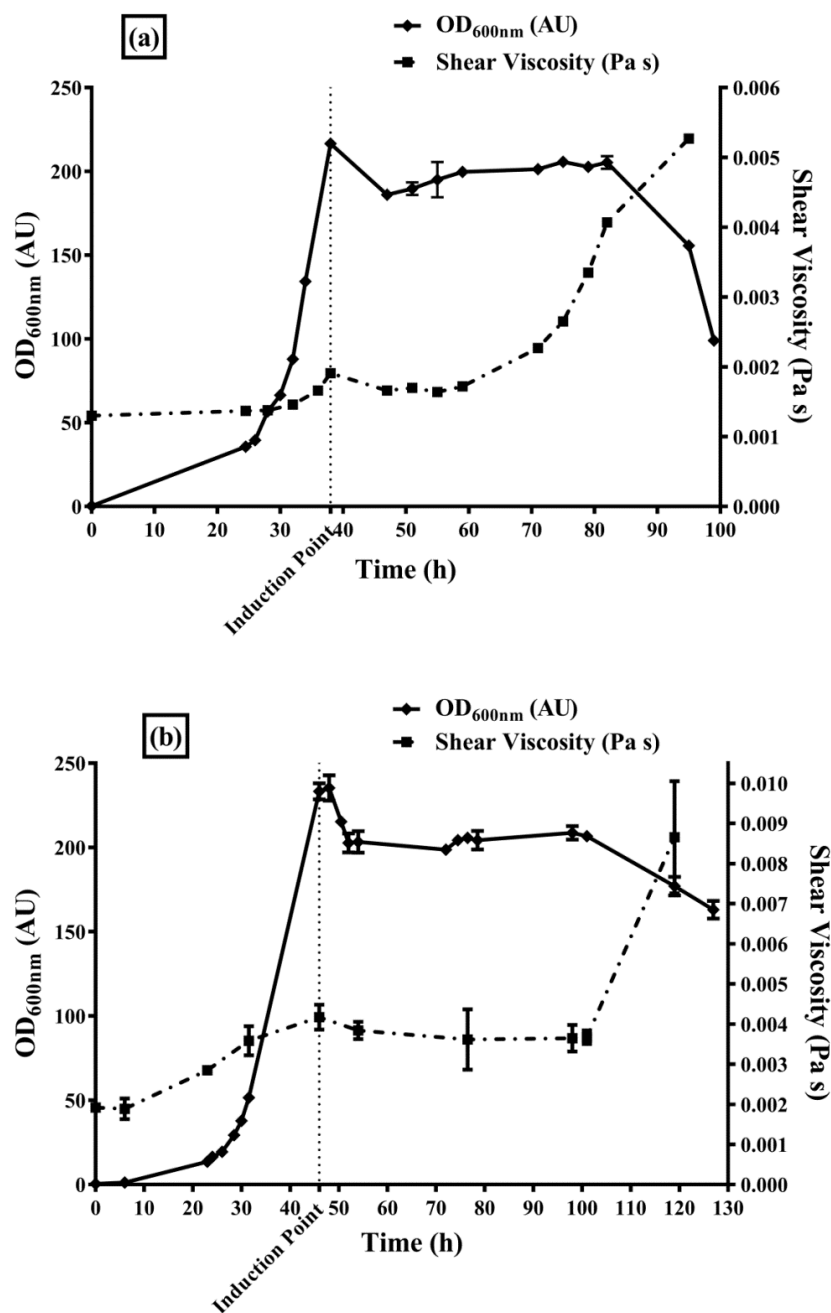
Figure 3-7: Comparison of two rheological instruments to measure viscosity. Optical density measured at 600 nm (absorbance units, AU, in triplicate). (a) Shear viscosity (Pa s, single measurement, held at steady state for 10 seconds) measured at 100 s^{-1} with a Malvern Instruments Kinexus Lab + rotational rheometer, at 25°C using 50 mm parallel plates and a 300 μm gap size. Induction point was at 38 h with IPTG. (b) Shear viscosity (Pa s, duplicate measurements) measured at 75 s^{-1} with a Brookfield DV-2+ viscometer at 25°C using a cup and bob setup (CP-40 cup, coaxial cylinder rotary viscometer). Induction point was at 46 h with IPTG. Error bars show standard deviation.

3.4.1.2.1 Comparing the viscosity profiles in fermentation using two different instruments

Figure 3-7 (b) shows the viscosity profile for a separate fermentation, using a Brookfield viscometer (coaxial cylinder rotary viscometer) using a cup and bob setup with a CP-40 spindle, measured at 75 s^{-1}, controlled at 25°C. Induction point for the fermentation run was at 46 h.

For the fermentation presented in Figure 3-7 (b), the PID control system had not yet been fully optimised (as described in Materials & methods section 2.2.4). In addition, there was both a very long exponential growth phase (excessive foaming disrupted growth), as well as a long stationary phase. However, as seen in Figure 3-7 (b), the Brookfield viscometer was able to monitor the viscosity profile of the cell broth. Following a similar trend to that observed with the Kinexus rheometer (Figure 3-7 (a)); the viscosity increased during the growth phase in alignment with the cell density increase, was relatively flat in stationary phase before increasing significantly as cell lysis occurred. This trend also corresponded well with dsDNA release and Fab' leakage during the fermentation.

Although the general viscosity trends during fermentation aligned well for both instruments, there were several issues with the Brookfield viscometer. First, the measurements must be manually carried out; rpm and torque must be converted into shear rate and shear stress, and viscosity then determined from the flow curve. Secondly, the gap size must be manually adjusted and set between each sample. This was extremely challenging as the viscosity is dependent on the gap size (for non-Newtonian materials), therefore small differences in gap size can have an impact on the viscosity. For this reason, duplicate measurements were carried out for all samples with the Brookfield viscometer. There were differences in the magnitude of the viscosity values between the instruments, however this could be for many reasons including the different shear rates used (75 s^{-1} vs. 100 s^{-1}), the different geometries used (parallel plates vs. cup and bob), in addition to batch-to-batch variation of the cell broth between fermentation runs. Furthermore, as mentioned above, for the fermentation run presented with the Brookfield instrument, the PID

control system had not yet been optimised, therefore, poor control throughout the fermentation would have led to different levels of lysis (and therefore viscosity values) in this fermentation. Temperature also significantly affects the viscosity, and the water bath used to control the temperature for the Brookfield viscometer offered poor control in comparison to the peltier plate system used in the Kinexus rheometer. Moreover, in practical terms, the old age of the Brookfield instrument and awkward manual set up of the instrument meant that the reliability of the measurements was questionable.

For the Kinexus rheometer, almost all steps in the measurement process were automated using the software provided, which is particularly important for setting the gap size, controlling temperature and obtaining rapid viscosity measurements. Data was analysed automatically; the flow curve was plotted on a graph in real-time during the measurements, and a table was populated with data including shear rate, shear stress and shear viscosity. Single measurements were able to be carried out for the Kinexus rheometer as the steady state measurement allowed multiple readings to be taken over 10 seconds and averaged. Duplicates and triplicates were measured occasionally, and the results were determined to be highly reproducible.

Considering that the aim of this study is to rapidly obtain at-line viscosity data in order to monitor cell lysis in fermentation, the high reproducibility of the Kinexus rheometer and the automated measurement process (including the ability to automate the setting of the gap size and temperature) was a more favourable option to rapidly obtain accurate viscosity data. In addition, the rheometer allows both viscometry testing as well as viscoelasticity testing, which offers the potential to characterise and investigate the rheology of the cell broth in a multitude of ways. However, the Brookfield instrument only offers the possibility to measure viscosity.

3.4.1.3 Batch vs. fed-batch fermentation

A batch fermentation was carried out to gain a deeper understanding of cell lysis and compare it to the fed-batch fermentation profile.

Figure 3-8 shows the viscosity profile for an *E. coli* fermentation ran in batch mode. DNA release to the cell broth, total protein release and the growth profile (OD_{600}) are also shown for reference. The viscosity was measured using the Brookfield viscometer, and the same trend can be seen in the growth phase; an increase in viscosity in relation to the cell density increase. Cells were induced with IPTG at 34 h after a dissolved oxygen spike was observed, however glycerol was not fed in the postinduction phase in order to observe cell lysis. The cell density can be seen to decrease slowly from the induction point. However, the DNA release, total protein leakage and viscosity increase rapidly from this point.

The DNA, protein and viscosity trends correlate well in Figure 3-8. Cell lysis was triggered immediately at induction point (seen by the rapid release of DNA and intracellular protein) because the addition of IPTG diverted the *E. coli* cells' energy away from maintenance, repair and cell growth and instead to the over-expression of the Fab' product. This energy demand for the production of Fab' coupled with a lack of carbon source (glycerol) caused the cells to lyse immediately.

This experiment also demonstrates an important consideration. Glycerol is highly viscous, and its addition in postinduction fermentation could result in an increase in the viscosity of the cell broth. For example, the viscosity trends observed in Figure 3-7 during cell lysis could have been caused by an accumulation of glycerol in the media (i.e. if cells are dying, the cells would consume less glycerol and the glycerol concentration would build up in the broth). However, as shown in Figure 3-8, the viscosity increased 5-fold from induction point to the end of the fermentation. Therefore, the batch fermentation profile presented shows that cell lysis (i.e. the release of intracellular content such as nucleic acids and host cell protein to the cell broth) correlates well with an increase in postinduction viscosity that is not attributable to glycerol feeding.
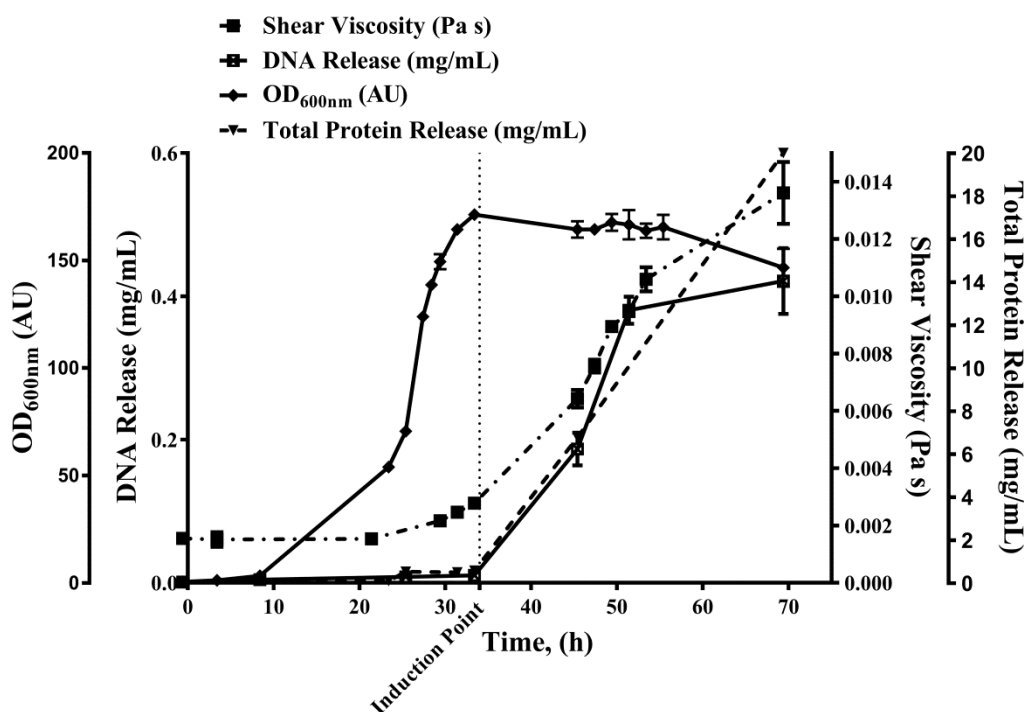
Figure 3-8: Shear viscosity trend in a batch *E. coli* fermentation. Shear viscosity measured at 75 s^{-1} (Pa s, duplicate measurements) with a Brookfield DV-2+ viscometer at 25°C using a cup and bob setup (CP-40 cup, coaxial cylinder rotary viscometer). Optical density (measured at 600 nm, absorbance units, AU, in triplicate), total protein release (mg/mL, measured in triplicate) and DNA release (mg/mL, measured in triplicate) presented to compare trends with fed-batch fermentation. Cells were induced with IPTG at 34 h, however glycerol was not fed in order to observe cell lysis. Rapid viscosity increase evident immediately after induction point. Fermentation terminated at 70 h. Error bars show standard deviation.

131

3.4.2   Detecting cell lysis and product loss using viscosity monitoring

Three fed-batch fermentation runs were carried out and evaluated, to assess whether cell lysis and product loss can be detected in a robust and reproducible manner by viscosity monitoring.

Figure 3-9 shows the three fed-batch fermentation runs (postinduction) and presents the shear viscosity data (following the protocol developed using the Kinexus rheometer) with the product leakage and the DNA release profiles. For all three fermentation runs, the postinduction viscosity increase correlated well with DNA release and product leakage. This also confirms what was shown in section 3.3; loss of cell viability, cell lysis and product loss occur simultaneously in postinduction fermentation, and (shown in section 3.4.1.3) that the release of intracellular content during cell lysis causes an increase in the viscosity of the cell broth.

As discussed in section 3.4.1.2, viscosity is determined by both the cell concentration and the solute concentration in the broth. The viscosity increase in the growth phase of fermentation can predominantly be attributed to the increase in cell concentration, and the change in viscosity in stationary phase can predominantly be attributed to the solute concentration in the broth. Cell density can vary significantly between fermentation batches, which can consequently influence the shear viscosity. However, cell density can be assumed to be constant in stationary phase (i.e. postinduction). Therefore, taking the viscosity at induction point as a reference (in order to negate differences in cell density between batches), i.e. determining the postinduction viscosity increase, enables the determination of the viscosity increase that is attributable to cell lysis:

$$\eta_{increase,postinduction} = \eta_t - \eta_0$$

Equation 3-1

where η_t is the viscosity of the cell broth at the time point of interest (postinduction), and η_0 is the viscosity of the cell broth at induction point.

Using this definition, it was determined that a 25% ± 5 increase in postinduction viscosity correlated to 10% product loss for the three fermentation runs shown in Figure 3-9.

It is straightforward to characterise the viscosity profile of a fermentation system in this way, and correlate this to product leakage and hence cell lysis. Using the results presented in this chapter to exemplify a practical application of this method; taking into account batch-to-batch variation, a postinduction viscosity increase of 20% may be an appropriate time to end the batch, in order to minimise product loss (taking into consideration the downstream processing time and operating environment that the cells are subject to).

This method of determining product loss is straightforward, and allows the operator to very quickly assess changes in cell viability and ascertain an appropriate harvest point by monitoring the viscosity in this way. In addition, results can be determined in under 2 minutes as no sample preparation is required.

To characterise a different fermentation system using this method; one should start by assessing the intracellular product profile and product leakage profile of the system, taking into account the scale and downstream processing requirements, and then determine the optimum harvest point. The harvest point can be correlated to the viscosity profile, and viscosity monitoring can then be used at-line to rapidly determine the harvest point in subsequent fermentations.

This methodology shows that viscosity monitoring may be used as an indicator of cell lysis in postinduction fermentation, and to determine the optimal harvest time (at-line) by indirectly identifying product leakage to the cell broth.
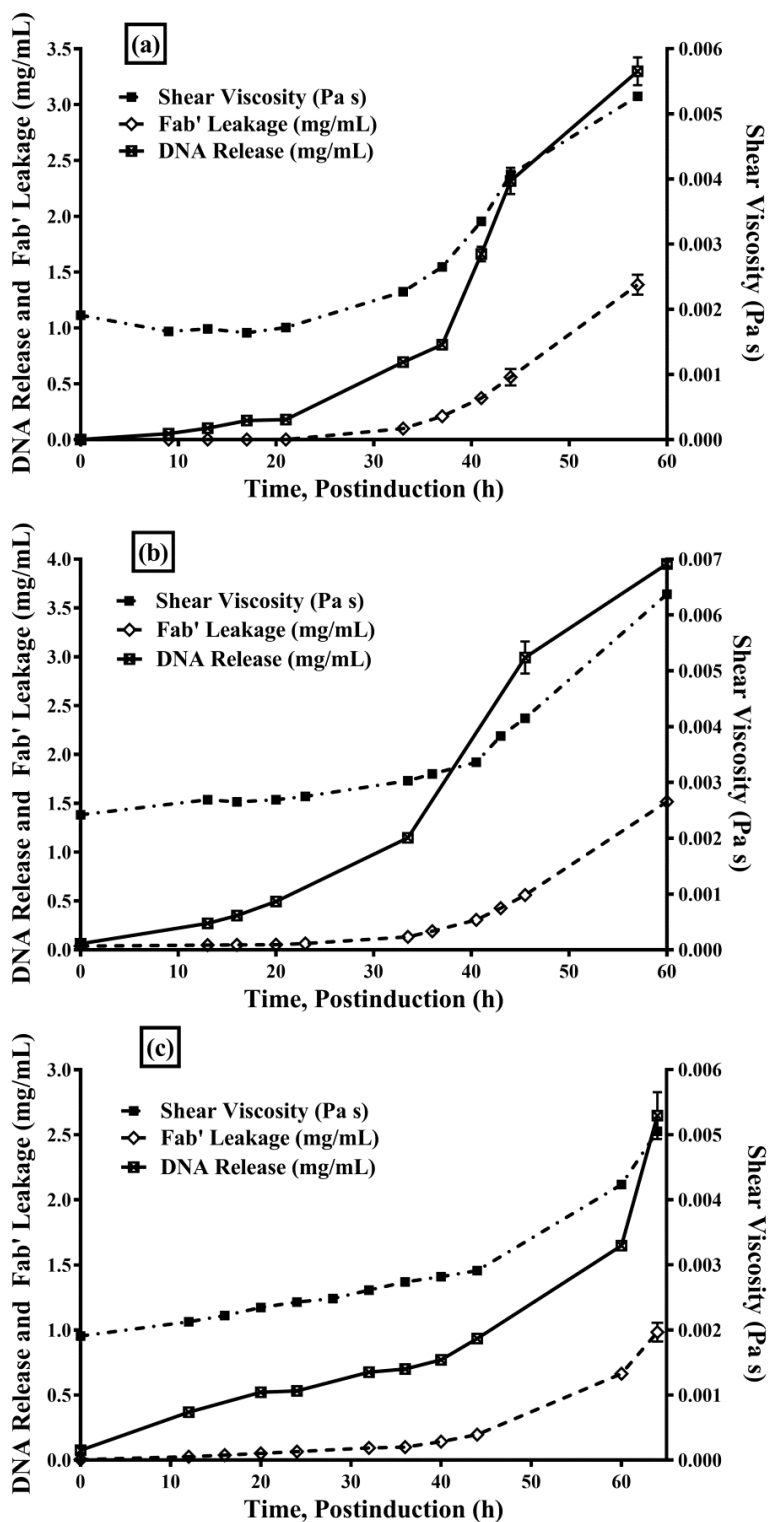
Figure 3-9: Effect of product leakage (mg/mL, measured in duplicate) and DNA release (mg/mL, measured in triplicate) on viscosity increase (Pa s, single measurement, held at steady state for 10 seconds) in postinduction fermentation for three fermentation runs. Error bars show standard deviation.

3.5 Evaluating viscosity monitoring against other common monitoring techniques

Viscosity monitoring may be able to observe changes in the physical properties of the cell broth during fermentation in order to detect cell lysis. However, there are several established technologies available on the market that are used to determine harvest time in fermentation by monitoring cell density, product titre, leakage or cell viability. This section discusses the advantages and disadvantages of some of these methods.

3.5.1 Biomass monitoring: optical density measurements and online capacitance measurements

Capacitance measurements were carried out using the Aber Instruments (Aber Instruments Ltd., Aberystwyth, UK) Futura biomass probe. The in-situ, online biomass probe measures the electrical capacitance of cells which can be converted to viable cells/mL and was calibrated offline with flow cytometry data. See section 2.3.2 in Materials & methods for a detailed explanation of its setup.

It was determined in Figure 3-3 and Figure 3-9 that the postinduction viscosity profile correlated well with DNA release and product leakage. Figure 3-10 shows the viscosity profile and growth profile (OD_{600}) with the capacitance data. According to the optical density profile, the first signs of lysis were observed at 44 h postinduction (82 h fermentation time), which corresponded to almost 40% product leakage. For the capacitance data shown in Figure 3-10, signs of cell lysis at 41 h postinduction (79 h fermentation time) corresponded to 30% product leakage.

Optical density (OD) measurements are routinely used to monitor biomass growth in fermentation. However, OD measurements give an indication of the total biomass obscuring the light path, and provide no insight into viable biomass (Hewitt and Nebe-Von-Caron, 2004). This means that OD measurements systematically underestimate lysis in late stage fermentation and miss the critical point of product leakage.

The capacitance probe was able to very successfully monitor cell viability during the exponential growth phase and early stationary phase, as seen in Figure 3-10. However, capacitance measurements tend to perform poorly in late stage fermentation, often missing the onset of cell lysis, as the plasma membranes of non-viable cells will still hold a certain amount of charge and therefore exhibit some form of capacitance (Sarra et al., 1996; Neves et al., 2000). This means that capacitance measurements can also overestimate the number of viable cells in the late stationary/decay phase of fermentation, as observed in Figure 3-10.

3.5.2   Offline analytical technologies

The postinduction viscosity profile closely aligns with the cell lysis trends observed through HPLC (product leakage), flow cytometry, DNA release and cytotoxicity. A comparison of the common monitoring techniques analysed in this chapter are presented in Table 3-2, assessing cost, time required and the ability to detect cell lysis and product leakage.

HPLC is the standard method to monitor product leakage. However, in comparison to monitoring viscosity, the up-front capital cost for the rheometer is much lower, the maintenance costs and cleaning downtime for the rheometer are minimal, no reagents are needed and analysis takes a fraction of the time. In order to assess leakage, the cell broth sample must first be centrifuged (in some cases, it is also necessary to filter), a standard curve must be prepared for each new HPLC run and each sample takes ~20 min to complete.

Flow cytometry is regularly employed to monitor cell viability in fermentation; however, it requires a lengthy and complicated staining procedure that also involves postmeasurement data analysis. Additionally, all cell-based monitoring techniques can only detect existing cells and are unable to measure the lysed cells, making it infeasible to monitor lysis effectively.

DNA release to the cell broth can give a very good indication of cell lysis. DNA release can be analysed using assays including Picogreen or spectrophotometric absorption such as the Nanodrop device. However, Picogreen assay requires a

comparatively complicated protocol and is time-consuming. In addition, proteins can interfere in Nanodrop measurements as they absorb light at the same wavelength as nucleic acids (Neves et al., 2000). In general, techniques for DNA analysis are susceptible to errors from losses due to degradation of DNA or from losses in sample preparation steps such as centrifugation (Neves et al., 2000).

Cytotoxicity assays, such as the Cytotox-96 assay presented in this chapter, can also very effectively monitor cell viability. However, the assay must be carried out offline and takes a relatively long time.

In summary, viscosity was able to rapidly monitor cell lysis and product loss in postinduction fermentation, which aligned very closely with data from DNA release, a cytotoxicity assay, product leakage (HPLC) and flow cytometry. Optical density and capacitance measurements performed poorly in the late stage of the fermentation and missed the critical point of product leakage.
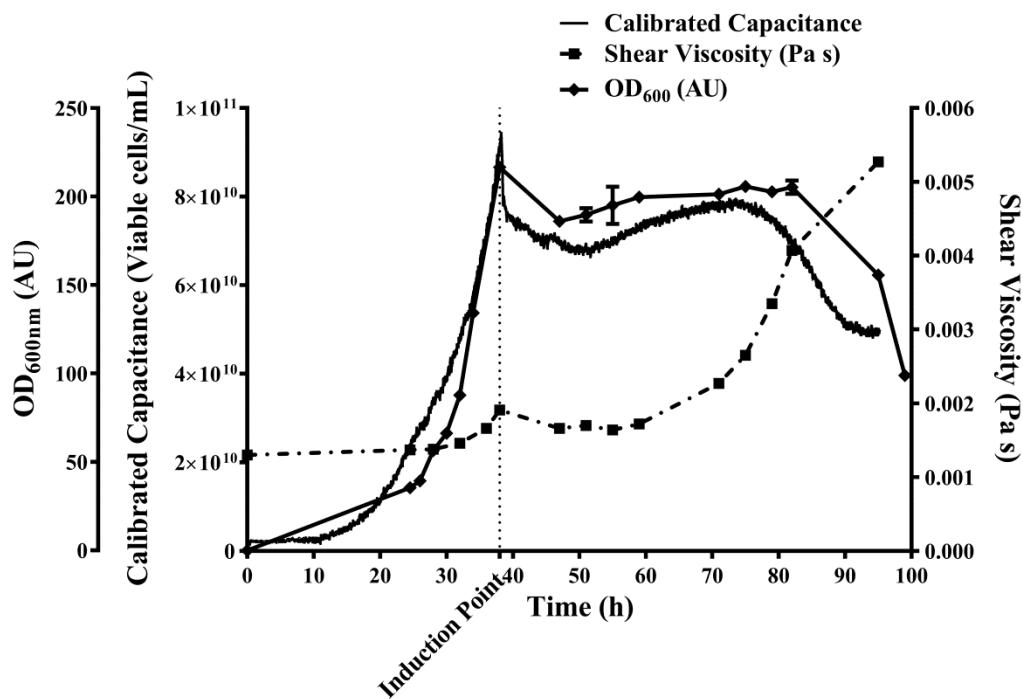
Figure 3-10: Evaluating online capacitance measurements against viscosity monitoring and optical density measurements to detect cell lysis. Capacitance profile measured online continuously and automatically converted to viable cells/mL. Capacitance data were calibrated offline with flow cytometry data (in triplicate). Shear viscosity measured at 100 s^{-1} (Pa s, single measurement, held at steady state for 10 seconds). Cell growth profile shown by optical density as a reference (measured at 600 nm, absorbance units, AU, in triplicate). Cells were induced with IPTG at 38 h. Error bars show standard deviation.

Table 3-2: Comparison of viscosity monitoring with common fermentation monitoring techniques used to detect cell lysis.

Analytical method	Cost	Time	Ability to detect lysis
Optical density	Low	2 min	Poor
HPLC	High	~40 min	Good
Flow cytometry	High	~30 min	Good
Online capacitance measurements	Medium	Online	Poor
DNA assays	Low	~40 min	Good
Cytotoxicity assays	Low	~70 min	Good
Viscosity monitoring	High	2 min	Good

3.6 Conclusions

This work represents an important first step in demonstrating the value of monitoring the physical properties of cell broths, and that rapid viscosity monitoring has the potential to be a useful tool for both process development and process operation at manufacturing scale to determine the optimal harvest time and minimise product loss. Cell lysis has been characterised for an industrially relevant *E. coli* fermentation using a range of analytical techniques in order to better understand the process and mechanisms of lysis. It was shown that product loss, cell viability and cell lysis occur simultaneously in fermentation.

The viscosity profile of the fermentation broth has been established and it has been shown that the viscosity correlated very well with product loss, cell viability and cell lysis in postinduction fermentation. A method was subsequently developed to rapidly detect cell lysis and product loss in postinduction fermentation using viscosity to monitor the cell broth. Viscosity monitoring showed an increase in viscosity during the exponential phase in relation to the cell density increase, a relatively flat profile in early stationary phase, followed by a rapid increase which correlated well with product loss, DNA release and loss of cell viability.

Viscosity monitoring was compared to several monitoring technologies that are commonly used to detect cell lysis in fermentation, and was shown to perform better than optical density measurements and online capacitance probes, and has equivalent performance to HPLC (product leakage), flow cytometry, a cytotoxicity assay and DNA quantification. However, monitoring viscosity at-line can provide information on lysis in a much shorter time period than the other methods presented; data can be obtained in under two minutes, which enables the operator to rapidly make decisions about cell harvesting.

It is thought that a combination of nucleic acids, host cell protein and other intracellular content may cause the increase in viscosity in postinduction fermentation broths. However, the picture is not clear; complex interactions between biomass and their polymers may be present in the composite system (Vlahopoulou and Bell, 1993; Vlahopoulou et al., 1994; Okamoto et al., 2001; Vlahopoulou et al.,

2001). Therefore, the next chapter will focus on investigating the rheological properties of cell broths in more detail, in order to determine the contribution that each of these components makes to the postinduction viscosity increase, and if important interactions are present between cells, cell debris and other intracellular content.

Chapter 4 Investigating and modelling the effects of cell lysis on the rheological properties of fermentation broths

The results presented in this chapter have been published in the Biochemical Engineering Journal, "Investigating and modelling the effects of cell lysis on the rheological properties of fermentation broths" (see Appendix).

4.1   Introduction

In the previous chapter, viscosity monitoring was shown to be a promising tool to monitor the physical properties of cell broths during fermentation. However, viscometry makes up only one part of the picture of rheology. In fact, rheology is defined as the study of the deformation and flow of matter, and can be divided into two types of physical properties; viscosity and viscoelasticity. Viscosity relates to the internal friction of a fluid and is a measure of its resistance to flow (for example, oil is more viscous than water). Viscoelasticity, however, describes both the solid-like (elastic) and liquid-like (viscous) characteristics of a non-Newtonian material undergoing deformation (either temporary or permanent), and these characteristics are indicative of the structural element interactions within the material. Essentially, viscoelasticity can be employed to define the properties of the internal structure and strength of a material. Rheology is frequently used to characterise materials across the processing industry, from oil and gas to cosmetics such as toothpaste and hand cream. In the biopharmaceutical industry, rheology is typically used in the formulation of therapeutics.

There are several technologies currently available on the market that monitor cell broths during fermentation, and a detailed review of these technologies has been carried out in the Introduction (section 1.4). Advanced technologies such as infrared spectroscopy monitor the chemical properties of a cell broth. However, developing rheology as a monitoring technology in fermentation, to detect changes in the physical properties of cell broth, has the potential to complement chemical and biological-based monitoring technologies, such as infrared or fluorescence spectroscopy, to provide comprehensive information on both the physical and

chemical properties of the fermentation broth. This has significance with respect to quality by design (QbD) initiatives in process development, i.e. characterising and monitoring key parameters in the process, and monitoring technologies (process analytical technologies, PAT) are central to the improvement of biopharmaceutical manufacturing (Perez-Pardo et al., 2011).

This chapter aims to gain a deeper understanding of the rheology of *E. coli* and investigate the effects of cell lysis on the rheological properties of cell broths in fermentation. This will involve using advanced rheological testing (both viscosity and viscoelasticity) to understand changes in the physical properties of cell broths, such as the cause of the increase in postinduction viscosity, and assess whether viscoelasticity can provide novel insight into fermentation by monitoring physical properties such as cell strength. Using the insight derived from these studies, it may be possible to develop a model to quantify cell lysis in postinduction fermentation using viscosity monitoring.

Therefore, the specific objectives of this chapter are to:

- Characterise the fundamental rheological properties of an *E. coli* cell broth to gain a deeper understanding of the physiological changes in *E. coli* cells during fermentation

- Assess whether viscoelastic measurements can provide novel insight in fermentation by monitoring physical properties such as cell strength

- Develop a mathematical model to quantify the extent of cell lysis in fermentation using viscosity monitoring

4.2   *E. coli* **fermentation**

High cell density fed batch *E. coli* fermentation runs producing antibody fragments (antigen-binding, Fab') were carried out as described in the previous chapter (Chapter 3).

143

4.3   Understanding the change in broth viscosity during fermentation

After characterising cell lysis in fermentation in the previous chapter, it was desired to gain a deeper understanding of the physiological changes that occur during cell lysis by determining the relative contributions that individual structural components of a cell broth make to the postinduction viscosity increase. In order to do this, the components were isolated (as described in Materials & methods section 2.5.4) and then viscometry experiments were carried out at various growth stages (i.e. over the course of a fermentation run) for cell broth, cell paste and supernatant, as shown in Figure 4-1, to obtain the flow curves.

Figure 4-1 (a) plots the flow curves of the cell broth throughout fermentation, showing a five-fold increase in viscosity from 0.0011 Pa s at the start of the fermentation to 0.0053 Pa s at the end of the fermentation, and an increase in shear thinning behaviour as the fermentation progressed (see Table 4-1) from 1.028 for SM6Gc media to 0.868 at 95 h postinduction. The viscosity increased steadily during the growth phase until induction point, and over a 70% increase (to 0.00191 Pa s) was observed in this phase. The increase in viscosity up to induction point can be attributed to the increase in cell concentration during exponential phase.

From induction point, the viscosity was relatively constant until a 25% increase was observed that correlated to 10% product loss (this was discussed in the previous chapter), and the viscosity rapidly increased thereafter. The increase in shear thinning behaviour observed in Figure 4-1 (a) correlated with cell lysis and the release of intracellular content to the cell broth.

Figure 4-1 (b) displays the flow curves for cell paste at various points during fermentation. The viscosity of the cell paste decreased slightly as the fermentation progressed through the growth phase from 0.35 Pa s to 0.28 Pa s, however this decrease was relatively small in contrast to the marked decrease observed between 33 h postinduction (the critical point of product leakage and cell lysis for the fermentation presented) and 57 h postinduction, from 0.22 Pa s to 0.10 Pa s. This aligns with the trend observed from the flow curves for the cell broth in Figure 4-1

(a), showing the rapid deterioration of the cells beyond 33 h postinduction and correspondingly a significant increase in the viscosity of the cell broth. Additionally, significant shear thinning behaviour was observed for all samples and in particular for the late stage fermentation sample (57 h postinduction), where a flow behaviour index of 0.587 ± 0.0289 was determined (see Table 4-2).

Figure 4-1 (c) shows flow curves for the supernatant of the fermentation broth in mid-exponential phase and late stage fermentation (57 h postinduction). A large increase in viscosity was seen for the supernatant at 57 h postinduction, from 0.00125 Pa s in mid-exponential phase to 0.0048 Pa s. In addition, a significant increase in shear thinning behaviour was observed, and the flow behaviour index was determined to be 0.766 ± 0.00542 for the 57 h postinduction supernatant sample (see Table 4-3). Considering that the SM6Gc media is a Newtonian fluid, and glycerol (a major component in the media) is also Newtonian, this reflects a significant change in the properties of the supernatant as the fermentation progressed.

Although the viscosity of the cells (cell paste) decreased significantly during fermentation, from 0.35 Pa s to 0.10 Pa s (Figure 4-1 (b)), the overall broth viscosity increased (Figure 4-1 (a)). Therefore, it can be seen that the increase in the viscosity of the cell broth is a result of the large increase in the supernatant viscosity (Figure 4-1 (c)). This confirms the hypothesis that the increase in broth viscosity in postinduction fermentation can be attributed to the release of intracellular content to the broth during cell lysis. In addition, the shear thinning behaviour of both the cells and the supernatant increased significantly as the fermentation progressed.
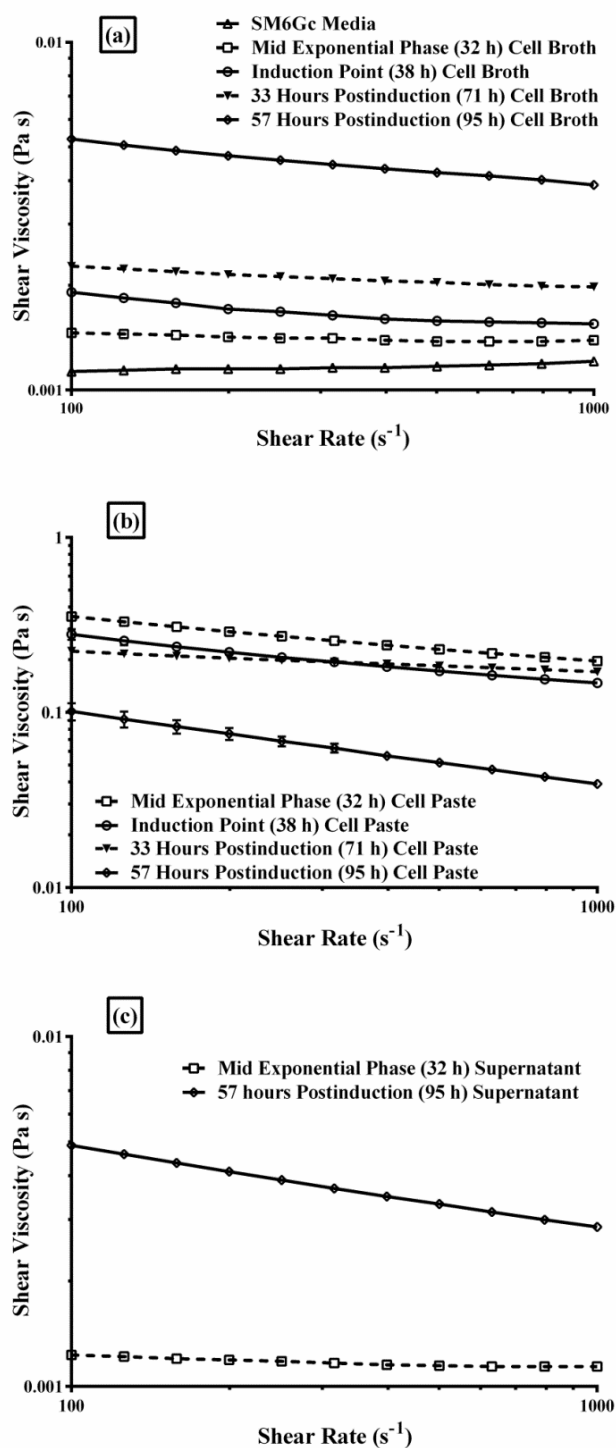
Figure 4-1: Understanding the relative contributions of components of a cell broth to the viscosity increase in postinduction fermentation. Flow curves of *E. coli* (a) cell broth, (b) cell paste and (c) supernatant at various time points in the fermentation. Single measurements were recorded at each shear rate, held at steady state for 10 seconds, over a shear rate range 100–1,000 s^{-1}. Viscometry measurements were carried out at 25°C using 50 mm parallel plates and a 300 μm gap size. Error bars show standard deviation.

Table 4-1: Flow behaviour index (n) values for the flow curves presented in Figure 4-1 (a) of *E. coli* cell broth at various times throughout fermentation, over a shear rate of 100-1000 s^{-1}, using a Malvern Instruments Kinexus Lab + rotational rheometer. Induction time was at 38 h using IPTG. Measurements were carried out at 25°C using 50 mm parallel plates and a 300 μm gap size. An increase in shear thinning behaviour is evident as the fermentation proceeded (flow behaviour index, n, was greater than 0.85 for all samples). Single viscometry measurements were recorded at each shear rate, and held at steady state for 10 seconds.

Sample	Flow behaviour index, n
SM6Gc media	1.028
Mid exponential phase (32 h)	0.977
Induction point (38 h)	0.908
33 h postinduction (71 h)	0.939
57 h postinduction (95 h)	0.868

Table 4-2: Flow behaviour index (n) values for the flow curves presented in Figure 4-1 (b) of *E. coli* cell paste at various times throughout fermentation, over a shear rate of 100-1000 s^{-1}, using a Malvern Instruments Kinexus Lab + rotational rheometer. Induction time was at 38 h using IPTG. Measurements were carried out at 25°C using 50 mm parallel plates and a 300 μm gap size. All samples show highly shear thinning behaviour. Triplicate viscometry measurements were recorded at each shear rate, and held at steady state for 10 seconds. Error bars show standard deviation.

Sample	Flow behaviour index, n
Mid exponential phase (32 h)	0.745 ± 0.0152
Induction point (38 h)	0.723 ± 0.0331
33 h postinduction (71 h)	0.881 ± 0.00888
57 h postinduction (95 h)	0.587 ± 0.0289

Table 4-3: Flow behaviour index (n) values for the flow curves presented in Figure 4-1 (c) of *E. coli* supernatant at various times throughout fermentation, over a shear rate of 100-1000 s^{-1}, using a Malvern Instruments Kinexus Lab + rotational rheometer. Induction time was at 38 h using IPTG. Measurements were carried out at 25°C using 50 mm parallel plates and a 300 μm gap size. An increase in shear thinning behaviour is evident as the fermentation proceeded. Triplicate viscometry measurements were recorded at each shear rate, and held at steady state for 10 seconds. Error bars show standard deviation.

Sample	Flow behaviour index, n
Mid exponential phase (32 h)	0.967 ± 0.000860
57 h postinduction (95 h)	0.766 ± 0.00542

4.4   Oscillatory tests

Viscoelasticity and its surrounding theory was discussed in the Introduction (section 1.5.3) and in Materials & methods (section 2.5.2.2). Having shown that monitoring the cell broth viscosity can be a useful tool to detect cell lysis in postinduction fermentation (see previous chapter), and having carried out viscometry tests on the components of the cell broth (supernatant, cell paste and cell broth); it was desired to further investigate the physical properties of the cells by carrying out oscillatory tests to assess whether additional rheological properties (i.e. viscoelastic properties) can provide novel insight into changes in the physical properties of cells during fermentation.

Oscillatory tests were carried out to characterise and provide insight into the viscoelastic properties of the *E. coli* cells, and to observe changes in their physical properties over the course of fermentation. Viscoelasticity can be measured by both amplitude sweeps and frequency sweeps. Oscillatory tests were carried out on cell paste only, as there was not enough structure present in the other materials studied to enable meaningful insight.

The linear viscoelastic range (LVER) can be defined as the limit at which the structure in a sample starts to break down and is where the rheological properties, i.e. the shear modulus (G' and G'') and phase angle (δ), are independent of frequency. The length, or critical strain limit, of the LVER relates to the stability and robustness of a material (i.e. permanent polymer cross-links), and G' is a direct measure of the structure in a sample, and therefore provides an indication of the strength of the material.

4.4.1   Elucidating the viscoelastic properties of *E. coli* cell paste

4.4.1.1   Amplitude sweeps

Figure 4-2 presents a comparison of the viscoelastic properties of *E. coli* at two different growth stages; in mid-exponential phase and at harvest point (33 h postinduction). An amplitude sweep was initially carried out to determine the LVER

by varying the amplitude (shear strain amplitude, %) from 0.05-10% and holding the frequency constant at 1 Hz.

Figure 4-2 (a) shows the storage (G') and loss (G") moduli for the two growth stages. The storage modulus is more commonly used to classify the LVER as it is more sensitive; the storage modulus is a combination of both the complex shear modulus (G*) and the phase angle (see Introduction section 1.5.3). The phase angle typically increases as the LVER breaks down (as a material breaks down, it becomes more fluid), and G* decreases.

Therefore, it can be seen from the G' profiles that the length of the LVER is greater for the 33 h postinduction cell paste than for the mid-exponential phase cell paste, i.e. the storage modulus starts to decline earlier for the mid-exponential phase cell paste. This means that the structure in the sample, i.e. the structure formed between the cells in the paste, starts to break down at an earlier time point for the mid-exponential phase cells. For the mid-exponential phase cell paste, the structure starts to break down at ~0.15% shear strain. For the harvest point cell paste, the structure starts to break down at ~0.4% shear strain. Therefore the strain limit of the LVER for the two samples (mid-exponential phase and harvest point cell paste) can be defined as 0.15% and 0.4%, respectively.

For both growth stages, it can also be seen in Figure 4-2 that the storage modulus, G', was greater than the loss modulus, G", which shows that both materials exhibited solid-like characteristics (i.e. the solid contribution was more pronounced than the liquid contribution). Although the cells at 33 h postinduction may be leaking product and other intracellular content to the broth due to porous membrane channels (as seen in the previous chapter), this result (i.e. the solid-like viscoelastic properties of the cell paste) indicates that the cells haven't fragmented and broken down at this point, and that the rod-like structure of the *E. coli* is still relatively intact.

However, the magnitude of the storage modulus, G', within the LVER is higher for mid-exponential phase cell paste than for 33 hours postinduction cell paste, at 339 Pa

and 40 Pa respectively, showing a considerable drop in the strength of the cells as the fermentation progresses.

The loss tangent, tanδ, is a ratio of the loss modulus to storage modulus (G"/G'), which provides a useful quantification of the elasticity (or solid-like structure) of a material. In Figure 3 (b), the loss tangent is plotted for the cell paste at the two different growth stages; mid-exponential phase and 33 h postinduction. The loss tangent was higher for the 33 h postinduction cell paste, throughout the amplitude range (0.05-10%). This indicates a more fluid (i.e. weaker) system, if the shear viscosity increases (the postinduction shear viscosity increase was observed in the previous chapter).

This result suggests that polymers in the sample are acting as fillers, and have a thickening effect (hence the increased viscosity), which could be caused by the formation of a network due to interactions between cells and leaked intracellular content. This confirms the insight derived from Figure 4-2 (a); the *E. coli* cells are still rod-like structures at 33 hours postinduction (although porous and leaking product), but the cells become weaker and lose rigidity as the fermentation progresses.
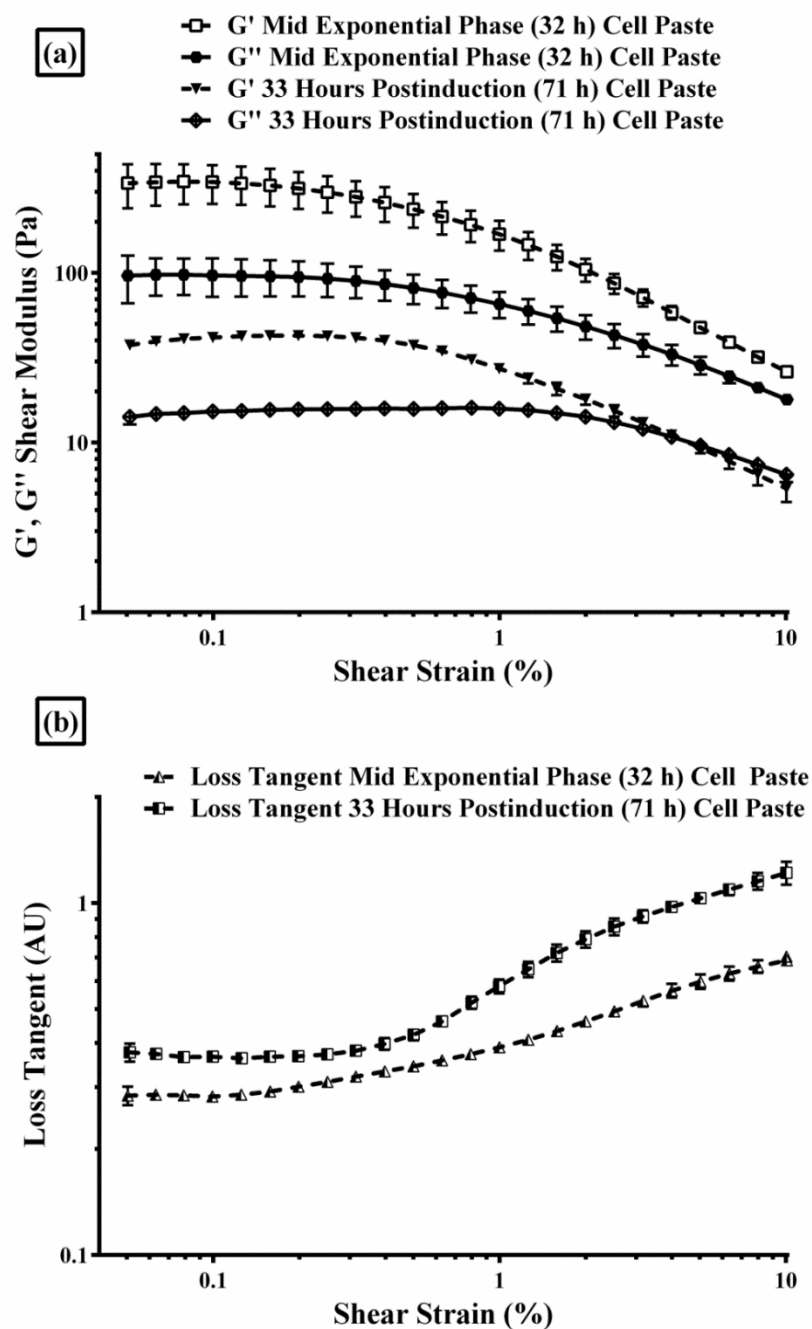
Figure 4-2: Elucidating the rheological properties of an *E. coli* cell paste. Measurements carried out to compare the rheological properties (storage (G') and loss (G'') moduli) of *E. coli* between two different growth stages; mid exponential phase and 33 hours postinduction (typical harvest point). (a) Dynamic oscillation measurements were taken using an amplitude sweep over a shear strain range 0.05-10%, holding frequency constant at 1 Hz. (b) The loss tangent, tanδ, is a ratio of the loss modulus to storage modulus (G''/G'), which gives a useful quantification of the elasticity of a material. Measurements were carried out at 25°C using 50 mm parallel plates and a 300 μm gap size. Error bars show standard deviation.

4.4.1.2 Frequency sweeps

After carrying out an amplitude sweep to characterise the cells and define the LVER, frequency sweeps were subsequently carried out on the *E. coli* cell paste. To carry out the frequency sweeps, the shear strain amplitude was held constant at 0.1% (within the LVER, as seen from Figure 4-2 (a)), and the frequency was varied from 1-10 Hz. A frequency sweep records a fingerprint spectrum of the material, and can be used to classify a material into three types of behaviour; a viscoelastic solid, a gel or a viscoelastic liquid. When G'>G", solid-like behaviour is exhibited, and the material can generally be classified as a viscoelastic solid; for a gel, the properties (phase angle (δ), G', G") are independent of frequency; and when G">G', liquid-like behaviour is exhibited, and the material can generally be classed as a viscoelastic liquid.

In Figure 4-3, it can be seen that for both materials (mid-exponential phase cell paste and harvest point cell paste), the storage modulus, G', is greater than the loss modulus, G", demonstrating that both materials have solid-like characteristics. This reflects the insight derived from the oscillatory tests carried out in Figure 4-2 (an amplitude sweep with the frequency held constant at 1 Hz (when within the LVER) should have the same result as the frequency data at 1 Hz, with the amplitude held constant within the LVER, i.e. they are the same measurement conditions).

However, both G' and G" are almost independent of frequency, suggesting that the behaviour of the materials are close to that of a gel. For the mid-exponential phase cell paste, the phase angle, δ, varied from 14-18° and for the 33 h postinduction cell paste, the phase angle varied from 22-35°. Therefore, although a mixture between gel-like behaviour and weak viscoelastic solid behaviour was seen for both materials, the phase angle change (over the frequency range) increased from mid-exponential phase to 33 h postinduction, showing a reduction in the solid-like properties as the fermentation progressed.

This shows that the cells decreased in strength over the fermentation, and became weaker i.e. more liquid-like, again confirming the insight derived from the amplitude sweep carried out in Figure 4-2.
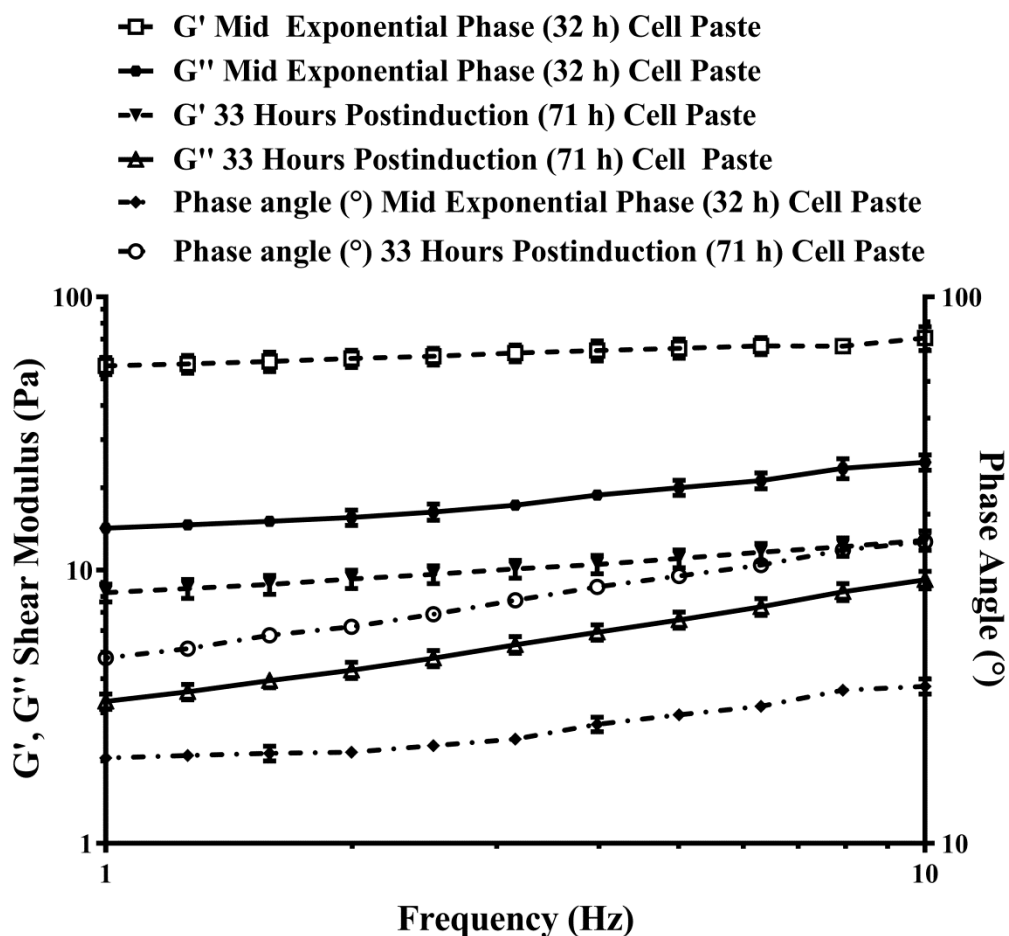
Figure 4-3: Frequency sweep of *E. coli* cell paste. Dynamic oscillation measurements were taken to determine the rheological properties of the cell paste. Amplitude was held constant at 0.1% (within the LVER) and frequency was varied between 1 and 10 Hz. Measurements carried out in triplicate to compare the rheological properties (storage (G') and loss (G") moduli and phase angle (δ, °)) of *E. coli* between two different growth stages; mid-exponential phase and 33 hours postinduction (typical harvest point). Measurements were carried out at 25°C using 50 mm parallel plates and a 300 μm gap size. Error bars show standard deviation.

4.4.2 Monitoring changes in viscoelasticity throughout fermentation

In section 4.4.1, it was observed that there were differences in the strength and structure of *E. coli* cells at two separate growth phases in fermentation (mid-exponential phase and at 33 h postinduction). In Figure 4-4, amplitude sweeps are presented for cell paste, monitored over several time points throughout the fermentation; and two phenomena are evident.

Firstly, it can be seen that the length (or critical strain limit) of the LVER increases as the fermentation progresses; the structure in the exponential phase cell paste started to break down at 0.15% (as described in section 4.4.1.1) and at the end of the fermentation (57 h postinduction), the structure started to break down at 1%. This shows that the stability of the cell paste increased as the fermentation progressed, and suggests an increase in network formation due to cross-linked polymers.

Secondly, it can be seen that the magnitude of the elastic component of the shear modulus (G') decreased with fermentation time, from 339 Pa in exponential phase to 20 Pa at 57 h postinduction. As G' is a direct measure of the structure in the sample, this implies that the strength of the cells decreased (G') significantly over the fermentation.

The results in Figure 4-4 therefore suggest that although the cell strength decreased, the critical strain limit increased due to interactions between cells and intracellular content such as DNA and host cell protein, which increased the "stickiness" of the cell paste as cell lysis occurred.

In Figure 4-5 (a), the growth profile for the *E. coli* fermentation (OD and dry cell weight), total Fab' production and shear viscosity profiles are shown as a reference (reproduced from the previous chapter). In Figure 4-5 (b), the average G' (averaged within the LVER, taken from Figure 4-4) was plotted for each time point, showing a rapid drop in cell strength between induction point and the harvest point (33 h postinduction). This suggests that after induction at 38 h, the strength of the cells

156

continued to decrease until reaching a critical point (e.g. ~40-60 Pa) where the cell membrane begins to deteriorate and product loss and cell lysis occur.

This result demonstrates the potential of viscoelastic parameters, such as G', to be determined, related to critical lysis factors and subsequently monitored in fermentation to provide useful information such as quantifying changes in cell strength during fermentation and providing insight into the physical state of the *E. coli* cells.

This study demonstrates a novel application in bioprocessing, using viscoelasticity to monitor cell strength in fermentation, which can be related to cell health. The useful insight derived from these experiments presents the potential to explore further opportunities using rheology-based monitoring in bioprocessing, such as using rheology to quantify and classify production processes or in primary recovery unit operations, for example as a novel process analytical technology for quality by design applications. In addition, monitoring the viscoelastic properties of cell broths shows significant potential to be used in combination with shear viscosity monitoring to enable superior classification of the physical properties of cell broths.
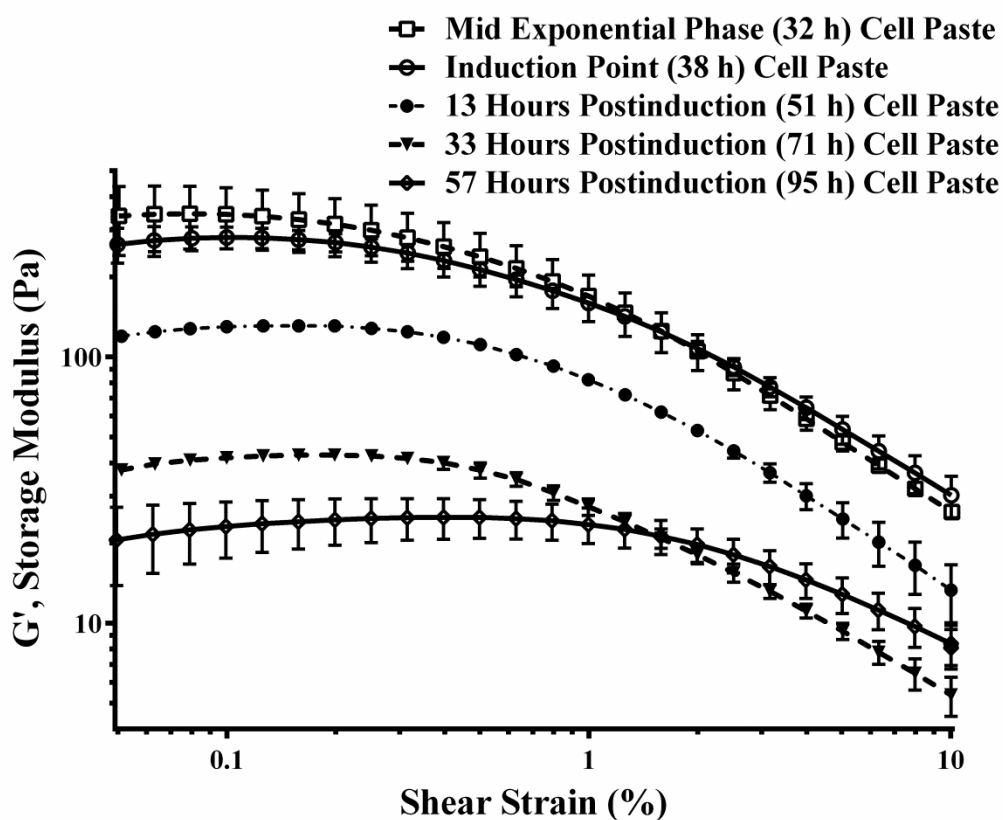
Figure 4-4: Amplitude sweeps of *E. coli* cell paste to determine the critical strain limit. Dynamic oscillation measurements were taken to determine the linear viscoelastic range (LVER, the critical strain limit before a material starts to break down), using an amplitude sweep over a shear strain range 0.05-10%, holding frequency constant at 1 Hz. Measurements carried out at various time points throughout fermentation, at 25°C using 50 mm parallel plates and a 300 μm gap size. Error bars show standard deviation.
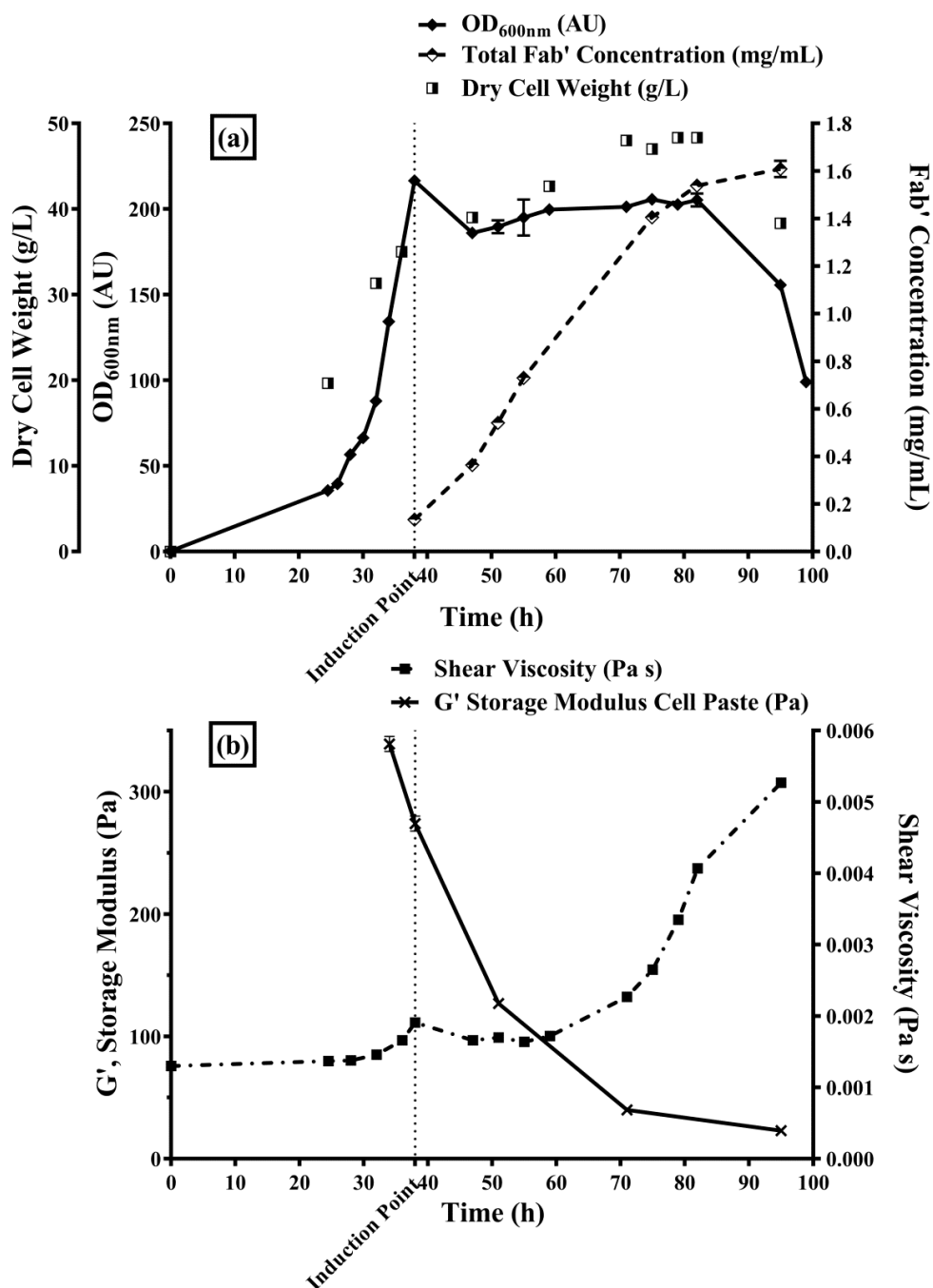
**Figure 4-5: Changes in cell strength during an *E. coli* (Fab') fermentation.
Induced with IPTG at 38 h. (a) Optical density at 600 nm (absorbance units
(AU), in triplicate), dry cell weight (g/L, in triplicate) and total Fab'
concentration (mg/mL, in duplicate). (b) Shear viscosity (Pa s, single
measurement, held at steady state for 10 s) and average storage modulus (G',
elastic component) of cell paste (Pa, measured in triplicate), calculated by
averaging G' over the linear viscoelastic range (LVER). Measurements were
carried out at 25°C using 50 mm parallel plates and a 300 μm gap size. Error
bars show standard deviation.**

4.5 Modelling cell lysis in postinduction fermentation

As discussed in the previous chapter, the viscosity of fermentation broths is determined by two factors; cell concentration and solute concentration in the broth (assuming other factors such as media composition, temperature, aeration and agitation are constant) (Reardon and Scheper, 1991). In section 4.3, it was demonstrated that the release of intracellular content during cell lysis in fermentation causes an increase in postinduction broth viscosity.

Cells, representative protein and DNA were isolated and prepared at various concentrations, in order to gain a deeper understanding of the contributions of these individual components to the overall viscosity of a fermentation broth. The aim was then to create a model to quantify cell lysis.

4.5.1 Viscosity and cell concentration

It is already known that the concentration of cells affects the viscosity of cell broths. Figure 4-6 (a) plots flow curves for cell suspensions at various concentrations (shown as dry cell weight). An increase in shear thinning behaviour was observed as the concentration of cells increased (shown in Table 4-4); which corresponded with the results shown in Figure 4-1.

As described in the previous chapter, 100 s^{-1} was chosen as the characteristic parameter to obtain apparent viscosity values for all studies presented, because at lower shear rates, the measurement will pick up more of the polymer interactions (such as nucleic acids) that are thought to cause an increase in viscosity during cell lysis in fermentation.

Taking the viscosity values from Figure 4-6 (a) at 100 s^{-1}, Figure 4-6 (b) shows a linear relationship between cell concentration and shear viscosity, with an R^2 value of 0.98. In exponential phase and early stationary phase fermentation, viscosity is predominantly determined by cell concentration. Therefore, it can be seen that a linear relationship exists between cell concentration and shear viscosity in the growth phase of *E. coli* fermentation.

The error bars for cell suspensions at higher concentrations are relatively large and it is thought that this may be caused by cell aggregation from centrifugation and re-suspension in sample preparation steps, as well as errors in the dry cell weight measurement process (typically not very robust). However, the relationship between cell concentration and shear viscosity is presented below in Equation 4-1, where C_{cells} is cell concentration (g.DCW/L) and η_{cells} is shear viscosity in Pa s;

$$\eta_{cells} = 5.38 \times 10^{-5} C_{cells} + 0.00062 \qquad \textbf{Equation 4-1}$$

This result confirms that Einstein's well-known viscosity equation, based on hydrodynamic theory for dilute suspensions of spherical particles (Einstein, 1906), is appropriate for the growth stage of the *E. coli* fermentation system presented in this study (see Introduction, section 1.5.2.2.1). The Einstein equation is of a linear form and based on the volume fraction of spherical particles, which can be considered to be roughly equivalent to the volumetric viable cell concentration. At higher cell concentrations, this linearity may not be appropriate, however further work must be carried out in a separate study to determine the fit of the Einstein equation (and extensions to the Einstein equation) to non-spherical *E. coli* cells at higher cell concentrations, as well as determining the influence of non-viable particles such as cell debris on the volume fraction.
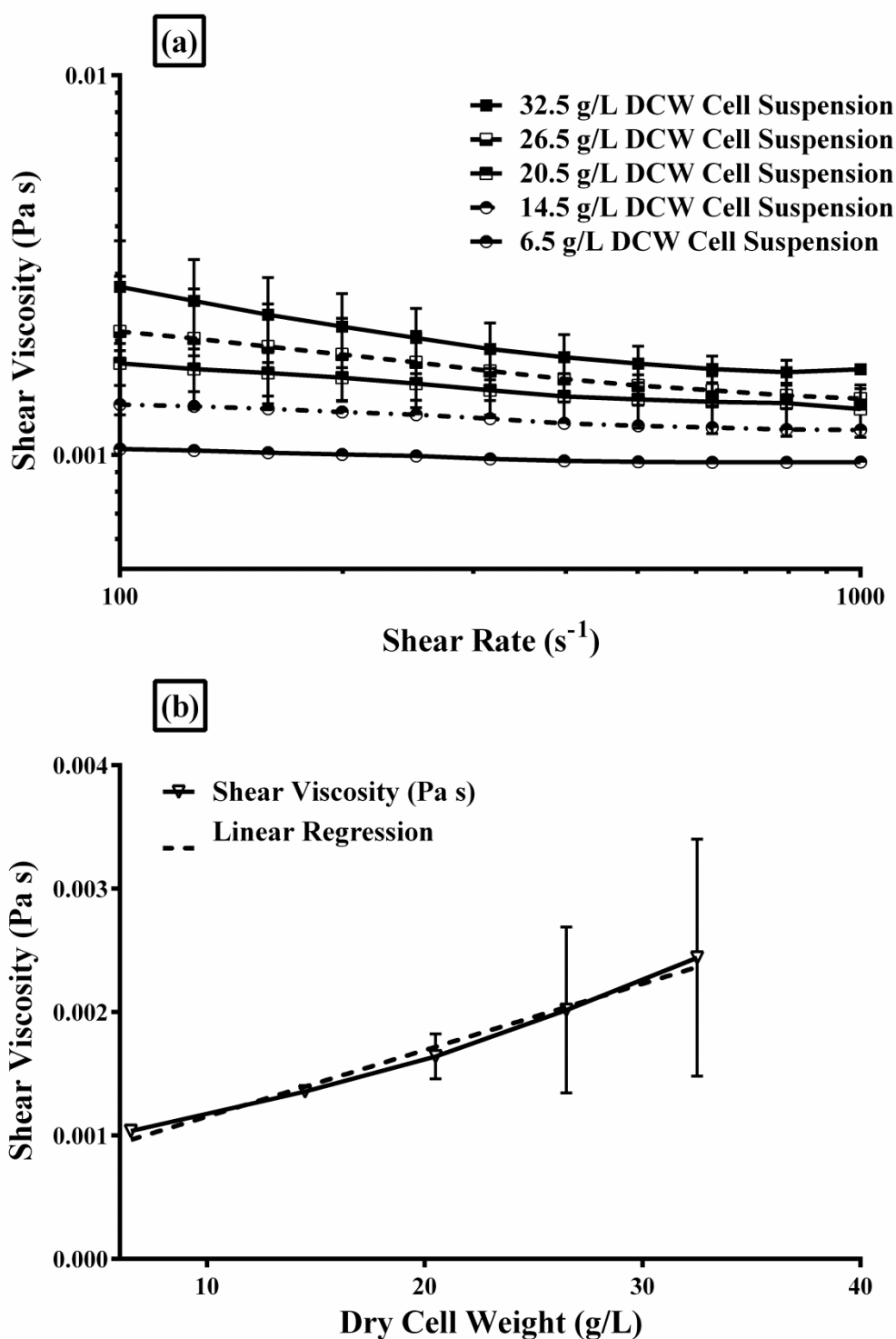
Figure 4-6: Determining the relationship between cell concentration and shear viscosity. (a) Flow curves of cell suspensions (shown as dry cell weight, g/L) measured over a shear rate 100-1,000 s^{-1}, carried out in triplicate, using 50 mm parallel plates at 25°C and a 300 μm gap size. (b) The linear relationship between cell concentration (dry cell weight, g/L) and shear viscosity at 100 s^{-1}; the R^2 value was 0.98. Error bars show standard deviation.

**Table 4-4: Flow behaviour index (n) values for the flow curves presented in
Figure 4-6 (a) of *E. coli* biomass at various times throughout fermentation, over
a shear rate of 100-1000 s^{-1}, using a Malvern Instruments Kinexus Lab +
rotational rheometer. Induction time was at 38 h using IPTG. Measurements
were carried out at 25°C using 50 mm parallel plates and a 300 µm gap size. An
increase in shear thinning behaviour is evident as the cell concentration
increased. Triplicate viscometry measurements were recorded at each shear
rate, and held at steady state for 10 seconds. Error bars show standard
deviation.**

Sample	Flow behaviour index, n
6.5 g/L DCW	0.965 ± 0.00189
14.5 g/L DCW	0.933 ± 0.00816
20.5 g/L DCW	0.880 ± 0.0433
26.5 g/L DCW	0.842 ± 0.140
32.5 g/L DCW	0.767 ± 0.105

4.5.2 Viscosity and protein concentration

Figure 4-7 displays flow curves of bovine serum albumin (BSA) protein at various concentrations, ranging from 10-50 g/L. At all concentrations, protein solutions exhibited highly shear thinning behaviour, as seen in Figure 4-7 (a) and in Table 4-5, ranging from a flow behaviour index of 0.6 - 0.7. Nonetheless, plotting the relationship between protein concentration and shear viscosity in Figure 4-7 (b) at 100 s^{-1}, there is a clear linear relationship evident, with an R^2 value of 0.92. The relationship between protein and shear viscosity is presented below in Equation 4-2, where η_{prot} is the viscosity of protein in Pa s and C_{prot} is the concentration of protein (g/L);

$$\eta_{prot} = 3.79 \times 10^{-5} C_{prot} + 0.0016 \qquad \textbf{Equation 4-2}$$

E. coli cells contain a vast range of proteins and although they differ from BSA (a globular protein), it is thought that the total concentration of protein in the cell broth is more important in determining the viscosity of the broth, than the viscosity of a specific protein (of which there is a wide range), and therefore it was assumed that the relationship between total protein in the fermentation broth and shear viscosity is linear. However, for this relationship to be used in a model, the rheological properties of host cell protein (i.e. *E. coli)* must be analysed in detail, as different proteins may also present very different rheological properties.
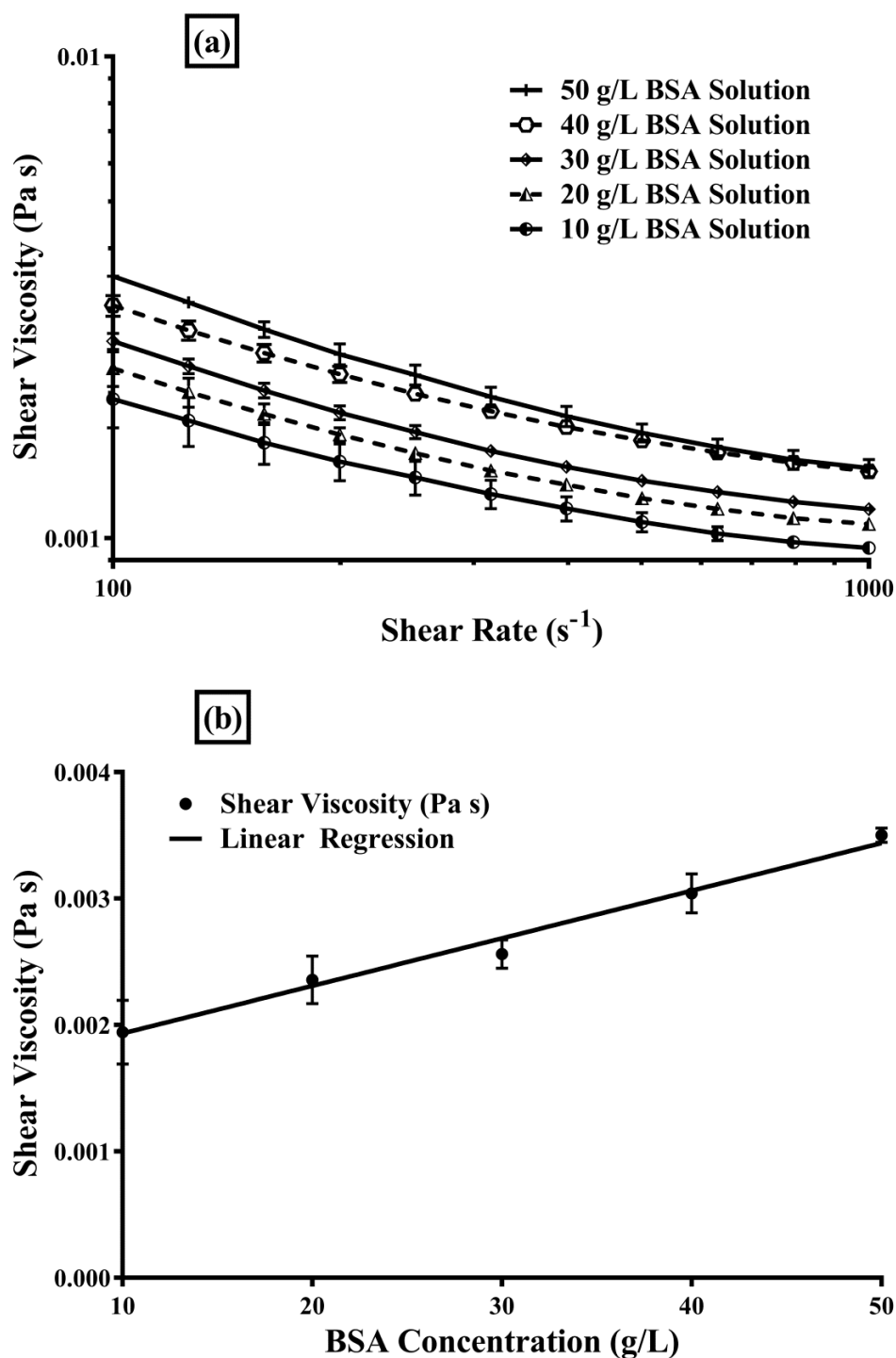
Figure 4-7: Determining the relationship between protein concentration and shear viscosity. (a) Flow curves of protein (BSA) solutions measured over a shear rate 100-1,000 s^{-1}, carried out in triplicate, using 50 mm parallel plates at 25°C and a 300 μm gap size. (b) The linear relationship between protein concentration and shear viscosity at 100 s^{-1}; the R^2 value was 0.92. Error bars show standard deviation.

Table 4-5: Flow behaviour index (n) values for the flow curves presented in Figure 4-7 (a) of protein at various concentrations (10 - 50 g/L), over a shear rate of 100-1000 s^{-1}, using a Malvern Instruments Kinexus Lab + rotational rheometer. Induction time was at 38 h using IPTG. Measurements were carried out at 25°C using 50 mm parallel plates and a 300 μm gap size. An increase in shear thinning behaviour is evident as the cell concentration increased, however all samples were highly shear thinning. Triplicate viscometry measurements were recorded at each shear rate, and held at steady state for 10 seconds. Error bars show standard deviation.

Sample	Flow behaviour index, n
10 g/L BSA	0.693 ± 0.0448
20 g/L BSA	0.657 ± 0.0329
30 g/L BSA	0.658 ± 0.0135
40 g/L BSA	0.655 ± 0.0155
50 g/L BSA	0.601 ± 0.0106

4.5.3 Viscosity and DNA concentration

Figure 4-8 (a) plots the flow curves for DNA at various concentrations (0.5 g/L to 4 g/L). All flow curves displayed Newtonian behaviour over the shear rate range studied (100-1000 s^{-1}), i.e. where the shear viscosity is independent of the shear rate, as shown in Table 4-6. As seen in Figure 4-8 (b), a linear relationship between DNA and viscosity is also evident, and an R^2 value of 0.99 was obtained. The relationship between DNA concentration and shear viscosity is shown below in Equation 4-3, where C_{DNA} is DNA concentration (g/L) and η_{DNA} is the viscosity of DNA in Pa s;

$$\eta_{DNA} = 0.0005123C_{DNA} + 0.001 \qquad \textbf{Equation 4-3}$$

This study used herring sperm DNA, a frequently studied and widely available DNA for research use. However, the wide range of nucleic acid content found in the cell broth during cell lysis is much more complex than this. This may include both DNA and RNA, as well as fragments of nucleic acids that have been degraded due to the harsh environment found inside the bioreactor. Therefore, although this study presented an interesting result, it only provides an indication of the complex mixture of nucleic acids found in the cell broth. In this way, it could be that RNA or fragments of nucleic acids have shear thinning behaviour, as well as a contribution to the overall broth viscosity.

4.5.4 Comparing the shear viscosity of DNA, protein and cells

From Figure 4-6, Figure 4-7 and Figure 4-8, it can be seen that cell concentration, protein concentration and DNA concentration all have linear relationships with shear viscosity. It is widely believed that the release of DNA during cell lysis causes the increase in viscosity in postinduction fermentation, and on a gram per gram basis, this is true; DNA has a much higher impact on the shear viscosity. This is reflected in the gradient of the linear equations; the gradient of the viscosity-DNA relationship is 0.0005123 and the gradient of the viscosity-protein relationship is 3.79 x 10^{-5}.

However, for the high cell density *E. coli* fermentation under study, extracellular protein concentration reached up to 40 g/L and extracellular DNA typically reached ~3 g/L. Comparing Figure 4-7 and Figure 4-8; protein at a concentration of 40 g/L has a shear viscosity of ~0.003 Pa s and DNA at a concentration of 3 g/L has a shear viscosity of ~0.0025 Pa s. Therefore, it can be seen that protein (in quantities typically found inside the bioreactor during cell lysis) has an equal or greater contribution to the shear viscosity as DNA.

In addition, the non-Newtonian behaviour of the cells increased as the cell concentration increased, exhibiting shear thinning behaviour. Moreover, for the entire shear rate range studied, 100-1000 s^{-1}, including the average shear rate found inside the bioreactor (100 s^{-1}, see Materials & methods section 2.5 for discussion of this) the DNA displayed Newtonian behaviour. However, the protein displayed strong non-Newtonian, shear thinning behaviour at all concentrations studied. This is interesting because it shows that protein has both a significant contribution to the shear viscosity increase during cell lysis, as well as a considerable effect on the shear thinning behaviour of the cell broth seen in late stage fermentation.
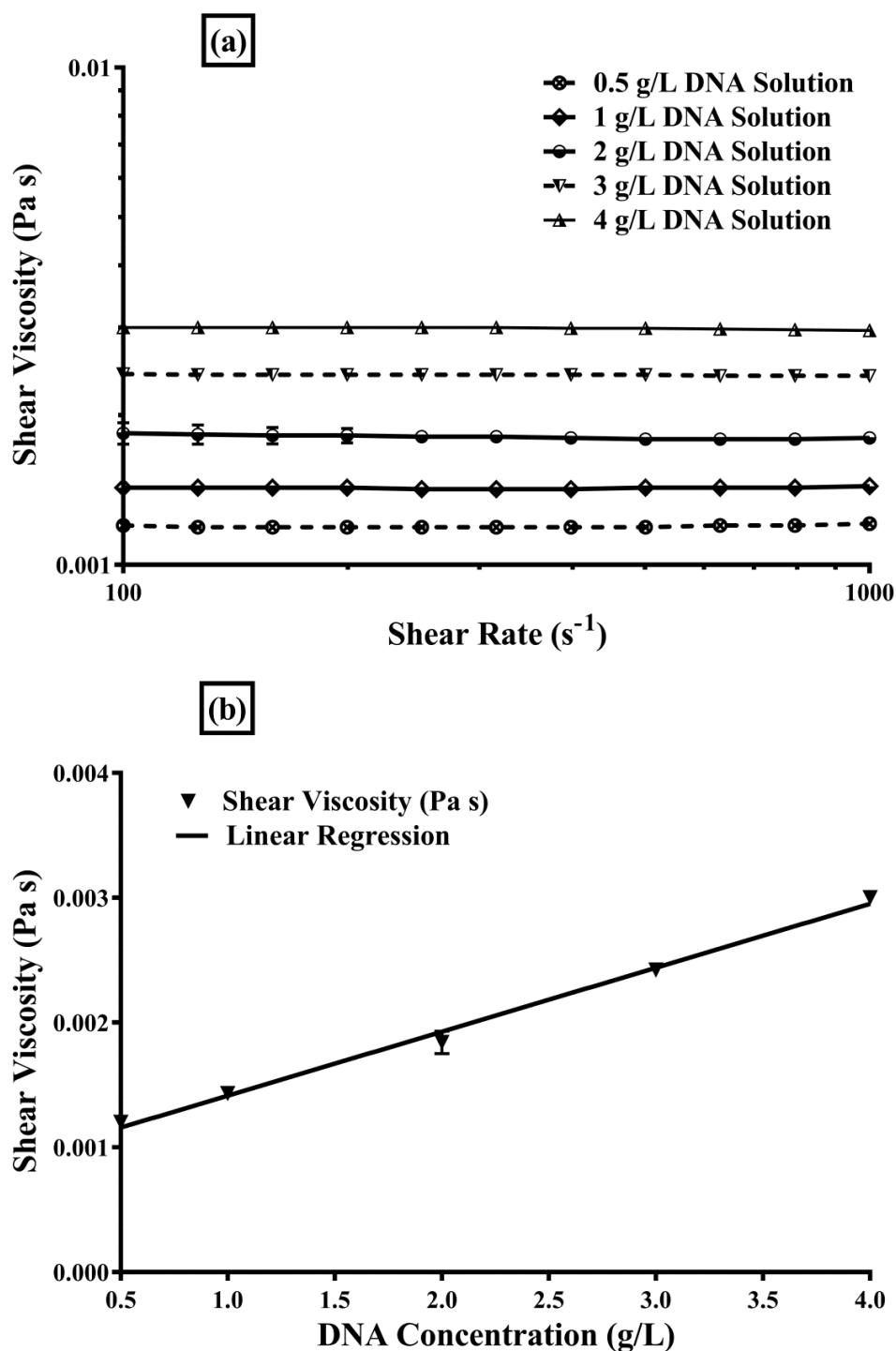
**Figure 4-8: Determining the relationship between DNA concentration and shear
viscosity. (a) Flow curves of DNA solutions at various concentrations, measured
over a shear rate 100-1,000 s^{-1}, carried out in triplicate, using 50 mm parallel
plates at 25°C and a 300 μm gap size. (b) The linear relationship between DNA
concentration and shear viscosity at 100 s^{-1}; the R^2 value was 0.99. Error bars
show standard deviation.**

169

Table 4-6: Flow behaviour index (n) values for the flow curves presented in Figure 4-8 (a) of DNA at various concentrations (0.5 - 4 g/L), over a shear rate of 100-1000 s^{-1}, using a Malvern Instruments Kinexus Lab + rotational rheometer. Induction time was at 38 h using IPTG. Measurements were carried out at 25°C using 50 mm parallel plates and a 300 μm gap size. Newtonian behaviour was observed for all samples under study. Triplicate viscometry measurements were recorded at each shear rate, and held at steady state for 10 seconds. Error bars show standard deviation.

Sample	Flow behaviour index, n
0.5 g/L DNA	1.01 ± 0.00325
1 g/L DNA	1.00 ± 0.000434
2 g/L DNA	0.991 ± 0.0207
3 g/L DNA	0.997 ± 0.00335
4 g/L DNA	0.995 ± 0.00197

4.5.5 Quantifying cell lysis using viscosity monitoring

The definition of cell lysis is that if cells are leaking DNA, then cell lysis is occurring. Therefore, DNA leakage to the fermentation broth can be used as a method to monitor and quantify cell lysis. From Figure 4-8, it can be seen that a linear relationship between DNA and viscosity exists.

In the growth phase of fermentation, viscosity is determined by cell concentration (i.e. such as the Einstein viscosity equation). However, in postinduction cell cultures (where cell concentration can be assumed to be constant), there are other factors affecting broth viscosity, such as the leakage of intracellular content. It has previously been shown (Voulgaris et al., 2016) that a relatively linear relationship exists between DNA leakage and product loss. In addition, the simultaneous leakage of DNA and the Fab' product during cell lysis was shown in the previous chapter. Therefore, assuming a proportional relationship between DNA and other intracellular content; by carrying out rapid viscosity monitoring during fermentation, DNA leakage to the broth can be modelled and quantified, and cell lysis and product loss can be inferred based on DNA release.

A linear model was created, shown in Figure 4-9, using experimental data from 3 identical fermentation runs, with 23 total data points. The model was created using MATLAB (The Mathworks, Inc., Natick, Massachusetts, USA), however this was done for convenience and to generate a logical methodology. It is recommended that users could execute this model very easily in Microsoft Excel or other more accessible software programs. Having previously determined a linear relationship between shear viscosity and DNA (Figure 4-8), the model was created using a linear "polyfit" function (n=1, where n is the degree of polynomial fit). The determined equation is presented below in Equation 4-4:

$$C_{DNA} = 905.8(\eta_t - \eta_0) + 0.1486 \qquad \textbf{Equation 4-4}$$

where C_{DNA} is the concentration of DNA that has leaked to the fermentation broth, η_t is the shear viscosity at the time point of interest (postinduction) and η_0 is the shear viscosity at induction point in fermentation, taken as a zero point in order to negate differences in cell density between batches (as discussed in the previous chapter).

By the time the cell density changes substantially in fermentation (see Figure 4-5), considerable cell lysis has already taken place (and a typical batch would be terminated at a much earlier time point), therefore it was assumed that cell density is constant throughout the stationary phase, and a cell concentration factor was not implemented into the model.

An R^2 value of 0.91 was determined for the model, which shows a highly linear relationship between the postinduction cell broth viscosity and DNA release. Generally, the model performed very well for all three fermentation datasets, and the majority of data points fell within the 90% confidence bands, with the exception of three outliers seen in Figure 4-9. A greater number of data points are at lower viscosities, and this is the most critical point to detect cell lysis and product leakage. In real fermentation runs, the batch would be ended before reaching such high viscosities (where the aim is to minimise product loss to the cell broth), which for this *E. coli* fermentation system corresponds to an increase in viscosity of up to 0.001 Pa s. Below an increase in shear viscosity of 0.001 Pa s, almost all data points were within the 10% confidence bands and the model performed particularly well in this region.

The model in Figure 4-9 demonstrates that by taking rapid at-line or indeed online viscosity measurements, it is possible to instantly quantify DNA leakage to the fermentation broth. This enables the operator to make rapid decisions about cell harvesting, as DNA leakage has implications on many downstream processing unit operations. The potential application of this model for other fermentation systems would be particularly useful for host cells with intracellularly-stored recombinant protein products. However, generally, it is useful to know DNA leakage during fermentation, including for mammalian cell processes where the product is secreted to the extracellular space; the DNA release would indicate cell lysis and hence the

level of contamination in the broth. This model also gives an indication of product loss, as product loss occurs simultaneously to DNA release (Voulgaris et al., 2016) (and see results in previous chapter, Chapter 3).
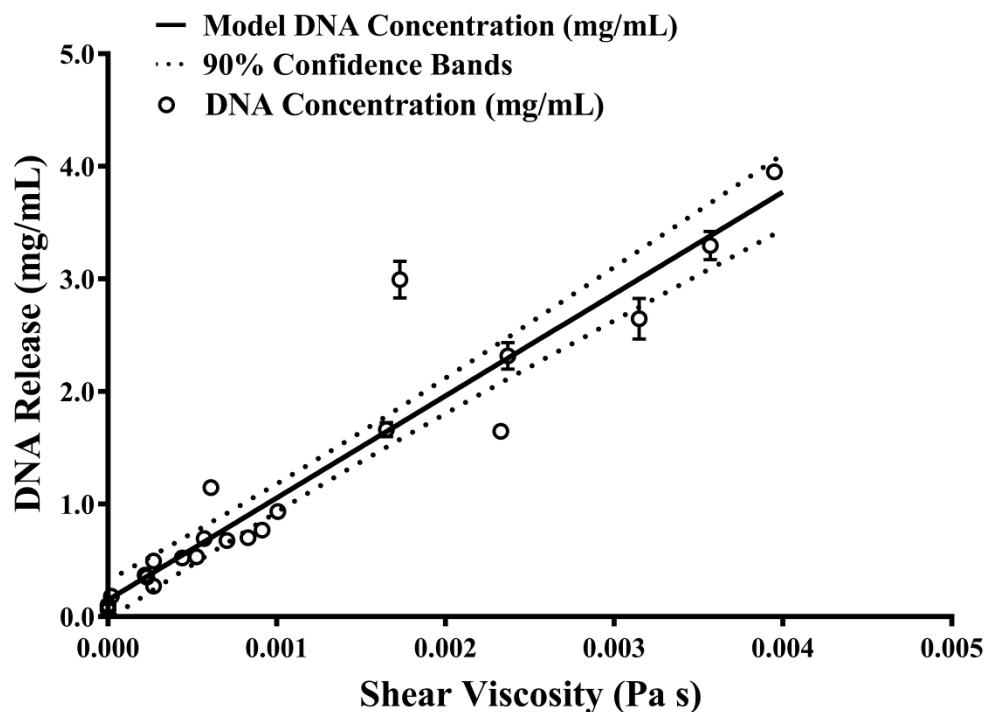
**Figure 4-9: Comparison of model prediction of cell lysis with experimental data.
Results of an empirical model built with three fermentation datasets (23 total
data points), to determine DNA concentration in extracellular space (mg/mL,
experiments carried out in triplicate), and hence cell lysis, from rapid viscosity
measurements. The R^2 value was 0.91, and the model had 3 outliers in the
dataset. 90% confidence bands are shown. Data was normalised to perform the
modelling and de-normalised to obtain the final results. Error bars show
standard deviation.**

4.6   Composition of an *E. coli* cell

The composition of an *E. coli* cell was published by Neidhardt & Umbarger (1996), and is shown below in Table 4-7. It was discussed in the previous section that protein has a significant contribution to the viscosity increase during cell lysis in postinduction fermentation, and in fact; protein makes up 55% of the dry weight of a cell.

In addition, high molecular weight DNA only makes up 3.1% of the dry weight of a cell. This shows that, although the DNA content of a cell is small, the relative impact that DNA has on the viscosity is large. However, although RNA is only a single strand of nucleotides and is much shorter than DNA, the RNA content of a cell makes up 20.5%; a significant component. Therefore, it is possible that in such a large proportion, RNA also has a significant contribution to the viscosity of the cell broth during cell lysis. This would be interesting to study further, although a study by Kong et al. (2009) showed that RNA does not significantly affect the viscosity during chemical lysis in *E. coli*.

Moreover, lipids (9.1%) and lipopolysaccharides (3.4%) make up a significant proportion of the dry weight of a cell, and may have a role in affecting the rheological properties of a cell broth during lysis. This may also be interesting to study in further detail.

It has also been shown that *E. coli* can secrete exopolysaccharides under stressed conditions such as osmotic and oxidative stresses (Lonescu & Belkin, 2009), which work to exhibit a protective effect on the *E. coli* cells*,* making them more resistant to heat and acid treatment (Chen and Mao, 2004). It would therefore be interesting to quantify colanic acid formation during late stage fermentation, and understand how this interacts with cell aggregation and cell lysis; cell aggregation has been shown to be affected by extracellular polymeric substances (Eboigbodin & Biggs, 2008), and would also affect the viscosity of the cell broth due to a change in the size of the particles (i.e. cells).

Table 4-7: Composition of an *E. coli* cell (Neidhardt & Umbarger, 1996)

Composition of an *E. coli* cell	% Dry weight
Protein	55
RNA	20.5
DNA	3.1
Lipids	9.1
Lipopolysaccharides	3.4
Peptidoglycan	2.5
Glycogen	2.5
Polyamines	0.4
Metabolites, Cofactors, Ions	3.5

4.7   Conclusions

The previous chapter focused on developing a method to detect cell lysis using rapid viscosity monitoring in postinduction fermentation. The present chapter has added to this work by carrying out advanced rheological studies on *E. coli* cells to develop a deeper understanding of the effects that cell lysis has on the physical properties of cell broths.

Components of the cell broth (cells and supernatant) were isolated and their viscosity was compared to whole cell broth. It was determined that the increase in shear viscosity in postinduction fermentation originates from the large increase in supernatant viscosity, which can be attributed to the release of intracellular content from the cells during lysis.

Oscillatory tests were then carried out on cell paste and used to gain insight into changes in the strength and stability of the cells over the course of fermentation. The change in cell strength was quantified and monitored using the storage modulus (G'). A decrease in the storage modulus and an increase in the LVER were observed, suggesting that although cell strength decreases over the fermentation, interactions are present between cells and leaked intracellular content such as DNA, which increases the "stickiness" of the paste.

These results demonstrate the power of rheology to characterise and monitor the physical properties of cell broths, which can provide useful information on cell health such as changes in cell strength. The insight derived here presents a useful opportunity to further explore rheology-based monitoring techniques in bioprocessing.

Cells, protein and DNA were isolated and viscometry tests were carried out at different concentrations. Linear relationships between shear viscosity and cells, protein and DNA concentration were observed. It was also shown that protein is shear thinning and has a significant contribution to viscosity in lysed cell broths, in addition to DNA, which has not previously been considered. Based on the linear

viscosity-DNA relationship, an empirical model was created, where it is possible to accurately quantify the level of cell lysis (by determining DNA concentration in the cell broth), by carrying out rapid at-line viscosity measurements. This directly indicates product loss, as a proportional relationship exists between DNA leakage and product loss, and therefore enables operators to make rapid decisions about harvest time. It is also envisaged that this model could be used for a wide range of industrial fermentation systems simply by characterising the relationship between viscosity and DNA leakage, and then implementing at-line viscosity monitoring.

The next chapter will focus on a process design case study, demonstrating the use of viscosity monitoring in fermentation to determine the optimal harvest time, where the aim is to understand the impact of upstream processing conditions on various primary recovery unit operations.

Chapter 5 Evaluating process options in Fab' primary recovery: crossflow filtration with flocculation to improve product yield, purity and process robustness

5.1 Introduction

Cell lysis in late stage fermentation represents a significant challenge in bioprocessing. In addition to product loss, impurities such as nucleic acids and host cell protein lead to large variations in the material properties of the cell broth, and therefore significantly impact both the operational performance of many downstream unit operations, as well as the robustness of the process. For the fermentation system under study in this thesis, the product is targeted to and stored in the periplasmic space, and therefore it is desired to harvest the cells at maximum intracellular product concentration. However, by doing this, there are many challenges to overcome with respect to cell lysis, such avoiding premature lysis during fermentation.

Considering the many problems associated with avoiding lysis in fermentation that have been observed and discussed throughout this thesis, this results chapter focuses on assessing a novel processing strategy, by running fermentations to maximum productivity (i.e. full autolysis), thereby achieving a much higher total product titre, and instead focusing on the recovery of the product from the extracellular space. It is proposed that this strategy may also reduce variability in the material properties of the cell broth and therefore improve the robustness of the process, as well as improve product yield. Therefore, this chapter aims to demonstrate an application of viscosity monitoring in fermentation to detect cell lysis and to inform novel process design strategies, focusing on assessing the impact that cell lysis has on several primary recovery unit operations.Two primary recovery sequences have been carried out using ultra scale-down (USD) technology, and evaluated alongside the existing Fab' primary recovery process, on the basis of total product recovered, impurity concentration, solids removal, processing time, capital costs and complexity.

5.1.1   Problems with the existing Fab' process

E. coli is extensively used for the production of recombinant proteins and has in fact become the most popular expression platform (Rosano and Ceccarelli, 2014). There are many advantages of using *E. coli* as a host organism to produce recombinant proteins, some of which include the ability to be grown to high cell density using inexpensive media, well-characterized genetic properties (Spadiut et al., 2014) and no requirement for glycosylation (Li et al., 2013). Recombinant proteins such as antibody fragments (Fab') produced in *E. coli* can be routinely targeted to the periplasmic space, however the capacity of the periplasm is limited (Schofield et al., 2016). As the periplasm reaches this capacity, cell lysis occurs and product is lost to extracellular space (see results Chapter 3 and Chapter 4). Traditionally, it is desired to retain the Fab' product within the periplasm during fermentation and harvest the cells before significant lysis and product leakage occurs. As such, the aim is to maximise intracellular product concentration in fermentation, however, there is a narrow processing window between optimal intracellular concentration and the rapid onset of cell lysis.

Upon reaching maximum intracellular product concentration, the cell broth is harvested. This typically includes holding time (up to several hours at large scale) and pumping the broth to the following unit operation i.e. beginning primary recovery operation. However, at the point of maximum intracellular product concentration, the cells are weak and fragile (Perez-Pardo et al., 2011). This means that cells will continue to lose viability while they are held and stirred in a holding tank, and will be susceptible to lysis from the shear experienced due to pumping. Therefore, the existing process lacks robustness, as the pumping and product hold step can lead to significant product loss, as well as variation in the level of lysis. For example, at harvest point, the level of product loss may be 10%, however after product hold and pumping, this can reach as high as 40%. In addition, previous studies suggested that the shear experienced due to discharge from disc stack centrifuges can result in 10-20% disruption of *E. coli* cells (Gray et al., 1972). These issues mean that the final product yield at the end of primary recovery can

significantly vary, which also presents issues with equipment sizing for both primary recovery as well as for the subsequent purification steps.

As seen in Figure 5-1 (a), the existing Fab' primary recovery sequence involves centrifugation to harvest the cells, re-suspension of the cell paste in extraction buffer to an appropriate level, periplasmic extraction to release the Fab' product from the cells, followed by centrifugation and depth filtration to remove the cell debris (Aucamp et al., 2014). However, due to the finite capacity of the periplasm to store the product, a constraint exists in the upstream process which limits the total amount of recoverable product in the downstream process. This is compounded by the limitations of each unit operation, as each unit operation also has a maximum achievable yield. Therefore, the large number of unit operations in the existing Fab' primary recovery process also reduce the overall product yield.
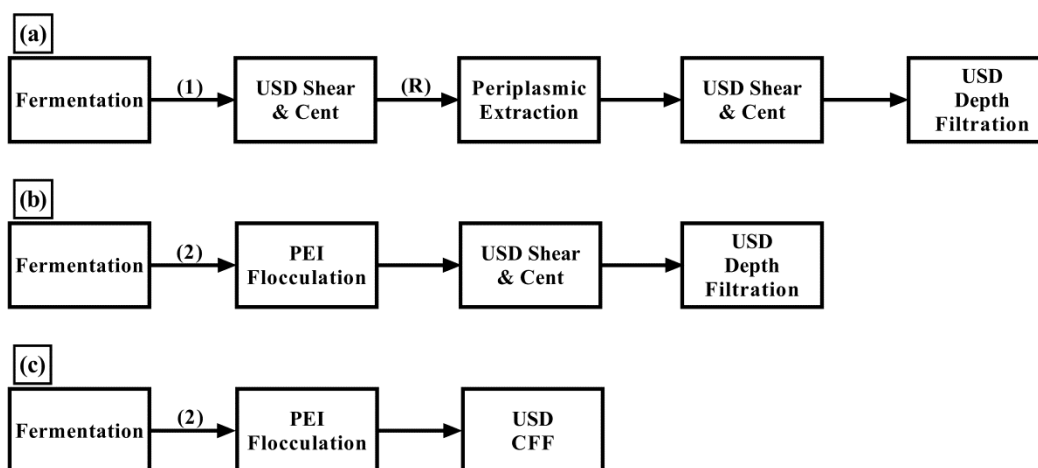
Figure 5-1: Process flowsheets of the primary recovery sequences under study. (a) USD study of the existing sequence for the primary recovery of Fab' from *E. coli* fermentation. (1) indicates Harvest Point 1 at maximum intracellular concentration (as seen in Figure 5-3, at 32 h postinduction). (R) indicates re-suspension with extraction buffer, carried out after centrifugation at a 70% dewatering level; (b) USD study carried out using a similar primary recovery sequence to that used by Voulgaris et al. (2016), with flocculation and centrifugation followed by depth filtration, after fermentation ran to maximum productivity i.e. fully autolysed cells. (2) indicates Harvest Point 2 at 57 h postinduction (as seen in Figure 5-3); (c) USD study carried out using a novel combination of flocculation with crossflow filtration, after fermentation ran to maximum productivity i.e. fully autolysed cells, and harvested at Harvest Point 2 (as seen in Figure 5-3).

5.1.2 Flocculation

A range of research has previously been carried out with the aim of overcoming the various challenges of cell lysis in fermentation, including the selective release of product from the periplasm (Jalalirad, 2013), or the co-expression of nuclease to reduce nucleic acid content in the cell broth (Balasundaram et al., 2009). However, these methods have their own unique challenges, such as the need to avoid premature cell lysis in fermentation (Mergulhão et al., 2005).

Previous work by Voulgaris et al. (2016) carried out a study to evaluate the ability to recover a recombinant protein product (domain antibody, dAb) from a fermentation ran to maximum productivity, (i.e. maximum total product titre) where the majority of cells had lysed, so that over 95% of product had been released to the cell broth, using a sequence similar to that shown in Figure 5-1 (b). In this work, polyethyleneimine (PEI) was used as a precipitant and flocculant at the end of fermentation to clean up the cell broth; selectively precipitating and flocculating host cell protein, nucleic acids and endotoxins, in addition to flocculating cells and cell debris (Voulgaris et al., 2016).

Some advantages of flocculation include the quick action of the PEI reagent and its ability to remove a wide range of impurities and cell debris by high speed centrifugation (due to the larger particle size of the flocculated material). A detailed review of the use of flocculation for lysed cell suspensions has been carried out elsewhere (Rayat et al., 2016; Voulgaris et al., 2016), however there are several studies demonstrating the successful use of flocculation in primary recovery (Milburn et al., 1990; Salt et al., 1995; Berrill et al., 2008; Espuny Garcia del Real et al., 2014; Voulgaris et al., 2015), such as a reduction of contaminants by over 50-fold when using a combination of flocculation, USD shear stress and centrifugation (Chatel et al., 2014).

5.1.3 Crossflow filtration

Microfiltration (MF) and ultrafiltration (UF) processes are established technologies across various industries including biopharmaceutical and pharmaceutical

manufacturing (Baruah et al., 2005). Crossflow filtration (CFF), where the feed flows tangentially to the membrane surface (as opposed to perpendicular flow in traditional depth filtration), is also used in primary recovery to separate recombinant protein from *E. coli* lysate (Forman et al., 1990), for example after homogenisation (Bailey and Meagher, 1997). Key advantages of using CFF instead of centrifugation or depth filtration include better separation in terms of clarification and product yield, better control over the process and lower capital and operating costs (Keefe and Dubbin, 2005). However, although CFF can achieve higher product yields by operating in diafiltration mode after the concentration step, the product will become increasingly diluted. In general, important challenges in the commercial development of microfiltration include process robustness, such as excessive membrane fouling due to high impurity loading in the feed material, and scalability, although CFF is thought to be more appropriate than depth filtration for large scale applications (Belfort et al., 1994; Yavorsky et al., 2003).

The use of flocculation in combination with centrifugation and/or depth filtration has previously been shown to improve product yield, throughput and clarification (Berrill et al., 2008; Roush and Lu, 2008; Chatel et al., 2014; Espuny Garcia del Real et al., 2014), however given the apparent processing advantages of CFF compared to both centrifugation and depth filtration, it may also be possible to obtain superior operational performance (i.e. throughput and capacity), clarification, product purity and yield by using CFF in combination with flocculation (see Figure 5-1 (c)). Therefore, if equivalent or superior operational performance can be achieved, CFF combined with flocculation may be able to replace both centrifugation and depth filtration unit operations. This would simplify the primary recovery process and open up a range of new possibilities for biopharmaceutical process design and operation.

5.1.4 Ultra scale-down technologies

To improve speed to market for groundbreaking therapies, a popular theme currently trending in the biopharmaceutical industry is leveraging technological innovation in order to streamline drug discovery and process development. There are a multitude of opportunities available within this space and some examples include the use of

computational biology for "virtual screening" in drug discovery (Lavecchia and Di Giovanni, 2013), upstream advances in synthetic biology and genome engineering techniques such as CRISPR (Hsu et al., 2014), the Tecan robotics platform (Dong et al., 2016), and TAP's AMBR 250 system (Xu et al., 2016) for automated, high-throughput analysis, the development of high-throughput microfluidic devices such as "lab on a chip" (Liu and Lu, 2016) or "organs-on-chips" devices (Esch et al., 2015) and ultra scale-down (USD) technologies (Rayat et al., 2016).

Ultra scale-down technologies use millilitre quantities of material to gain an understanding of how a process will behave at large scale. A comprehensive review of the development of this technology has been carried out elsewhere (Rayat et al., 2016), however some of the benefits include the ability to carry out high-throughput experiments, process automation, reduced scale-up risk, the ability to assess process design alternatives at small scale (e.g. following quality by design (QbD) principles and a design of experiments approach (DoE)) and the rapid optimisation of processing conditions. USD technologies have received most attention in the early primary recovery stages of the bioprocess, which therefore enables researchers to investigate the interactions and trade-offs between upstream processing conditions and downstream operation efficiency (Rayat et al., 2014). This permits the researcher to take a process integration approach in order to rapidly optimise sections of, or even the entire bioprocess from end to end, which has traditionally been difficult to carry out due to the complexity, cost and time requirements for large scale bioprocessing.

There are several examples of ultra scale-down applications for process integration and process design, some highlights include studying the interaction between fermentation, homogenisation and centrifugation for the recovery of antibody fragments from *E. coli* (Li et al., 2013), the integration of host strain bioengineering and bioprocess development to screen and evaluate process robustness for a range of engineered strains (Aucamp et al., 2014), characterisation of the impact of conditioning methods (e.g. flocculation) on clarification performance by continuous centrifugation (Chatel et al., 2014) and the evaluation of options for the harvest of recombinant protein in *E. coli* fermentation, based on the extent of cell lysis

(Voulgaris et al., 2016). There are also many published studies demonstrating the ability of various USD technologies to mimic both pilot and large scale bioprocessing (Hutchinson et al., 2006; Perez-Pardo et al., 2011; Li et al., 2012; Lopes and Keshavarz-Moore, 2012; Espuny Garcia del Real et al., 2014). Additionally, the development of an ultra scale-down CFF device has previously been carried out by Ma et al. (2010), and a microscale CFF device has been developed by Rayat et al. (2014) to facilitate parallel analysis and integration for automated bioprocessing, and both devices included verification at pilot and large scale.

5.1.5 Aims & objectives

The research presented in this chapter uses USD technology as a platform to rapidly evaluate the performance of three bioprocess designs, based on a set of criteria including total product recovered, purity (total protein and nucleic acid impurity profiles) and clarification performance. In doing so, this chapter also aims to demonstrate that the novel use of CFF in combination with flocculation can achieve equivalent or superior clarification performance compared to the existing primary recovery process for Fab' produced in *E. coli*, in addition to a reduction of nucleic acid and host cell protein levels, whilst improving overall product yield, reducing primary recovery processing time, reducing the number of unit operations and lowering capital costs.

The overall aim of this chapter is to carry out a case study demonstrating an application of viscosity monitoring in process development. This will involve using viscosity monitoring to make decisions about harvest time and to influence an approach to create a novel process design in primary recovery.

The specific objectives of this chapter are to:

- Demonstrate an application of viscosity monitoring in fermentation process development by carrying out a case study

- Use ultra scale-down technology to gain an understanding of the impact of upstream processing conditions on downstream operation efficiency

- Evaluate the performance of a novel process design, based on several criteria such as clarification performance, total product yield, product purity, capital costs and processing time

5.2   Upstream processing

High cell density *E. coli* fermentations were carried out in fed-batch mode in a 5 L working volume Applikon fermenter, as previously described in results Chapter 3 and Chapter 4. Figure 5-2 shows the growth profile of typical duplicate fermentation runs, where dry cell weight reached a maximum of 60 g/L which corresponded to an OD_{600} of ~200. The exponential phase began at ~24 h and recombinant protein expression (Fab') was induced at 36 h with IPTG, after a dissolved oxygen spike was observed due to complete utilisation of the carbon source. At this point, glycerol was fed at a constant rate (6.4 mL/min), enabling rapid Fab' production in stationary phase. Harvest Point 1 and Harvest Point 2 are displayed in Figure 5-2, which correspond to 32 h postinduction and 57 h postinduction, respectively.

The duplicate product (Fab') profiles for the fermentation are shown in Figure 5-3 (a). After induction, rapid Fab' production began and reached a total of 1.9 mg/mL by the end of the fermentation. Intracellular product concentration increased rapidly until 32 - 36 h postinduction, where the concentration peaked and rapidly decreased thereafter. It can also be seen that product loss to the broth, i.e. Fab' leakage, remained low until reaching 32 h postinduction, and rapidly increased thereafter.

To carry out the primary recovery sequences presented in this chapter, cells were harvested at two separate time points. First, cells were harvested at maximum intracellular product concentration (0.8 mg/mL) at Harvest Point 1 (denoted on graph, Figure 5-3 (a)), in order to carry out process scenario 1 (see Figure 5-1 (a)). Second, cells were harvested at maximum productivity i.e. maximum total product titre, where significant cell autolysis had taken place (Harvest Point 2, 1.85 mg/mL

total product titre) to carry out process scenarios 2 and 3 (Figure 5-1 (b) and (c) respectively).

Therefore, for process scenarios 2 and 3, where the fermentation was ran to maximum productivity, the product titre was much higher than for scenario 1 (harvested at maximum intracellular concentration). In addition to the increase in product titre, this fermentation strategy also removed the need to avoid premature lysis in stationary phase, as it was desired to maximise the recovery of product in extracellular space (i.e. in the cell broth).

At Harvest Point 2, almost 60% of product had leaked to the broth, and material was then frozen and stored at -80°C before carrying out the DSP sequences. After thawing, cells were shaken gently for 1 h at room temperature before carrying out the process scenarios, at which point over 99% of product was found in extracellular space. For a real fermentation run using fresh cell broth, it is believed that ~100% lysis could rapidly be achieved at the end of fermentation by turning off fermenter controls (i.e. aeration and glycerol feeding) and continuing to agitate the cell broth for a short period.

The process sequence shown in Figure 5-1 (a) was carried out with fresh cells, after stirring gently for 1 h at room temperature to mimic holding time at large scale, as it was desired to retain the product within the periplasm and avoid cell lysis. At Harvest Point 1, ~10% product leakage to the broth had taken place. After holding time in process scenario 1, ~26% of product had leaked to the broth, which is a typical level of lysis after holding time at large scale. However, as discussed in section 5.1, this level can vary significantly, which can have a major impact on the product yield, process robustness and the performance of downstream unit operations, due to large variations in the material properties of the harvested cell broth.

In Figure 5-3 (b), the postinduction viscosity and nucleic acid profiles are shown. Shear viscosity was used to monitor the level of cell lysis in fermentation, using the method previously described in results Chapter 3 and Chapter 4. The nucleic acid

concentration in the broth increased from 2 to ~5 mg/mL between 0 and 20 h postinduction, showing that some lysis took place in early stationary phase. Between 20 - 32 h postinduction, the nucleic acid concentration increased to ~7.5 mg/mL (i.e. at Harvest Point 1), and rapidly increased thereafter until reaching almost 12 mg/mL at Harvest Point 2. The shear viscosity profile correlated well with the nucleic acid profile, increasing slightly between 0 and 20 h postinduction, then increasing to reach ~0.003 Pa s at Harvest Point 1, and rapidly increasing from this point onwards to 0.008 Pa s at Harvest Point 2.

The nucleic acid and viscosity profiles also provide an indication of the ease of processing for the two different harvest points; it is known that high viscosity is challenging for many downstream unit operations (see Introduction, section 1.3.3), and the nucleic acid content gives an indication of contaminants in the cell broth. Therefore, by monitoring the viscosity profile, it could be possible in the future to quantify the level of cell lysis and determine the amount of flocculant to add in the primary recovery step directly after fermentation (for process scenarios 2 and 3).

The Fab' titre and dry cell weight were slightly higher for the experiments presented in this chapter, in comparison to the results presented in Chapter 3 and Chapter 4. This is due to a recalibration issue; the tubing for the fermentation system was replaced before carrying out these experiments (i.e. the tubing for glycerol feeding), and the feeding rates were subsequently recalibrated. After recalibration, it is likely that the glycerol feed rate was slightly higher than in the fermentation runs reported in the previous results chapters, due to limitations imposed by discrete pump increments. This can be seen in Figure 5-2, where the dry cell weight continued to increase after induction point at 36 h. The overfeeding of glycerol and increased biomass also explains the increase in Fab' titre to 1.85 mg/mL. In addition, the final shear viscosity reached at Harvest Point 2 was higher than in previous fermentation runs, at 0.008 Pa s. However, the Fab' leakage profile, seen in Figure 5-3 (a), remained the same as in previous fermentation runs, where the onset of leakage was consistently observed between 32 - 36 h postinduction. This is due to the limited capacity of the periplasm.

Nucleic acid concentration and viscosity were used in this chapter to monitor the level of cell lysis. In Chapter 3 and Chapter 4, Picogreen assay was used to monitor double stranded DNA (dsDNA) in the cell broth, as dsDNA has a greater contribution to the viscosity, due to its longer length and higher molecular weight. However, Table 4-7 presented in Chapter 4 showed that RNA makes up a significant amount of a cell's weight, and may also have a contribution to the viscosity increase in postinduction fermentation. Furthermore, this chapter focuses on the performance of primary recovery unit operations. It is not only double stranded DNA that causes problems in downstream processing, but also single stranded DNA and RNA. In addition, for the purpose of monitoring the performance of contaminant removal in the flocculation step, total nucleic acid concentration is more meaningful, as PEI will precipitate and flocculate all nucleic acids, not only double stranded DNA. Therefore, total nucleic acid concentration was monitored in this chapter.
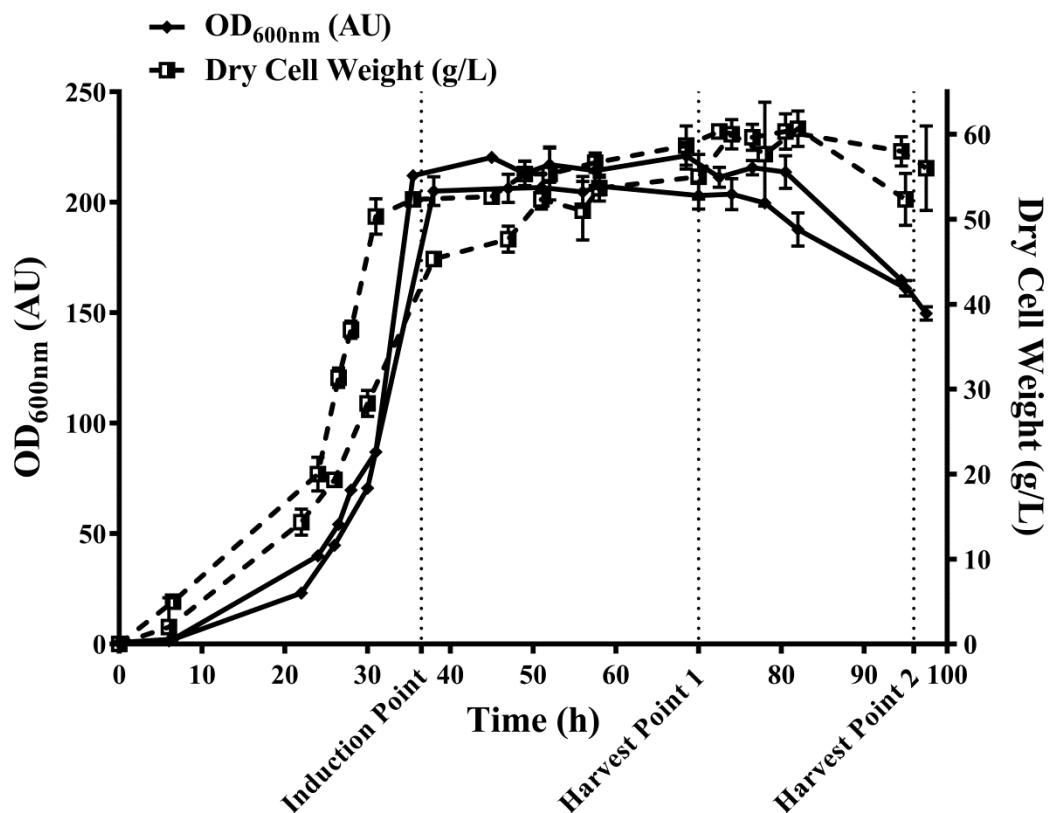
Figure 5-2: Fermentation growth profile for duplicate *E. coli* Fab' fermentations. Cells induced with IPTG at 36 h and fed with glycerol thereafter. Optical density at 600 nm (absorbance units (AU), in triplicate) and dry cell weight (g/L, in triplicate). Harvest Point 1 and 2 denote harvest at 32 h postinduction (process sequence 1) and 57 h postinduction (process sequence 2 and 3), respectively. Error bars show standard deviation.
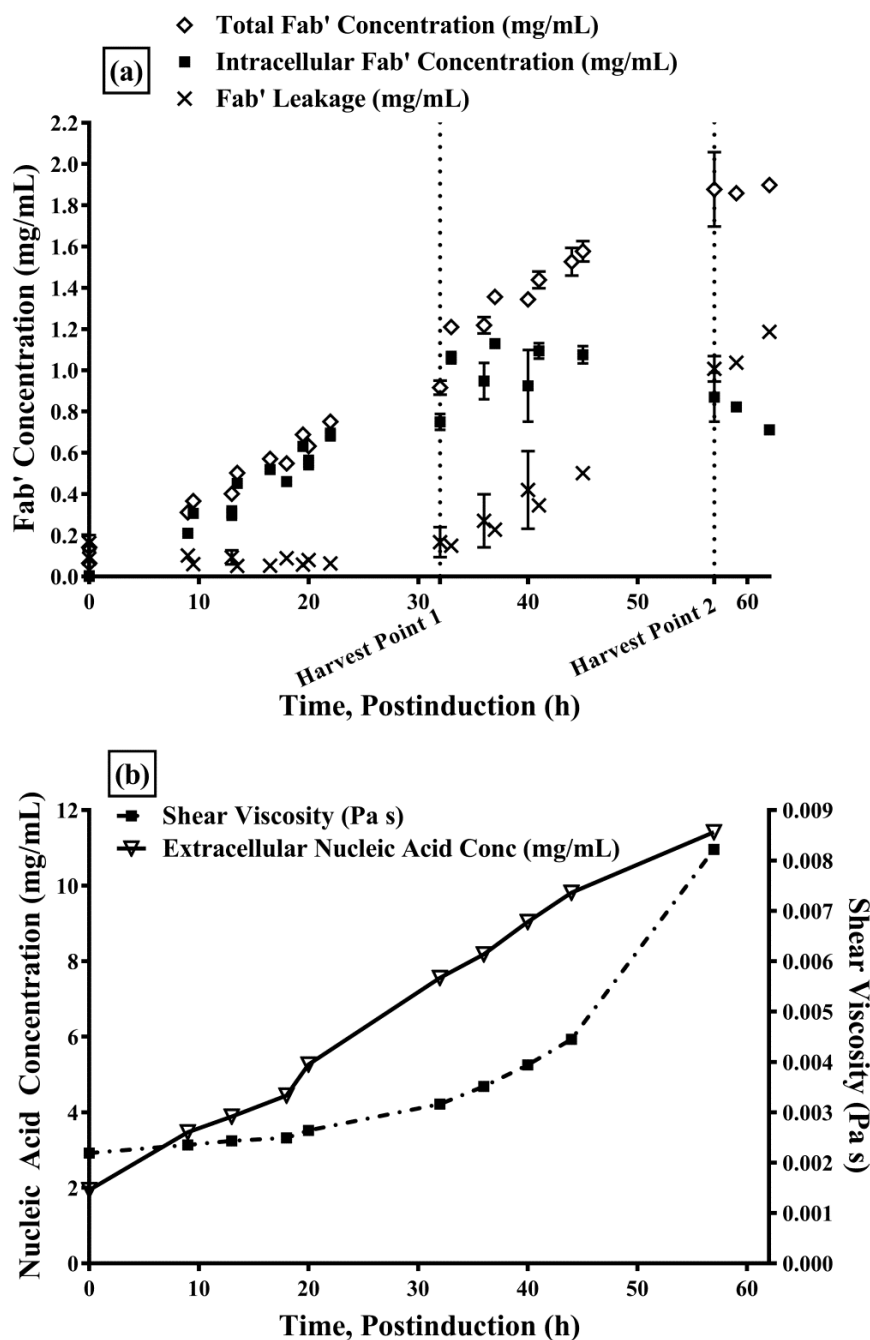
Figure 5-3: Product, nucleic acid and viscosity profiles for *E. coli* Fab' fermentation. Cells induced with IPTG at 36 h and fed with glycerol thereafter. Data shown postinduction. Harvest Point 1 and 2 denote harvest at 32 h postinduction (process sequence 1) and 57 h postinduction (process sequence 2 and 3) respectively. (a) Total Fab' concentration, intracellular Fab' concentration and Fab' leakage, (mg/mL, in duplicate); (b) Shear viscosity (Pa s, single measurement, held at steady state for 10 s) and extracellular nucleic acid concentration (mg/mL, in triplicate at 230 nm absorbance). Viscosity measurements were carried out at 25°C using 50 mm parallel plates and a 300 μm gap size. Error bars show standard deviation.

5.3   Flocculation studies

In preliminary studies carried out by Voulgaris et al. (2016), PEI concentration was assessed between 0.1 and 6% w/v of the broth (final concentration in the broth), and 0.5% PEI was chosen based on its ability to aggregate particles in the submicron range i.e. particles that are difficult to remove through centrifugation. In this section, the aim was to evaluate flocculation conditions for the *E. coli* cell broth at Harvest Point 2. PEI was therefore assessed at a range of concentrations, across several dimensions; the ability to flocculate cells and cell debris i.e. aggregate submicron particles, the removal of nucleic acids and host cell protein, and reduction of the supernatant viscosity.

The cell broth was harvested at 57 h postinduction and was fully autolysed. Cell broth was flocculated with PEI and assessed at three concentrations; 0.5%, 1.0% and 1.5% w/v final concentration in the broth. Figure 5-4 (a) presents the particle size distributions before and after flocculation, at each of the PEI concentrations, showing that all three concentrations successfully flocculated the material, with the smallest particle size around 2 μm and a median particle size, or d_{50}, of 139.65 μm (in comparison to a median particle size of 2.50 μm before PEI addition).

Figure 5-4 (b) shows the supernatant viscosity, extracellular nucleic acid concentration and extracellular protein concentration before and after PEI addition. It can be seen that increasing the concentration of PEI caused a reduction in extracellular protein and nucleic acid, which was also reflected in the reduction in supernatant viscosity. However, a trade-off exists; although higher levels of PEI increased the removal of nucleic acids and host cell protein, the flocculated material became extremely difficult to pipette at higher PEI concentrations due to the high solids concentration. Further, high levels of PEI create additional challenges downstream where there would also be a need to demonstrate its removal after the primary recovery steps. However, due to batch to batch variability in fermentation, adding enough PEI to the broth is also necessary to ensure robustness in the flocculation process. Therefore, 1% PEI was chosen to go forward, on the basis that it successfully flocculated cells and cell debris (above ~2 μm particle size), reduced

the supernatant viscosity by 17.6% and reduced the concentration of nucleic acids and host cell protein in the supernatant by 34.7% and 16.1%, respectively, without causing significant processability issues.
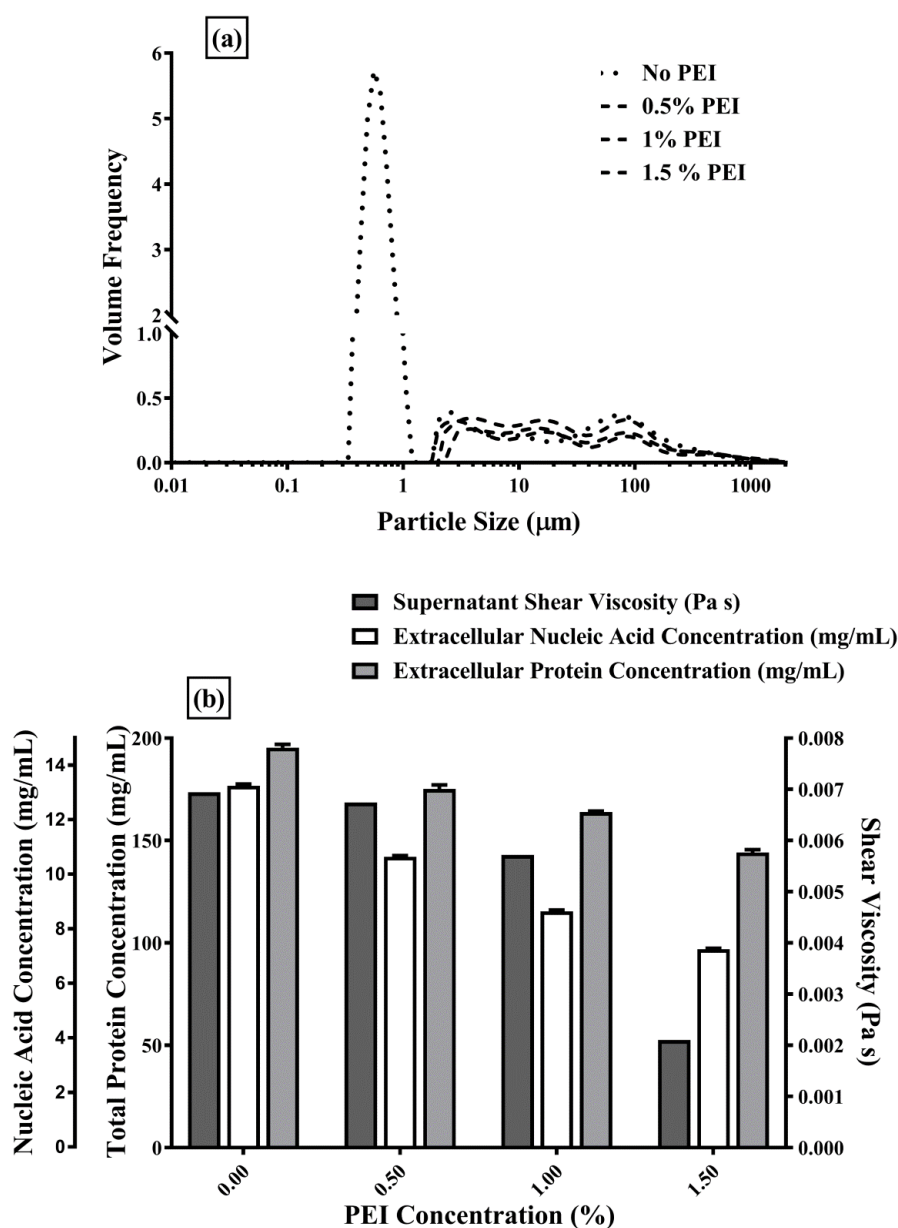
Figure 5-4: Evaluating flocculation conditions for *E. coli* cell broth. Cell broth used was autolysed and harvested at 57 h postinduction. (a) particle size distributions for *E. coli* cell broth with and without flocculation (PEI). Data recorded in triplicate and averaged before being treated using a method previously described by Chatel et al. (2014), to convert from volume % to volume frequency; (b) Extracellular nucleic acid concentration (measured in triplicate at 230 nm absorbance), extracellular total protein concentration (measured in triplicate at 280 nm absorbance) and shear viscosity of the supernatant of *E. coli* cell broth (Pa s, single measurement, held at steady state for 10 s) for different concentrations of PEI. Viscosity measurements were carried out at 25°C using 50 mm parallel plates and a 300 μm gap size. Error bars show standard deviation.

5.4   USD primary recovery studies

Ultra scale-down (USD) operating parameters (e.g. centrifugation and depth filtration) were selected based on both USD experimental data and previous studies by Voulgaris et al. (2016), to mimic typical conditions for large scale bioprocessing. This section presents an overview of the primary recovery processing sequences under study.

5.4.1   Process scenario 1

After harvesting cells at Harvest Point 1 (see Figure 5-3 (a)) and holding the broth for 1 h, the primary recovery sequence for process scenario 1 was carried out (see Figure 5-1 (a)). USD shear studies and centrifugation were first carried out. The broth was exposed to a shear stress (maximum energy dissipation rate) equivalent to 1.04×10^6 W/kg to mimic the shear level experienced in the feed zone and due to solids discharge in an industrial disc stack centrifuge. Following shear studies, small scale (bench-top) centrifugation was carried out at 6,800 rpm for 5 min, which was equivalent to industrial scale CSA centrifuge operation at 48 L/h, based on an equivalent settling area, $V_{lab}/t\sum_T$ of 1.96×10^{-8} m/s (see Materials & methods section 2.6.4 for calculation). The broth was subsequently dewatered to 70%.

After dewatering, the cell paste was re-suspended in extraction buffer at a ratio of 1 g cells: 7 mL extraction buffer, and periplasmic extraction was carried out for 12 h at 60°C and 250 rpm in a shaker-incubator to release the Fab' product. After extraction, USD shear studies and centrifugation were again carried out to remove the cells and cell debris. For the second shear study, a shear stress of 1.30×10^5 W/kg was used to mimic the shear experienced in the feed zone of an industrial disc stack centrifuge. Centrifugation conditions for the second centrifugation step were the same as stated above.

Following centrifugation, depth filtration was carried out on the supernatant stream, at constant pressure (300 mbar) using a nominal pore size of 0.1 μm. Figure 5-5 (a) shows the permeate volume vs. time for the duplicate USD depth filtration runs. The filtration performance was good, and had high reproducibility. It can be seen that the

196

filters became blocked at around 160 seconds after 4,800 µL had passed through to the permeate stream. To obtain the V_{max} (capacity), i.e. to assess the performance of the filtration unit, (time/volume) vs. time could be plotted for both duplicates, as shown in Figure 5-5 (b).

Lines of best fit were subsequently fitted to the t/v vs. t plots, and the R^2 values for duplicate 1 and 2 were determined to be 0.994 and 0.9896, respectively. For the filter used, i.e. of area 2.8 x 10^{-5} m^2, the V_{max} was proportional to 1/gradient of the straight line, which was determined to be 21,688 and 20,446, respectively. Dividing these values by the area of the filter used gives the V_{max} value per m^2, which was calculated to be 752 ± 31 L/m^2. This is the capacity of the filter for the material under study, i.e. the limit before the filter blocks, per unit area of the filter. The capacity can be used to scale the operation, and determine the area of the filter required at large scale production.
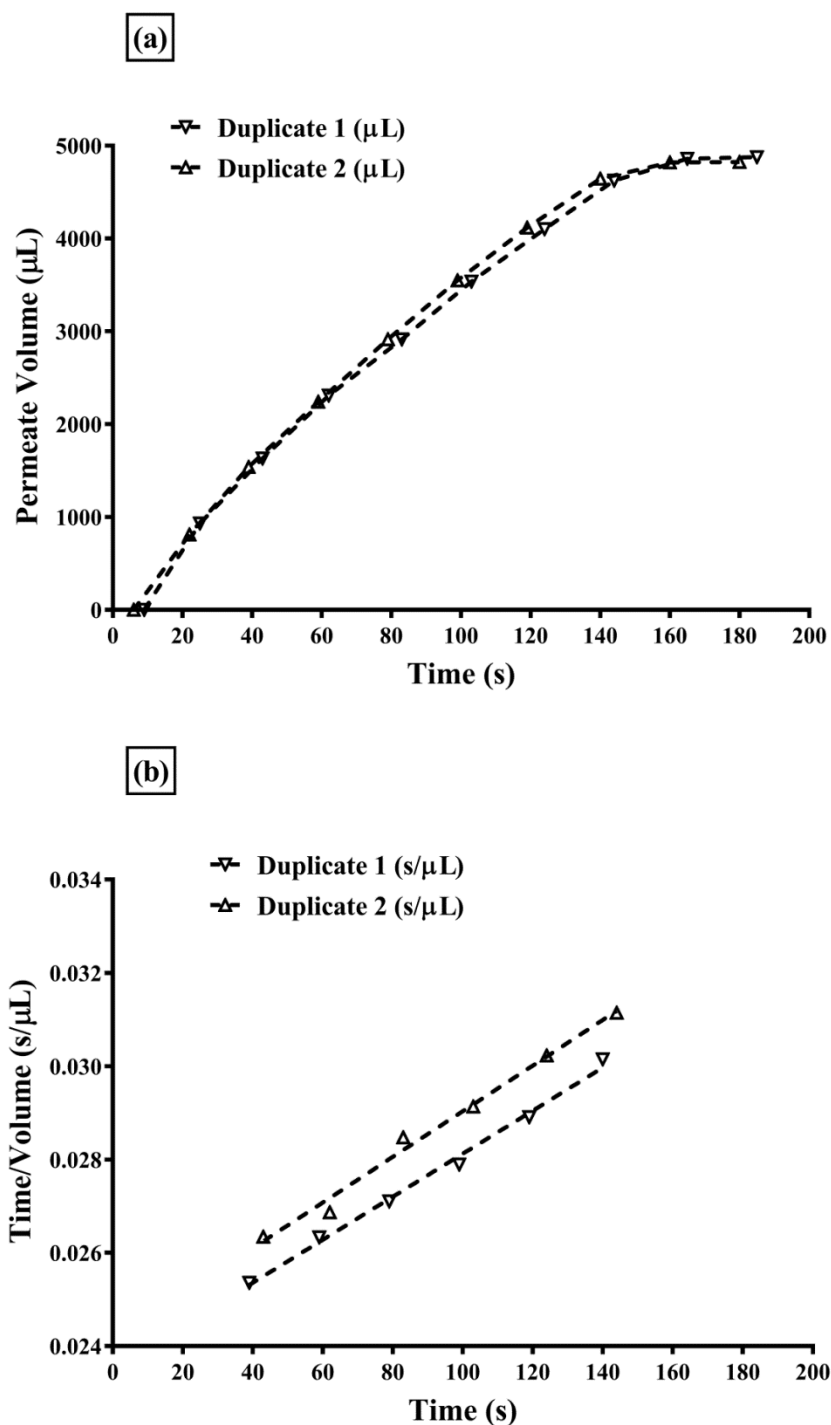
Figure 5-5: Depth filtration step for process scenario 1. Depth filtration performed in duplicate on a liquid handling robotic platform (Tecan Freedom EVO₁), fitted with depth filter media with an area of 2.8 x 10⁻⁵ m², and 0.1 μm nominal pore size. Vacuum filtration carried out at constant pressure (ΔP = 300 mbar), with 5 mL of process material. (a) permeate volume (μL) vs. time (seconds); (b) plot of t/v (seconds/μL) vs. t (seconds), used to determine the V_{max}. R^2 values for duplicate 1 and 2 were 0.994 and 0.9896, respectively.

5.4.2   Process scenario 2

After harvesting cells at Harvest Point 2 (see Figure 5-3 (a)), the primary recovery sequence for process scenario 2 was carried out with fully autolysed cell broth (see Figure 5-1 (b)). The cell broth was flocculated with PEI for 30 min at 1,080 rpm, in order to reach maximum floc strength (see Materials & methods, section 2.6.1). After flocculation, USD shear studies were carried out at a maximum energy dissipation rate of 1.30×10^5 W/kg, followed by centrifugation at 6,800 rpm for 5 min, which was equivalent to industrial scale CSA centrifuge operation at 48 L/h, based on an equivalent settling area, $V_{lab}/t\sum_T$ of 1.96×10^{-8} m/s.

As seen in Figure 5-6, particle size distributions were taken to assess floc breakup after USD shear studies, as flocculated material is known to be shear sensitive. In Figure 5-6, the cell broth is shown before flocculation as a reference and had a median particle size (d_{50}) of 11.7 μm. The particle size distributions after flocculation and after USD shear studies are presented, and a small amount of floc breakup due to shearing can be seen. After shear studies, the two peaks around 100 μm and 1000 μm became more pronounced, and shifted slightly to the left. This shifted the median particle size, or d_{50}, from 213.8 μm to 144.7 μm. In addition, a very small number of particles were detected at just below 1 μm after USD shear studies. Although the average particle size reduced, the vast majority of particles remained above 2 μm (over 99%), showing minimal floc breakup due to shearing, and a significant improvement in the particle size distribution profile after both flocculation and shear studies.

Following USD shear studies and centrifugation, depth filtration was carried out at constant pressure (300 mbar) using a filter with 0.1 μm nominal pore size, in the same manner as for process scenario 1 (described in section 5.4.1). Figure 5-7 (a) shows the permeate volume vs. time for duplicate runs with the supernatant stream from the centrifugation step. In comparison to the plots shown in Figure 5-5 (a) for process scenario 1; although the filter did not block, the total permeate volume was much lower, at ~2,000 μL and it took longer to reach this volume; the runs were ended after 500 seconds.

The same procedure was followed to determine the V_{max} (as described for process scenario 1 in section 5.4.1) and Figure 5-7 (b) shows the straight line plots of t/v vs. t, where the R^2 values for duplicate 1 and 2 were 0.9868 and 0.9736, respectively. The duplicate values for 1/gradient of the straight line (shown in Figure 5-7 (b)) were calculated to be 6913 and 6275, respectively. The V_{max} was subsequently calculated to be 236 $L/m^2 \pm 16$. The capacity of the filter was significantly lower for process scenario 2 than for process scenario 1, which is to be expected due to the increase in impurities in the cell broth attributable to cell lysis.

5.4.3 Process scenario 3

After harvesting cells at Harvest Point 2 (see Figure 5-3 (a)), the primary recovery sequence for process scenario 3 was carried out with fully autolysed cell broth (see Figure 5-1 (c)). The cell broth was flocculated with PEI for 30 min at 1,080 rpm, in order to reach maximum floc strength (see Materials & methods, section 2.6.1). Directly after flocculation, crossflow filtration (CFF) was carried out.

For crossflow filtration, it was possible to use a 500 kDa pore size, whilst achieving good operational performance. However, as seen in Figure 5-7 (a), using a filter size lower than 0.1 μm for process scenario 2 would have been challenging, and insufficient material (permeate volume) would have been available for further analysis. The next section will discuss flocculation with crossflow filtration in more detail.
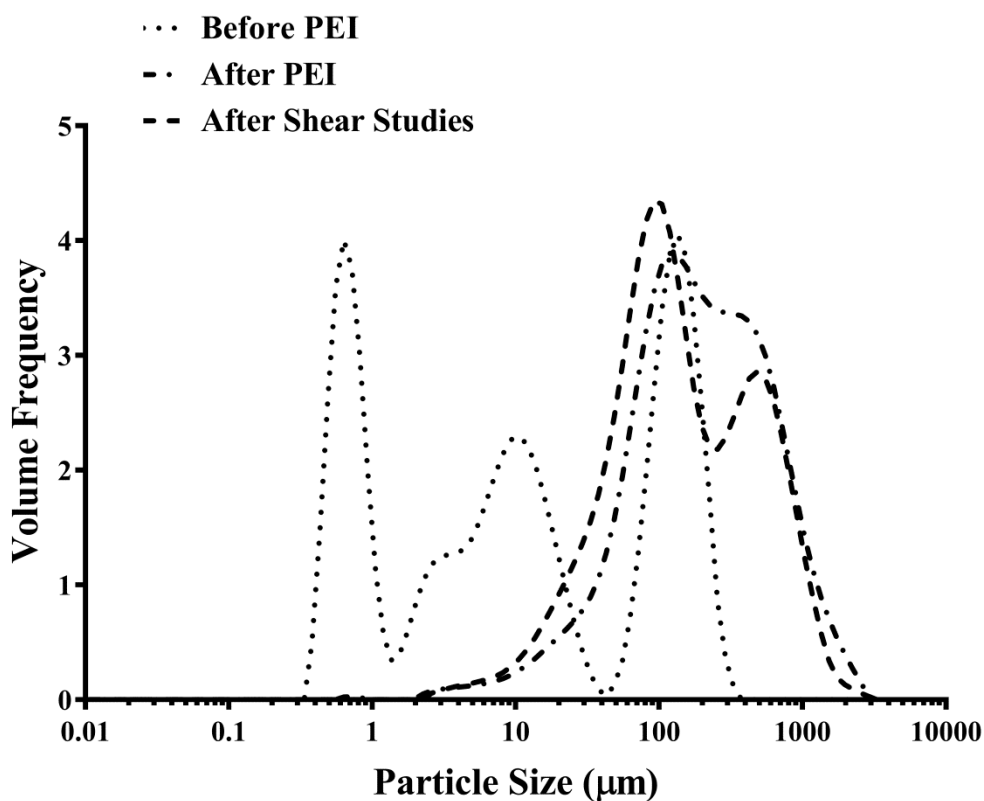
Figure 5-6: Particle size distributions taken to assess floc breakup before and after USD shear studies. Cell broth was autolysed and harvested at 57 h postinduction and the PSD is shown as a reference. Flocculation was carried out at 1% w/v PEI concentration (final concentration in the broth). USD shear studies carried out at 1.30 x 10^5 W/kg. Data recorded in triplicate and averaged before being treated using a method previously described by Chatel et al. (2014), to convert from volume % to volume frequency.

(a)

(b)
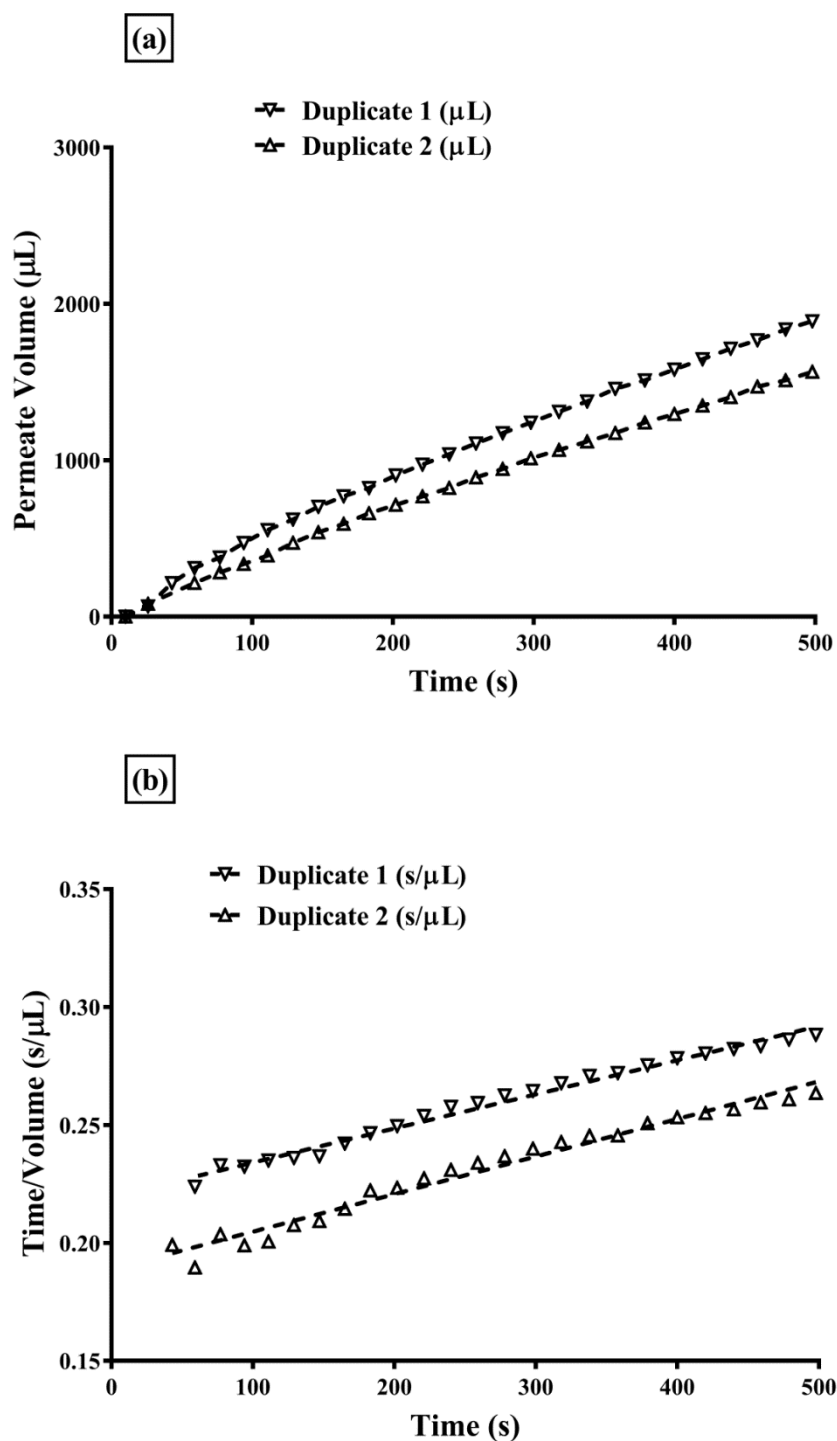
Figure 5-7: Depth filtration for process scenario 2. Depth filtration performed in duplicate on a liquid handling robotic platform (Tecan Freedom EVO1), fitted with depth filter media with an area of 2.8×10^{-5} m^2, and 0.1 μm nominal pore size. Vacuum filtration carried out at constant pressure ($\Delta P = 300$ bar), with 5 mL of process material. (a) permeate volume (μL) vs. time (seconds); (b) plot of t/v (seconds/μL) vs t (seconds), used to determine the V$_{max}$. R^2 values for duplicate 1 and 2 were 0.9868 and 0.9736, respectively.

5.5   Flocculation and crossflow filtration

Flocculated material is known to be shear sensitive, therefore, having determined the concentration of PEI to use for the flocculation step, it was also necessary to understand the extent of floc breakup that occurs due to the shear experienced during crossflow operation, particularly at high feed flow rates. Particle size distributions were taken to assess floc breakup during operation with CFF at two different feed fluxes; 1350 and 1950 L/m^2/h (i.e. at 4,000 and 6,000 rpm in the USD device), where typical values range from 300 - 2100 L/m^2/h for a V-screen cassette. Therefore, the feed fluxes used in this study were in the mid and high range for the typical use of this cassette.

Particle size distributions are shown in Figure 5-8 for the two feed fluxes. The particle size distribution for a typical *E. coli* cell broth before flocculation is shown as a reference, and had a median particle size of 2.47 μm. The same trend can be seen for both feed fluxes; after flocculation with PEI, the minimum particle size of the flocs was around 2 μm and the median particle size after flocculation was 370.8 μm for the 1350 L/m^2/h feed flux, and 308.2 μm for the 1950 L/m^2/h feed flux (a separate flocculation was carried out for each feed flux experiment; this variability will be discussed in more detail later).

After 30 min operation with the CFF device, no particles can be seen in the 200 to 1000 μm size range, and a greater number of particles are in the 1 to 100 μm size range. The median particle sizes for the two flux rates after 30 min CFF operation were 27.4 μm and 19.7 μm, respectively for the 1350 L/m^2/h and 1950 L/m^2/h feed fluxes. After 60 min operation, the peak at around 5 μm increased, whilst the tail decreased in the 30 to 100 μm range. The median particle sizes for the two flux rates after 60 min CFF operation were subsequently 19.2 μm and 11.4 μm, respectively for the 1350 L/m^2/h and 1950 L/m^2/h feed fluxes. This shows that floc breakup occurred over the 60 min period for both feed fluxes; 1350 and 1950 L/m^2/h.

In comparison to non-PEI treated cell broth, where the smallest particle was around 0.3 μm; the smallest particle size after 60 min CFF operation was still much greater

for both feed fluxes (~1 μm). However, after 60 min CFF operation, the smallest particle size and the median particle size for the 1350 L/m^2/h feed flux was slightly higher than for the 1950 L/m^2/h feed flux. Therefore, 1350 L/m^2/h was chosen to operate the CFF device as less floc breakup occurred with this feed flux.

It can also be seen that floc breakup after CFF operation (for both feed fluxes) was much higher than for the USD shear studies carried out in Figure 5-6. This is largely due to the long exposure time in the CFF device compared to the shear studies (i.e. 30 - 60 min vs. 20 s). Although CFF is regarded as lower shear operation than centrifugation in general, this result shows that the shear impact of the long operating time on the floc could be more severe than that in disc-stack centrifugation.
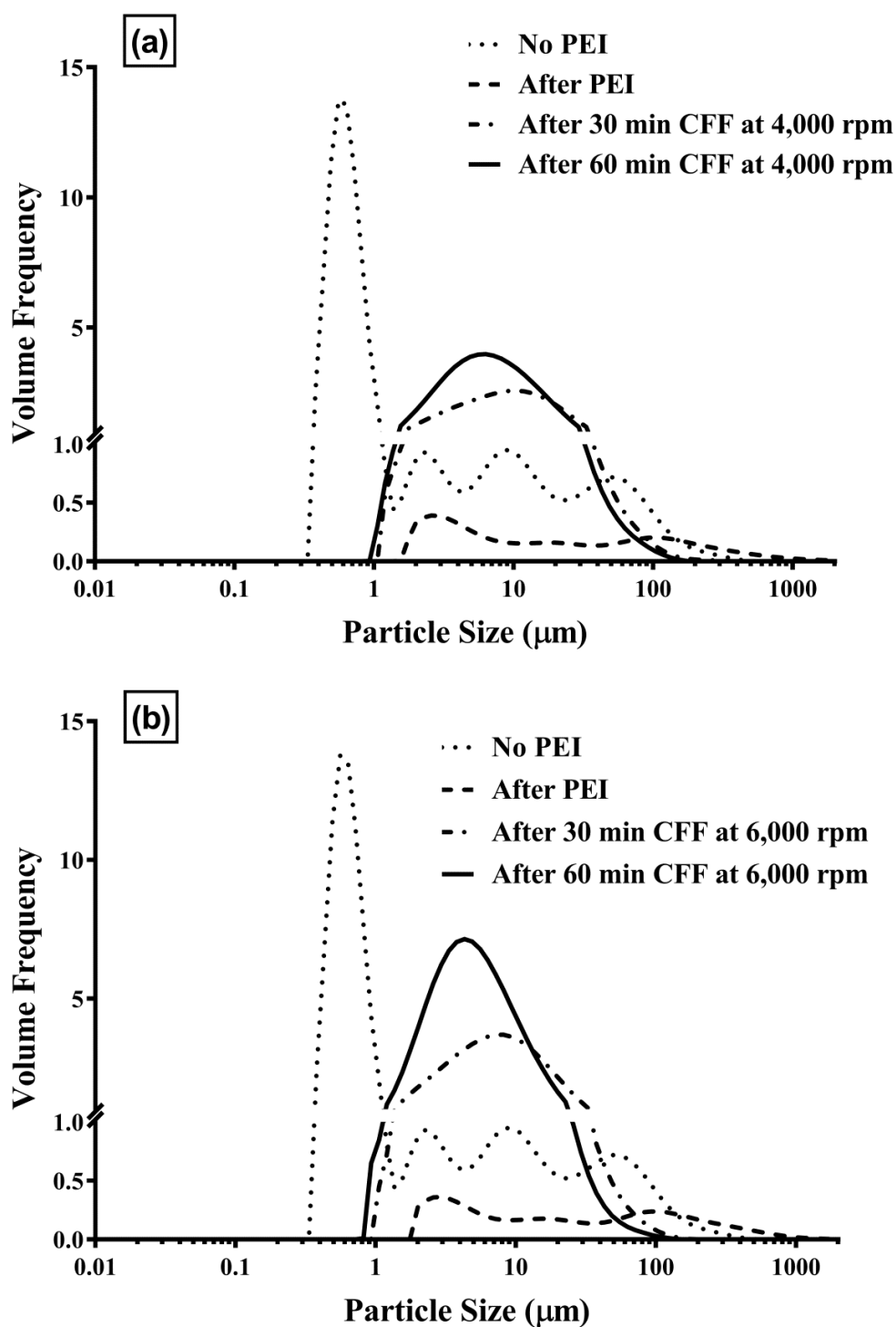
Figure 5-8: Particle size distributions before and after flocculation, and after 30 and 60 min operation with CFF to show floc breakup vs. time for two feed fluxes. Data recorded in triplicate and averaged before being treated using a method previously described by Chatel et al. (2014), to convert from volume % to volume frequency; (a) 1350 L/m^2/h feed flux (4,000 rpm in the USD CFF device) and (b) 1950 L/m^2/h feed flux (6,000 rpm in the USD CFF device).

After establishing the flocculation conditions and determining the feed flux to use for CFF operation, CFF runs were carried out in concentration mode with both flocculated material and non-flocculated material, to provide a comparison between their respective performances.

For the purpose of comparison of the process sequence, the CFF device was selected to be operated at constant permeate flux in concentration mode only, at a typical mid-range flux rate for industrial microfiltration operation of 45.5 $L/m^2/h$ (1 mL/min for the USD device). All runs were carried out until the transmembrane pressure (TMP) reached 2 bar. Figure 5-9 (a) shows the time taken for the transmembrane pressure to reach 2 bar, i.e. the time before the membrane can be considered to be blocked, for CFF operation both with and without flocculation.

For non-flocculated cell broth, harvested at 57 h postinduction and fully autolysed, the membrane blocked almost immediately after 2.2 min ± 0.7. The capacity for CFF operation can be determined by dividing the throughput (i.e. 2.2 mL) by the area of the membrane (13.2 cm^2). Therefore, the capacity for non-flocculated, fully autolysed cell broth was determined to be 1,677 $L/m^2 \pm 485$.

For CFF runs with flocculated, fully autolysed cell broth, a good operating time was achieved of 16.7 min ± 7, and it was calculated (as described above) that the capacity was 12,687 $L/m^2 \pm 5,600$. Although there was significant variation in the runs, as seen in the error bars in Figure 5-9 (a), this nonetheless represents a 5-10-fold improvement in throughput by using flocculation, in comparison to non-flocculated broth. The variation observed for CFF operation with the non-flocculated cell broth was 32%, and the variation for the flocculated cell broth was 44%.

Water flux tests were carried out before and after each CFF run, in order to assess the extent of irreversible fouling on the membrane. Figure 5-9 (b) presents the water flux tests as normalised water permeability (NWP), normalised to 25°C for CFF operation with and without flocculation. The NWP was determined by increasing the permeate flux (in $L/m^2/h$, or LMH) in a step-wise fashion and measuring the corresponding change in TMP (in bar), using milliQ water before and after each CFF

run. Plotting the TMP vs. flux relationship for each water flux test yielded a straight-line plot, and the gradient of the line was equal to the NWP (LMH/bar), which was then normalised to 25°C using a correction factor (actual temperature values varied between 21 and 23°C between runs).

It was observed in Figure 5-9 (b) that significant fouling occurred during runs both with and without flocculation, however fouling occurred at a much slower rate for flocculated material, as seen by the increase in throughput in Figure 5-9 (a). Further, fouling on the membrane was 34% higher after CFF runs without flocculation than with flocculation (different starting permeability values). Although a high level of fouling for both runs was observed, the higher level of fouling observed for the runs without flocculation is due to the higher soluble content in the material, for example soluble nucleic acids and protein. However, further characterisation of the relationship between flux and transmembrane pressure is needed for optimal design of the process in the future.

In addition, variation in the NWP was seen between runs; the average NWP value before runs with flocculated broth was considerably lower than before the non-flocculated runs. A new membrane was used for each CFF run, and this shows that there was a large variation between the permeability of each of the membranes. This variation in the NWP between CFF runs could explain the variation seen in Figure 5-9 (a); as mentioned above, the variation seen between the runs was 32% and 44% for non-flocculated and flocculated broth, respectively. Another explanation for the high variation seen in the CFF runs is that lysed *E. coli* cell broth consists of a diverse and complex mixture of biological material, which leads to a challenging downstream process. Further, flocculation at 100 mL scale was difficult due to the presence of dead volumes in the small-scale vessel. For large scale flocculation, it is believed that this would not be a problem, however this could have contributed to the variability seen in the runs with flocculation.

Even though variation was observed, a significant improvement was seen in CFF performance by using PEI, in comparison to non-flocculated material. A mid-range permeate flux was used, and a high capacity was attained. However, the

reproducibility would need to be addressed when scaling up to large scale crossflow filtration operation.
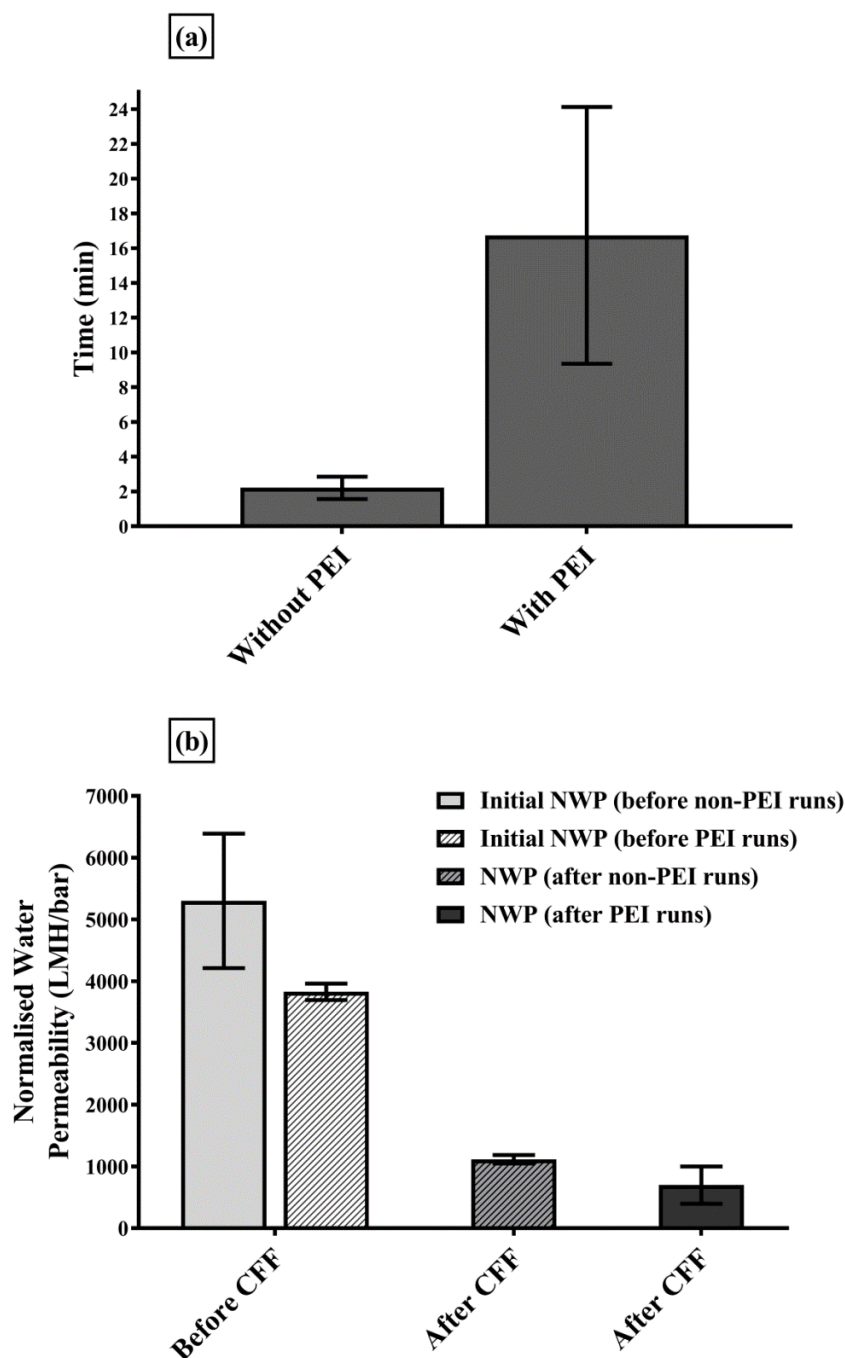
Figure 5-9: Crossflow filtration with and without flocculation. (a) Time taken before membrane blocked for CFF operation at constant permeate flux of 45.5 L/m²/h (1 mL/min for USD device operation) and 1350 L/m²/h feed flux, showing duplicate runs with and without flocculation (1% w/v PEI). CFF runs stopped upon reaching a transmembrane pressure (TMP) of 2 bar. Average operating time without flocculation was 2.2 min ± 0.7 (capacity = 1,677 L/m² ± 485), and average time with flocculation was 16.7 min ± 7 (capacity = 12,687 L/m² ± 5,600); (b) water flux tests before and after CFF, shown as normalised water permeability (NWP) at 25°C (in duplicate). Error bars show standard deviation.

5.6   Evaluating the performance of the three primary recovery scenarios

After establishing the various USD operating parameters, the three process sequences were then carried out. This section aims to evaluate the performance of the three scenarios based on several criteria, including clarification performance (i.e. solids removal), total product yield and product purity.

Figure 5-10 shows the optical density profiles after each unit operation across the three process scenarios. The OD_{600} profiles for process scenario 1 are shown in Figure 5-10 (a), where it can be seen that the optical density of the harvested fermentation feed at 32 h postinduction (see Figure 5-2) was 203 ± 6.24. After carrying out USD shear studies and centrifugation, the OD_{600} of the supernatant was determined to be 2.30 ± 0.172. The solids remaining for this step was calculated to be 0.783% (see Materials & methods, section 2.6.4 for calculation). As described in section 5.4.1, dewatering was carried out to a level of 70% and the cell paste was then re-suspended in extraction buffer, at a ratio of 1 g cells: 7 mL buffer. The OD_{600} after re-suspension and periplasmic extraction was 25.2 ± 1.19. Following the second USD shear studies and centrifugation step, the OD_{600} of the supernatant was determined to be 0.887 ± 0.0137 and the solids remaining at this stage was 3.35%. Both centrifugation steps in process scenario 1 were able to achieve high solids separation, which is due to the settings used to mimic a low-medium flow rate for an industrial CSA centrifuge, of 48 L/h. After the depth filtration step, the OD_{600} was determined to be 0.668 ± 0.00429 and the level of solids remaining was determined to be 74%. The separation performance was relatively poor for depth filtration, and the rate at which the material passed through the filter (see Figure 5-5) suggests that either the pore size of 0.1 μm may have been too large, or that the solids removal was already high as many of the large particles had been removed in the centrifugation step. The overall solids remaining for the primary recovery process sequence 1 was determined to be 0.307%.

The OD_{600} profiles for process scenario 2 are shown in Figure 5-10 (b). After harvest at 57 h postinduction, the OD_{600} was 52.2 ± 4.75. Flocculation was carried out, followed by USD shear studies and centrifugation, and the OD_{600} of the supernatant

was determined to be 0.179 ± 0.0146. The solids remaining after the centrifugation step was subsequently calculated to be 0.194%, and the good separation performance can be attributed to the use of flocculation. After centrifugation, depth filtration was carried out in the same manner as for process scenario 1 (described above), and the OD_{600} of the permeate after filtration was 0.1195 ± 0.00569. The solids remaining after the depth filtration step was therefore determined to be 41.7%.

The relatively poor depth filtration performance could be due to the high concentration of soluble impurities remaining in the supernatant after centrifugation (which would affect the optical density), and could have also caused the slow rate of increase in permeate volume seen in Figure 5-7 (a) due to interactions with the filter media (nucleic acids are charged). However, the high number of solids remaining (41.7%) may also be because there were few solids remaining in the broth, as the preceding centrifugation performance was very good. To improve the permeate flow rate for this depth filtration step, the pore size of the filter could be increased above 0.1 μm, as the flocculated solid material had a particle size much larger (>1 μm, see Figure 5-6 and Figure 5-4 (a)).

The optical density profiles for process scenario 3 are shown in Figure 5-10 (c). After harvest, the starting OD_{600} of the fully autolysed cell broth was 67.3 ± 3.38. The solids remaining, S_{CFF}, for CFF runs was calculated in a different way to the centrifugation solids remaining calculations:

$$S_{CFF} = \frac{OD_s}{OD_f} \times 100\% \qquad \textbf{Equation 5-1}$$

where OD_s is the optical density (at 600 nm) of the permeate and OD_f is the optical density of the feed sample.

After CFF runs, the OD_{600} of the non-flocculated permeate was 0.121 ± 0.00611 and 0.0723 ± 0.00234 for the flocculated permeate. The solids remaining after CFF was

therefore determined to be 0.173% for CFF runs without flocculation and 0.112% for CFF runs with flocculated cell broth. Therefore, a 40% improvement in clarification between CFF runs with and without flocculation can also be seen, which can be attributed to the removal of submicron particles in the flocculation step and the larger particle size of the flocs, which improved separation in the CFF step.

Although the starting optical densities were different between process scenario 1 (harvested at 32 h postinduction, at the onset of cell lysis) and process scenarios 2 and 3 (both harvested at 57 h postinduction, cells were fully autolysed), it should be noted that for scenarios 2 and 3, the cell broth contained a much higher concentration of impurities in the liquor, as the lysed cells had released their intracellular content to the broth. Therefore, although the cell concentration was lower, the primary recovery steps were more challenging due to the increased impurity content. In addition, it should be noted that the starting optical densities for process scenarios 2 and 3 were slightly different, due to variation between repeated fermentation runs.

Given this, the clarification efficiency achieved in both scenarios 2 and 3 was superior to that in scenario 1, which can be attributed to the use of flocculation. However, clarification performance for all three scenarios was good.
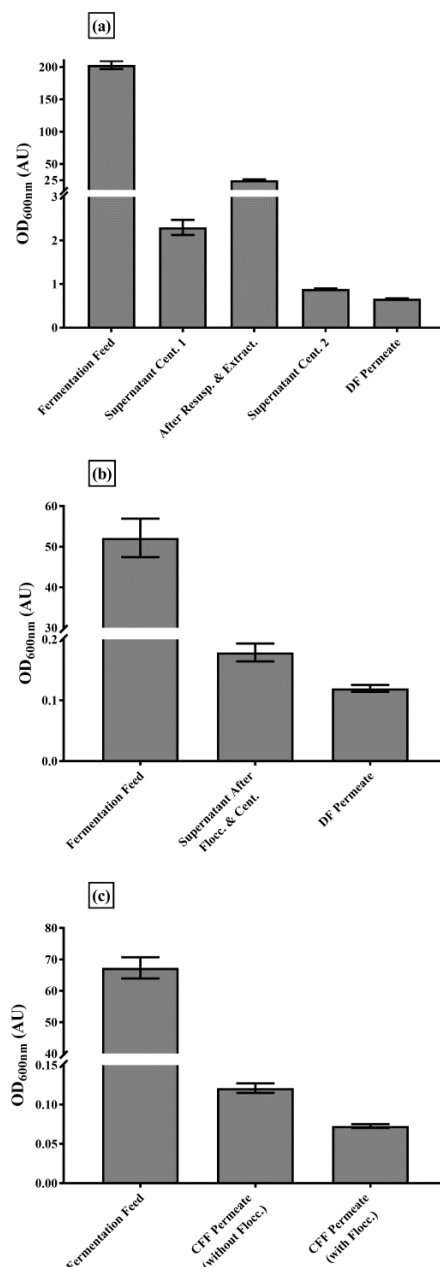
Figure 5-10: Optical density profiles across each of the three process scenarios. All runs carried out in duplicate. Optical density measured at 600 nm (absorbance units, AU, in triplicate); (a) fermentation harvested at Harvest Point 1 (see Figure 5-3); (b) and (c) fermentation harvested at Harvest Point 2. Centrifugation (coupled with USD shear studies as described) carried out at 6,800 rpm for 5 min (equivalent to industrial scale CSA centrifuge operation at 48 L/h, based on an equivalent settling area, $V_{lab}/t\sum_T$ of 1.96×10^{-8} m/s). Re-suspension carried out at a ratio of 1g cells: 7 mL extraction buffer, and periplasmic extraction carried out for 12 h at 60°C and 250 rpm in a shaker-incubator. Depth filtration performed at constant pressure ($\Delta P = 300$ mbar) using a nominal pore size of 0.1 μm. PEI concentration was 1% for all runs (w/v of broth). CFF runs were carried out at a constant permeate flux of 45.5 L/m^2/h (1 mL/min) and feed flux of 1350 L/m^2/h using a 500 kDa pore size. Error bars show standard deviation.

Figure 5-11 displays the contaminant profiles (nucleic acid and total protein) and product profiles (intracellular and extracellular Fab' concentration, where appropriate) across each of the three process scenarios. Figure 5-12 shows the same profiles, however they have been normalised to the starting concentrations for ease of comparison across the scenarios.

The starting nucleic acid and total protein concentrations in the fermentation broth for process scenarios 2 and 3 (Figure 5-11 (b) and (c)) were over double that of the fermentation feed for scenario 1 (Figure 5-11 (a)), however the recoverable Fab' titre was also more than double.

Figure 5-11 (a) shows the starting nucleic acid and total protein concentrations in the broth for process scenario 1 to be 6.02 ± 0.85 mg/mL and 112 ± 6.54 mg/mL, respectively, and both concentrations stayed relatively constant after centrifugation. After re-suspension of the cell paste, the contaminants in the broth were low, as expected, however the presence of 0.898 ± 0.00347 mg/mL nucleic acids and 16.9 ± 0.147 mg/mL total protein in the broth were due to the 70% dewatering level, i.e. the broth was not fully dewatered and some soluble contaminants remained in the stream. After extraction, the concentration of contaminants increased due to cell lysis. The aim of extraction is to extract the Fab' product from the periplasm, whilst minimising the release of host cell protein and nucleic acids. However, the concentration of both nucleic acids and total protein after extraction increased to 2.94 ± 0.0160 mg/mL and 61.6 ± 0.62 mg/mL, respectively. Following the second centrifugation step and depth filtration, the contaminants in the supernatant stayed relatively constant, which is to be expected as these steps were focused on separating solids and liquid, and the contaminants were solubilised in the broth.

The initial Fab' concentrations are shown in Figure 5-11 (a) as both intracellular and extracellular, which were 0.783 ± 0.0219 mg/mL and 0.275 ± 0.0160 mg/mL, respectively (~26% product loss due to lysis). Following centrifugation, the Fab' concentration in the supernatant was 0.192 ± 0.00758 mg/mL; which was lost due to the 70% dewatering level. After re-suspension of the cell paste (1:7 dilution), the desired intracellular product concentration was 0.291 ± 0.000989 mg/mL and after

extraction, the product concentration in the broth was 0.140 ± 0.00115 mg/mL. The product concentration stayed relatively constant for the subsequent primary recovery unit operations, however a small amount of product was lost at each stage, and the final product concentration after depth filtration was 0.137 ± 0.00168 mg/mL.

Figure 5-11 (b) shows the starting concentrations of host cell protein and nucleic acid as 220 mg/mL and 12.4 mg/mL, respectively; significantly higher concentrations than in process scenario 1. After flocculation and centrifugation, the contaminant concentration in the broth reduced considerably to 167 mg/mL total protein and 8.48 mg/mL nucleic acids. After depth filtration, the concentration of contaminants stayed relatively constant, as the remaining contaminants were solubilised in the cell broth and therefore able to pass through the filter.

The initial Fab' concentration in the broth for process scenario 2, harvested at 57 h postinduction and fully autolysed, is shown in Figure 5-11 (b) at 1.75 ± 0.00450 mg/mL. The product concentration decreased after flocculation and centrifugation to 1.54 ± 0.172 mg/mL, which suggests that some product was lost in the centrifugation step (typically 5% is lost) and some product was lost in the flocculation step. Following centrifugation, depth filtration was carried out and the final product concentration in the permeate was determined to be 1.42 ± 0.32 mg/mL. The high variation in the duplicates could be due to variation observed in the flocculation setup at small-scale (previously described) which was then propagated through the subsequent unit operations.

Figure 5-11 (c) shows the contaminant and product profiles for process scenario 3. The initial total protein and nucleic acid concentrations were 268 ± 0.713 mg/mL and 13.9 ± 0.125 mg/mL, respectively. After carrying out flocculation and crossflow filtration, a significant reduction in contaminants was observed, to 150 ± 0.699 mg/mL total protein and 7.74 ± 0.0117 mg/mL nucleic acids. The product concentration in the broth of the harvested fermentation feed at 57 h postinduction (fully autolysed) was 1.95 ± 0.0235 mg/mL. After flocculation and CFF operation in concentration mode, the final Fab' concentration was 1.23 ± 0.143 mg/mL. Therefore, a significant drop was observed in the product titre after this unit

operation. This will be discussed in more detail in the following sections. The variation also seen in the product titre after flocculation and CFF could be due to the variation in the flocculation setup and CFF runs, as seen in Figure 5-9 (a).
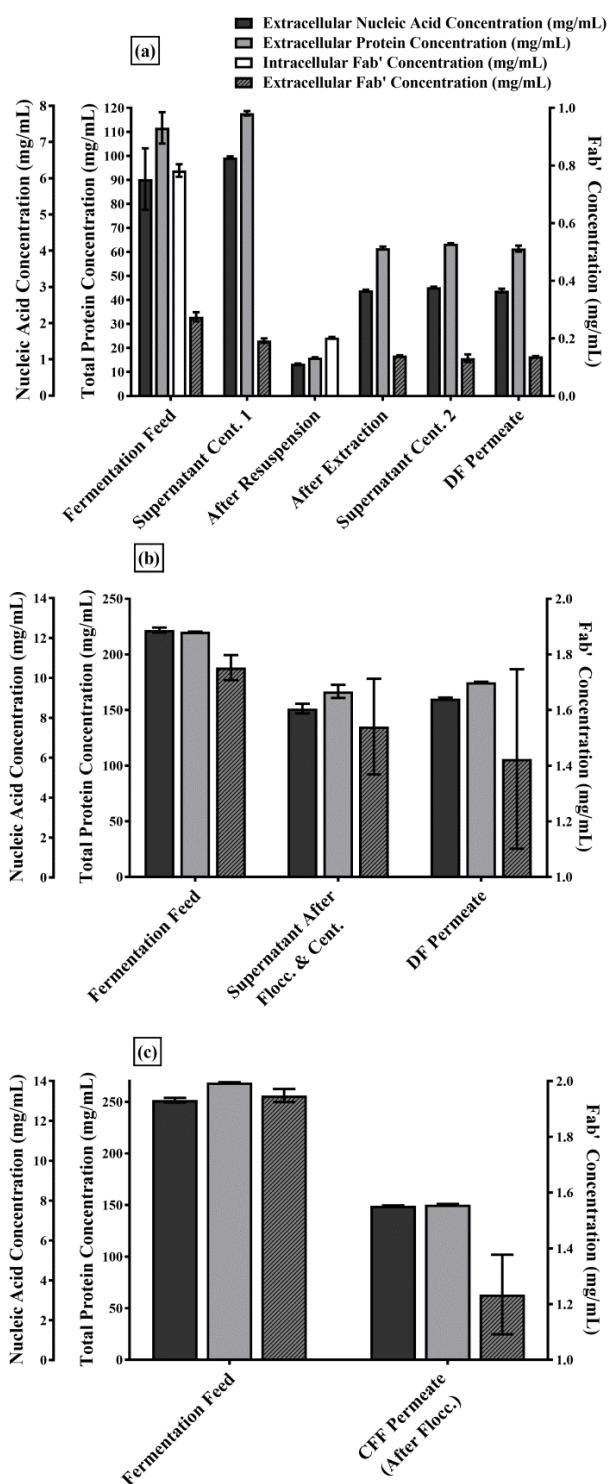
Figure 5-11: Nucleic acid, total protein and product (Fab') profiles across each unit operation for the three process scenarios. All runs carried out in duplicate. Fab' was measured in duplicate (mg/mL), total protein in triplicate (at 280 nm absorbance, mg/mL) and nucleic acids in triplicate (at 230 nm absorbance, mg/mL); (a) process scenario 1; (b); process scenario 2; (c) process scenario 3. Error bars show standard deviation.
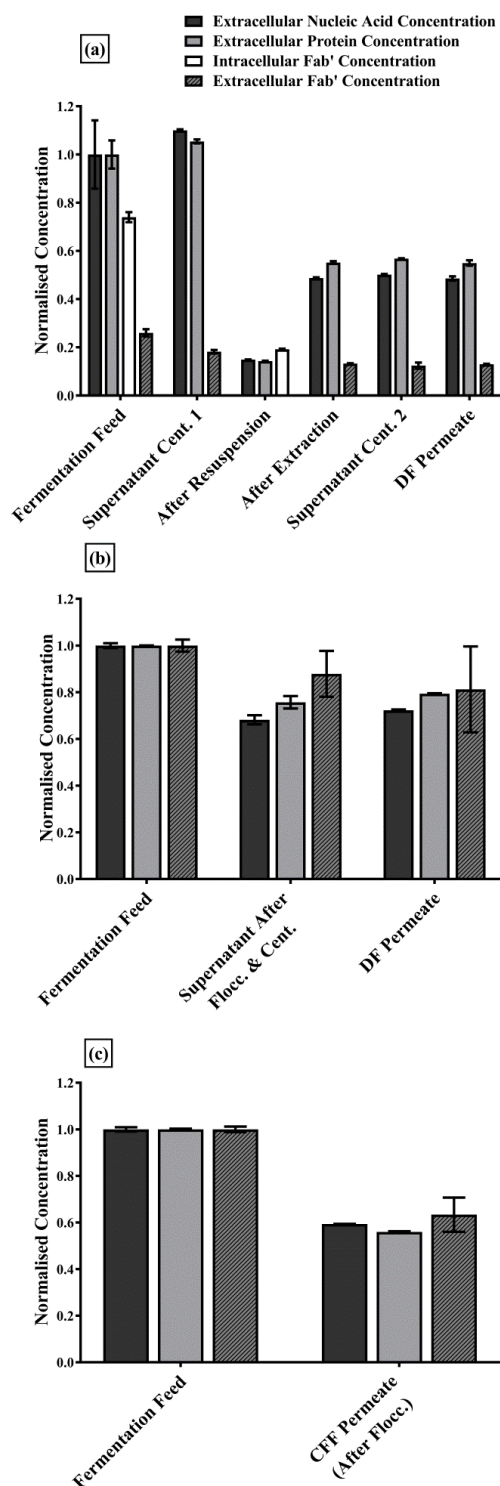
Figure 5-12: Normalised nucleic acid, total protein and product (Fab') profiles across each unit operation for the three process scenarios. All runs carried out in duplicate. Fab' was measured in duplicate (mg/mL), total protein in triplicate (at 280 nm absorbance, mg/mL) and nucleic acids in triplicate (at 230 nm absorbance, mg/mL); (a) process scenario 1; (b); process scenario 2; (c) process scenario 3. Error bars show standard deviation.

218

Figure 5-13 summarises the performance of the three process scenarios, in terms of overall product yield, solids removal and product purity. Figure 5-13 (a) shows the total solids remaining for each of the primary recovery sequences, where a 3-fold improvement in solids removal was achieved for scenario 3, in comparison to scenario 1. A 4-fold improvement in solids removal was also achieved for scenario 2, compared to scenario 1. The overall product yield is also shown, where it can be seen that process scenarios 2 and 3 achieved significant improvements in comparison to process scenario 1; this was calculated by mass balance and will be discussed in more detail in the next section.

Figure 5-13 (b) shows the impurity profiles for each primary recovery sequence. The use of flocculation and CFF in scenario 3 achieved a 3.6-fold improvement in product purity, in comparison to the existing Fab' primary recovery process seen in scenario 1. Flocculation with centrifugation in scenario 2 also achieved a 3-fold improvement in product purity, in comparison to scenario 1. As mentioned above, although the contaminant levels in process scenarios 2 and 3 were higher than observed in process scenario 1, the product titre was also higher. Therefore, process scenarios 2 and 3 achieved superior results than process scenario 1, in terms of solids removal, product yield and product purity.
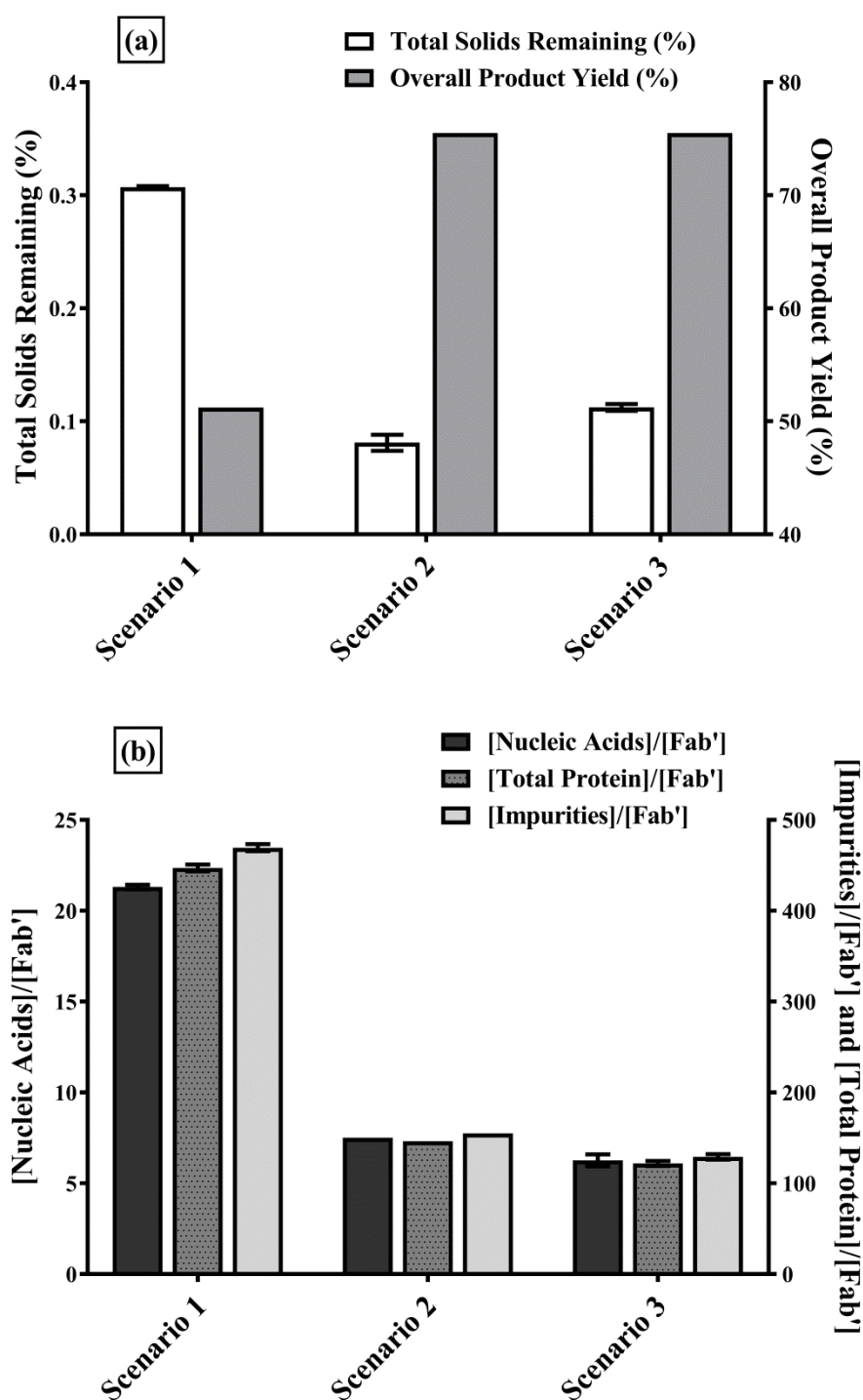
Figure 5-13: Summary of the three DSP process scenarios. All runs carried out in duplicate; (a) Total solids remaining (%) at the end of each primary recovery scenario and overall product yield (%) calculated by mass balance; (b) Comparison of impurity levels for each process scenario; [Nucleic acids]/[Fab'], [total protein]/[Fab'] and [total impurities]/[Fab']. Fab' measured in duplicate (mg/mL), and nucleic acid and total protein measured in triplicate (at 280 nm and 230 nm, respectively, mg/mL). Error bars show standard deviation.

5.7   Mass balances

In order to determine the total product recovered and impurity profiles for each process sequence, as well as the capital costs and downstream processing time, mass balances were carried out for the solids, the Fab' product, total protein and nucleic acids. The following sections detail the assumptions made to carry out the mass balances, the calculations required and the results for each process sequence.

5.7.1   Assumptions for the mass balances

The assumptions made to carry out the mass balances are listed below:

- All mass balances were calculated on the basis of 1,000 L feed fermentation broth

- For the centrifugation steps, a 70% dewatering level was assumed; the highest level in an industrial disc stack centrifugation process were assumed so that the results drawn from the analysis are more reliable (Salte et al., 2006)

- For scenario 1, the experimentally-determined periplasmic extraction performance was poor (~30%). Therefore, for the mass balance calculations, the efficiency for the periplasmic extraction step was raised to 80%, a typical level for industrial extraction processes (personal communication with a colleague in the Department of Biochemical Engineering, University College London)

- Starting concentrations for product, solids, nucleic acids and total protein for process scenarios 2 and 3 were normalised to enable an equal comparison, as there was a slight variation in the starting experimental concentrations due to repeated fermentation runs (e.g. 1.95 mg/mL and 1.75 mg/mL were normalised to 1.85 mg/mL starting Fab' concentration in the fermentation feed)

- Cell concentration was measured by optical density, and converted to wet cell weight in order to carry out the mass balances. This was done by converting OD_{600} measurements to dry cell weight measurements using a ratio of 1

absorbance unit (AU): 0.261 g/L dry cell weight (determined experimentally). Following this, the dry cell weight was multiplied by 3 to get wet cell weight (a typical rule of thumb is that wet cell weight is 3x dry cell weight for *E. coli* cells) (Bratbak and Dundas, 1984)

- For the depth filtration steps, it was assumed that all liquor passed through to the permeate, however the total protein, nucleic acids and product were assumed to have a 10% rejection coefficient, i.e. 10% of solutes were retained by the membrane

- For the flocculation steps in process scenarios 2 and 3, 10% product was assumed to be lost in the solids fraction after PEI addition (Ma et al., 2010). In addition, taking estimates from experimental data (Figure 5-4), 30% nucleic acids and 15% total protein were assumed to precipitate into the solids fraction after PEI addition

- It was assumed that the volume of liquor was equivalent to the mass of liquor (i.e. the density of the liquor was that of water, as only small molecules were present in the water)

- It was assumed that the density of solids debris, ρ_{sol}, was 1.05 kg/L (Wong et al., 1997)

5.7.2 **Process sequence 1**

Table 5-1 shows the results of the mass balances carried out for process scenario 1. Mass balances were carried out for solids, product, nucleic acids and total protein. As discussed in the previous section (section 5.6), the clarification performance for the first centrifugation step was 99.21% (solids remaining = 0.79%) and the clarification performance for the second centrifugation step was 96.65% (solids remaining = 3.35%).

The starting solids concentration (wet cell weight) was calculated to be 158.831 g/L, shown in Table 5-1, and the starting feed volume was assumed to be 1000 L. The mass of solids remaining in the supernatant after the first centrifugation step was therefore calculated as:

$$M_{sol,\text{sup}} = M_{sol,feed} \times (1 - clarification_{cent})$$ **Equation 5-2**

where $M_{sol,sup}$ is the mass of solids in the supernatant (kg), $M_{sol,feed}$ is the mass of solids in the feed stream (kg) and $clarification_{cent}$ is the clarification performance for the first centrifugation step, described above as 99.21%.

Therefore, the mass of solids remaining in the supernatant after the first centrifugation step was calculated to be 1.255 kg and the mass of solids in the sediment stream could be calculated as:

$$M_{sol,\text{sed}} = M_{sol,feed} \times clarification_{cent}$$ **Equation 5-3**

where $M_{sol,sed}$ is the mass of solids in the sediment stream after centrifugation (kg).

Thus, the mass of solids in the sediment stream was determined to be 157.577 kg for the first centrifugation step. In the same way, the mass balance for the solids in the second centrifugation step was calculated to be 4.434 kg in the supernatant stream and 127.930 kg in the sediment stream (with a clarification efficiency of 96.65%).

To calculate the volume of liquor in the sediment stream, the experimental dewatering level (*DW*) of 70% was used. The dewatering level can be calculated as:

$$DW = \frac{V_{sol,sed}}{V_{tot,sed}} = \frac{V_{sol,sed}}{V_{sol,sed} + V_{liq,sed}}$$ **Equation 5-4**

where $V_{sol,sed}$ is the volume of solids in the sediment stream (L), $V_{tot,sed}$ is the total volume in the sediment stream (L) and $V_{liq,sed}$ is the volume of liquor in the sediment

stream (L). This can then be rearranged to obtain the volume of liquor in the sediment stream ($V_{liq,sed}$):

$$V_{liq,sed} = (\frac{1-DW}{DW}) \times \frac{M_{sol,sed}}{\rho_{sol}}$$

Equation 5-5

where ρ_{sol} is the density of solids debris, assumed to be 1.05 kg/L.

The volume of liquor in the sediment stream was thus calculated to be 64.317 L and it was assumed that the volume of liquor was equivalent to the mass of liquor. Therefore, the mass of liquor was determined to be 64.317 kg in the sediment stream after the first centrifugation step. The mass of liquor in the supernatant stream could then be determined to be 784.415 kg.

The mass of liquor was calculated in the second centrifugation step using the same method; 52.216 kg and 1589.368 kg were determined to be in the sediment and supernatant streams, respectively.

The total mass in each of the streams could also be calculated as:

$$M_{tot} = M_{liq} + M_{sol}$$

Equation 5-6

where M_{tot} is the total mass in the stream (kg), M_{liq} is the total mass of liquor in the stream (kg) and M_{sol} is the total mass of solids in the stream (kg).

In addition, the total volume in each of the streams could be calculated. For example, in the supernatant stream after the first centrifugation step:

$$V_{tot,\text{sup}} = V_{sol,\text{sup}} + V_{liq,\text{sup}} = \left(\frac{M_{sol,\text{sup}}}{\rho_{sol}}\right) + V_{liq,\text{sup}} \qquad \textbf{Equation 5-7}$$

where $V_{tot,sup}$ is the total volume in the supernatant (L), $V_{sol,sup}$ is the volume of solids in the supernatant (L) and $V_{liq,sup}$ is the volume of liquor in the supernatant (L).

Therefore, the total volume in the supernatant stream after the first centrifugation step was 785.610 L, and the total volume in the sediment stream was therefore determined to be 214.390 L, based on a starting feed of 1000 L. For the second centrifugation step, the total volumes in the sediment and supernatant streams were calculated in the same way as above, and it was determined that 174.055 L and 1593.591 L were in the sediment and supernatant streams, respectively.

As described previously, the cells were diluted in a ratio of 1 g cells: 7 mL extraction buffer for the periplasmic extraction step. The volume was thus adjusted accordingly for this step in the mass balance (i.e. 1553.256 L buffer was added to the 214.390 L centrifugation sediment stream and the sediment was re-suspended, while the mass of solids remained constant).

After extraction, the mass of solids was calculated by:

$$M_{sol,aftext} = M_{sol,beforeext}(1 - \varepsilon_{ext}) + M_{sol,beforeext} \times \varepsilon_{ext} \times f \quad \textbf{Equation 5-8}$$

where $M_{sol,aftext}$ is the mass of solids in the stream after extraction (kg), $M_{sol,beforeext}$ is the mass of solids in the stream before extraction (kg), ε_{ext} is the extraction efficiency (set to 80%, see assumptions) and f is 0.8, a factor to account for the remaining weight of the lysed cells (i.e. 80% of the mass of the lysed cells (80%) was assumed to remain, so that 20% of the mass of the lysed cells was lost to extracellular space as

liquid). The mass of solids remaining after extraction was therefore calculated to be 132.364 kg.

To carry out the mass balance for the solids in the depth filtration unit operation, the mass in the permeate stream was calculated as:

$$M_{sol,DFpermeate} = M_{sol,DFfeed} \times S_{DF}$$ **Equation 5-9**

where $M_{sol,DFpermeate}$ is the mass of solids in the permeate stream (kg), $M_{sol,DFfeed}$ is the mass of solids in the feed stream (i.e. the supernatant stream from the second centrifugation step, kg) and S_{DF} is the solids remaining for the depth filtration unit operation, calculated in section 5.6 as 74%. Therefore the mass of solids in the permeate stream was determined to be 3.281 kg. As described in the assumptions, it was assumed that all of the liquor from the supernatant in the second centrifugation step passed through to the permeate stream in the depth filtration step. Therefore, 1589.368 L (or 1589.368 kg) of liquor was found in the permeate stream.

Subsequently, the volume in the permeate stream could be calculated:

$$V_{tot,DFpermeate} = V_{liq,DFpermeate} + \frac{M_{sol,DFpermeate}}{\rho_{sol}}$$ **Equation 5-10**

where $V_{tot,DFpermeate}$ is the total volume in the permeate stream (L) and $V_{liq,DFpermeate}$ is the volume of liquor in the depth filtration permeate (L). $V_{tot,DFpermeate}$ was determined to be 1592.493 L.

For the product, total protein and nucleic acid mass balances, the depth filtration unit was assumed to have a 10% rejection coefficient, i.e. 90% of soluble material would pass through the filter. The product mass balance is shown in Table 5-1 for process

scenario 1, and both intracellular and extracellular balances are shown, to demonstrate how their profiles changed over each unit operation. The final product recovered in the first primary recovery process sequence was 0.542 kg, based on a starting fermentation feed of 1000 L. This product was recovered in a total volume of 1592.493 L (at a concentration of 0.340 mg/mL), which can be attributed to the significant dilution (1: 7) required in the periplasmic extraction step. The product yield achieved for each step (where appropriate) is also shown in Table 5-1, and the overall yield for the primary recovery sequence was calculated to be 51.2%.

Table 5-1 also shows the mass balances for nucleic acids and total protein, respectively. These calculations were carried out by using both experimentally determined values and the method described above to determine the total volume, which enabled the determination of the mass. It can be seen that 4.523 kg nucleic acids and 94.915 kg total protein remained in the broth at the end of the primary recovery sequence, in 1592.493 L final volume.

Table 5-1: Mass balance for solids, product (Fab'), nucleic acids and total protein in process scenario 1. Cells harvested at 32 h postinduction and held for 1 h to mimic large scale holding time. Mass balance based on starting feed of 1000 L. Centrifugation carried out at 48 L/h using a disc stack centrifuge and dewatered to a level of 70%. Cell paste (sediment stream) after the first centrifugation step was re-suspended in extraction buffer in a ratio of 1: 7. Fab' data measured by HPLC (Agilent 1200, Agilent Technologies Inc., California, USA) and shown as both intracellular and extracellular concentration, where appropriate. Cell concentration was measured by optical density, and converted to wet cell weight. Nucleic acid and total protein concentration measured using the Nanodrop (Nanodrop 1000 spectrophotometer, Thermo Scientific, Wilmington, DE, USA).

	Ferm. Feed	Cent. 1 Sup.	Cent. 1 Sed.	Before Ext.	After Ext.	Cent. 2 Sup.	Cent. 2 Sed.	DF Perm.
C_{sol} (g/L)	158.831	1.597	735.000	89.145	74.882	2.783	735.000	2.060
M_{sol} (kg)	158.831	1.255	157.577	157.577	132.364	4.434	127.930	3.281
M_{liq} (kg)	848.732	784.415	64.317	1617.573	1641.585	1589.368	52.216	1589.368
$C_{prod,int}$ (mg/mL)	0.783	0.008	3.622	0.439	0.088	0.003	0.862	/
$C_{prod,ext}$ (mg/mL)	0.275	0.307	0.156	0.019	0.370	0.378	0.302	0.340
$M_{prod,int}$ (kg)	0.783	0.006	0.777	0.777	0.155	0.005	0.150	/
$M_{prod,ext}$ (kg)	0.275	0.241	0.034	0.034	0.655	0.602	0.053	0.542
C_{NucAc} (mg/mL)	6.024	7.087	2.129	0.258	2.937	3.154	0.949	2.840
M_{NucAc} (kg)	6.024	5.567	0.456	0.456	5.191	5.026	0.165	4.523
$C_{TotProt}$ (mg/mL)	111.688	131.394	39.478	4.788	61.622	66.178	19.906	59.601
$M_{TotProt}$ (kg)	111.688	103.224	8.464	8.464	108.926	105.461	3.465	94.915
M_{Tot} (kg)	1007.563	785.670	221.894	1775.150	1773.949	1593.802	180.147	1592.649
V_{Tot} (L)	1000.000	785.610	214.390	1767.646	1767.646	1593.591	174.055	1592.493
Product yield (%)	/	/	76.6	100	80	92	/	90

5.7.3   Process sequence 2

Table 5-2 shows the mass balances carried out for the second process scenario. As seen in Table 5-2, the starting concentration of solids in the fermentation feed was 45.824 g/L, in a volume of 1000 L. 41.667 L of PEI (the volume of 25% w/v PEI solution required to achieve 1% final concentration in the broth) was then added to the broth to carry out the flocculation step. This volume diluted the total concentrations of protein, product and nucleic acids, however their respective total masses stayed the same. Furthermore, due to the precipitation and flocculation with PEI, some soluble nucleic acids, protein and Fab' product were assumed to precipitate into solids, which caused the mass and concentration of solids to almost double after PEI addition (to 86.644 kg and 83.178 g/L, respectively). Therefore, the masses and concentrations of product, nucleic acids and total protein are shown in Table 5-2, broken down into the total, soluble and solids fractions. To determine this, 10% product was assumed to be lost in the solids fraction after PEI addition. In addition, taking estimates from experimental data (Figure 5-4), 30% nucleic acids and 15% total protein were assumed to precipitate into the solids fraction after PEI addition.

The mass balance was then carried out for the centrifugation step, in the same manner as described in section 5.7.2. Here, the clarification performance was 99.8%, and the mass of solids in the sediment stream was determined to be 86.476 kg, and 0.168 kg in the supernatant stream. For a 70% dewatering level, the total volume in the supernatant after the centrifugation step was 979.443 L. The depth filtration step was carried out as described in section 5.7.2; and the solids remaining was calculated in section 5.6 to be 41.7%. Therefore, the remaining solids in the permeate stream were determined to be 0.07 kg.

The mass balances for the Fab' product, nucleic acids and total protein were carried out using the same method as described above. As seen in Table 5-2, the final mass of soluble Fab' in the depth filtration permeate stream was determined to be 1.372 kg. In addition, the use of PEI in this primary recovery sequence enabled an overall reduction in nucleic acid content by 39.3% (to 8.013 kg) and a 26.3% reduction in

total protein (to 180.191 kg), in comparison to the starting masses (as seen in Table 5-2). The final volume was determined to be 944.045 L. The product yield achieved for each step (where appropriate) is also shown in Table 5-2, and the overall yield for the second primary recovery sequence was calculated to be 74.2%.

Table 5-2: Mass balance for solids, product (Fab'), nucleic acids and total protein in process scenario 2. Cells harvested at 57 h postinduction and fully autolysed. Mass balance based on starting feed of 1000 L. Flocculation carried out using 25 % w/v PEI solution and added to reach a final broth concentration of 1%. Centrifugation carried out at 48 L/h using a disc stack centrifuge and dewatered to a level of 70%. Fab' data measured by HPLC (Agilent 1200, Agilent Technologies Inc., California, USA). Cell concentration was measured by optical density, and converted to wet cell weight. Nucleic acid and total protein concentration measured using the Nanodrop (Nanodrop 1000 spectrophotometer, Thermo Scientific, Wilmington, DE, USA).

	Ferm. Feed	After PEI	Cent. 1 Sup.	Cent. 1 Sed.	DF Perm.
C_{sol} (g/L)	45.824	83.178	0.172	1389.745	0.074
M_{sol} (kg)	45.824	86.644	0.168	86.476	0.070
M_{liq} (kg)	956.358	959.149	923.852	35.296	923.852
$C_{prod,tot}$ (mg/mL)	1.851	1.777	1.556	5.242	1.453
$C_{prod,soluble}$ (mg/mL)	1.851	1.599	1.556	2.274	1.453
$C_{prod,solids}$ (mg/mL)	0.000	0.178	0.0004	2.968	0.0002
$M_{prod,tot}$ (kg)	1.851	1.851	1.524	0.326	1.372
$M_{prod,soluble}$ (kg)	1.851	1.665	1.524	0.141	1.372
$M_{prod,solids}$ (kg)	0.000	0.185	0.0004	0.185	0.0002
$C_{NucAc,tot}$ (mg/mL)	13.199	12.671	9.094	68.978	8.488
$C_{NucAc,soluble}$ (mg/mL)	13.199	8.870	9.086	5.464	8.484
$C_{NucAc,solids}$ (mg/mL)	0.000	3.801	0.008	63.514	0.003
$M_{NucAc,tot}$ (kg)	13.199	13.199	8.907	4.292	8.013
$M_{NucAc,soluble}$ (kg)	13.199	9.240	8.900	0.340	8.010
$M_{NucAc,solids}$ (kg)	0.000	3.960	0.008	3.952	0.003
$C_{TotProt,tot}$ (mg/mL)	244.503	234.723	204.454	711.173	190.872
$C_{TotProt,soluble}$ (mg/mL)	244.503	199.514	204.381	122.910	190.840
$C_{TotProt,solids}$ (mg/mL)	0.000	35.208	0.073	588.263	0.032
$M_{TotProt,tot}$ (kg)	244.503	244.503	200.251	44.252	180.191
$M_{TotProt,soluble}$ (kg)	244.503	207.827	200.179	7.648	180.161
$M_{TotProt,solids}$ (kg)	0.000	36.675	0.071	36.604	0.030
M_{Tot} (kg)	1002.182	1045.793	924.021	121.772	923.923
V_{Tot} (L)	1000.000	1041.667	979.443	62.224	944.045
Product yield (%)	/	90	91.5	/	90

5.7.4   Process sequence 3

Table 5-3 shows the mass balances carried out for the third process scenario with flocculation and crossflow filtration. As seen in Table 5-3 the starting concentration of solids in the fermentation feed was 45.824 g/L, in a volume of 1000 L. Carried out in the same way as for process scenario 2, described in section 5.7.3, 41.667 L of PEI (the volume of 25% w/v PEI solution required to achieve 1% final concentration in the broth) was then added to the broth for the flocculation step, which caused an increase in the total solids concentration to 83.178 g/L.

To carry out the mass balance for the subsequent CFF step (in concentration mode), the total volumes in the permeate and retentate were first calculated. To calculate the volume in the permeate stream for a 1000 L starting fermentation feed volume, the concentration factor (CF) must first be calculated:

$$CF = \frac{V_{CFFpermeate,experimental} + V_{CFFchamber}}{V_{CFFchamber}}$$

Equation 5-11

where $V_{CFFpermeate,experimental}$ is the experimentally determined permeate volume (16.7 mL) and $V_{CFFchamber}$ is the working volume of the chamber in the USD CFF device (5.3 mL).

The concentration factor was therefore determined to be 4.15. Following this, the volume in the retentate could be calculated as:

$$V_{CFFretentate} = \frac{V_{Feed,CFF}}{CF}$$

Equation 5-12

where $V_{CFFretentate}$ is the volume in the retentate (L) and $V_{Feed,CFF}$ is the volume in the feed of the CFF device (for the mass balance, this was 1041.667 L after the flocculation step).

The volume in the retentate was therefore 250.947 L and the volume in the permeate could then be determined to be 790.720 L.

The clarification performance, described in section 5.6 as 0.112% solids remaining in the CFF permeate stream, was used to calculate the mass of solids in the retentate and permeate streams after CFF. These were determined to be 0.0973 kg in the permeate stream and 86.644 kg in the retentate stream.

For the product mass balance, displayed in Table 5-3, it can be seen that after the CFF step (carried out in concentration mode), 1.172 mg/mL soluble product was found in the permeate stream, based on a total feed product concentration of 1.777 mg/mL (1.599 mg/mL soluble product). This amounted to a total product mass of 0.927 kg; a 1.71-fold increase in product recovered in comparison to that seen in process scenario 1. However, ~44% of the soluble product remained inside the CFF chamber (0.739 kg). In addition, for process scenario 2, the total product recovered was calculated to be 1.372 kg.

For large scale CFF operation, diafiltration would be carried out to recover the remaining product inside the chamber, therefore, the diavolume required to achieve an equal product recovery to that of scenario 2 was calculated. First, the overall desired yield was set to 1.372 kg (to match process scenario 2). This meant that an additional 0.445 kg Fab' product was required to be recovered in the diafiltration step. Next, the rejection coefficient (σ_{prod}) of the product was calculated (from the CFF concentration step) using the equation:

$$C_{\mathrm{Pr}od,CFFretentate1} = C_{\mathrm{Pr}od,CFFfeed} \times CF^{\sigma_{prod}} \qquad \textbf{Equation 5-13}$$

Which can be rearranged to determine the rejection coefficient, σ_{prod}:

$$\sigma_{prod} = \frac{\ln(\frac{C_{Prod,CFFretentate1}}{C_{Prod,feed}})}{\ln(CF)}$$

Equation 5-14

where σ_{prod} is the rejection coefficient for the Fab' product, $C_{Prod,CFFretentate1}$ is the concentration of the product in the retentate stream after the CFF step carried out in concentration mode (3.680 mg/mL), $C_{Prod,CFFfeed}$ is the concentration of product in the starting feed before CFF (1.777 mg/mL) and CF is the concentration factor (4.15, as described above). Therefore, the rejection coefficient for the Fab' product was determined to be 0.512.

Following this, the number of diavolumes, D (i.e. the additional buffer volume in the diafiltration step), required to achieve a total yield of 1.372 kg Fab', was calculated using the equation:

$$C_{Prod,CFFretentate2} = C_{Prod,CFFretentate1}e^{-D(1-\sigma_{prod})}$$

Equation 5-15

Which can be rearranged to determine the number of diavolumes required, D:

$$D = \frac{\ln(\frac{C_{Prod,CFFretentate2}}{C_{Prod,CFFretentate1}})}{(\sigma_{prod} - 1)}$$

Equation 5-16

where D is the number of diavolumes, $C_{Prod,CFFretentate2}$ is the concentration of product in the retentate after the diafiltration step (1.906 mg/mL) and $C_{Prod,CFFretentate1}$ is the concentration of product in the retentate after the CFF concentration step (3.680 mg/mL), as described above.

Consequently, the number of diavolumes required, D, was determined to be 1.347, which was equivalent to a total buffer volume of 337.658 L. This meant that the total volume at the end of the third primary recovery sequence was 1128.820 L, with a total product of 1.372 kg. For both scenario 2 and 3, this represents a 2.53-fold improvement in total product recovered, in comparison to the existing Fab' process (process scenario 1). A further increase in product recovery would be possible using diafiltration after CFF ran in concentration mode, however this would increasingly dilute the recovered product in the permeate stream. The product yield achieved for each step (where appropriate) is also shown in Table 5-3 and the overall yield for the third primary recovery sequence was subsequently calculated to be 74.2% (equivalent to process scenario 2). Additionally, the total product yield for the CFF steps (concentration with diafiltration) was calculated to be 82.4%.

As seen in Table 5-3, nucleic acids and total protein mass balances were carried out in the same way as described above, using experimental values to establish the concentration of protein and nucleic acids in the permeate and retentate streams, and to determine the rejection coefficients in the CFF step ran in concentration mode. The rejection coefficient for nucleic acids, σ_{NucAc}, was determined to be 0.595 and the rejection coefficient for total protein, $\sigma_{TotProt}$, was determined to be 0.589. The starting total mass of nucleic acids was 13.199 kg, and after PEI addition (30% of the total nucleic acids were assumed to precipitate to the solids fraction, as described in section 5.7.3) and CFF in concentration mode, 5.963 kg total nucleic acids was found in the permeate stream. For the total protein mass balance, the initial mass was 244.503 kg and 109.390 kg total protein was found in the permeate stream after PEI addition (15% of the total protein was assumed to precipitate to the solids fraction, as described in section 5.7.3) and the CFF step in concentration mode. Therefore, for flocculation with PEI followed by CFF (scenario 3), a 55% reduction in both total protein and nucleic acids was achieved.

Table 5-3: Mass balance for solids, product (Fab'), nucleic acids and total protein in process scenario 3. Cells harvested at 57 h postinduction and fully autolysed. Mass balance based on starting feed of 1000 L. Flocculation carried out using 25 % w/v PEI solution and added to reach a final broth concentration of 1%. Cell concentration was measured by optical density, and converted to wet cell weight. Total protein and nucleic acid concentration measured using the Nanodrop (Nanodrop 1000 spectrophotometer, Thermo Scientific, Wilmington, DE, USA). Fab' data measured by HPLC (Agilent 1200, Agilent Technologies Inc., California, USA). CFF carried out at a flux rate of 45.5 L/m^2/h in concentration mode, and then a mass balance for a diafiltration step was carried out to determine the buffer volume required to reach 1.372 kg total product recovered (equal to process scenario 2).

	Ferm. Feed	After PEI	CFF Perm.	CFF Retent.	Diafil. Perm.	Diafil. Retent.	Total Prod. Rec.
C_{sol} (g/L)	45.824	83.178	0.123	344.881	0.000287	344.880	0.0000863
M_{sol} (kg)	45.824	86.644	0.0973	86.547	0.0000972	86.547	0.0974
M_{liq} (kg)	956.358	959.149	790.627	168.521	338.100	168.522	1128.727
$C_{prod,tot}$ (mg/mL)	1.851	1.777	1.173	3.680	1.317	1.906	1.216
$C_{prod,soluble}$ (mg/mL)	1.851	1.599	1.172	2.943	1.316	1.170	1.215
$C_{prod,solids}$ (mg/mL)	0.000	0.178	0.000263	0.737	0.00061	0.736	0.000368
$M_{prod,tot}$ (kg)	1.851	1.851	0.927	0.923	0.445	0.478	1.372
$M_{prod,soluble}$ (kg)	1.851	1.665	0.927	0.739	0.445	0.294	1.372
$M_{prod,solids}$ (kg)	0.000	0.185	0.000208	0.185	0.000208	0.185	0.000415
$C_{NucAc,tot}$ (mg/mL)	13.199	12.671	7.541	28.837	/	/	/
$C_{NucAc,soluble}$ (mg/mL)	13.199	8.870	7.535	13.075	/	/	/
$C_{NucAc,solids}$ (mg/mL)	0.000	3.801	0.00562	15.762	/	/	/
$M_{NucAc,tot}$ (kg)	13.199	13.199	5.963	7.237	/	/	/
$M_{NucAc,soluble}$ (kg)	13.199	9.240	5.958	3.281	/	/	/
$M_{NucAc,solids}$ (kg)	0.000	3.960	0.00445	3.955	/	/	/

$C_{TotProt,tot}$ (mg/mL)	244.503	234.723	138.342	538.412	/	/	/
$C_{TotProt,soluble}$ (mg/mL)	244.503	199.514	138.290	392.428	/	/	/
$C_{TotProt,solids}$ (mg/mL)	0.000	35.208	0.052	145.984	/	/	/
$M_{TotProt,tot}$ (kg)	244.503	244.503	109.390	135.113	/	/	/
$M_{TotProt,soluble}$ (kg)	244.503	207.827	109.349	98.479	/	/	/
$M_{TotProt,solids}$ (kg)	0.000	36.675	0.0412	36.634	/	/	/
M_{Tot} (kg)	1002.182	1045.793	790.724	255.068	338.100	255.068	1128.824
V_{Tot} (L)	1000.000	1041.667	790.720	250.947	338.100	250.947	1128.820
Product yield (%)	/	90	55.7	/	60.3	/	82.4

5.7.5   Capital costs and processing time

After carrying out the mass balances, the total processing time and capital costs for each of the primary recovery sequences were determined. First, equipment was sized appropriately and capital costs were obtained using Biosolve (Biopharm Services, Chesham, UK); shown in Table 5-4 below.

Table 5-4: Equipment sizes and capital costs (taken from Biosolve (Biopharm Services, Chesham, UK)) for each of the units used in the three process sequences carried out in this study. Costing data obtained from January 2016 and in US dollars ($). Sizing based on the most appropriate fit for the volumes required in this study, and on available equipment in the Biosolve database.

Equipment	Size	Capital cost ($)
Bioreactor	1000 L	486722
Disc Stack Centrifuge	Max. 600 L/h	648614
Vessel (flocculation)	1000 L	62353
Vessel (extraction)	3000 L	78578
CFF	5 m^2	167400
Depth Filtration	5 m^2	5647

After obtaining appropriate equipment sizes, the processing times for each of the unit operations could be determined. These are shown for each process scenario in Table 5-5, Table 5-6 and Table 5-7 below. It was assumed that 2 h was required for product transfer between each unit operation at large scale.

For the depth filtration step in process scenario 1, the flux rate could be determined from the data shown in Figure 5-5 (a). This was determined by obtaining the permeate volume per unit of time (within the linear region in Figure 5-5 (a)). The permeate flow rate was therefore determined to be 0.1152 L/h and dividing this value

by the USD depth filter area (2.8×10^{-5} m^2), the flux rate was calculated to be 4114 L/m^2/h. For a 5 m^2 filter area, the time required to filter 1593.591 of broth was 0.0775 h (rounded to 1 h in Table 5-5 below).

For the depth filtration step in process scenario 2, the flux rate was determined to be 514.3 L/m^2/h (with a permeate flow rate of 0.0144 L/h), calculated in the same way as described above, from the data shown in Figure 5-7 (a). For a 5 m^2 filter area, the time required to filter 979.443 L broth was 0.381 h (rounded to 1 h in Table 5-6 below).

To calculate the time required for the CFF steps in process scenario 3, both concentration and diafiltration time were calculated by:

$$t_{CFF} = \frac{V_{Feed,CFF}}{(Flux_{CFF} \times A_{Membrane})}$$

Equation 5-17

where t_{CFF} is the time required for each of the CFF steps (in concentration or diafiltration mode), $V_{Feed,CFF}$ is the volume of feed, $Flux_{CFF}$ is the flux rate used for CFF operation (45.5 L/m^2/h) and $A_{Membrane}$ is the area of the membrane used (5 m^2).

Table 5-5: Processing time (h) required for each unit operation in process scenario 1. Centrifugation carried out at 48 L/h, using a disc stack centrifuge. Periplasmic extraction carried out for 16 h, according to standard protocol at large scale. Depth filtration determined based on a filter area of 5 m². 2 h product transfer time assumed between each step for large scale operation (not included in calculations below).

	Centrifugation 1	Periplasmic Extraction	Centrifugation 2	Depth Filtration
Time (h)	20.833	16.000	36.826	1.000

Table 5-6: Processing time (h) required for each unit operation in process scenario 2. Flocculation at large scale assumed to take 2 h total for 1000 L broth. Centrifugation carried out at 48 L/h, using a disc stack centrifuge. Depth filtration determined based on a filter area of 5 m². 2 h product transfer time assumed between each step for large scale operation (not included in calculations below).

	Flocculation	Centrifugation	Depth Filtration
Time (h)	2.000	21.701	1.000

Table 5-7: Processing time (h) required for each unit operation in process scenario 3. Flocculation at large scale assumed to take 2 h total for 1000 L broth. CFF steps calculated based on flux rates in both concentration mode and diafiltration mode. 2 h product transfer time assumed between each step for large scale operation (not included in calculations below).

	Flocculation	CFF (Concentration)	CFF (Diafiltration)
Time (h)	2.000	4.579	1.609

5.7.6 Summarising the performance of the three process scenarios

Table 5-8 shows a summary of the three process scenarios. It can be seen that both scenario 2 and 3 achieved a 2.53-fold improvement in total product recovered, in comparison to the existing Fab' recovery process (scenario 1). By running the fermentation to maximum productivity for process scenarios 2 and 3, i.e. full autolysis, the initial total product concentration was significantly greater than for process scenario 1 (where the aim was to avoid product loss and maximise the intracellular product concentration).

However due to the diafiltration step with CFF (337 L additional buffer volume), the concentration of Fab' in scenario 3 (1.216 mg/mL) was lower in comparison to scenario 2 (1.453 mg/mL). A further increase in product recovery would be possible using diafiltration after CFF, however this would increasingly dilute the concentration of the recovered product in the permeate stream.

The capital costs for the downstream processing sequences as well as total downstream processing (DSP) time were estimated using Biosolve, based on 1,000 L starting fermentation feed. The use of CFF with flocculation demonstrated a significant reduction in processing time (14 h) and capital costs ($230,000) in comparison to both scenario 1 and 2. The intensified process designs in scenario 2 and 3 were able to achieve higher product yields largely due to the reduction in the number of unit operations in the sequences. At a scale of 1,000 L feed material, the third process sequence is favourable, however it should be noted that as the scale increases to full industrial production, centrifugation may be a more feasible unit operation than crossflow filtration, as it can be ran continuously at high flow rates and the capital costs become more economical at a larger scale in comparison to CFF.

Table 5-8: Summary of the three DSP process scenarios. Product concentration (Fab', mg/mL) measured in duplicate. Total product recovered and overall product yield at end of DSP were calculated by mass balance, based on 1,000 L of feed fermentation broth. Total solids remaining and [Impurity]/[Fab'] were calculated from experimental data (runs carried out in duplicate). Capital costs and downstream processing (DSP) time were calculated using both Biosolve (Biopharm Services, Chesham, UK) and mass balances, based on processing 1,000 L of feed fermentation broth. The starting points for scenario 2 and 3 mass balances were normalised, so that experimental variation between fermentation runs was removed.

	Scenario 1	Scenario 2	Scenario 3
Product concentration (mg/mL)	0.340	1.453	1.216
Product recovered (kg)	0.542	1.372	1.372
Overall product yield (%)	51.2	74.2	74.2
Total solids remaining (%)	0.307	0.0810	0.112
[Impurity]/[Fab']	469	155	129
Capital costs ($)	1,400,000	700,000	230,000
DSP time (h)	82.659	30.701	14.188
Final volume (L)	1,592.493	944.045	1,128.820

5.8   Conclusions

This study demonstrates an approach to assess alternative primary recovery options using ultra scale-down technology to gain insight into large scale processing. Three primary recovery sequences were evaluated and compared, with a focus on a novel process design using CFF with flocculation directly after fermentation ran to maximum productivity i.e. full cell autolysis.

The use of flocculation with CFF in concentration mode achieved a 1.71-fold improvement in total product recovered, which was increased to 2.53-fold by carrying out diafiltration (using a diavolume of 1.347x the CFF chamber volume). In addition, a 3-fold improvement in solids removal and a 3.6-fold improvement in product purity were achieved, in comparison to the existing Fab' recovery process (process scenario 1). Acceptable operation (in terms of permeate flux) was attained for CFF at USD scale, which was equivalent to mid-range operation at large scale. This process design is deemed to be more robust, as the need to avoid premature lysis in fermentation is removed and the process sequence is simplified. Further, it was shown that this approach to process design i.e. by taking a holistic view of the process to understand the impact of upstream processing conditions on downstream operation efficiency, demonstrated a significant reduction in both DSP time and capital costs.

This study provides a basis for rapidly assessing alternative process designs, using USD technology to identify suitable primary recovery process designs before taking through to large scale. In doing so, this study also demonstrated an application of fermentation viscosity monitoring in process development, and its utility in rapidly assessing challenges such as detecting the level of lysis in the cell broth, inferring the level of contaminants and understanding the impact of high viscosity on the process, such as pumping.

It would also be interesting to investigate additional process variables such as effects on product quality due to lysis or flocculation, although a previous study showed no effect on the aggregation of a domain antibody (dAb) using PEI (Chatel et al., 2014).

Another factor to consider is the need to demonstrate removal of the PEI reagent after downstream processing. The process sequences studied here may be used to assess their application to other cell lines and products such as yeast and mammalian cells.

Chapter 6   Considerations for the commercialisation of viscosity monitoring

The central aim of this thesis is to develop a method to rapidly detect cell lysis and product loss in fermentation using viscosity monitoring, in order to enable decision making about harvest time, and to demonstrate the application and value of viscosity monitoring in process development and optimisation.

Process monitoring technologies in fermentation typically focus on monitoring biomass growth or cell viability, and do so by monitoring chemical or biological variables. However, the work in this thesis has demonstrated that physical properties can be monitored to provide useful information about the cell broth. In this research, a deeper understanding of changes in the physical properties of cell broths during fermentation has been obtained, as well as insight into the impact of lysis on various primary recovery unit operations. The novel use of viscosity monitoring in biopharmaceutical fermentation to rapidly detect lysis and product loss has been shown to be a promising analytical tool for both process development and large scale manufacturing, to enable rapid decision-making about cell harvesting in order to minimise product loss. In addition, the application of viscosity monitoring has been demonstrated in process development, in combination with high-throughput, ultra scale-down technology to rapidly evaluate novel primary recovery process designs. Therefore, this work additionally demonstrates the value of developing an online, in-situ probe to monitor the viscosity and other rheological parameters in biopharmaceutical fermentation.

Procellia Ltd., the industrial sponsor of this thesis, are working to commercialise an online, in-situ viscosity sensor for industrial biopharmaceutical fermentation, that will ultimately be used as part of a platform technology for the predictive modelling of novel cell quality indicators. The product will be a hardware (probe)/software (modelling) combination, that is able to monitor both the volume fraction (biomass concentration) and the viscosity of the cell broth.

The current in-line probe uses ultrasound spectroscopy to measure both the amplitude attenuation and the change in ultrasound velocity of the fermentation

broth. By employing a set of equations called the ECAH equations (Epstein, Carhart, Allegra and Hawley), the amplitude attenuation can be converted into to the volume fraction (i.e. to determine the biomass concentration of the cell broth). In addition to monitoring the biomass concentration, the Einstein equations can be implemented, in order to determine the viscosity of the cell suspension, based on the cell concentration.

The work carried out in this thesis has demonstrated that significant value can be derived from monitoring the physical properties of an industrially relevant, high cell density *E. coli* fermentation. Therefore, the first step towards the commercialisation of this technology should be to take forward the use of viscosity monitoring to demonstrate its application in large scale fermentation, for a range of products and host cells. This will further demonstrate the proof of concept and the value of viscosity monitoring for a wide range of biopharmaceutical fermentation systems, and will also provide a reference point for the subsequent validation with the in-situ viscosity sensor.

In order to develop the product to reach this point, there are several issues that need to be addressed. First, after integrating the ECAH equations to successfully measure the volume fraction from the amplitude attenuation, the models need to be able to accurately determine the viscosity of the cell broth, particularly at high cell concentrations. The volume fraction can be converted to viscosity via the Einstein equations, which become increasingly complex as the volume fraction increases. For high cell density fermentation systems, this may be challenging as the model complexity may require significant computational power, and the accuracy of the models needs to be verified at high volume fractions.

In addition, it is known that the viscosity in fermentation is not only affected by the volume fraction, but also by the solute concentration in the broth. The work in this thesis has demonstrated that the intracellular content released during cell lysis has a significant impact on the viscosity in late stage fermentation. The amplitude attention can be used to determine the volume fraction, however the sound velocity may be used to monitor chemical changes in the media. By developing the capability to

detect chemical changes in the media (changes in ultrasound velocity), this can be integrated with the models to detect volume fraction (amplitude attenuation), to create a new model to accurately monitor the viscosity of the cell broth throughout the entire fermentation, based on both volume fraction and chemical content in the cell broth. This will bring the probe to the point of accurately monitoring the viscosity of fermentation broths.

A further challenge to address that is generic to all in-situ fermentation probes includes minimising the effect of aeration (i.e. gas bubbles) and agitation on signal interference. Some early work has been undertaken by the company to mitigate this, however further development must be carried out in order to ensure the success of the technology. This could be done with post-measurement modifications to reduce the noise. It should be noted that the in-situ probe has also been designed to withstand high temperature sterilisation procedures.

After developing the product to the point of being able to accurately monitor viscosity in fermentation, the work carried out in this thesis can be integrated into the software part of Procellia's product. The model created in Chapter 4 can be integrated in order to detect and quantify lysis (based on DNA release to the cell broth) and product loss in real-time by online viscosity monitoring. The ability to achieve this will be a major milestone for the company, and will demonstrate the significant commercial value of the technology. Further relationships can be characterised in a similar way, for example by developing models for the relationship between viscosity and total protein release or product leakage in postinduction fermentation. This will provide operators with extremely useful information by directly quantifying cell lysis as well as indicating the level of contaminants in the broth (i.e. to specify the downstream conditions required). This information is useful because it will enable real-time connectivity and integration between the upstream and downstream unit operations.

In addition to monitoring the viscosity, it may be possible to monitor other physical parameters using ultrasound spectroscopy, such as the storage modulus of the cell broth. This would be particularly useful in fermentation systems that have significant

structure, i.e. strong viscoelastic behaviour (for example, mycelial fermentations). The work carried out in this thesis (see Chapter 4) has demonstrated that monitoring the storage modulus can provide unique information regarding changes in the strength of the cells during fermentation. Therefore, an opportunity exists to develop the capability to monitor the storage modulus as a key cell quality indicator (i.e. to monitor cell strength). In order to do this, the storage modulus will need to be extensively characterised in fermentation and subsequently validated. As a result, the ultimate aim of Procellia's software is to be able to model and interpret valuable information such as volume fraction (biomass concentration), viscosity (cell lysis) and storage modulus (cell strength) to create a novel predictive modelling system to indicate cell health in fermentation.

With regards to the hardware element of Procellia's technology (i.e. the physical probe), several aspects need to be considered for its commercialisation. First, the probe has been designed to be able to measure a range of ultrasound frequencies (1-10 MHz), however it currently operates at a fixed frequency of 5 MHz. The ECAH equations may also be able to provide information on particle size as an output from the model. By adjusting the probe hardware to measure the ultrasound properties of the cell broth across a range of frequencies, it may be possible to determine the particle size distribution and therefore provide useful information on the cell broth, for example, the level of cell debris in the broth. This would be extremely useful for process operation as cell debris can impact downstream unit operations such as centrifugation and microfiltration.

Moreover, when considering the commercialisation of Procellia's technology in the bioprocessing industry, it is important to assess the evolution and impact of single-use technology. Over the last 10 years, single-use technology has become increasingly prevalent in the bioprocessing industry, and this has led to a change in the way that process monitoring technologies are applied. To avoid contamination issues, DOT, pH and temperature probes are now routinely used as ex-situ technologies, i.e. to monitor the respective variables from outside of the bioreactor wall. This is an important consideration if Procellia want to move into the single-use market; not only must a new probe prototype be developed to monitor the cell broth

ex-situ, but it will also be necessary to work with single-use manufacturers to integrate Procellia's technology with the existing set up.

The ultimate aim of PAT is to be able to control all critical parameters in the process. The further development of Procellia's technology will enable the monitoring and eventual control of a range of physical parameters in fermentation to provide a wealth of information regarding cell health. The work in this thesis has demonstrated the commercial value of monitoring the physical properties of cell broths and an exciting opportunity exists to commercialise Procellia's technology. The work carried out in this thesis has therefore laid the foundation for the further development and commercialisation of an in-situ, online viscosity sensor.

Chapter 7   Conclusions & future work

Cell lysis is a considerable challenge in biopharmaceutical fermentation, and is particularly important for host cells that store the product in the intracellular space (for example, in the periplasm), as product loss occurs at the point of lysis. Apart from product loss during cell lysis, impurities such as nucleic acids and host cell protein are released simultaneously to the cell broth, which leads to large variations in the material properties of the broth. This significantly impacts both the operational performance of many downstream unit operations as well as the robustness of the process, as many downstream processes are sensitive to the process material properties.

Cell lysis in fermentation has been observed for decades, however our ability to monitor and detect lysis is limited. The ability to detect lysis has significance both academically and commercially, however it is challenging as the complex nature of the cell broth means that it is difficult to observe lysis directly, and current analytical technologies are unable to rapidly and accurately monitor the shift between optimum intracellular product concentration and leakage to the cell broth. Therefore, there exists a need to improve our understanding of the phenomenon of cell lysis, and by improving understanding, it is possible to develop solutions to monitor and ultimately control lysis. As a result, this thesis has focused on characterising cell lysis in *E. coli* fermentation to improve process understanding, and subsequently developing a novel methodology to monitor and detect cell lysis in fermentation.

To investigate cell lysis and develop a deeper understanding of the associated problems, fermentations have been carried out using an industrially relevant, high cell density *E. coli* strain producing antibody fragments (antigen-binding, Fab'), and a range of analytical techniques have been used to characterise the progression of cell lysis in late stage fermentation. Following this, the viscosity profile of the fermentation broth has been characterised, which showed an increase in viscosity during exponential phase in relation to the cell density increase, a relatively flat profile in stationary phase, followed by a rapid increase during late stage fermentation which correlated well with product loss, DNA release and loss of cell

viability. After establishing a strong correlation between cell lysis and postinduction viscosity, a methodology has been developed to monitor the viscosity of the cell broth at-line, in order to rapidly detect cell lysis and product loss in postinduction fermentation. The at-line viscosity monitoring method was then evaluated against several common monitoring technologies, and results confirmed that viscosity monitoring can accurately identify lysis and product leakage at an earlier time point than optical density measurements and online capacitance measurements, and can obtain results in under 2 minutes; faster than flow cytometry, DNA assays, cytotoxicity assays and HPLC measurements. The ability to accurately and rapidly detect cell lysis is critical to enable rapid decision making for industrial process operation. This work has therefore demonstrated the utility of rapidly monitoring the physical properties of fermentation broths for recombinant protein production, and that viscosity monitoring has the potential to be a valuable tool for process development to determine the optimal harvest time and minimise product loss.

After determining the viscosity profile during fermentation, establishing a correlation between postinduction viscosity and then developing a method to rapidly detect cell lysis, it was desired to further investigate the physical properties of fermentation broths to understand whether rheological testing could provide information relating to the causes of the postinduction viscosity increase during fermentation. Therefore, components of the cell broth have been isolated (cell broth, cells and supernatant) and it was observed that the increase in cell broth viscosity in postinduction fermentation is a result of the large increase in the supernatant viscosity, which can be attributed to the release of intracellular content to the broth during lysis. In addition, oscillatory rheological testing has been carried out on cell paste to understand changes in the strength and stability of cells during fermentation, which was quantified and monitored using the storage modulus. A decrease in the storage modulus and an increase in the LVER were observed, suggesting that although cell strength decreases over the fermentation, interactions exist between cells and leaked intracellular content such as DNA, which increases the "stickiness" of the cell paste. Therefore, monitoring the viscoelastic properties of cells has also demonstrated potential as a tool to detect changes in cell strength during fermentation. Cell strength is an important property that significantly impacts the downstream process,

including the performance in cell harvesting, cell disruption and cell debris removal such as centrifugation or microfiltration unit operations.

Cell lysis can be defined as the release of DNA from the cell. The release of DNA to the cell broth during cell lysis in late stage fermentation causes significant problems in the downstream process. Therefore, having demonstrated a linear correlation between DNA and viscosity, a model has been developed to quantify the extent of cell lysis in postinduction fermentation, using rapid at-line viscosity monitoring. This model enables results in under 2 minutes, to provide information regarding the level of DNA present in the cell broth (i.e. the level of contaminants), and provides useful information to fermenter operators to determine the optimal harvest time and to assess the impact of the contaminants on downstream unit operations, for example to determine the conditions to be used in centrifugation. Product leakage and DNA release have been shown to occur simultaneously in fermentation; therefore the model also directly indicates product loss. This model has the potential to be used in a wide range of industrial fermentation systems, simply by characterising the relationship between viscosity and DNA leakage, and then implementing rapid, at-line viscosity monitoring.

Following the studies to understand and characterise cell lysis in fermentation using rheology, a process design case study has been carried out, where two alternative primary recovery process sequences have been designed and evaluated to avoid the problems associated with cell lysis in fermentation and simultaneously intensify the primary recovery process. The focus of this study was on taking an integrated approach to process design by understanding and assessing the impact of upstream processing conditions (i.e. harvest time) on primary recovery unit operations. Fermentation was carried out and ran to full autolysis (i.e. maximum productivity) in order to remove the challenges associated with avoiding product loss and lysis in fermentation and to therefore minimise process variation. Running the fermentation to full autolysis enables a higher product titre to be achieved, however it also creates a high level of contaminants in the cell broth. To overcome this, PEI was proposed as a primary recovery step directly after fermentation to precipitate and flocculate the contaminants, followed by a crossflow filtration step. The novel primary recovery

sequence achieved a significant improvement in total product recovered, solids removal and product purity in comparison to the existing primary recovery process, whilst reducing capital costs, processing time and intensifying the process.

This study has provided a basis for rapidly assessing alternative design options, by using ultra scale-down technology to identify suitable primary recovery process designs before taking through to large scale. In doing so, this study has also demonstrated an application of fermentation viscosity monitoring in process development, and its utility in rapidly assessing challenges such as detecting the level of lysis in the cell broth, inferring the level of contaminants and understanding the impact of high viscosity on the process.

The work undertaken in this thesis has opened up avenues for further research projects to be carried out. In Chapter 3, the PID controller for the 7 L Applikon fermenter online controls (T, DOT, agitation) were improved. However, it was observed that significant fluctuation occured in exponential phase. It would be interesting to develop and integrate a PID controller that would enable different PID settings at different growth stages in the fermentation, which may enable higher cell densities and product titres.

The viscosity profile has been established and characterised in Chapter 3 for a high cell density *E. coli* fermentation system, and related to cell lysis. In order to develop this work further, it would be interesting to integrate viscosity measurements with online control data, for example stirrer rate (shear rate) to determine the Reynold's number throughout the fermentation, and integrate this into a computational fluid dynamics model to deliver insight into fluid flow patterns and mixing, which would be particulary useful as a scale-up tool in fermentation.

The rheological properties of *E. coli* cells (i.e. bulk rheological properties) have been characterised in Chapter 4. Atomic force microscopy can be carried out to elucidate the rheological properties of a single *E. coli* cell. It would be interesting to be able to observe changes in the rheological properties (i.e. microrheology) of individual cells over fermentation time, and compare this information to the bulk rheological

behaviour of the cells. In doing so, this would facilitate a deeper understanding of cell lysis, in particular the interactions between cells, cell debris and leaked intracellular content as cell lysis occurs.

In addition, a cell concentration factor could be integrated into the model developed in Chapter 4, which could be done using online viable biomass measurements with the Aber Instruments capacitance probe. This would enable a more accurate quantification of cell lysis, based on both viable biomass and viscosity (i.e. DNA and intracellular content release).

Further, investigating the impact of colanic acid formation during late stage fermentation, and understanding how this interacts with cell aggregation and cell lysis would be interesting to study further; cell aggregation has been shown to be affected by extracellular polymeric substances (Eboigbodin & Biggs, 2008), and would also affect the viscosity of the cell broth due to a change in the size of the particles (i.e. cells). The in-line viscosity probe being developed by Procellia Ltd. may be able to determine particle size distribution in real-time, and this could be incredibly useful for a range of fermentation systems.

In order to establish viscosity monitoring as a valuable and robust analytical technology, the methodology developed in this thesis needs to be extended to a range of biopharmaceutical applications. First, it is important to demonstrate the use of viscosity monitoring in *E. coli* strains that produce other periplasmically-stored products, for example domain antibodies or plasmid DNA products. This can be done by carrying out fermentations and then ascertaining the relationship between the shear viscosity, cell lysis and product loss. Following this, other microbial strains could be examined, for example the yeast *P. pastoris*, which can be grown to high cell densities and stores the product intracellularly (for example, virus-like particles). Additionally, the viscosity profile of mammalian cell cultures could be explored. This would be interesting as mammalian host cells such as CHO will typically secrete the product to the cell broth, and it would be necessary to gain an understanding of the impact of product secretion on the viscosity of the broth, and whether cell lysis in mammalian cell culture can be detected by viscosity monitoring.

Furthermore, viscosity monitoring could be applied to other unit operations where viscosity has a significant impact on the operational performance. Some examples include homogenisation, in which viscosity monitoring could be a valuable process development tool to detect and optimise cell disruption levels against the number of passes and the pressure. Also, viscosity monitoring could be applied to the periplasmic extraction step to optimise extraction time, i.e. by minimising DNA release and maximising product release. Viscosity monitoring could also be used in microfiltration operation, to monitor the viscosity of both the retentate and permeate streams in order to detect the level of fouling on the membrane.

Above all, the work carried out in this thesis demonstrates that significant value can be found in using rheology to monitor the physical properties of cell broths, and that viscosity monitoring could be used in combination with other analytical technologies such as infrared spectroscopic monitoring to provide a comprehensive picture of the cell broth, by monitoring both the physical and chemical properties. Therefore, this work additionally demonstrates the value of developing an online, in-situ probe to monitor the viscosity and other rheological parameters in biopharmaceutical fermentation.

The ultimate aim of the sponsor company, Procellia Ltd., is to bring to market an in-line probe for real-time viscosity monitoring in fermentation, that can be used as part of a platform technology for the predictive modelling of novel cell quality indicators. The technology will be a hardware (probe)/software (modelling) combination, that is able to monitor both the volume fraction (biomass concentration) and the viscosity of the cell broth. In addition to monitoring the viscosity, it may be possible to monitor other physical parameters such as particle size distribution and the storage modulus of the cell broth in fermentation systems that have significant structure (for example, mycelial fermentations). This would enable monitoring of the storage modulus as a cell quality indicator (i.e. to monitor cell strength). In order to do this, the storage modulus will need to be extensively characterised in fermentation and validated, along with the volume fraction (biomass concentration) and viscosity, as parameters to indicate cell health. Additionally, the model developed in this thesis to quantify DNA release based on viscosity measurements can be integrated with the software

part of Procellia's technology. This will enable the online determination and monitoring of cell lysis, which will be a powerful tool for process operation. The development of the software part of the product will be key to its success, in particular the models required to ultimately control cell lysis in fermentation using a range of inputs such as volume fraction, viscosity and storage modulus will be highly complex.

In addition to the commercialisation of an online, in-situ ultrasound probe, this may then be able to be brought together with various online monitoring technologies to create an integrated control platform in fermentation. For example, online viscosity monitoring, cell lysis quantification, cell strength and particle size distribution could then be integrated with the online determination of the Reynold's number and computational fluid dynamics models (as discussed above), online fermenter controls such as temperature, DOT and stirrer rate, the Aber Instruments online capacitance probe for viable biomass determination and infrared technologies providing chemical information of the cell broth. This would enable a robust view to be obtained of chemical, biological and physical properties of the cell broth and through this, a control system to be developed for optimal fermentation monitoring and control.

In summary, the work carried out in this thesis has laid a solid foundation for the further development of viscosity monitoring as a tool to detect cell lysis and product loss in recombinant protein production. In addition, the novel primary recovery process designs created and evaluated in this thesis have demonstrated significant improvements to the existing process, and the value of the integrated process design concept to find a global process optimum, i.e. by considering the impact of upstream processing conditions on downstream unit operations has been demonstrated. In order to validate these process designs, the product quality should first be assessed for each unit operation in the process. These processes can then be further optimised through a design of experiments (DoE) approach, to achieve an even higher product titre, product yield, solids removal and improved impurity profiles.

Chapter 8   References

Abuchowski A, McCoy JR, Palczuk NC, van Es T and Davis FF. 1977. Effect of covalent attachment of polyethylene glycol on immunogenicity and circulating life of bovine liver catalase. J. Biol. Chem. 252 (11), pp. 3582-3586.

Adams R, Popplewell G, Rapecki S and Tickle S. 2009. Neutralising Antibody Molecules Having Specificity for Human IL-17, United States of America: Patent No. US 20090117126A1.

Ambler CM. 1961. Theory of centrifugation. Ind. Eng. Chem. 53(6), pp. 430-433.

Arnold SA, Gaensakoo R, Harvey LM and McNeil B. 2002. Use of at-line and in-situ near-infrared spectroscopy to monitor biomass in an industrial fed-batch *Escherichia coli* process. Biotechnol. Bioeng. 80(4), pp. 406-413.

Assawajaruwan S, Eckard P and Hitzmann B. 2017. On-line monitoring of relevant fluorophores of yeast cultivations due to glucose addition during the diauxic growth. Process. Biochem. 58, pp. 51-59.

Aucamp JP, Davies R, Hallet D, Weiss A and Titchener-Hooker NJ. 2014. Integration of host strain bioengineering and bioprocess development using ultra-scale down studies to select the optimum combination: an antibody fragment primary recovery case study. Biotechnol. Bioeng. 111, pp. 171-181.

Badino Jr AC, Facciotti MCR and Schmidell W. 1999. Estimation of the rheology of glucoamylase fermentation broth from the biomass concentration and shear conditions. Biotechnol. Tech. 13, pp. 723-726.

Badino Jr AC, Facciotti MCR and Schmidell W. 2001. Volumetric oxygen transfer coefficients (kLa) in batch cultivations involving non-Newtonian broths. Biochem. Eng. J. 8, pp. 111-119.

Bailey S and Meagher M. 1997. Crossflow microfiltration of recombinant *Escherichia coli* lysates after high pressure homogenization. Biotechnol. Bioeng. 56, pp. 304-310.

Balasundaram B, Nesbeth D, Ward J, Keshavarz-Moore E and Bracewell D. 2009. Step change in the efficiency of centrifugation through cell engineering: co-expression of Staphylococcal nuclease to reduce the viscosity of the bioprocess feedstock. Biotechnol. Bioeng. 104, pp. 134-142.

Baruah G, Venkiteshwaran A and Belfort G. 2005. Global model for optimizing crossflow microfiltration and ultrafiltration processes: a new predictive and design tool. Biotechnol. Prog. 21, pp. 1013-1025.

Becker T, Hitzmann B, Muffler K, Pörtner R, Reardon KF, Stahl F and Ulber R. 2007. Future aspects of bioprocess monitoring. Adv. Biochem. Engin. Biotechnol. 105, pp. 249-293.

Belfort G, Davis R and Zydney A. 1994. The behaviour of suspensions and macromolecular solutions in crossflow microfiltration. J. Membr. Sci. 96, pp. 1-58.

Bell D and Dunnill P. 1982. Shear disruption of soya protein precipitate particles and the effect of aging in a stirred tank. Biotechnol. Bioeng. 24(6), pp. 1271-1285.

Bensmira M, Nsabimana C and Jiang B. 2010. Effects of fermentation conditions and homogenization pressure on the rheological properties of Kefir. LWT Food. Sci. Technol. 43, pp. 1180-1184.

Bentley W and Kompala DS. 1990. Optimal induction of protein synthesis in recombinant bacterial cultures. Annals of the New York Academy of Sciences. 589, pp. 121-138.

Bentley WE, Mirjalili N, Andersen DC, Davis RH and Kompala DS. 1990. Plasmid-encoded protein: The principal factor in the "metabolic burden" associated with recombinant bacteria. Biotechnol. Bioeng. 35, pp. 668-681.

Berrill A, Ho S and Bracewell D. 2008. Ultra scale-down to define and improve the relationship between flocculation and disc-stack centrifugation. Biotechnol. Prog. 24, pp. 426-431.

Better M, Chang CP, Robinson RR and Horwitz AH. 1988. *Escherichia coli* secretion of an acove chimeric antibody fragment. Science. 240, pp. 1041-1043.

Beutel S and Henkel S. 2011. In situ sensor techniques in modern bioprocess monitoring. Appl. Microbiol. Biotechnol. 91, pp. 1493-1505.

Biechele P, Busse C, Solle D, Scheper T and Reardon K. 2015. Sensor systems for bioprocess monitoring. Eng. Life. Sci. 15, pp. 469-488.

Bird RE, Hardman KD, Jacobson JW, Johnson S, Kaufman BM, Lee SM, Lee T, Pope SH, Riordan GS and Whitlow M. 1988. Single-chain antigen-binding proteins. Science. 242, pp. 423-426.

Blanch HW and Bhavaraju SM. 1976. Non-Newtonian fermentation broths: rheology and mass transfer. Biotechnol. Bioeng. 18, pp. 745-790.

Boehl D, Solle D, Toussaint H-J, Menge M, Renemann G, Lindemann C, Hitzmann B and Scheper T. 2001. Application of fluorescence spectroscopy for on-line bioprocess monitoring and control. Proc. SPIE. 4201, pp. 50-57.

Bowering LC. 2004. Microbial Systems for the Manufacture of Therapeutic Antibody Fragments. BioProcess Int. 2, pp. 40-47.

Bratbak G and Dundas I. Bacterial dry matter content and biomass estimations. Appl and Environ.Microbiol. 48 (4), pp. 755-757.

Bryan WL and Silman RW. 1990. Rolling-sphere viscometer for in situ monitoring of shake-flask fermentations. Enzyme Microb. Technol. 12, pp. 818-823.

Carvalho C. 2012. Biofilms: New Ideas for an Old Problem. Recent Patents on Biotechnology. 6(1), pp. 13-22.

Chan G, Booth AJ, Mannweiler K and Hoare M. 2006. Ultra scale-down studies of the effect of flow and impact conditions during *E. coli* cell processing. Biotechnol. Bioeng. 95, pp. 671-683.

Chatel A, Kumpalume P and Hoare M. 2014. Ultra scale-down characterization of the impact of conditioning methods for harvested cell broths on clarification by continuous centrifugation - recovery of domain antibodies from rec *E. coli*. Biotechnol. Bioeng. 111, pp. 913-924.

Chen Y, Chen L, Chen S, Chang M and Chen T. 2004. A modified osmotic shock for periplasmic release of a recombinant creatinase from *Escherichia coli*. Biochem. Eng. J. 19, pp. 211-215.

Chen H-C, Hwang C-F and Mou D-G. 1992. High-density *Escherichia coli* cultivation process for hyperexpression of recombinant porcine growth hormone. Enzyme Microb. Technol. 14(4), pp. 321-326.

Chen J and Mao Y. 2004. Protective effect of exopolysaccharide colanic acid of *Escherichia coli* O157:H7 to osmotic and oxidative stress. International Journal of Food Microbiology. 93(3), pp. 281-6.

Chew W and Sharratt P. 2010. Trends in process analytical technology. Anal. Methods. 2, pp. 1412-1438.

Chopda VR, Gomes J and Rathore AS. 2016. Bridging the gap between PAT concepts and implementation: An integrated software platform for fermentation. Biotechnol. J. 11, pp. 164-171.

Ciccolini LAS, Ayazi Shamlou P, Titchener-Hooker NJ, Ward JM and Dunnill P. 1999. Rheological properties of chromosomal and plasmid DNA during alkaline lysis reaction. Bioprocess Eng. 21, pp. 231-237.

Cohen SN, Chang ACY, Boyer HW and Helling RB. 1973. Construction of biologically functional bacterial plasmids in vitro. Proc. Nat. Acad. Sci. 70(11), pp. 3240-3244.

Coppella SJ and Dhurjati P. 1987. Low-cost computer-coupled fermenter off-gas analysis via quadrupole mass spectrometer. Biotechnol. Bioeng. 29(6) pp. 679-689.

Crowley J, Arnold SA, Wood N, Harvey LM and McNeil B. 2005. Monitoring a high cell density recombinant *Pichia pastoris* fed-batch bioprocess using transmission and reflectance near infrared spectroscopy. Enzyme Microb. Technol. 36, pp. 621-628.

Deindoerfer FH and West JM. 1960. Rheological properties of fermentation broths. Adv. Appl. Microbiol. 2, pp. 265-273.

Dhillon GS, Brar SK, Kaur S and Verma M. 2013. Rheological studies during submerged citric acid fermentation by *Aspergillus niger* in stirred fermentor using apple pomace ultrafiltration sludge. Food Bioprocess Technol. 6, pp. 1240-1250.

DiMasi JA, Grabowski HG and Hansen RW. 2016. Innovation in the pharmaceutical industry: New estimates of R&D costs. J. Health Econ. 47, pp. 20-33.

Doak DL and Phillips JA. 1999. In Situ Monitoring of an *Escherichia coli* fermentation using a diamond composition ATR probe and mid-infrared spectroscopy. Biotechnol. Prog. 15, pp. 529-539.

Dong J, Migliore N, Mehrman S, Cunningham J, Lewis M and Hu P. 2016. High-throughput, automated protein A purification platform with multi-attribute LC-MS analysis for advanced cell culture process monitoring. Anal. Chem. 88, pp. 8673-8679.

Doran P. 1995. Bioprocess Engineering Principles. Australia: Elsevier Science & Technology Books.

Eboigbodin K and Biggs C. 2008. Characterization of the Extracellular Polymeric Substances Produced by *Escherichia coli* Using Infrared Spectroscopic, Proteomic, and Aggregation Studies. Biomacromolecules. 9, pp. 686-695.

Ecker DM, Jones SD and Levine HL. 2015. The therapeutic monoclonal antibody market. mAbs. 7(1), pp. 9-14.

Einstein A. 1906. Eine neue Bestimmung der Molekülldimensionen. Annalen der Physik. 19, pp. 289-306. Correction, ibid., 34 (1911), pp. 591-592, A new determination of molecular dimensions, in: R. Fürth, A.D. Cowper (Eds.), Investigation on the theory of the brownian movement, Dover Publications, USA, 1956, pp. 36-54.

Esch E, Bahinski A and Huh D. 2015. Organs-on-chips at the frontiers of drug discovery. Nat. Rev. Drug Discov. 14, pp. 248-260.

Espuny Garcia del Real G, Davies J and Bracewell D. 2014. Scale-down characterization of post-centrifuge flocculation processes for high-throughput process development. Biotechnol. Bioeng. 111, pp. 2486–2498.

Fehrenbach R, Comberbach M and Petre JO. 1992. On-line biomass monitoring by capacitance measurement. J. Biotechnol. 23, pp. 303-314.

Finn B, Harvey LM and McNeil B. 2006. Near-infrared spectroscopic monitoring of biomass, glucose, ethanol and protein content in a high cell density baker's yeast fed-batch bioprocess. Yeast. 23, pp. 507-517.

Food and Drug Administration. 2004. Guidance for industry PAT - A framework for innovative pharmaceutical development, manufacturing and quality assurance. Rockville, MD: U.S. Department of Health and Human Services.

Forman S, DeBernandez E, Feldberg R and Swartz R. 1990. Cross-flow filtration of inclusion bodies from soluble proteins in recombinant *E. coli* cell lysate. J. Membr. Sci. 48, pp. 263-279.

Formenti LR, Nørregaard A, Bolic S, Hernandez DQ, Hagemann T, Heins A-L, Larsson H, Mears L, Mauricio-Iglesias M, Kruehne U and Gernaey KV. 2014. Challenges in industrial fermentation technology research. Biotechnol. J. 9, pp. 727-738.

Franz C, Jürgen K, Florentina P and Karl B. 2005. Sensor combination and chemometric modelling for improved process monitoring in recombinant *E. coli* fed-batch cultivations. J. Biotechnol. 120, pp. 183-196.

Frenzel A, Hust M and Schirrmann T. 2013. Expression of recombinant antibodies. Front. Immunol. 4, pp. 1-20.

Furuse H, Amari T, Miyawaki O, Asakura T and Toda K. 2002. Characteristic behaviour of viscosity and viscoelasticity of *Aureobasidium pullulans* culture fluid. J. Biosci. Bioeng. 93(4), pp. 411-415.

Galindo E and Nienow AW. 1992. Mixing of highly viscous simulated xanthan fermentation broths with the lightnin A-315 impeller. Biotechnol. Prog. 8, pp. 233-239.

Garcia-Arrazola R, Chau Siu S, Chan G, Buchanan I, Doyle B, Titchener-Hooker N and Baganz F. 2005. Evaluation of a pH-stat feeding strategy on the production and recovery of Fab' fragments from *E. coli*. Biochem. Eng. J. 23, pp. 221 - 230.

Gasser B, Maurer M, Gach J, Kunert R and Mattanovich D. 2006. Engineering of *Pichia pastoris* for improved production of antibody fragments. Biotechnol. Bioeng. 94(2), pp. 353-361.

Glassey J, Gernaey KV, Clemens C, Schulz TW, Oliveira R, Striedner G and Mandenius C-F. 2011. Process analytical technology (PAT) for biopharmaceuticals. Biotechnol. J. 6, pp. 369-377.

Gray P, Dunnill P and Lilly M. 1972. The continuous-flow isolation of enzymes. In: Terui, G. (Ed.) Fermentation Technology Today, pp. 347-351. Kyoto: Society of Fermentation Technology.

Hakemeyer C, Strauss U, Werz S, Jose GE, Folque F and Menezes JC. 2012. At-line NIR spectroscopy as effective PAT monitoring technique in Mab cultivations during process development and manufacturing. Talanta. 90, pp. 12-21.

Hall JW, McNeil B, Rollins MJ, Draper I, Thompson BG and MacAloney G. 1996. Near-infrared spectroscopic determination of acetate, ammonium, biomass and glycerol in an industrial *Escherichia coli* fermentation. Appl. Spectrosc. 50(1), pp. 102-108.

Harms P, Kostov Y and Rao G. 2002. Bioprocess monitoring. Curr. Opin. Biotechnol. 13, pp. 124-127.

Hewitt CJ and Nebe-Von-Caron G. 2004. The Application of Multi-Parameter Flow Cytometry to Monitor Individual Microbial Cell Physiological State. Adv. Biochem. Eng./Biotechnol. 89, pp. 197-223.

Hoffman F and Rinas U. 2004. Stress induced by recombinant protein production in Escherichia coli. Adv. Biochem. Engin. Biotechnol. 89, pp. 73-92.

Hsu P, Lander E and Zhang F. 2014. Development and applications of CRISPR-Cas9 for genome engineering. Cell. 157, pp. 1262-1278.

Hutchinson N, Bingham N, Murrell N, Farid S and Hoare M. 2006. Shear stress analysis of mammalian cell suspensions for prediction of industrial centrifugation and its verification. Biotechnol. Bioeng. 95(3), pp. 483-491.

Jain RK. 1990. Physiological barriers to delivery of monoclonal antibodies and other macromolecules in tumors. Cancer Res. 50, pp. 814-819.

Jalalirad R. 2013. Selective and efficient extraction of recombinant proteins from the periplasm of *Escherichia coli* using low concentrations of chemicals. J. Ind. Microbiol. Biotechnol. 40, pp. 1117-29.

Jeong KJ, Jang SH and Velmurugan M. 2011. Recombinant antibodies: engineering and production in yeast and bacterial hosts. Biotechnol. J. 6(1), pp. 16-27.

Jespers L, Schon O, Famm K and Winter G. 2004. Aggregation-resistant domain antibodies selected on phage by heat denaturation. Nat. Biotechnol. 22(9), pp. 1161-1165.

Joosten V, Lokman C, van Den Hondel CA and Punt PJ. 2003. The production of antibody fragments and antibody fusion proteins by yeasts and filamentous fungi. Microb. Cell. Fact. 2(1). DOI: 10.1186/1475-2859-2-1.

Justice C, Brix A, Freimark D, Kraume M, Pfromm P, Eichenmueller B and Czermak P. 2011. Process control in cell culture technology using dielectric spectroscopy. Biotechnol. Adv. 29, pp. 391-401.

Kaiser C, Pototzki T, Ellert A and Luttmann R. 2008. Applications of PAT-process analytical technology in recombinant protein processes with *Escherichia coli*. Eng. Life. Sci. 8(2), pp. 132-138.

Keefe R and Dubbin D. 2005. Specifying microfiltration systems. Chem. Eng. 112(8), pp. 48-51.

Kiviharju K, Salonen K, Moilanen U and Eerikäinen T. 2008. Biomass measurement online: the performance of in situ measurements and software sensors. J. Ind. Microbiol. Biotechnol. 35, pp. 657-665.

Kleman GL and Strohl WR. 1994. Developments in high cell density and high productivity microbial fermentation. Curr. Opin. Biotech. 5, pp. 180-186.

Kola I. 2008. The state of innovation in drug development. Clin. Pharmacol. Ther. 83(2), pp. 227-230.

Kong S, Day AF, O'Kennedy RD, Shamlou PA and Titchener-Hooker NJ. 2009. Using viscosity-time plots of *Escherichia coli* cells undergoing chemical lysis to measure the impact of physiological changes occurring during batch cell growth. J. Chem. Technol. Biotechnol. 84, pp. 696-701.

Larson SM, Carrasquillo JA, Krohn KA, Brown JP, McGuffin RW, Ferens JM, Graham MM, Hill LD, Beaumier PL and Hellström KE. 1983. Localization of 131l-labeled p98-specific Fab fragments in human melanoma as a basis for radiotherapy. J. Clin. Invest. 72(6), pp. 2101-2114.

Lavecchia A. and Di Giovanni C. 2013. Virtual screening strategies in drug discovery: a critical review. Curr. Med. Chem. 20, pp. 2839-2860.

Leduy A, Marsan AA and Coupal B. 1974. A Study of the rheological properties of a non-Newtonian fermentation broth. Biotechnol. Bioeng. 16, pp. 61-76.

Lee SY. 1996. High cell-density culture of *Escherichia coli.* Trends Biotechnol. 14, pp. 98-105.

Lee HLT, Boccazzi P, Gorret N, Ram RJ and Sinskey AJ. 2004. In situ bioprocess monitoring of *Escherichia coli* bioreactions using raman spectroscopy. Vib. Spectrosc. 35, pp. 131-137.

Lee HW, Carvell J, Brorson K and Yoon S. 2015. Dielectric spectroscopy-based estimation of VCD in CHO cell culture. J. Chem. Technol. Biotechnol. 90, pp. 273-282.

Levy M, Ciccolini L, Yim S, Tsai J, Titchener-Hooker N, Ayazi Shamlou P and Dunnill P. 1999. The effects of material properties and fluid flow intensity on plasmid DNA recovery during cell lysis. Chem. Eng. Sci. 54, pp. 3171-3178.

Lewis G, Taylor IW, Nienow AW and Hewitt CJ. 2004. Application of Multi-Parameter Flow Cytometry to the Study of Recombinant *Escherichia Coli* Batch Fermentation Processes. J. Ind. Microbiol. Biotechnol. 31(7), pp. 151-158.

Li Q, Aucamp J, Tang A, Chatel A and Hoare M. 2012. Use of Focused Acoustics for Cell Disruption to Provide Ultra Scale-Down Insights of Microbial Homogenization and its Bioprocess Impact - Recovery of Antibody Fragments from rec *E. coli*. Biotechnol. Bioeng. 109(8), pp. 2059 - 2069.

Li Q, Mannall G, Ali S and Hoare M. 2013. An ultra scale-down approach to study the interaction of fermentation, homogenization, and centrifugation for antibody fragment recovery from rec *E. coli*. Biotechnol. Bioeng. 110, pp. 2150-2160.

Liu Y and Lu H. 2016. Microfluidics in systems biology - hype or truly useful? Curr. Opin. Biotechnol. 39, pp. 215-220.

Lonescu M and Belkin S. 2009. Overproduction of Exopolysaccharides by an *Escherichia coli* K-12 rpoS Mutant in Response to Osmotic Stress. Applied and Environmental Microbiology. 75(2), pp. 483-492.

Lopes A and Keshavarz-Moore E. 2012. Prediction and verification of centrifugal dewatering of *P. pastoris* fermentation cultures using an ultra scale-down approach. Biotechnol. Bioeng. 109, pp. 2039-2047.

Mandenius C-F and Titchener-Hooker NJ. 2013. Measurement, monitoring, modelling and control of bioprocesses. Adv. Biochem. Engin. Biotechnol. 132, pp. 1-285.

Mason TG, Dhople A and Wirtz D. 1996. Linear viscoelastic moduli of concentrated DNA solutions. Macromolecules. 81(2), pp. 153-157.

McNeil B, Harvey LM, Rowan NJ and Giavasis I. 2013. Fermentation monitoring and control of microbial cultures for food ingredient manufacture. In: Woodhead Publishing Series in Food Science, T.a.N. Microbial Production of Food Ingredients, Enzymes and Nutraceuticals, pp. 125–143: Woodhead Publishing Ltd.

Meireles M, Lavoute E and Bacchin P. 2003. Filtration of a bacterial fermentation broth: harvest conditions effects on cake hydraulic resistance. Bioprocess Biosystems Eng. 25, pp. 309-314.

Mergulhão F, Summers D and Monteiro G. 2005. Recombinant protein secretion in *Escherichia coli*. Biotechnol. Adv. 23, pp. 177-202.

Metzner AB and Otto RE. 1957. Agitation of Non-Newtonian Fluids. American Institute of Chemical Engineers. 3(1), pp. 3-10.

Mewis J and Wagner NJ. 2012. Colloidal suspension rheology, 1st edition, Cambridge: Cambridge University Press.

Milburn P, Bonnerjea J, Hoare M and Dunnill P. 1990. Selective flocculation of nucleic acids, lipids, and colloidal particles from a yeast cell homogenate by polyethyleneimine, and its scale-up. Enzyme Microb. Technol. 12, pp. 527-532.

Mohseni M, Kautola H and Grant D. 1997. The viscoelastic nature of filamentous fermentation broths and its influence on the directly measured yield stress. J. Ferment. Bioeng. 83(3), pp. 281-286.

Morrow T and Felcone LH. 2004. Defining the difference: what makes biologics unique. Biotechnol. Healthc. 1(4), pp. 24-26.

Navratil M, Norberg A, Lembren L and Mandenius C. 2005. On-line multi-analyzer monitoring of biomass, glucose and acetate for growth rate control of a *Vibrio cholerae* fed-batch cultivation. J. Biotechnol. 115, pp. 67-79.

Neidhardt F and Umbarger H. 1996. Chapter 3: Chemical Composition of *Escherichia Coli*. In: edition 2. *Escherichia Coli* and Salmonella: Cellular and Molecular Biology, American Society of Microbiology.

Nelson AL and Reichert JM. 2009. Development trends for therapeutic antibody fragments. Nat. Biotechnol. 27, pp. 331-337.

Nesbeth DN, Perez-Pardo M, Ali S, Ward J and Keshavarz-Moore E. 2011. Growth and productivity impacts of periplasmic nuclease expression in an *Escherichia coli* Fab' fragment production strain. Biotechnol. Bioeng. 109, pp. 517-527.

Neves AA, Pereira DA, Vieira, LM and Menezes JC. 2000. Real time monitoring biomass concentration in *Streptomyces clavuligerus* cultivations with industrial media using a capacitance probe. J. Biotechnol. 84, pp. 45-52.

Ni Y and Chen R. 2009. Extracellular recombinant protein production from *Escherichia coli.* Biotechnol. Lett. 31, pp. 1661-1670.

Noui L, Hill J, Keay PJ, Wang RY, Smith T, Yeung K, Habib G and Hoare M. 2002. Development of a high resolution UV spectrophotometer for at-line monitoring of bioprocesses. Chem. Eng. Process. 41, pp. 107-114.

Okamoto Y, Ohmori K and Glatz CE. 2001. Harvest time effects on membrane cake resistance of *Escherichia coli* broth. J. Membr. Sci. 190, pp. 93-106.

Ozturk S and Hu W-S. 2004. Cell Culture Technology for Pharmaceutical and Cell-Based Therapies, CRC Press.

Perez-Pardo M, Ali S, Balasundaram B, Mannall G, Baganz F and Bracewell D. 2011. Assessment of the manufacturability of *Escherichia coli* high cell density fermentations. Biotechnol. Prog. 27, pp. 1488-1496.

Perley CR, Swartz JR and Cooney CL. 1979. Measurement of cell mass concentration with a continuous-flow viscometer. Biotechnol. Bioeng. 21, pp. 519-523.

Picque D and Corrieu G. 1988. New instrument for online viscosity measurement of fermentation media. Biotechnol. Bioeng. 31, pp. 19-23.

Pons M-N, Le Bonté S and Potier O. 2004. Spectral analysis and fingerprinting for biomedia characterisation. J. Biotechnol. 113, pp. 211-230.

Rayat A, Chatel A, Hoare M and Lye G. 2016. Ultra scale-down approaches to enhance the creation of bioprocesses at scale: impacts of process shear stress and early recovery stages. Curr. Opin. Chem. Eng. 14, pp. 150-157.

Rayat A, Lye G and Micheletti M. 2014. A novel microscale crossflow device for the rapid evaluation of microfiltration processes. J. Membr. Sci. 452, pp. 284-293.

Read EK, Park JT, Shah RB, Riley BS, Brorson KA and Rathore AS. 2009. Process Analytical Technology (PAT) for Biopharmaceutical Products: Part 1. Concepts and Applications. Biotechnol. Bioeng. 105, pp. 276-284.

Reardon KF and Scheper TH. 1991. Determination of cell concentration and characterization of cells. In: Rehm, HJ and Reed G. (Ed.) Measuring, Modelling and Control. Second Edition, vol. 4. Germany: Biotechnology, VCH.

Revers L and Furczon E. 2010. An introduction to biologics and biosimilars. Part I: Biologics: What are they and where do they come from? CPJ/RPC. 143(3), pp. 134-139.

Riesenberg D and Guthke R. 1999. High-cell-density cultivation of microorganisms. Appl. Microbiol. Biotechnol. 51, pp. 422-430.

Rosano G and Ceccarelli E. 2014. Recombinant protein expression in *Escherichia coli*: advances and challenges. Front. Microbiol. 5(172). DOI: 10.3389/fmicb.2014.00172.

Roush D and Lu Y. 2008. Advances in primary recovery: centrifugation and membrane technology. Biotechnol. Prog. 24, pp. 488-495.

Salt D, Hay S, Thomas O, Hoare M and Dunnill P. 1995. Selective flocculation of cellular contaminants from soluble proteins using polyethyleneimine: a study of several organisms and polymer molecular weights. Enzyme Mircob. Technol. 17, pp. 107-113.

Salte H, King JMP, Baganz F, Hoare M, Titchener-Hooker NJ. 2006. A methodology for centrifuge selection for the separation of high solids density cell broths by visualisation of performance using windows of operation. Biotechnol. Bioeng. 95 (6), pp. 1218-1227.

Sandor M, Rüdinger F, Bienert R, Grimm C, Solle D and Scheper T. 2013. Comparative study of non-invasive monitoring via infrared spectroscopy for mammalian cell cultivations. J. Biotechnol. 168, pp. 636-645.

Sarra M, Ison AP and Lilly MD. 1996. The relationships between biomass concentration, determined by a capacitance-based probe, rheology and morphology of *Saccharopolyspora erythraea* cultures. J. Biotechnol. 51, pp. 157-165.

Schelden M, Lima W, Doerr EW, Wunderlich M, Rehmann L, Buechs J and Regestein L. 2017. Online measurement of viscosity for biological systems in stirred tank bioreactors. Biotechnol. Bioeng. 114, pp. 990-997.

Schmidt FR. 2004. Recombinant expression systems in the pharmaceutical industry. Appl. Microbiol. Biotechnol. 65, pp. 363-372.

Schofield D, Templar A, Newton J and Nesbeth D. 2016. Promoter engineering to optimize recombinant periplasmic Fab' fragment production in *Escherichia coli*. Biotechnol. Prog. 32(4), pp. 840-847.

Shibasaki S, Ueda M, Lizuka T, Hirayama M, Ideka Y, Kamasawa N, Osumi M and Tanaka A. 2001. Quantitative evaluation of the enhanced green fluorescent protein displayed on the cell surface of *Saccharomyces cerevisiae* by fluorometric and confocal laser scanning microscopic analyses. Appl. Microbiol. Biotechnol. 55(4), pp. 471-475.

Shiloach J and Fass R. 2005. Growing *E. coli* to high cell density - A historical perspective on method development. Biotechnol. Adv. 23, pp. 345-357.

Shimmons W, Svrcek Y and Zajic JE. 1976. Cell concentration control by viscosity. Biotechnol. Bioeng. 18, pp. 1793-1805.

Skerra A and Plückthun A. 1988. Assembly of a functional immunoglobulin Fv fragment in *Escherichia coli*. Science. 240, pp. 1038-1041.

Sletta H, Nedal A, Aune TEV, Helleburst H, Hakvåg S, Aune R, Ellingsen TE, Valla S and Brautaset T. 2004. Broad-host-range plasmid pJB658 can be used for industrial-level production of a secreted host-toxic single-chain antibody fragment in *Escherichia coli*. Appl. Environ. Microbiol. 70(12), pp. 7033-7039.

Sørensen HP and Mortensen KK. 2005. Advanced genetic strategies for recombinant protein expression in *Escherichia coli*. J. Biotechnol. 115, pp. 113-128.

Spadiut O, Capone S, Krainer F, Glieder A and Herwig A. 2014. Microbials for the production of monoclonal antibodies and antibody fragments. Trends Biotechnol. 32, pp. 54-60.

Stärk E, Hitzmann B, Schügerl K, Scheper T, Fuchs C, Köster D and Märkl H. 2002. In-situ-fluorescence-probes: a useful tool for non-invasive bioprocess monitoring. In: Scheper T (ed.), Advances in Biochemical Engineering/Biotechnology. Berlin: Springer-Verlag.

Suhr H, Wehnert G, Schneider K, Bittner K, Scholz T, Geissler P, Jähne B and Scheper T. 1995. In situ microscopy for on-line characterization of cell-populations in bioreactors, including cell-concentration measurements by depth from focus. Biotechnol. Bioeng. 47, pp. 106-116.

Tosi S, Rossi M, Tamburini E, Vaccari G, Amaretti A and Matteuzzi D. 2003. Assessment of in-line near-infrared spectroscopy for continuous monitoring of fermentation processes. Biotechnol. Prog. 19, pp. 1816-1821.

Ulber R, Frerichs J-G and Beutel S. 2003. Optical sensor systems for bioprocess monitoring. Anal. Bioanal. Chem. 376, pp. 342-348.

Vlahopoulou I and Bell AE. 1993. Effect of various starter cultures on the viscoelastic properties of bovine and caprine yoghurt gels. Int. J. Dairy Technol. 46, pp. 61-63.

Vlahopoulou I, Bell AE and Wilbey A. 1994. Starter culture effects on caprine yoghurt fermentation. Int. J. Dairy Technol. 47, pp. 121-123.

Vlahopoulou I, Bell AE and Wilbey A. 2001. Effects of starter culture and its exopolysaccharides on the gelation of glucono-δ-lactone-acidified bovine and caprine milk. Int. J. Dairy Technol. 54(4), pp. 135-140.

Vojinovic V, Cabral JMS and Fonsecca LP. 2006. Real-time bioprocess monitoring part I: in situ sensors. Sensors and Actuators B. 114, pp. 1083-1091.

von Behring E and Kitasato S. 1890. The mechanism of immunity in animals to diphtheria and tetanus. Deutsche Medizinische Wochenschrift. 16, pp. 1113-1114.

Voulgaris I, Chatel A, Hoare M, Finka G and Uden M. 2016. Evaluation of options for harvest of a recombinant *E. coli* fermentation producing a domain antibody using ultra scale-down techniques and pilot-scale verification. Biotechnol. Prog. 32(2), pp. 382-392.

Voulgaris I, Finka G, Uden M and Hoare M. 2015. Enhancing the selective extracellular location of a recombinant *E. coli* domain antibody by management of fermentation conditions. Appl. Microbiol. Biotechnol. 99(20), pp. 8441-8453.

Ward ES, Güssow D, Griffiths AD, Jones PT and Winter G. 1989. Binding activities of a repertoire of single immunoglobulin variable domains secreted from *Escherichia coli*. Nature. 341, pp. 544-546.

Ward M, Lin C, Fox BP, Fox JA, Wong DL, Meerman HJ, Pucci JP, Fong RB, Heng MH, Tsurushita N, Gieswein C, Park M and Wang H. 2004. Characterization of humanized antibodies secreted by *Aspergillus niger*. Appl. Environ.Microbiol. 70(5), pp. 2567-2576.

Wong HH, O'Neill BK and Middelberg APJ. Cumulative sedimentation analysis of *Escherichia coli* debris size. 1997. Biotechnol. Bioeng. 55 (3), pp. 556-564.

Wörn A and Plückthun A. 2001. Stability engineering of antibody single-chain Fv fragments. J. Mol.Biol. 305(5), pp. 989-1010.

Wunderlich M, Trampnau PP, Emanuel FL, Buechs J and Regestein L. 2016. Online in situ viscosity determination in stirred tank reactors by measurement of the heat transfer capacity. Chem. Eng. Sci. 152, pp. 116-126.

Wu P, Ozturk SS, Blackie JD, Thrift JC, Figueroa C and Naveh D. 1994. Evaluation and applications of optical cell density probes in mammalian cell bioreactors. Biotechnol. Bioeng. 45, pp. 495-502.

Xiong Z-Q, Guo M-J, Chu J, Zhuang Y-P and Zhang S-L. 2015. On-line specific growth rate control for improving reduced glutathione production in *Saccharomyces cerevisia*. Biotechnol. Bioprocess Eng. 20, pp. 887-893.

Xiong Z-Q, Guo M-J, Guo Y-X, Chu J, Zhuang Y-P and Zhang S-L. 2008. Real-time viable-cell mass monitoring in high-cell-density fed-batch glutathione fermentation by *Saccharomyces cerevisiae* T65 in industrial complex medium. J. Biosci. Bioeng. 105(4), pp. 409-413.

Xu P, Clark C, Ryder T, Sparks C, Zhou J, Wang M, Russell R and Scott C. 2016. Characterization of TAP Ambr 250 disposable bioreactors, as a reliable scale-down model for biologics process development. Biotechnol. Prog. DOI: 10.1002/btpr.2417.

Yavorsky D, Blanck R, Lambalot C and Brunkow R. 2003. The clarification of bioreactor cell cultures for biopharmaceuticals. Pharm. Technol. pp. 62-70.

Yokota T, Milenic DE, Whitlow M and Schlom J. 1992. Rapid tumor penetration of a single-chain Fv and comparison with other immunoglobulin forms. Cancer Res. 52(12), pp. 3402-3408.

Zabriskie DW and Humphrey AE. 1978. Estimation of fermentation biomass concentration by measuring culture fluorescence. Appl. Environ. Microbiol. 35(2), pp. 337-343.

Zanzotto A, Szita N, Boccazzi P, Lessard P, Sinskey AJ and Jensen KF. 2004. Membrane-aerated microbioreactor for high-throughput bioprocessing. Biotechnol. Bioeng. 87(2), pp. 243-254.

Zhao L, Fu H-Y, Zhou W and Hu W-S. 2015. Advances in process monitoring tools for cell culture bioprocesses. Eng. Life Sci. 15, pp. 459-468.

Chapter 9   Appendix

9.1   **Publication 1: Detecting cell lysis using viscosity monitoring in *E. coli* fermentation to prevent product loss (Biotechnology Progress)**

9.2 Publication 2: Investigating and modelling the effects of cell lysis on the rheological properties of fermentation broths (Biochemical Engineering Journal)

9.3 **Publication 3: Evaluating process options in Fab' primary recovery: crossflow filtration with flocculation to improve product yield, purity and process robustness (in preparation for submission, 2018)**

Evaluating process options in Fab' primary recovery: crossflow filtration with flocculation to improve product yield, purity and process robustness

Joseph M Newton[1], Mohd S Hussain[1], Alex Chatel[1], Ioannis Voulgaris[1], Andrea CME Rayat[1], Joanna Vlahopoulou[2], Yuhong Zhou[1].

[1] Department of Biochemical Engineering, UCL, Torrington Place, London, WC1E 7JE, UK; telephone: +44-20-76793795; fax: +44-20-79163943; e-mail: y.zhou@ucl.ac.uk

[2] Procellia Ltd., Netpark Incubator, Thomas Wright Way, Sedgefield, County Durham, TS21 3FD, UK; telephone: +44-1740-625250; email: joanna@procellia.com

Corresponding author: Yuhong Zhou, telephone: +44-20-76793815, e-mail: y.zhou@ucl.ac.uk

Running title: Improving product yield, purity and process robustness with crossflow filtration and flocculation

Abstract

Cell lysis and intracellular product loss in fermentation represent a significant challenge in bioprocessing; impurities such as nucleic acids and host cell protein lead to large variations in the material properties of the cell broth and therefore impact process robustness in downstream processing unit operations. In this article, two alternative primary recovery approaches were carried out using ultra scale-down (USD) technology, and evaluated alongside the existing Fab' primary recovery process on the basis of total product recovered, impurity concentration, solids removal, processing time, capital costs and complexity.

This research verified the novel use of crossflow filtration (CFF) in combination with flocculation as a microfiltration step directly after fermentation to intensify the primary recovery process. This process design achieved a 2.53-fold increase in total product recovered, a 3-fold improvement in solids removal and a 3.6-fold improvement in product purity in comparison to the existing Fab' recovery process. Acceptable operation in terms of permeate flux was attained with CFF at USD scale, which was equivalent to mid-range operation at large scale. This process is deemed to be much more robust, as the need to avoid premature lysis in fermentation is removed and the primary recovery sequence is simplified. Further, it was shown that this approach to process design i.e. by taking a holistic view of the process to understand the impact of upstream processing conditions on downstream operation efficiency, demonstrated a significant reduction in both DSP time and capital costs.

Keywords: fermentation; primary recovery; *E. coli*; crossflow filtration; flocculation; ultra scale-down.